8-2011

Evaluation Of Intensity Modulated Radiation Therapy (Imrt) Delivery Error Due To Imrt Treatment Plan Complexity And Improperly Matched Dosimetry Data

Jacqueline R. Tonigan

EVALUATION OF INTENSITY MODULATED RADIATION THERAPY (IMRT)

DELIVERY ERROR DUE TO IMRT TREATMENT PLAN COMPLEXITY AND

IMPROPERLY MATCHED DOSIMETRY DATA

by

Jacqueline Renee Tonigan, B.S.

APPROVED:

_____

Supervisory Professor – David Followill, Ph.D.

_____

[Lei Dong, Ph.D.]

_____

[Geoffrey Ibbott, Ph.D.]

_____

[Stephen Kry, Ph.D.]

_____

[R. Allen White, Ph.D.]

(All signatures must be in black ink.)

APPROVED:

_____

Dean, The University of Texas
Graduate School of Biomedical Sciences at Houston

EVALUATION OF INTENSITY MODULATED RADIAITON THERAPY (IMRT)

DELIVERY ERROR DUE TO IMRT TREATMENT PLAN COMPLEXITY AND

IMPROPERLY MATCHED DOSIMETRY DATA

A

THESIS

Presented to the Faculty of

The University of Texas

Health Science Center at Houston

and

The University of Texas

M. D. Anderson Cancer Center

Graduate School of Biomedical Sciences

in Partial Fulfillment

of the Requirements

for the Degree of

MASTER OF SCIENCE

By

Jacqueline R. Tonigan, B.S.

Houston, Texas

August, 2011

Dedication

In dedication to the loving memory of

Eric and Diane Tonigan.

Acknowledgements

EVALUATION OF INTENSITY MODULATED RADIATION THERAPY (IMRT) DELIVERY ERROR DUE TO IMRT TREATMENT PLAN COMPLEXITY AND IMPROPERLY MATCHED DOSIMETRY DATA

Abstract

Jacqueline R. Tonigan, B.S.

Supervisory Professor: David Followill, Ph.D.

Intensity modulated radiation therapy (IMRT) is a technique that delivers a highly conformal dose distribution to a target volume while attempting to maximally spare the surrounding normal tissues. IMRT is a common treatment modality used for treating head and neck (H&N) cancers, and the presence of many critical structures in this region requires accurate treatment delivery. The Radiological Physics Center (RPC) acts as both a remote and on-site quality assurance agency that credentials institutions participating in clinical trials. To date, about 30% of all IMRT participants have failed the RPC's remote audit using the IMRT H&N phantom. The purpose of this project is to evaluate possible causes of H&N IMRT delivery errors observed by the RPC, specifically IMRT treatment plan complexity and the use of improper dosimetry data from machines that were thought to be matched but in reality were not. Eight H&N IMRT plans with a range of complexity defined by total MU (1460-3466), number of segments (54-225), and modulation complexity scores (MCS) (0.181-0.609) were created in Pinnacle v.8m. These plans were delivered to the RPC's H&N phantom on a single Varian Clinac. One of the IMRT plans (1851 MU, 88 segments, and MCS=0.469) was equivalent to the median H&N plan from 130 previous RPC H&N phantom irradiations. This average IMRT plan was also delivered on four matched Varian Clinac machines and the dose distribution calculated using a different 6MV beam model. Radiochromic film and TLD within the phantom were used to analyze the dose profiles and absolute doses, respectively. The measured and calculated were compared to evaluate the dosimetric accuracy. All deliveries met the RPC acceptance criteria of ±7% absolute dose

difference and 4 mm distance-to-agreement (DTA). Additionally, gamma index analysis was performed for all deliveries using a ±7%/4mm and ±5%/3mm criteria. Increasing the treatment plan complexity by varying the MU, number of segments, or varying the MCS resulted in no clear trend toward an increase in dosimetric error determined by the absolute dose difference, DTA, or gamma index. Varying the delivery machines as well as the beam model (use of a Clinac 6EX 6MV beam model vs. Clinac 21EX 6MV model), also did not show any clear trend towards an increased dosimetric error using the same criteria indicated above.

Table of Contents

List of Figures

List of Tables

Chapter 1   Introduction

1.1 Statement of Problem

Intensity modulated radiation therapy (IMRT) is a relatively new technique that is widely used in radiotherapy clinics across the nation. IMRT utilizes a linear accelerator (linac)-mounted multi-leaf collimator (MLC) to shape the radiation beam into multiple segments per beam angle, creating fluence maps of varying intensity. Upon delivery, these fluence-modulated beams sum in three dimensions to create a highly conformal dose distribution. This technique increases the ability to cover tumor targets of irregular shape with the prescription dose while sparing nearby normal tissues and organs at risk (OARs). These advantages in target dose conformity and OAR dose sparing make IMRT very desirable for radiotherapy treatment situations in which tumor targets are in close proximity to OARs and steep dose gradients are required. For these reasons, IMRT is commonly used to treat head and neck (H&N) cancers, where many OARs exist such as the spinal cord, orbits, parotid glands, and may be near the target. In these situations a complex dose distribution is needed to avoid unacceptable or undesirable normal tissue toxicities.

In order to create these more conformal dose distributions, IMRT utilizes a technique of breaking up a large beam into a grid of several smaller beams known as "beamlets." These beamlets are given an intensity weight between 0% and 100% of the total beam intensity. The beamlets are combined to create a pattern of intensities known as an intensity map. This intensity map represents the radiation output from the specific angle of incidence of that beam required to deliver dose to the target and spare other tissues. This process is carried out for each of the beams used in an IMRT treatment plan and all intensity maps are then summed in three dimensions to create the desired dose distribution. Intensity maps are translated into deliverable MLC configurations, known as segments, for each beam. IMRT treatments can then be delivered in a step-and-shoot method, during which the radiation beam is off between segments, or with the dynamic method, during which the radiation beam remains on while the MLC form the different segments. The ability of this technique to modulate the fluence and create highly conformal dose distributions with varying dose levels makes it much more complex than conventional radiotherapy.

IMRT treatment plan complexity has been associated with a large numbers of monitor units (MU), small segment size, large numbers of segments, complex segment shape, and overall complex fluence maps (for a single beam). It has been quantified by Webb using the modulation index (MI) which compares adjacent bixel (or beamlet) intensities. The MI measures the complexity of a treatment plan by evaluating the number of changes in intensity of adjacent bixels that exceed one half the standard deviation of the bixel intensities, therefore quantifying the amount of modulation required. In this study, three types of treatment plans were used to evaluate the possible gains of fully modulated, more complex beams. One plan was created with full modulation, allowing each beamlet to vary as necessary to create the desired dose distribution. A second plan was created with the idea of few-segment IMRT (fsIMRT), in which each beam was allowed two segments for modulation, one including the entire beam's eye view (BEV) of the PTV and one of the BEV of the PTV excluding any overlap with the OAR. The simplest plan was an example of conventional conformal radiotherapy (CRT) in which each beam conformed to the PTV with one segment and had a single weight. In Webb's study, plans with these three levels of complexity were created for two challenging planning situations and it was verified that the MI increases with increased complexity and in turn with increased conformity. Webb also showed that the plans created with more modulation and with higher MIs were able to achieve better PTV coverage and OAR sparing [1].

More recently, McNiven *et al* introduced the concept of the modulation complexity score (MCS) which takes into account leaf position variability, degree of field shape irregularity, segment weight, and segment area by using the leaf sequence variability (LSV) and aperture area variability (AAV). The MCS has a value from 0.0-1.0, with 1.0 being the most simple open square field. In their study, they evaluated the MCS of treatment plans for various sites and found that sites with more complex anatomy, such as the head and neck, required plans with a lower MCS (increased complexity). They also evaluated several radical lung plans that covered a range of MCS values, MU, and segment numbers to compare plan and delivery. While no direct correlation between MCS and gamma index analysis percentage pass rate was found, it was identified that any plan with MCS > 0.8 or less than 50 MU were always (100% specificity) considered dosimetrically robust (>90%

pass rate for 2%/1mm criteria). The MCS offered higher sensitivity in identifying threshold criteria than the MU. The MCS is used in this study and is further described in Section 2.3.1.The increased complexity that comes with IMRT affects many stages of the IMRT delivery process, including treatment planning, treatment delivery, and quality assurance. The complexity and its effect on dose calculations, plan quality and delivery accuracy must be considered if accurate and safe radiation doses are to be delivered to patients [2].

To optimize radiotherapy doses, treatment planning systems can implement either forward planning or inverse planning. In forward treatment planning, the planner determines the treatment beam parameters such as the beam angle, collimator shape, modifiers to be used and the weight of each beam. The dose is then calculated and evaluated. The planner can iteratively make adjustments to the beam parameters to alter the dose distribution as desired until an acceptable plan is reached. In inverse treatment planning, the planner establishes dose objectives such as tumor prescriptions and OAR dose limitations. The treatment planning computer then determines the beam parameters required to meet those objectives. This is also an iterative process in that the planner can continue to add or adjust objectives to increase the quality of the plan.

Currently commercial treatment planning systems (TPSs) allow inverse treatment planning methods for IMRT plans, which can easily allow a plan to become more complex than necessary. During the dose calculation and optimization process, artifacts and noise can lead to small but sharp fluctuations in the intensity maps making the treatment plan more complex without any benefit to the quality of the plan [3]. In addition, the planner does not have direct control over the segments generated in IMRT inverse planning and thus, with a large number of possible solutions to the input objectives, the TPS may choose a more complex set of segments with minimal or no increase in treatment plan quality. Finally, with the ability of IMRT to conform to tumor targets so well, a planner may continue to optimize a plan passed the objectives required by the physician resulting in a plan of superior quality, but of unnecessary complexity, requiring more time to deliver and more mechanical work.

One technique suggested to reduce IMRT plan complexity and increase the treatment deliverability is fluence smoothing performed during optimization. An algorithm can be used to reduce the unwanted fluctuations in fluence in a treatment plan, hence smoothing the

intensity map and decreasing its complexity. Giorgia *et al* evaluated the effects of smoothing fluences on the IMRT treatment plan complexity, as measured by the modulation index (MI), the plan quality, and the dose delivery accuracy. It was found that IMRT plans created with less smoothing had an increased number of MUs and a decreased average MLC aperture and, as expected, were more complex (had a higher MI). There was not much difference noted in the quality of plans with varying levels of smoothing, as evaluated by the dose volume histograms (DVHs). It was, however, found that a poorer gamma index analysis pass rate (±3%/3mm criteria) resulted from decreased smoothing and that the correlation between the percentage of failing pixels with MI decreased with increasing fluence smoothness. Giorgia *et al* concluded that these correlations could indicate that when an IMRT plan was simple (low MI), failures were caused by dose calculation errors and when a plan was complex (high MI), failures were more likely to be caused by delivery errors [3].

Craft *et al* studied the tradeoff between number of MU (a measure of complexity) and the plan quality by adding a direct measure of the number of MU required, the sum of positive gradients (SPG), as a linear function to the treatment planning objectives. The SPG is the sum of all positive increases in intensity between adjacent beamlets. It was found that significant reductions in MU could usually be made without greatly affecting plan quality. However, there was a certain amount of complexity required and plans that were too simple did not provide adequate target coverage and normal tissue sparing. The authors concluded that a tradeoff tool could be implemented into treatment planning to avoid over-complicating treatment plans while providing an acceptable treatment plan that met the prescription requirements and normal tissue constraints [4].

Accuracy of an IMRT treatment dose calculation is imperative. Several different characteristics of the radiation delivery system in this calculation can contribute to uncertainty in IMRT dose calculations such as the definition of the source, MLC leaf positioning and speed, MLC leaf end shape, MLC transmission and scatter, and MLC tongue-and-groove effects. In one study by Li *et al*, a maximum PTV dose difference of 5.4% was found between calculations with and without MLC leakage. When the effects of

MLC tongue-and-groove effects were evaluated in the same study, a maximum of 5.1% difference was found [5].

In a study by Mohan *et al*, the effects of increasing the frequency and amplitude of intensity fluctuations of an IMRT field, as might be seen in complex treatment plans, were evaluated. It was observed that high frequency and amplitude fluctuations in the intensity require increased MU and small window widths for delivery. This resulted in a limitation on the minimum dose to the target region, possibly affecting plan quality by imposing a lower limit on the dose normal tissues could receive. Also for a complex plan with many small segments, a large amount of the dose comes from indirect sources (MLC leaf transmission and scatter), increasing the dose calculation dependence on empirical corrections and possibly decreasing the accuracy of this calculation [6].

In addition, the resolution of the MLC leaf position and size can impact on the dose calculation and can affect the quality and accuracy of the plan. Zhang *et al* found that with increasing beamlet step-size: maximum dose values of the PTV (hotspots) increased, the mean dose of the OAR increased, uniformity and conformity decreased, PTV coverage decreased, and the objective function increased. These changes indicated that an coarse resolution as defined by the width of the MLC leaves and the beamlet step-size negatively affected treatment plan quality as one might observe in complex IMRT plans [7].

In a dose accuracy study mentioned previously, Li *et al* compared dose distribution calculations between Monte Carlo and Corvus (Best Inc., Springfield, VA) treatment plans of varying intensity map resolution and found a maximum of 8% difference in mean dose and a maximum 4% standard deviation for treatment plans with a 1×1 mm^2 resolution in the dose calculation grid. The authors suggested that a 0.2×0.2 mm^2 intensity map at isocenter was necessary for accurate IMRT dose calculations [5].

IMRT treatment plan complexity also affects the radiation delivery itself. Steep dose gradients between targets and adjacent OARs greatly increase the need for accurate patient localization and set up. Hong *et al* studied the effects of daily setup variations on H&N IMRT treatments by measuring setup errors made when using conventional thermoplastic immobilization masking, laser alignment, and weekly portal films for setup. An average error of 3.33 mm in a single dimension was found and when all six degrees of freedom were

accounted for, an average composite vector offset of 6.97 mm was found. These errors would result in as much as 20-30% PTV under dosing and increases in OAR doses exceeding the toxicity limitations in the plans evaluated. Hong's study illustrated that small errors along one axis can add up in three dimensional space to create offsets that are not measured by conventional setup techniques and that could result in significant dosimetric consequences [8].

In addition, Siebers *et al* studied the effects of random and systematic setup errors on H&N simultaneous integrated boost (SIB) IMRT treatments and found that while the plans were relatively insensitive to random setup errors, systematic errors of 1.5 mm and 3 mm resulted in a dose error of greater than 3% for approximately 10% and 50% of patients, respectively. Twenty-eight percent of the plans evaluated with a 3 mm systematic error had a dose error of greater than 5%. This study illustrated the need for techniques to detect and reduce systematic setup errors and demonstrated the need for appropriate PTV margins to ensure dosimetric accuracy in tumor dose coverage [9].

Also, the accelerator's mechanical ability to deliver the treatment is a key issue in IMRT that could increase with increasing plan complexity. Luo *et al*, using prostate treatment log file-based Monte Carlo calculations, discovered that for every 0.2 mm systematic leaf position error, there was a 1% target dose error [10]. In another study, Mu *et al* evaluated the effects of random and systematic MLC leaf position errors on the quality of IMRT plans. Overall, it was found that while plans are unaffected by random errors, systematic MLC leaf position errors of only 1 mm resulted in a 4% average change in the dose received by 95% of the target ($D_{95\%}$) for simple plans (with less than 50 segments) and an 8% change for more complex plans (with more than 100 segments). This 1 mm systematic MLC leaf position error also resulted in 9% and 13% dose changes in the parotid glands for simple and complex plans, respectively [11]. These studies described above indicate just how sensitive IMRT dose delivery is to MLC leaf position and with complex plans there is an increase in the number MLC leaf positions because of the larger number of segments used.

As described above, since there are numerous possible contributors to errors in IMRT treatment delivery and the possible delivery of an unsafe radiation dose, IMRT

quality assurance (QA) becomes all that more important. However, even though most medical physicists recognize the need for IMRT QA, a standard IMRT QA procedure and evaluation criteria have not been agreed upon. Several methods and products exist for patient-specific IMRT QA. One commonly implemented technique is "per-beam" or "single field" planar QA. This is performed by delivering each beam of a treatment plan individually to a planar detector such as a diode array, ion chamber array, film or EPID device followed by a gamma analysis on the expected dose distribution of that individual beam. Currently, 3%/3mm gamma or composite distance-to-agreement (DTA) criteria is commonly held, though there is minimal evidence of its predictive power [12].

In a study by Kruse *et al*, three clinically acceptable plans were modified by reoptimizing with aggressive objectives and constraints to create three complex, and unacceptable, plans. The clinically acceptable plans had a calculated dose that agreed to within 4% of the dose measured at several low gradient points using an ion chamber in a cylindrical phantom, while the dose comparison with the unacceptable plans exceeded the 4% criterion. Single field IMRT QA was performed on both sets of plans using an EPID and an ion chamber array with a gamma index analysis of 3%/3mm and 2%/2mm. The EPID 3%/3mm analysis resulted in an average percent of pixels passing of 97.6% and 97.1% for acceptable and unacceptable plans, respectively. With the 2%/2mm criteria, these pass rates were 90.7% and 89.0% for acceptable and unacceptable plans, respectively. Similarly, pass rates of 98.8% and 98.7% were found with the 3%/3mm ion chamber array gamma analysis for acceptable and unacceptable plans, respectively, and of 93.4% and 91.0% with the 2%/2mm criteria. Pass rates for the acceptable and unacceptable plans were comparable in each evaluation and in some cases the unacceptable plan had a higher planar gamma analysis pass rate than the acceptable plan, therefore the fraction of pixels passing the gamma analysis was found to be a poor predictor of IMRT dosimetric accuracy [13].

Other methods of patient-specific IMRT QA include single-angle composite dose delivery to a planar detector and phantom measurements. With single-angle composite IMRT QA, all treatment fields are delivered to a planar detector, such as a diode array, at a normal angle and the summation of these fields is evaluated as compared to a calculation of the dose expected by the TPS. In this process, all high dose, steep gradient, and low dose

regions are summed together, possibly masking the complexity of the fields and making error detection difficult [12]. With phantom measurements for IMRT QA, the entire treatment plan is recalculated on the phantom geometry and then delivered to the phantom as it would be to a patient. Ion chamber measurements are made in low dose gradient regions and planar film measurements are taken to evaluate steep dose gradients. Again, it is common to implement a 3%/3mm gamma or composite DTA criteria.

While any of these IMRT QA methods may be sufficient for certain plans, the consistency of these techniques is unknown and therefore they are unreliable. With increased dose gradients and more complex intensity maps, complex IMRT treatment plans increase the difficulty as well as the importance of the measurements, and may increase the uncertainty of the these QA methods.

With the many possible causes of errors in IMRT delivery and minimal means to measure them, it is not surprising that almost 30% of institutions participating in NCI funded clinical trials failed a QA audit using the Radiological Physics Center's (RPC) IMRT H&N phantom [14]. This failure rate is very alarming, especially considering that these institutions put forth their best effort in order to pass the audit in order to be allowed to participate in clinical trials using IMRT. It is extremely important for institutions to be able to deliver these treatments accurately, to be consistent with each other for the purpose of the clinical trials, as will be discussed in the next section, but even more importantly for the safety and the health of the patients. Unfortunately advanced treatment techniques have not always proved to be beneficial to the patients, as highlighted in several NY Times articles in the past few years [15,16].

For all of the above mentioned reasons, it is critical to evaluate the IMRT treatment process to identify causes of delivery error so they can be detected, avoided, and fixed. Aside from the multiple components contributing to IMRT complexity, mistakes in IMRT treatment delivery can be caused by a plethora of factors. Some of these include incorrect photon beam dosimetry data, malfunctioning MLC, improper treatment planning, and failed or incorrect data transfer. A common oversight when performing IMRT QA is to assume that the TPS beam models are accurate when in fact the inaccuracies in the beam model may be contributing to the dose delivery error. One must ensure that the very basic dosimetry

parameters used to calculate dose for IMRT plans are accurate since this is the starting point for a very complex IMRT dose calculation. Once the basic dosimetry parameters and associated beam models have been verified then attention to the MLC parameters, etc. can be considered in the IMRT QA process. Current IMRT QA techniques may or may not be sensitive to these factors depending on the rigor of the measurements and agreement criteria used. For example, a study by Nelms *et al* used IMRT treatment plans calculated with intentionally incorrect beam models, and found that per-beam planar IMRT QA gamma analysis pass rate was not sensitive to clinically relevant dose errors. In fact, significant moderate correlations were found indicating that larger errors occur with higher pass rates. Nelms concluded that per-beam planar IMRT QA was not very useful in predicting IMRT dose delivery errors [17]. In fact, many of the RPC's IMRT H&N phantom irradiation failures were found after the institution had performed its own IMRT QA measurements that showed no IMRT delivery errors.

Until now, no one to our knowledge has attempted to measure the effects of treatment plan complexity or mismatched (incorrect beam model dosimetry parameters) dosimetry data by comparing treatment plan calculations to measurements made in an anthropomorphic phantom. In this project, we evaluated the dose delivery accuracy of H&N IMRT treatments of varying complexity. Additionally, we evaluated the ability of matched machines using a single TPS beam model even though there was some degree of variability in dosimetry parameters between the machines to deliver a standard H&N IMRT treatment accurately.

1.2 The Radiological Physics Center and Anthropomorphic QA Phantoms

Assigned with the task of ensuring clinical consistency and comparability in radiation doses delivered at institutions participating in clinical trials, the Radiological Physics Center (RPC) was founded in the late 1960's as a National Cancer Institute (NCI) funded group. It is crucial for institutions participating in multi-clinic studies to have uniform radiation therapy delivery quality and accuracy to ensure trial results are not influenced by dosimetric differences between clinics. The RPC monitors the machine output and brachytherapy source strength, dose calculation algorithms, dosimetry data, and quality assurance procedures of participating institutions by means of off-site remote auditing and on-site dosimetry review visits. The RPC performs chart checks, QA procedure review, treatment planning algorithm verification, and dosimetry data comparisons. Additionally included in the RPC's off-site programs are mailable TLD and OSLD machine output checks and six different mailable anthropomorphic phantoms.

Anthropomorphic phantoms enable the RPC to evaluate the ability of an institution to accurately deliver therapeutic dose distributions to a patient, including patient imaging, treatment planning, set up, and dose delivery processes. The RPC currently utilizes different anthropomorphic phantoms for thorax, spine, liver, pelvis/prostate, head and neck, and stereotactic radiosurgery treatments. These phantoms are made of anatomically shaped plastic shells which can be filled with water to simulate soft tissue. Also present in the plastic shell is a removable section containing imageable target and avoidance structures as well as dosimeters. Relative planar dose distributions are measured with radiochromic film and absolute point doses are measured with TLD. The dose distribution is generally measured with film in two major planes of the phantom and is normalized to the absolute point doses measured by the TLD. These phantoms are mailed to institutions for remote auditing and returned to the RPC for dosimeter reading and evaluation of the agreement between the dose distribution planned by the institution and that delivered. The RPC is also involved in helping institutions in implementing corrective action if deemed necessary.

Currently, the IMRT head and neck (H&N) phantom is used for IMRT credentialing of institutions for many clinical trials including eight active Radiation Therapy Oncology Group (RTOG) protocols. Recently, it was reported that about 30% of the institutions

participating in the IMRT H&N phantom audit are not passing the 7% absolute dose and 4 mm distance-to-agreement (DTA) criteria. Within the clinical trial community, there is a desire to better understand why such a large percentage of institutions fail the H&N phantom irradiation test. The RPC has decided to investigate the possible causes of the phantom failures in order to provide the radiotherapy community guidance as to how to improve the delivery of IMRT treatments. In the present study, the IMRT H&N phantom will be utilized to evaluate two of the possible causes of IMRT dosimetric inaccuracy, treatment plan complexity and mismatched dosimetry data.

1.3 Hypothesis and Specific Aims

We hypothesized that increased IMRT treatment plan complexity or the use of improperly matched accelerator dosimetry data can lead to errors in head and neck IMRT deliver, as measured with the RPC's H&N phantom, that result in differences between the measured and planned dose distributions.

This hypothesis was tested with the following specific aims:

1. We created clinically relevant treatment plans for the RPC IMRT H&N phantom for: a) a standard 6 MV delivery b) three increasingly more simple 6 MV deliveries and c) four increasingly more complex 6 MV deliveries as defined by MCS, MU and number of segments.

2. We delivered the eight planned IMRT treatments to the RPC IMRT H&N phantom on a single linear accelerator three times and measured the dose distribution delivered by each.

3. We delivered the standard treatment plan to the RPC IMRT H&N phantom on four matched machines that use the same dosimetry data three times each.

4. We calculated the standard plan dose distribution on an unmatched machine.

5. We compared the measured and calculated doses using the common RPC criteria of 7% and 4mm DTA as well as criteria of 5% and 3 mm DTA.

The dose distributions delivered using the eight treatment plans were measured with TLD and radiochromic film and both absolute point doses and planar dose distributions were compared to those calculated with the treatment planning system. Likewise, the delivery of the standard plan was measured with TLD and radiochromic film on four matched machines and the absolute point doses and planar dose distributions were compared to those calculated with the treatment planning system. A composite measure of the percent point dose agreement and the distance to agreement (DTA), the gamma index, was also be evaluated for each of these measurements.

The completion of this study will give the RPC direction into to what is causing the high rate of IMRT credentialing failure. With the growing use of advanced technologies

including IMRT and the increased need for strong QA, this study hopes to highlight some of the indicators of plans that are likely to contain dosimetric errors. The results of this study could decrease the amount of time and effort it takes to determine the cause of irradiation failures post-irradiation. Ideally the results will provide guidance to institutions as to treatment plan criteria that should be noted and avoided to increase the robustness of the treatment plan and treatment delivery, such as a complexity threshold above which dosimetric failure is expected.

Chapter 2   Methods and Materials

2.1 Phantom

This study utilizes the RPC's IMRT head and neck phantom, which was designed as a means of auditing and credentialing institutions wishing to participate in Radiation Therapy Oncology Group (RTOG) head and neck protocols using IMRT. It was designed to mimic a patient for an RTOG oropharyngeal protocol (H-0022) with two target volumes, a primary tumor and a secondary node, and an organ at risk (OAR) within close proximity to the primary target. This phantom was created with tissue-equivalent materials containing radiation dosimeters to measure the dose delivered.

The phantom consists of an anthropomorphic clear plastic shell and a polystyrene block insert, as shown in Figure 2.1. The plastic shell is hollow and can be filled with water through two plugs in the bottom to simulate soft tissue.
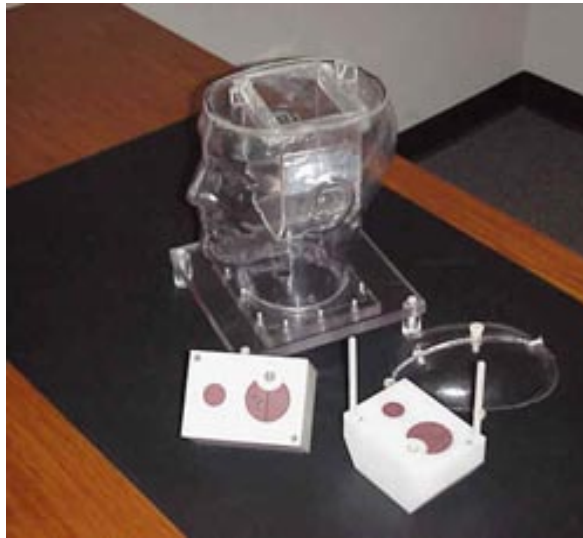
Figure 2.1 RPC IMRT Head and Neck phantom with dosimetry insert

The removable polystyrene insert measures 13 cm by 10.5 cm by 7.5 cm and contains the two targets and OAR volumes as well as the radiation dosimeters. The insert is cut along the axial plane for insertion and removal of dosimeters. The targets and OAR are visible at this opening as seen in Figure 2.1. **Error! Reference source not found.Error! Reference source not found.** shows the superior half of the insert alongside a cross-sectional CT image of the same half. The solid water planning target volumes (PTVs) and

the acrylic OAR are labeled in the images in Figure 2.2, as well as the locations for the TLD. The phantom dosimetry insert materials were chosen to ensure visibility on CT images with minimal effects on the delivery. The three structures within the insert are cylinders with central axes that lay along the superior-inferior axis of the phantom. The primary PTV has a posterior semi-circular cut-out the OAR sits, separated by a 0.8 cm gap. Dimensions of the PTVs and OAR can be found in Table 2.1.
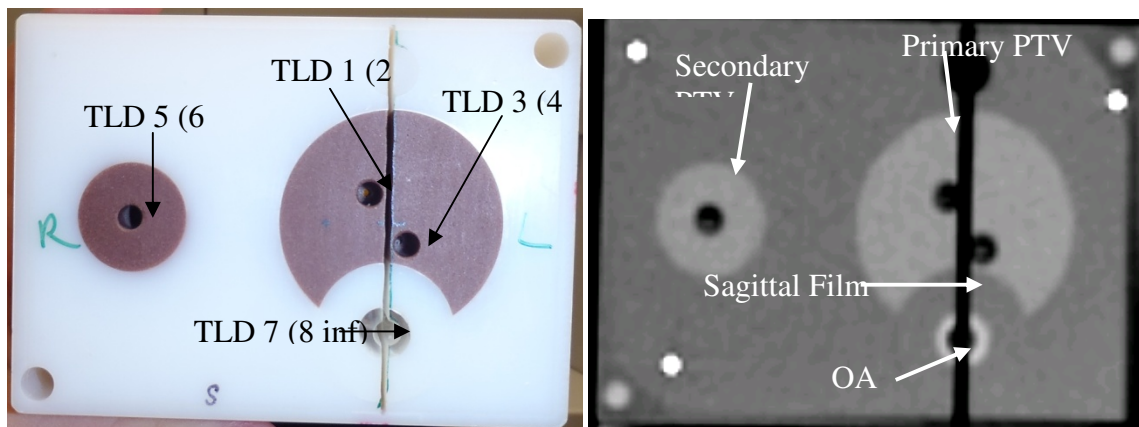
Figure 2.2 Picture (left) and CT image (right) of superior axial half of IMRT Head and Neck phantom with two PTVs and an OAR. Eight TLD are numbered as those in the superior half (those in the inferior half).

Structure	Diameter (cm)	Length (cm)
Primary PTV	4	5
Secondary PTV	2	5
OAR	1	13

Table 2.1 Dimensions of structures within RPC IMRT Head and Neck phantom dosimetry insert

The phantom insert houses a total of eight thermoluminescent dosimeter capsules (TLDs). There are four holes in each half of the insert, that hold the TLD. The TLD are placed in pairs at the same location in the superior and inferior half of the insert. There is one pair of TLD in the center of each the secondary PTV and the OAR. In the primary PTV, one pair of TLD lies anterior and right of the center of the cylinder and one pair lies posterior and left of the center.

15

The insert also houses radiochromic film in the axial and sagittal planes. The film along the sagittal plane bisects the primary PTV and the OAR and is cut in two pieces where it intersects the axial film. There is also a region of the sagittal film cut to allow for TLDs in the OAR. Small holes are pricked in designated points of the film for registration purposes. These holes are pricked in the axial film by three pins located in the axial plane of the insert. The sagittal films are pricked by a placing a small, sharp tool through five holes that are drilled in the left side of the insert. Details on film registration are provided in Section 2.4.4.

2.2 Treatment Planning

2.2.1 Treatment Plan Goals

To determine if treatment plan complexity is directly related to dosimetry errors in IMRT delivery, we created eight IMRT treatment plans of varying complexity to deliver to the RPC's H&N phantom. One plan was created to represent the average IMRT H&N phantom plan, the baseline plan. From there, treatment plan complexity was increased or decreased by extensive re-optimization, influencing the number of MU, number of segments, segment size, and MCS.

In order to establish a baseline plan, a sample of 130 previous irradiations of the RPC's IMRT H&N phantom completed at institutions across the country with Pinnacle treatment planning, Varian linear accelerators, and using one fraction to deliver the full prescription were evaluated. The median number of MU, number of segments, and number of beams were used to establish planning goals for the baseline plan of this study.

2.2.2 Phantom Imaging

To acquire images of the RPC IMRT H&N phantom for treatment planning, a CT simulation on a Philips Mx8000 IDT 16 slice CT scanner (Philips Healthcare, Andover, MA) with the AcQSim workstation was performed. The phantom was filled with water and the insert containing TLD was put in place. The phantom was set up on the imaging table supine and "head first." Screws on the posterior side of the inferior support were adjusted to ensure the insert was approximately level with the table. The anterior-posterior laser was aligned along the central line of the face. A radio-opaque marker (bb fiducial) was placed at the position of the laser crosshairs on the nose and each ear to mark the simulation isocenter. These bb's were taped down to ensure they did not move over the course of irradiation and

the laser crosshair position was drawn on the tape. Scan parameters similar to the commonly used MD Anderson adult head and neck protocol was used with 1.5 mm slice thickness, 120 kV, and 250 mAs contiguous imaging, resulting in 174 images. The fine slice thickness was used to ensure TLD visibility. These images were imported into the Pinnacle (Philips Medical, Madison, WI) for treatment planning.

2.2.3 Planning Parameters

Treatment planning was performed on Pinnacle version 8.0m (Philips Medical, Madison, WI). The couch was removed from the CT scan at the interface between the phantom and the table. We used electron density lookup table that is routinely used at MD Anderson and was created for this and two other simulation CT scanners. This table allows the TPS to convert CT numbers to electron densities for the dose calculation.

Using the region of interest (ROI) tool set, contours required by the RPC for the primary PTV (PTV_66), secondary PTV (PTV_54), OAR (CORD), and all eight TLD were created manually. TLD contours were created to include the TLD powder visible on the CT images. The skin was contoured with the autocontour function and a normal tissue structure was created by subtracting the PTVs with an additional margin of 5 mm from the total volume defined by the skin. Several planning structures were also contoured, including a 5 mm expanded OAR, total PTV and several hot spots.

The isocenter for these plans were created at the intersection of the three bb's placed during simulation on the slice in which all three bb's are visible. This point was used for laser localization.

As commonly done at MDACC, nine beams were used in our IMRT planning. The nine coplanar beams were placed at gantry angles of 200°, 240°, 280°, 320°, 0°, 40°, 80°, 120°, and 160°. In some cases, the beam angle was change from 160° to 165° to increase the ability to avoid the OAR. The MLC for each beam was initially set to expose both PTVs with an additional margin of 5 mm. All beams used 6 MV photons with couch and collimator angles of 0°.

2.2.4 Dose Prescription

The dose prescription used in this study is based on the dosimetric requirements set by the RPC for credentialing irradiations of the phantom. At least 95% of the primary PTV is to receive 6.6 Gy, and less than 1% can receive less than 93% of 6.6 Gy. At least 95% of

the secondary PTV is to receive 5.4 Gy, and less than 1% can receive less than 93% of 5.4 Gy. The OAR may receive at maximum 4.5 Gy and the normal tissue may receive at maximum 110% of the full prescription dose of 6.6 Gy. These criteria are summarized in Table 2.2. The prescription was set to deliver 660 cGy to 96% of the ROI mean dose to the primary PTV for all plans. The dose grid was set to include the entirety of the phantom and used a 0.4 cm^3 resolution unless otherwise noted.

Structure	Dosimetric Criteria
Primary PTV	$D_{95\%} \geq 6.60$ Gy
	$D_{99\%} \geq 6.14$ Gy
Secondary PTV	$D_{95\%} \geq 5.40$ Gy
	$D_{99\%} \geq 5.03$ Gy
OAR	Maximum dose < 4.50 Gy
Normal Tissue	Maximum dose ≤ 7.26 Gy

Table 2.2 RPC IMRT Head and Neck phantom dose prescription and constraints

2.2.5 Objectives/Inverse Planning

Inverse planning was performed using Direct Machine Parameter Optimization (DMPO). Iterations of the optimization used the Adaptive Convolve dose calculation algorithm and the final dose was computed with the CC Convolution algorithm. The IMRT parameters (number of iterations, convolution dose iteration, minimum MU, maximum number of segments, stopping tolerance, minimum segment size) and the planning objectives were manipulated to create plans of the desired complexity. The objectives, their weights, and IMRT parameters for each of the eight plans used in this study can be found in Appendix A Treatment Planning Dose Objectives and IMRT Parameters

2.2.6 Mismatched Beam Dosimetry Dose Calculation

To investigate the effects of improper beam modeling on dosimetric accuracy, a calculation of the baseline plan dose was performed using an incorrect beam model. This was done using a script that copies the beams and respective control points from one plan to another using a different designated beam model. At MDACC, different beam models are utilized for the Varian 2100 series machines and the Varian 600 series machines to account for variations in the machine designs. The main mechanical differences in these machines exist at the wave guide. Since the Varian 600 series machines output only 6 MV photon beams, the waveguide can be shorter than that of the Varian 2100 series machines. The 600

series waveguide is therefore vertical and no bending magnet is used. This results in a different electron beam focus on the target than a machine using a bending magnet. The Varian 2100 CD machine that the 2100 series model is based off will be referred to in this study as the "baseline machine." The 600 series beam model was used to calculate the dose of the baseline plan to compare against the delivery on a 2100 series machine to demonstrate a case of forced mismatched beams.

2.3 Treatment Plan Evaluation

2.3.1 Complexity

2.3.1.1 Modulation Complexity Score

In addition to number of MU and number of segments, we used the modulation complexity score (MCS) as a measure of plan complexity in this study [2]. The modulation complexity score (MCS) uses two parameters, the leaf sequence variability (LSV) and aperture area variability (AAV), to take into account leaf position variability, degree of field shape irregularity, segment weight, and area. The LSV considers the difference in position of adjacent MLC leaves for each segment and is calculated as shown in Equation 2.1. The AAV considers the area of each segment as defined by the MLC compared to the maximum aperture of that segment and is calculated as shown in Equation 2.2. Finally, these two terms are combined for each beam as the sum of their MU-weight product, as in Equation 2.3. The MCS of an entire plan is equal to the MU-weighted sum of the MCS for each beam in the plan, shown in Equation 2.4. An MCS of 1.0 has "zero" complexity and is defined by an open rectangular field. More highly complex plans have a lower MCS [2]. A Pinnacle script written by Tom Purdie was used to compute the MCS for each of the treatment plans.

$$LSV_{segment} = \left[\frac{\sum_{n=1}^{N}(pos_{max} - (pos_n - pos_{n+1}))}{N \times pos_{max}}\right]_{left\ bank}$$

$$\times \left[\frac{\sum_{n=1}^{N}(pos_{max} - (pos_n - pos_{n+1}))}{N \times pos_{max}}\right]_{right\ bank}$$

Equation 2.1

$$AAV_{segement} = \frac{\sum_{a=1}^{A} <pos_a>_{left\ bank} - <pos_a>_{right\ bank}}{\sum_{a=1}^{A} <max(pos_a)>_{left\ bank\ \in beam} - <max(pos_a)>_{right\ bank \in beam}}$$

<div align="center">Equation 2.2</div>

$$MCS_{beam} = \sum_{i=1}^{I} AAV_{segment\ i} \times LSV_{segment\ i} \times \frac{MU_{segment\ i}}{MU_{beam}}$$

<div align="center">Equation 2.3</div>

$$MCS_{plan} = \sum_{j=1}^{J} MCS_{beam\ j} \times \frac{MU_{beam\ j}}{MU_{plan}}$$

<div align="center">Equation 2.4</div>

2.3.1.2   Segment Size

Additional effort was made to evaluate the open area per segment, the segment size, for each plan. This information is not provided in Pinnacle v.8m but is in Pinnacle v.9. Treatment plans were copied and opened with Pinnacle v.9 to use this feature. Doses were not recalculated in the copied plans, but segment weights were provided and multiplied by the beam MU calculated in Pinnacle v.8m to find the MU per segment. The minimum, maximum, and average MU per segment size and per segment were evaluated along with the minimum segment size for each beam.

2.3.2   Plan quality

To ensure all plans met prescription and were comparable, we evaluated each plan's ability to achieve the dose objectives set by the RPC. To do this, the percent of the PTVs receiving 100% and 93% of the prescription dose, the maximum dose to the OAR, and the maximum dose to the normal tissue were assessed.

2.4 Dosimetric Accuracy Evaluation

To determine if dosimetric accuracy is affected by treatment plan complexity, each of the eight treatment plans was delivered to the RPC's H&N phantom three times on the baseline machine and the dose distribution measured by TLD and radiochromic film. Additionally, the baseline plan was delivered to the phantom on another Varian 2100 CD, a Varian 21EX, and a Varian Trilogy three times each and the dose distribution measured by TLD and radiochromic film to assess the possible effects of beam model matching.

2.4.1   Phantom Irradiation

We delivered the baseline plan on the baseline machine, a Varian Clinac 2100 CD linac at MD Anderson Cancer Center in Houston, TX. This machine was equipped with the Varian Millennium 120 MLC. This multi-leaf collimator has 120 total leaves, sixty leaves on each bank. The forty central leaves are 5 mm wide at isocenter and the ten peripheral leaves on each side are 10 mm wide at isocenter. Following the AAPM TG-51 protocol, this linac was calibrated to 1.000 cGy/MU in muscle at d_{max} under reference conditions of 100 cm SSD and 10 cm X 10 cm field size.

The phantom was positioned at the head of the treatment couch, above the mesh top to avoid possible effects of the mesh on the film. It was positioned supine and "head first" as it was for the simulation as shown in Figure 2.3. The lasers were aligned to the simulation isocenter using the bb's and intersecting marks. The alignment of the lasers with the cross hairs of the gantry was checked several times throughout these measurements. This was done by setting the phantom up according to the lasers and checking that the position was correct with the cross hairs also.

Figure 2.3 RPC IMRT Head and Neck phantom set up for irradiation on linac table

We delivered each treatment using the record and verify system, Mosaiq (IMPAC Medical Systems, Inc., Sunnyvale, CA), with the linac in clinical mode. Each treatment was delivered three separate times, loading new TLD and film prior to each irradiation. Since the

exchange of dosimeters requires removing the phantom insert, the phantom was completely repositioned and proper set up confirmed for each individual irradiation.

The baseline plan was also delivered following the same process on three additional machines which employ the same beam model in our TPS. Another Varian 2100CD linac, a Varian 21EX linac, and a Varian Trilogy linac each with Millennium 120 MLC and calibrated in the same manner as the baseline machine were used. These linacs employ the same basic physics machinery and ideally should be the same. The Varian 2100CD linac became commercially available about 2002. The Varian 21EX machine was the next in the series and includes an EPID. Finally, the Trilogy was released and in addition to on-board imaging accessories contains a mini filter to allow for higher dose rates at small field sizes, an addition that did not affect this study. On the Trilogy machine, the treatment table is slightly different in that it is designed for imaging. All other machines had a mesh top in place. For the Trilogy couch, the phantom was placed on the imaging top (as opposed to at the head of the couch above the mesh top) and the rails were moved for beams which intersected them at angles of 160° (or 165°) and 240°. These machines were all matched to the baseline machine upon acceptance and are maintained at 2% absolute agreement of percent depth dose and machine output by following AAPM TG-51 annual quality assurance [18]. Monthly machine output checks around the time of the irradiations performed for this study matched each machine with the baseline machine with 1% deviation or less.

2.4.2 Dosimeters

This study utilized TLD and radiochromic film for radiation measurements as routinely performed by the RPC for auditing and credentialing. Each of these radiation dosimeters measures the radiation dose passively, making them optimal for remote measurements such as the RPC's mailable phantom audit program. The absolute point doses and planar relative dose distributions delivered in this study were measured by the TLD and radiochromic film, respectively.

2.4.2.1   Thermoluminescent Dosimetry

Thermoluminescent (TL) dosimetry is based upon the phenomena of certain inorganic crystals absorbing radiation energy and emitting it as light when heated. These crystals, TL phosphors, have high concentrations of imperfections known as trapping

centers. Electron-hole pairs can be created in the crystal by incident radiation, followed by the migration of these electrons and holes to various traps located off the conduction and valence bands, respectively. When the crystal is heated, the electrons and holes are excited out of the traps and can recombine, resulting in the release of a light photon. TL phosphors are integrating dosimeters, meaning continuous exposure of the crystal to radiation will lead to a progressive accumulation of trapped electrons and holes. Therefore, the number of electron-hole pairs formed by the incident radiation is reflected by the number of trapped electrons and holes and the intensity of light created by their recombination can be measured. This, in turn, can be related to the radiation dose received by the TL material.

The RPC uses a TL material known as TLD100. TLD100 is a lithium fluoride crystal powder doped with magnesium and titanium to serve as the primary trapping centers and luminescent recombination centers, respectively. The TL powder is housed in a plastic capsule measuring 15 mm long and 4 mm in diameter. These capsules contain two packets of approximately 20 mg of the radiation-sensitive powder each, providing two absolute dose measurements.

To determine the radiation dose received by a TLD capsule, each packet of powder is weighed, heated, and the amount of light released is measured with a photomultiplier tube (PMT). The measured amount of light is then converted to absorbed dose to muscle, D, using a number of correction factors as in Equation 2.5.

$$D = T \times S \times K_E \times K_L \times K_F$$

Equation 2.5

In the above equation, T is the average TL response reading per mass of powder, as determined by the PMT and scale. The system sensitivity, S, is the absorbed dose per system response, which is determined by measuring the system's response for a set of TLD (the "standards") irradiated to a known dose with ^{60}Co under standard conditions. K_E is a factor to take into account the varying response of TLD to different radiation energies. K_L accounts for the response of TLD to radiation, which is approximately linear up to 4 Gy (for TLD100), past which it is supralinear [19]. Finally, K_F is a function of time and takes into account TL response signal fading that occurs over time due to electrons and holes being excited and recombining at room temperature. Some traps are shallow (do not differ much in

23

energy level from the conduction or valence band) and are unstable and therefore electrons and holes in them are more likely to escape without thermal excitation. Fading decreases exponentially with time, becoming mostly constant after ten days [20]. The RPC waits a minimum of ten days to read TLD in order to reduce unstable fading and the effects of uncertainty in the exact time since irradiation.

The corrections mentioned for energy response, fading, and linearity are found by the RPC for each batch of TLD they use. This study used TLD from one single batch and the corresponding corrections determined by the RPC were used. A control set and a standard set of TLD were irradiated to a known dose the same week as a phantom irradiation and read out at the same time as the phantom TLD to determine the system's response. All TLD used in this study were read out at least 10 days post-irradiation. This TLD system has a precision of 3% and agrees with ion chamber measurements within ±4% at a 90% confidence level [20].

2.4.2.2   *Radiochromic Film Dosimetry*

Radiochromic film is comprised of a material that changes color upon exposure to radiation without any chemical, optical, or heat processing. The resultant image which is a pattern of optical densities (OD), or reduced transmission of light, can be measured to obtain a planar dose distribution. Radiochromic film has high spatial resolution (<0.1 mm), relatively low spectral sensitivity, and is insensitive to light [21]. It also is approximately tissue equivalent and has no significant angular dependence, making it ideal to make dosimetric measurements [22].

In this study, we used GafChromic® EBT2 (International Specialty Products, Wayne, NJ) film which is specifically intended for use in external beam radiotherapy applications. EBT2 film is made of an active microcrystalline monomeric dispersion coated on a flexible polyester film base. EBT2 film turns blue upon irradiation which occurs as a result of partial polymerization of the active component of the film [21]. In this irradiated state, the film has a primary absorption peak at about 636 nm and a secondary absorption peak at 565 nm. The active layer of this film contains a yellow dye which decreases it's sensitivity to light by about ten times and provides a reference background. This dye causes the irradiated portion of the film to appear dark green.

EBT2 film is designed to be used to measure doses from 1 cGy to 40 Gy. Within the range of therapeutic and scattered radiation energies EBT2 has a low energy dependence, with less than 10% response difference for 100 keV and 6 MV photons, as reported by the manufacturer. A recent study by Arjomandy *et al* showed that the energy dependence is even weaker, varying about 4.5% for photon energies from 75 kVp to 18 MeV [23]. The spatial resolution of EBT2 film is reported by the manufacturer to be at least 100 μm. The effective atomic number is reported to be 6.84 compared to the effective atomic number of water of 7.3.

For each of the phantom irradiations in this study, three pieces of film were cut from a pattern. An axial film was cut to fit between the two halves of the insert. Two sagittal films were cut to fit within the superior and inferior halves of the insert, with a section cut out for the OAR TLD. All films came from the same batch and were marked to maintain orientation and irradiation number.

The recommendations of AAPM Radiation Therapy Committee Task Group 55 were followed in regards to handling and measuring the film [21]. All film was kept in closed, dark envelopes to reduce the exposure to light. The film was kept at room temperature with low humidity and blank film was kept with the measurement pieces to record background radiation. All film was read at least two days post-irradiation.

To evaluate the resultant distribution of optical densities of the EBT2 film, we used a transmission densitometer, the CCD100 Microdensitometer (Photoelectron Corporation, Lexington, MA). In this system, a light-emitting diode (LED) light box, emitting light with a wavelength centered at 665 nm to approximately match the primary absorption of the film, was used to shine through a piece of film. The light transmitting through was recorded by a charge-coupled device (CCD) camera directly above. The CCD camera was set at a height appropriate to focus on the 150 mm by 150 mm we desired to measure and the focus checked by acquiring an image of a ruler. The region of the light box not contained in the central measurement area was covered with a black mask. The CCD camera had a resolution of 512 by 512 pixels, which produces a pixel size of approximately 0.3 mm for this set up. This system was contained in a light-tight cabinet to prevent external light contamination.

A piece of blank film was imaged and stored as a "flat field" to be subtracted from the following images to account for variations in the scanner. Next, a 10 mm by 10 mm grid was imaged to set the spatial calibration. Once the scanner was calibrated, the experimental films were measured. A consistent orientation was maintained for all film measurements. Axial films were imaged alone and sagittal films from the same irradiation were imaged together as they were in the phantom, with a small gap in between. All measurements were saved as .FIT files for further analysis.

To find the relationship between OD and dose for our batch of film, we performed a film calibration. We irradiated film to several different doses with 6 MV photons as in the IMRT plans, and evaluated the resultant ODs to generate a dose response curve. Nine 3 cm by 3 cm squares were cut from the same piece of film and marked for unique identification and orientation. On the baseline machine treatment table, these pieces of film were arranged in a square on the center of 9 cm stack of solid water for adequate backscatter and covered by 5 cm of solid water. The top of the solid water stack was set to 100 cm SSD and a 35 cm by 35 cm field was centered on the stack using the field light. We then irradiated the stack with all pieces of film present, removed one piece, and delivered additional MU to the remaining film. Another piece of film was removed and the process continued until a different number of MU was delivered to each piece of film. The alignment of all pieces was maintained during this process. To determine the total dose delivered to each piece of film, the number of MU was multiplied by the appropriate machine output factor. The machine output factor was calculated using Equation 2.6, where S_c is the collimator scatter factor, S_p is the phantom scatter factor, and PDD is the percent depth dose at 5 cm depth in water. The output factor for this machine and field size was 0.9632. The films were irradiated to a range of 48 cGy to 1300 cGy, which covers the range of doses expected in the phantom irradiations. These values are reported in

.

$$Output\ factor = S_c \times S_p \times PDD$$

Equation 2.6

Square #	Total MU	Dose (cGy)
1	50	48.16
2	150	144.48
3	250	240.80
4	350	337.13
5	550	529.77
6	750	722.41

7	950	915.05
8	1150	1107.70
9	1350	1300.34

Table 2.3 EBT2 film irradiation for dose calibration

These calibration films were imaged using the technique described above and the average OD of three readings for the center of each square was recorded. These net ODs were plotted against the calculated dose delivered and fit with a third-order polynomial, as shown in Figure 2.4. The resulting equation was used to convert the experimental film OD, x, to dose, D as in Equation 2.7 and had R^2 of 0.9984.
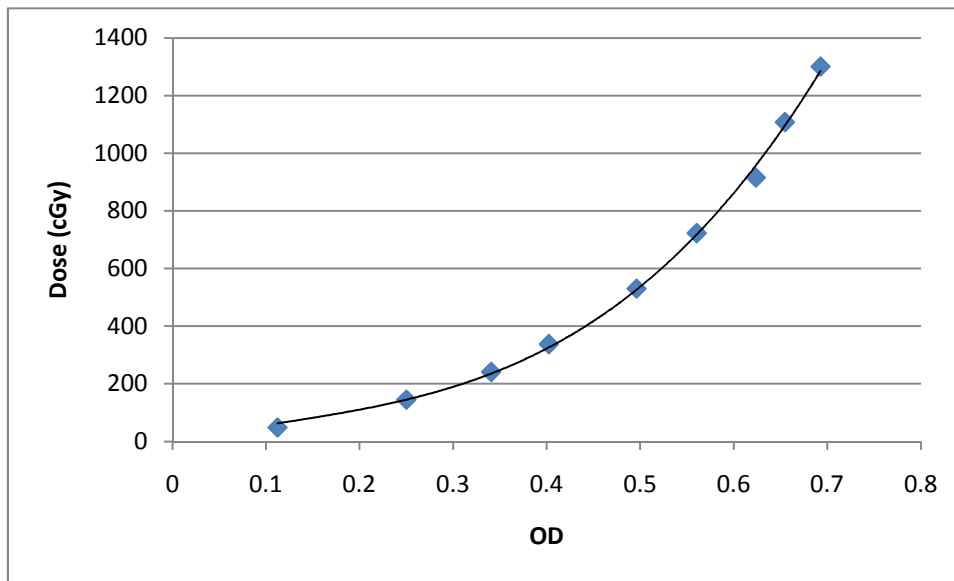
Figure 2.4 Dose response curve for EBT2 film used in this study

$$D = 4707.8x^3 - 1556.3x^2 + 675.08x$$

Equation 2.7

2.4.3   Absolute Point Dose Analysis

In order to assess the quality of a treatment planning system, the planned dose distribution should be compared to a physical measurement of the dose distribution. Different techniques are used to quantitatively evaluate the agreement between planned and

delivered doses in low and high dose gradient regions. In low gradient regions, the absolute doses are directly compared and held to a percentage standard.

To evaluate the absolute dose to a specific point in the phantom, the dose to eight TLDs in the phantom insert was measured for each irradiation as described in Section 2.4.2.1. Doses measured by the TLD were then compared to the mean dose to the corresponding TLD ROI calculated by the TPS. The percentage difference between the measured dose and the predicted dose for each TLD was calculated. This percentage must be ±7% for both the primary PTV and secondary PTV point doses in order to comply with the RPC standards. The RPC does not include the TLD in the OAR in this analysis because they are generally within or near a steep dose gradient and small positional errors can result in large dosimetric errors.

2.4.4 Film, Plan, and Phantom Registration

In order to compare the measured dose distributions with those calculated in the TPS, we had to register the irradiated films and the treatment planning data to a single coordinate system. This was done using a program built using the MATLAB® language (The MathWorks, Inc., Natick, MA) known as the Computational Environment for Radiotherapy Research (CERR) (J.O. Deasy and Washington University, St. Louis, MO) which can be used to view and analyze treatment plans in a standard format. All treatment plans, including the CT image set, were exported in DICOM-RT format from Pinnacle and imported into CERR. Then, by identifying a set of known points on the CT images, we were able to register each of the treatment plans to the phantom coordinate system. To allow for a comparison of the planar dose distributions, the film was registered to these same coordinates using another program written in MATLAB, RPCFILM. With the RPCFILM program, the .FIT files containing the OD images of the film were opened and registered to the phantom coordinate system using the pin pricks. The location of each pin prick was identified and matched to its corresponding point within the phantom. Our dose response curve generated in Section 2.4.2.2 was then used to convert the OD distributions of the films to dose distributions.

To allow for a comparison of the absolute doses, the film doses were normalized to the matching primary PTV TLD doses. On the axial films, the percent difference between

the average doses of the superior and inferior TLD in the primary PTV to the film-measured doses at those two points were determined. On the sagittal films, the percent difference between the dose measured with TLD to that measured by film was determined at all four of the TLD locations within the primary PTV.

2.4.5 Planar Dose Analysis

Using the above described registration process and the RPCFILM program, we compared the dose distributions recorded by the film to those of the treatment plan. Dose profiles were taken through the center of the primary PTV in each orthogonal direction. On the axial films, a lateral dose profile was taken through the center of the primary and secondary PTV and an anteroposterior dose profile was taken through the center of the primary PTV. On the sagittal films, a dose profile was recorded in the superior-inferior direction through the center of the primary PTV. The dose profiles were generated by a 0.3 mm resolution sampling of the film and each profile was visually inspected for shifts in the dose distributions. We used a moving average at 3 mm intervals to smooth the dose profiles.

In high gradient regions, small spatial errors can lead to large dose differences in planned and delivered treatments and thus a distance-to-agreement (DTA) criteria is used. The DTA is a measurement of the distance between a measured dose point and the closest matching dose point in the planned dose distribution.

To evaluate the ability of the system to plan and deliver the steep dose gradient required between the primary PTV and the OAR, the distance to agreement (DTA) was evaluated. The dose profile between the primary PTV and OAR in the anteroposterior direction on the axial films was used for this analysis. A linear regression of the penumbra was performed on the film data and corresponding treatment plan data with the boundaries at the approximate max and min points of the dose gradient between the two. These points were considered to be at the relatively flat regions of dose, evaluated individually for each film. From both the film and treatment plan profiles, 75%, 50%, and 25% dose values were determined and the differences in position at each point recorded. The average of all these values was taken to be the DTA for that film.

2.4.6 Gamma Analysis

RPCFILM was also used to compare the measured planar dose distributions to the corresponding treatment plans in RPCFILM with a gamma analysis, a quantitative technique described by Low *et al*. A gamma analysis quantifies both the absolute dose difference and DTA criterion into a single metric for evaluating dose distribution agreement, with the measured dose as reference and the calculated dose assessed for comparison. Using the gamma analysis, these two criteria are assessed and agreement of the measured and calculated dose distributions is quantified by the γ-index.

To perform a gamma analysis, one first defines the criteria to hold the dose distribution agreement to. ΔD_M is the dose difference criteria and Δd_M is the DTA criteria, for example we used $\Delta D_M/\Delta d_M$ of 7%/4mm. These two acceptance criterion are used to form an ellipsoid surface when combined in a space of major axis DTA, $r(r_m,r)$, and dose difference, $\Delta(r_m, r)$ which is defined by Equation 2.8 below:

$$\sqrt{\frac{r^2(r_m,r)}{\Delta d_M^2} + \frac{\delta^2(r_m,r)}{\Delta D_M^2}} = 1$$

Equation 2.8

Where $r(r_m,r) = |r - r_m|$, $\delta(r_m,r) = D(r) - D_m(r_m)$, m denotes measurement and D(r) is the dose at point r.

Assessment of the calculated dose distribution can then be performed and evaluation of its ability to meet acceptance criteria by finding the minimum value of $\Delta(r_m, r_c)$ as defined below:

$$\gamma(r_m) = \min\{\Gamma(r_m,r_c)\}\,\forall\{r_c\}$$

Equation 2.9

With

$$\Gamma(r_m,r_c) = \sqrt{\frac{r^2(r_m,r_c)}{\Delta d_M^2} + \frac{\delta^2(r_m,r_c)}{\Delta D_M^2}}$$

Equation 2.10

Where c denotes calculated.

If $\gamma(r_m)$, the γ-index, is less than or equal to one, that measured point is within the ellipsoid of acceptance and passes the criteria as acceptably agreeing with the calculated dose. The γ-index is then generally found at all points in the measured distribution and a percentage of points passing can be used to assess the overall agreement between calculated and measured dose.

The program RPCFILM has a masking tool which allows the user to define regions of the film not to include in the gamma analysis. This is particularly useful for the H&N IMRT phantom sagittal films where the OAR TLD section is cut out. It is also useful at some film edges where the film was affected by the cutting action and the dose it reflects may be corrupted.

The RPC is not currently using a gamma analysis to credential institutions with the H&N IMRT phantom, but has been collecting data using a criterion of 7%/4mm on a region of the axial film as shown below in Figure 2.5. Therefore, we performed a 7%/4mm gamma analysis on the same region of all our films to compare to the percent of pixels passing the RPC's evaluation.
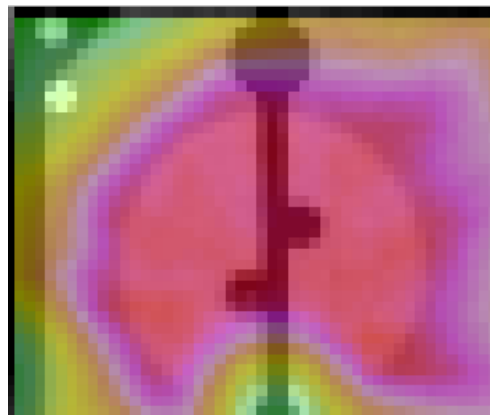

Figure 2.5 Primary PTV region on axial films used for gamma analysis to compare with gamma analysis done at the RPC

In addition, we performed a gamma analysis on a more complete region of the axial films as shown in Figure 2.6 and a region of the sagittal films as shown in Figure 2.7 with criteria of 7%/4mm and 5%/3mm for each. The masking tool was used to cover all pin pricks, cuts, and uneven edges, defined individually for each film.
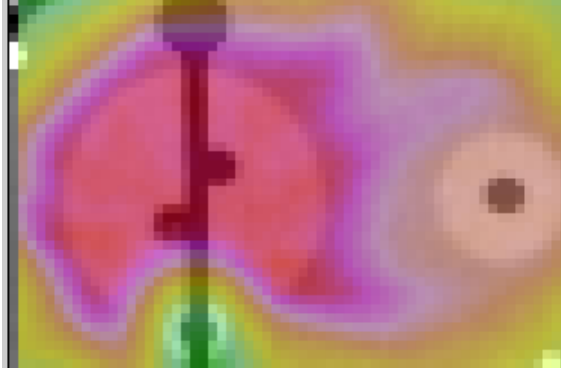
Figure 2.6 Complete axial film area used for gamma analysis in this study
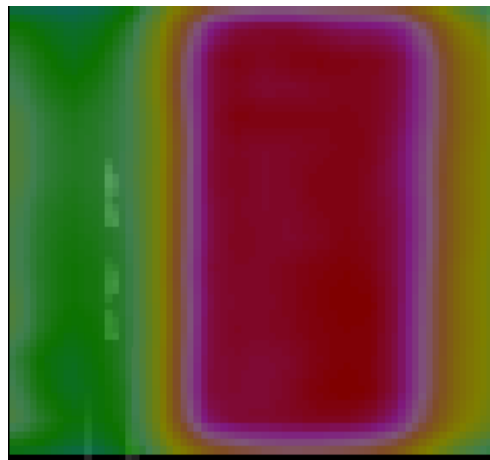
Figure 2.7 Complete sagittal film area used for gamma analysis in this study

Chapter 3   Results

3.1 Treatment Plans

3.1.1   Treatment Planning Goals

To establish a baseline treatment plan, 130 previous irradiations of the RPC's IMRT H&N phantom performed with the Pinnacle TPS and Varian linear accelerators (linacs) were evaluated. Table 3.1 shows the resultant median, standard deviation, maximum, and minimum for each the number of beams, number of MU, and number of segments.

	Number of beams	Total MU	Total number of segments
Median	9	1863	87
Standard Deviation	1.3	417	76
Minimum	5	557	29
Maximum	13	2961	581

Table 3.1 Summary of characteristics of comparable irradiations of the RPC IMRT Head and Neck phantom

Of the plans included in Table 1, 108 of these plans had passed the RPC audit and 22 had failed. Figure 3.1 and Figure 3.2 show the distribution as a histogram of each plan's total MU and number of segments, respectively, and whether it passed or failed the RPC audit. Note that there is not a clear distinction between passing and failing treatment plans for either of these measures of complexity.
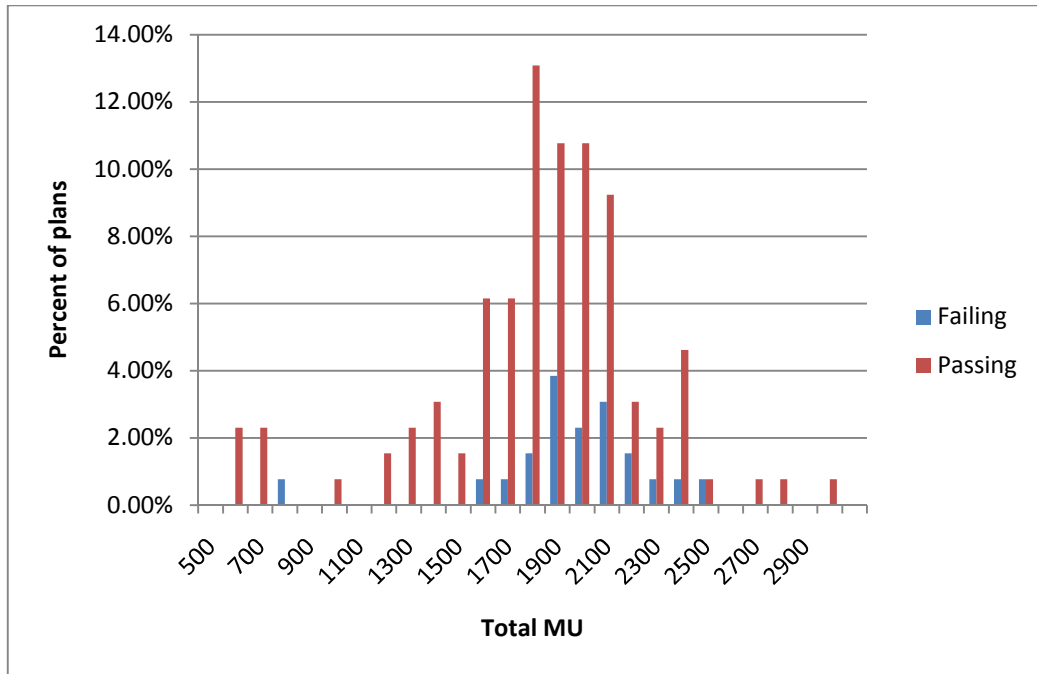
Figure 3.1 Distribution of total MU in plans passing and failing an RPC audit with the IMRT Head and Neck phantom
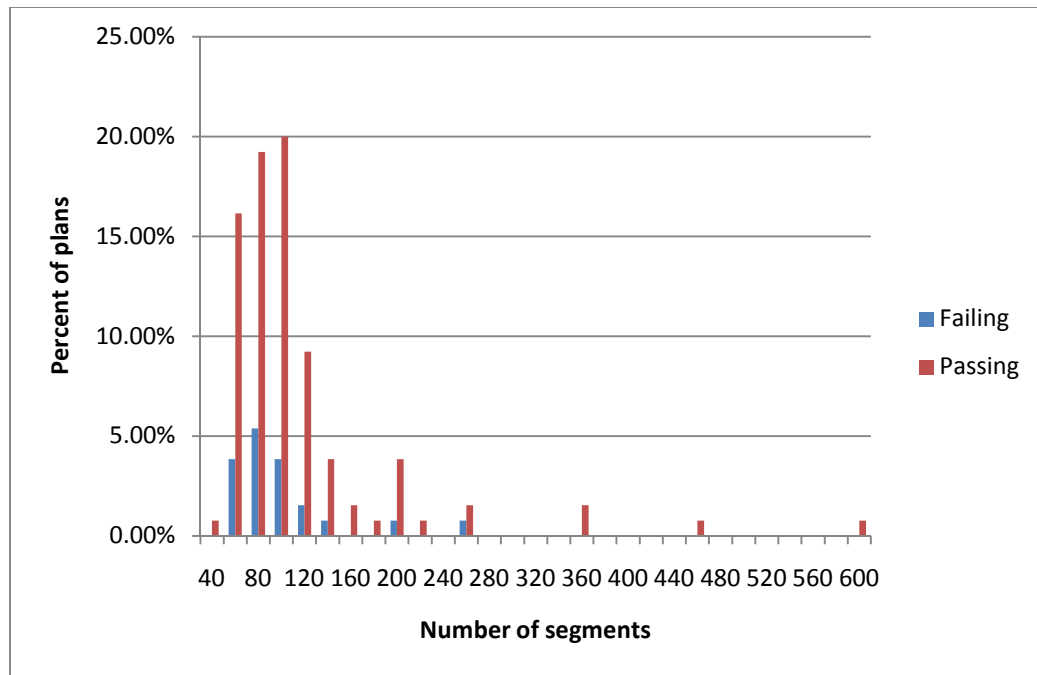

Figure 3.2 Distribution of total number of segments in plans passing and failing an RPC audit with the IMRT Head and Neck phantom

3.1.2 Treatment Plans

The analysis performed above in Section 3.1.1 provided treatment planning goals for a baseline plan as well as goals for the most simple and complex plans as defined by the number of MU and number of segments. The median number of beams, nine, matched with the commonly used number at our institution and was used for all treatment plans.

After establishing a baseline plan and re-optimizing extensively to both decrease and increase treatment plan complexity, a total of fifty IMRT treatment plans for the RPC's H&N phantom meeting prescription and OAR constraints were created. From these, eight treatment plans were chosen based on the distribution of the modulation complexity score (MCS), which for our plans range from 0.181 (most complex) to 0.609 (least complex). The number of MU, number of segments, and MCS for each of the plans used in this study are shown in Table 3.2. Also included are the average number of MU per segment and the minimum segment area allowed by the TPS for each plan. The blue row highlights the baseline plan, chosen to represent the median RPC plan from the previous analysis. The plan numbering convention used in Table 3.2 will be used for the remainder of this report. Plans 6 and 7 used a grid size of 0.3 mm^3 and the remaining plans used a grid size of 0.4 mm^3.

Plan	MCS	MU	# segments	MU/segment	Min Segment Area (cm^2)
1	0.609	1460	54	27	6
2	0.574	1585	134	12	0.5
3	0.532	1712	53	32	6
4	0.469	1932	88	22	4
5	0.392	2058	225	9	0.5
6	0.338	2488	89	28	0.1
7	0.269	2527	225	11	0.25
8	0.181	3469	216	16	0.1

Table 3.2 Summary of measures of complexity of treatment plans used in this study, blue highlight indicates baseline plan

Segment size and MU per segment were evaluated to further understand the complexity of each treatment plan. The minimum segment size actually used in the treatment plan, the minimum, maximum and average number of MU per cm^2 of all segments in each plan, and the minimum and maximum MU per segment are reported in Table 3.3.

Notice that the minimum and maximum MU per cm^2 tend to become more extreme with the more complex plans, that is not always the case. Most importantly, notice that there are segments in the more complex plans that plan fractional MU for some segments, some with only 0.1 MU/segment. Some linacs would not be allowed to deliver fractional MU and the accuracy of fractional MU delivery on those that do allow it is questionable since it is not generally calibrated or evaluated.

Plan	MCS	MU	# segments	min segment size (cm^2)	min MU/cm^2	max MU/cm^2	avg MU/cm^2	min MU/seg	max MU/seg
1	0.609	1460	54	6	0.36	6.01	1.78	16.0	55.2
2	0.574	1585	134	0.51	0.02	24.36	1.35	1.0	83.3
3	0.532	1641	54	6.02	0.15	14.76	2.27	5.0	89.1
4	0.469	1851	88	4	0.02	18.01	2.19	1.0	72.0
5	0.392	2058	225	1.28	0.01	20.98	1.58	0.5	55.2
6	0.338	2410	89	0.25	0.13	334.60	9.46	0.1	87.0
7	0.269	2417	225	0.96	0.00	106.60	2.33	0.1	107.7
8	0.181	3466	216	0.29	0.00	54.42	3.64	0.1	72.0

Table 3.3 Summary of segment size and MU/segment of treatment plans used in this study, blue highlight indicates baseline plan

The relationship between the three measures of complexity used in this study, total MU, number of segments, and MCS for the eight treatment plans chosen are illustrated in Figure 3.3-Figure 3.5. It can be seen that while the total MU and MCS trend together with an R^2 value of 0.93, the number of segments does not directly relate to either the total MU or the MCS.
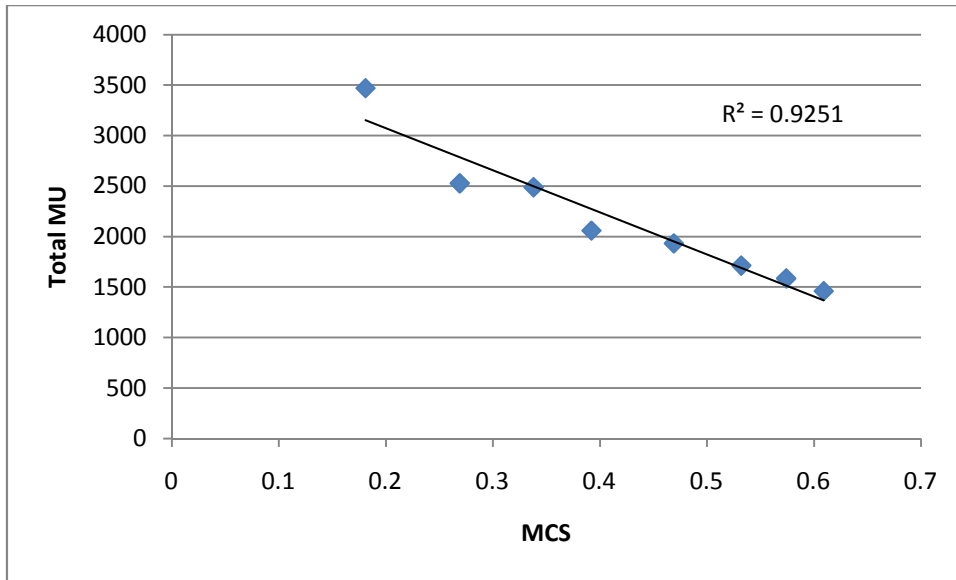
Figure 3.3 Relationship between total MU and MCS for the eight plans used in this study with linear trendline
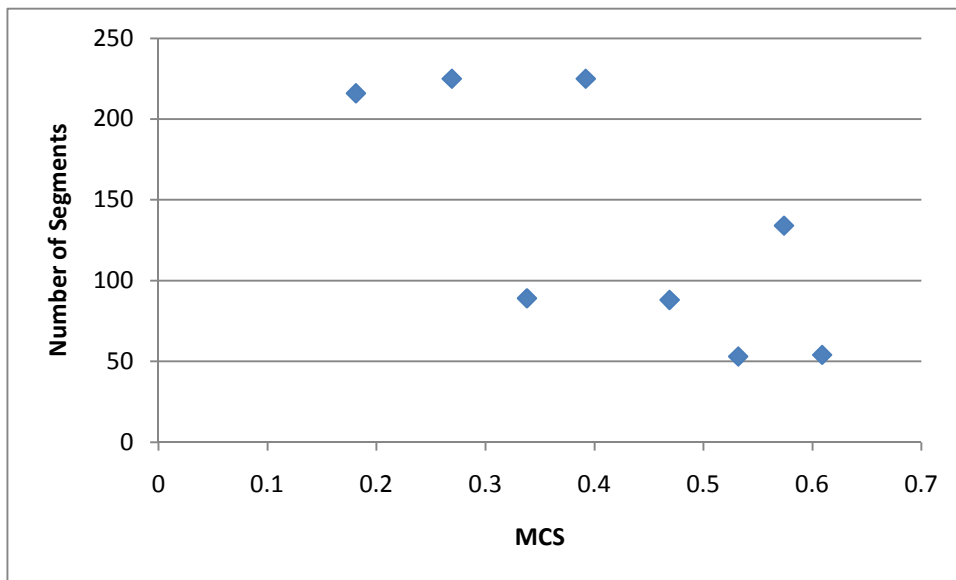
Figure 3.4 Relationship between number of segments and MCS for the eight plans used in this study
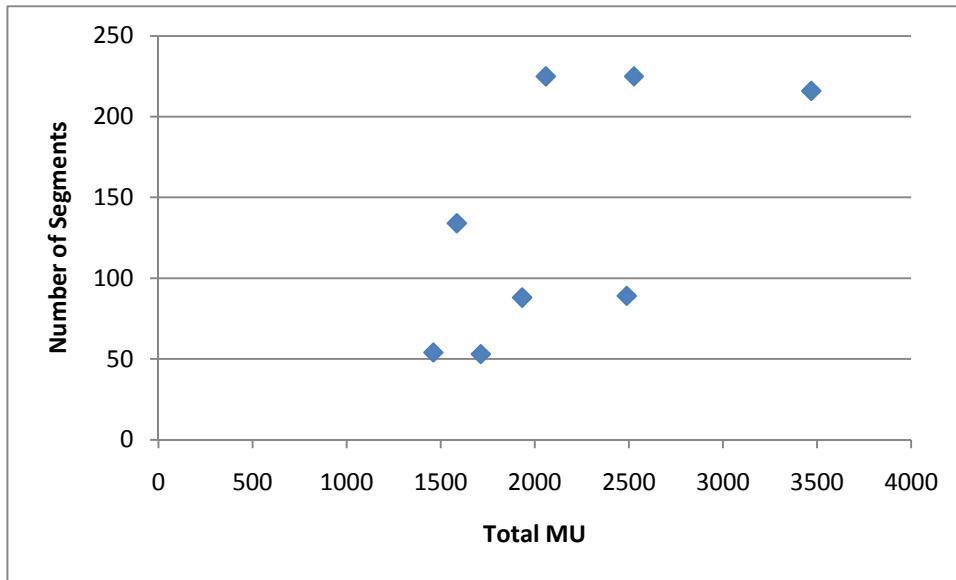
Figure 3.5 Relationship between number of segments and total MU for the eight plans used in this study

3.2 Treatment Plan Quality Comparison

To ensure all plans used in this study were comparable, we evaluated the quality of each plan through three means. We first looked at the ability to meet the RPC prescription and constraints, which were presented in Table 2.2. The results of this evaluation are presented below in Table 3.4.

Plan Number	Primary PTV V_{660}	Primary PTV Max Dose (cGy)	Secondary PTV V_{540}	OAR Max Dose (cGy)	NT Max Dose (cGy)	NT Max Dose %of Rx
1	96.0%	719.2	99.9%	450	679.7	103.0%
2	95.0%	738.2	100.0%	444.8	692.1	104.9%
3	97.4%	712.0	100.0%	422.7	704.3	106.7%
4	97.7%	712.4	100.0%	410	690	104.6%
5	98.4%	718.8	100.0%	409	644	97.6%
6	98.9%	748.0	99.9%	389.1	690.8	104.7%
7	96.3%	746.1	98.0%	402.7	674.6	102.2%
8	98.6%	742.5	98.0%	425.9	778	117.9%

Table 3.4 The values of each dosimetric objectives for the eight plans used in this study, including prescriptions and constraints.

The second column of Table 3.4 shows the percent of the primary PTV volume receiving the prescribed dose of 660 cGy (as required for irradiating the RPC H&N

38

phantom), known as V_{660}. For each of the plans, the dose distribution was normalized to 96% of the prescription dose to the primary PTV. The percent of the primary PTV volume receiving the prescribed 660 cGy is not always 96% because the dose distribution does not always perfectly match the volume of the primary PTV. All plans exceed the required 95% primary PTV coverage. In addition, the next column contains the maximum dose in cGy received by the primary PTV. These values are between 710 cGy and 750 cGy, generally increasing with treatment plan complexity. The fourth column of Table 3.4 shows the percent of the secondary PTV volume receiving the prescribed dose of 540 cGy, known as V_{540}. All plans cover greater than 97% of the secondary PTV with this dose, therefore meeting and exceeding the requirement of 95% secondary PTV coverage. The fifth column of Table 3.4 shows the maximum dose for each plan in cGy received by the OAR, which should not exceed 450 cGy according to the RPC constraints. All plans met this requirement. The sixth and seventh columns of Table 3.4 show the maximum dose in cGy received by the normal tissue (NT) as defined in Section 17 and the percentage that dose is of the prescribed 660 cGy, respectively. The RPC constraint states that the normal tissue should not receive greater than 110% of the prescribed dose. All plans met this requirement with the exception of plan number 8, which exceeds by almost 8% or about 53 cGy. Note that plan number 8 is the most complex of the plans. This was deemed acceptable since the study is not evaluating the effects of complexity on plan quality and the plan meets all other constraints. Overall, note that increased complexity does not necessarily increase the quality for this sample of IMRT treatment plans.

3.3 Dosimetric Accuracy Evaluation

3.3.1 Absolute Point Dose Analysis

Each of the eight plans was delivered on the RPC IMRT H&N phantom using the baseline linac three times to evaluate the possible effects of treatment plan complexity on dosimetric accuracy. In addition, the baseline plan was run on three additional machines three times each and re-calculated using a different beam model and compared to the baseline measurement in order to evaluate the possible effects of beam matching on

dosimetric accuracy. This H&N phantom holds eight TLD, numbered as shown in Figure 2.2.

The point dose measured with each TLD for all irradiations are reported in Appendix B Absolute Point Dose Measurements. The absolute point dose analysis is summarized in Table 3.5 and Table 3.6. The percent difference between the average measured dose and the calculated dose to each of the six TLD in the PTVs of the phantom for all irradiations as well as the standard deviation of the three TLD measurements for each point is provided. A positive percent difference indicates a greater calculated dose than measured for that specific TLD. Note that all TLD measurements meet the RPC standard of 7% agreement. Recall that TLD in the OAR (TLD #7 and #8) are not included in this analysis because of their position with respect to steep dose gradients. Differences between the delivered and planned doses tend to be positive more often than negative, indicating a higher dose delivered than planned, but this effect does not reveal a consistent trend. Plan 5 has all negative differences and Plan 6 and 7 have all positive differences. Plan 3 had errors of greater than 5% for four out of six TLD measurements. Plan 6 had errors of 5% or greater for each of the analyzed points. . Only two other absolute point dose measurements evaluating the effects of complexity on dosimetric error (Table 3.5) had an error of 4% or greater. None of the TLD measurements evaluating the effects of beam matching on dosimetric accuracy (Table 3.6) exceed 4% dose difference.

	TLD Average Measured vs. Calculated % Difference (standard deviation)					
Plan	TLD #1	TLD #2	TLD #3	TLD #4	TLD #5	TLD #6
1	2.7% (2.3%)	3.1% (2.2%)	-0.1% (1.3%)	-0.1% (1.1%)	2.4% (0.7%)	2.2% (1.2%)
2	2.5% (0.7%)	3.4% (1.5%)	-0.6% (0.6%)	-0.9% (1.2%)	3.9% (2.3%)	2.2% (2.0%)
3	5.7% (0.8%)	6.3% (1.3%)	2.5% (1.4%)	3.6% (1.9%)	6.3% (1.1%)	5.5% (1.4%)
4	2.3% (2.4%)	3.1% (1.3%)	0.4% (1.0%)	-1.3% (2.5%)	2.8% (0.7%)	1.5% (0.3%)
5	-0.1% (0.7%)	-0.2% (2.9%)	-2.7% (0.3%)	-2.6% (2.1%)	-1.7% (0.9%)	-1.4% (1.3%)
6	4.8% (0.7%)	6.5% (2.4%)	5.6% (1.4%)	5.9% (1.7%)	4.7% (1.7%)	4.7% (2.2%)
7	3.9% (0.5%)	2.9% (1.6%)	2.1% (0.9%)	3.1% (1.7%)	1.6% (0.5%)	3.1% (0.7%)
8	2.7% (1.4%)	-0.2% (2.2%)	-2.1% (0.7%)	-2.5%(0.9%)	1.7% (1.4%)	3.7% (2.1%)

Table 3.5 Average difference between measured and calculated TLD doses and standard deviation of the three TLD measurement differences for the six PTV TLD for all eight plans used in this study

	TLD Average Measured vs. Calculated % Difference (standard deviation)					
Machine	TLD #1	TLD #2	TLD #3	TLD #4	TLD #5	TLD #6
Baseline	2.3% (2.4%)	3.1% (1.3%)	0.4% (1.0%)	-1.3% (2.5%)	2.8% (0.7%)	1.5% (0.3%)
2100 CD	2.9% (1.5%)	1.4% (1.9%)	0.3% (1.5%)	-1.5% (1.2%)	3.4% (1.4%)	1.1% (1.4%)
21EX	1.1% (0.8%)	1.5% (0.6%)	-1.5% (0.5%)	-2.5% (1.1%)	3.5% (0.8%)	0.2% (1.2%)
Trilogy	-0.9% (0.4%)	-1.2% (0.4%)	-2.5% (1.0%)	-1.5% (2.1%)	1.1% (0.1%)	-0.9% (0.7%)
6EX	2.4% (2.4%)	2.9% (1.3%)	0.2% (1.0%)	-1.6% (2.5%)	2.5% (0.7%)	1.3% (0.3%)

Table 3.6 Average difference between measured and calculated TLD doses and standard deviation of the dose (cGy) for the six PTV TLD for irradiations of the baseline plan on four different machines and recalculated with the incorrect beam model (6EX)

The percent error for each of the six PTV TLDs was compared to our three measures of treatment plan complexity: MCS, number of MU, number of segments, and minimum segment size. These comparisons are shown graphically in Figure 3.6, Figure 3.7, Figure 3.8, and Figure 3.9. None of these measures of complexity appear to relate to absolute point dose errors, as there is no trend in any of these figures. There also appears to be no relationship between absolute point dose measurements and beam matching.
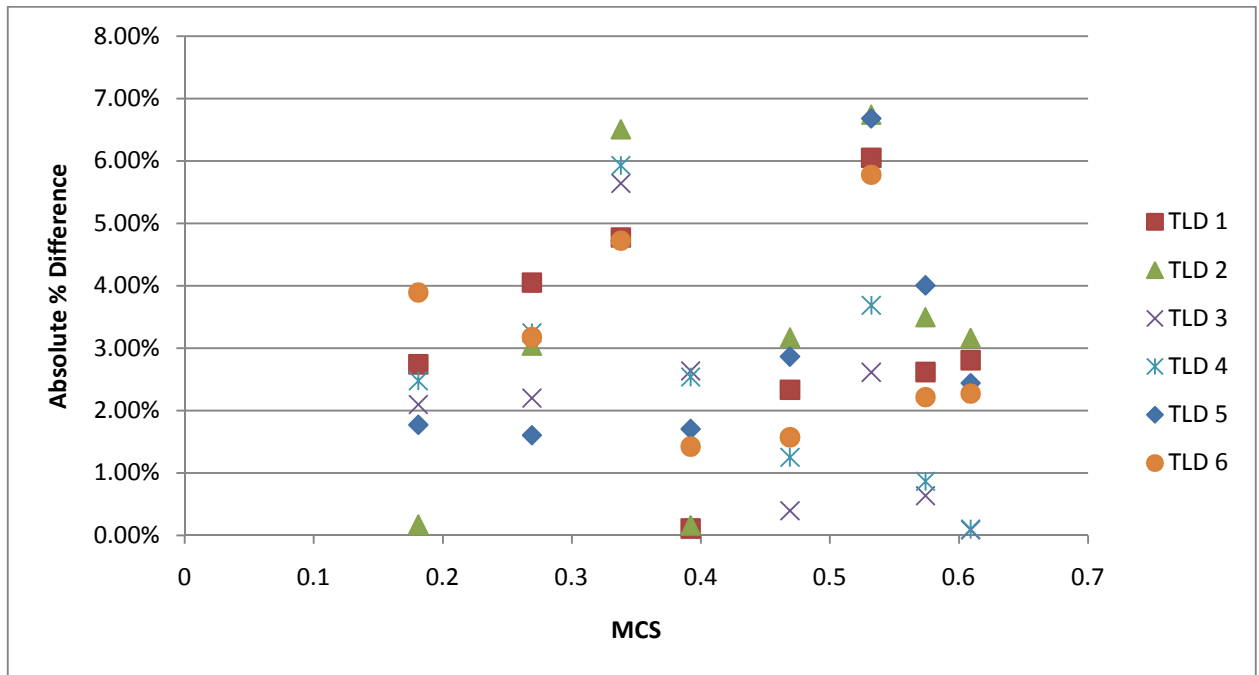
Figure 3.6 Distribution of absolute percent difference in calculated and measured TLD doses with the MCS of the corresponding eight treatment plans
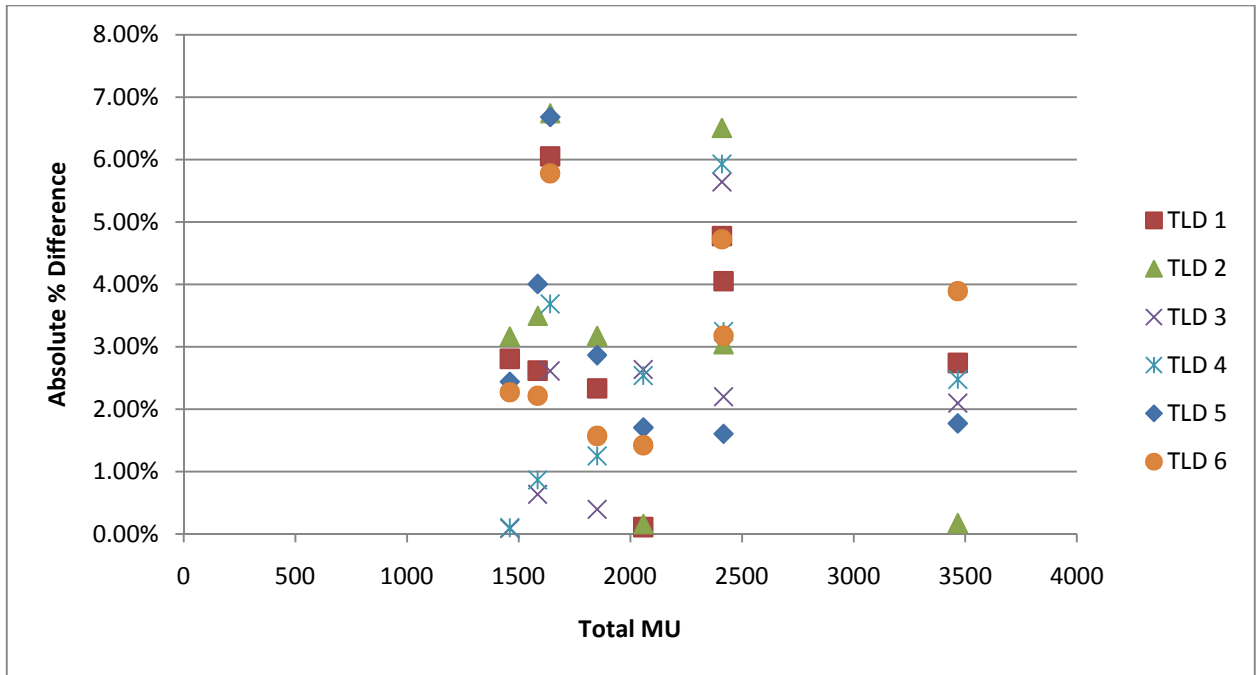
Figure 3.7 Distribution of percent difference in calculated and measured TLD doses with the total number of MU of the corresponding eight treatment plans
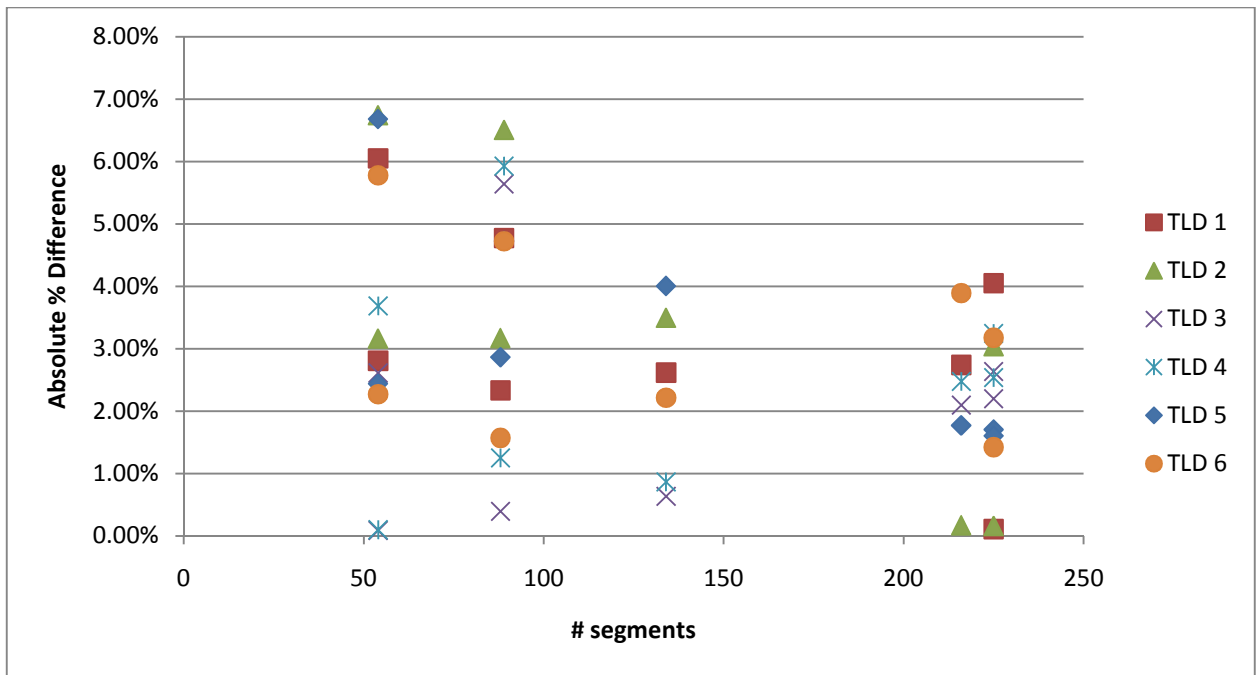
Figure 3.8 Distribution of percent difference in calculated and measured TLD doses with the total number of segments of the corresponding eight treatment plans
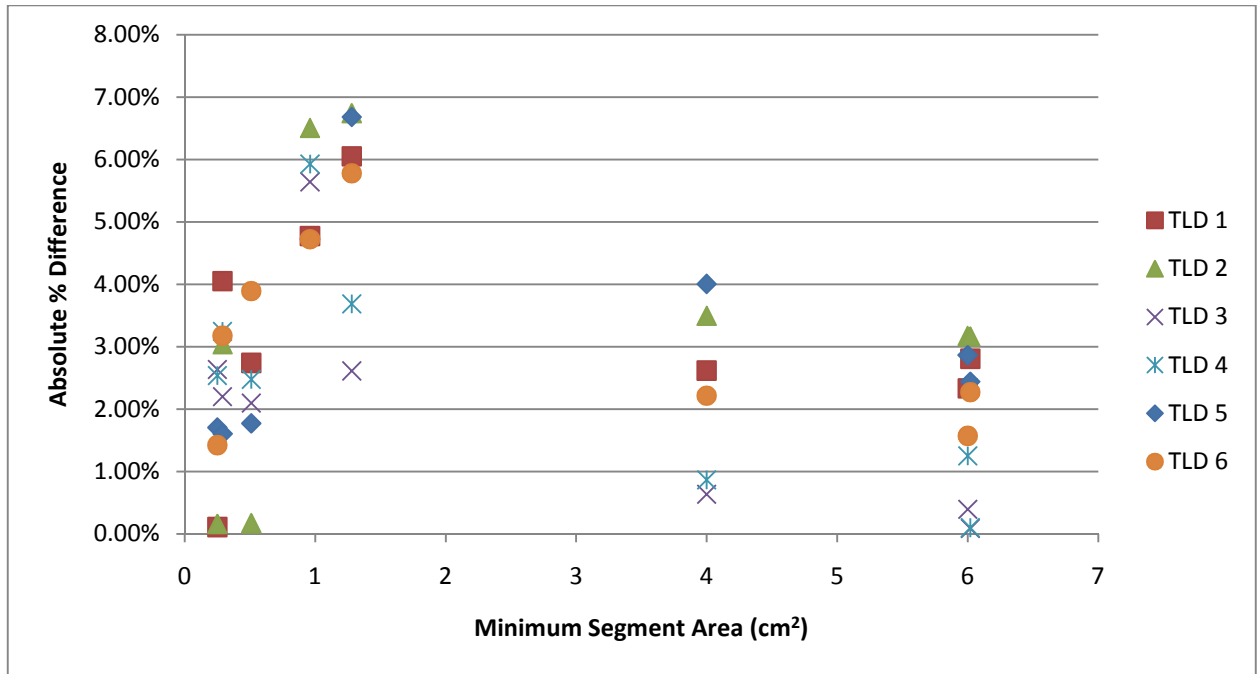
Figure 3.9 Distribution of percent difference in calculated and measured TLD doses with the minimum segment size (cm^2) of the corresponding eight treatment plans

3.3.2 Planar Dose Analysis

As mentioned in Section 2.4.2.2, the RPC IMRT H&N phantom holds film in two planes. To evaluate the planar agreement between planned and measured doses, three different dose profiles were measured for each of the irradiations. On the axial films, a lateral dose profile was taken through the center of the primary and secondary PTV and an anterior-to-posterior dose profile was taken through the center of the primary PTV and OAR. On the sagittal films, a dose profile was recorded in the superior-inferior direction through the center of the primary PTV and OAR, where a cut-out for the OAR TLD exists. The profiles for the baseline plan (Plan 4) are presented below in Figure 3.10-Figure 3.12. The profiles for all other plans are presented in Appendix C Dose Profiles. These profiles display the calculated dose, each of the three measurements, and the average of all three measurements. The measured sagittal superior-inferior profiles have a gap in the data along the y-axis where the axial film separated the two sagittal films.
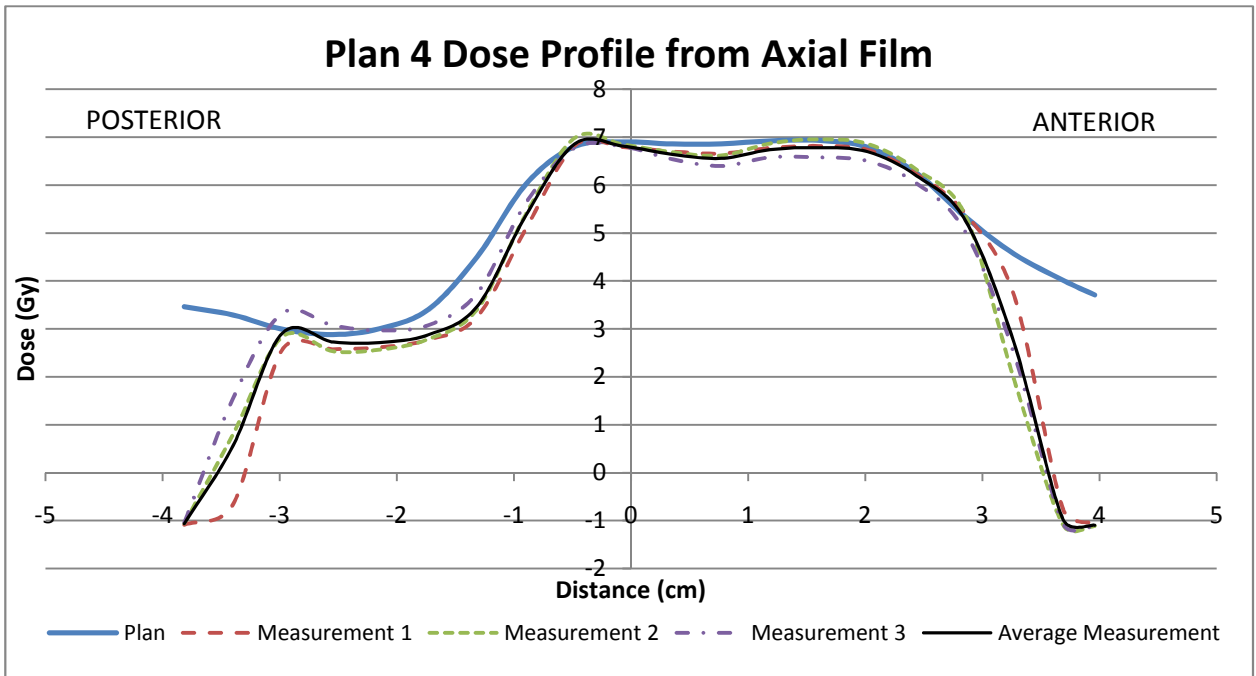
Figure 3.10 Posterior-to-anterior dose profile of Plan 4 as planned by the TPS and measured with the three axial films
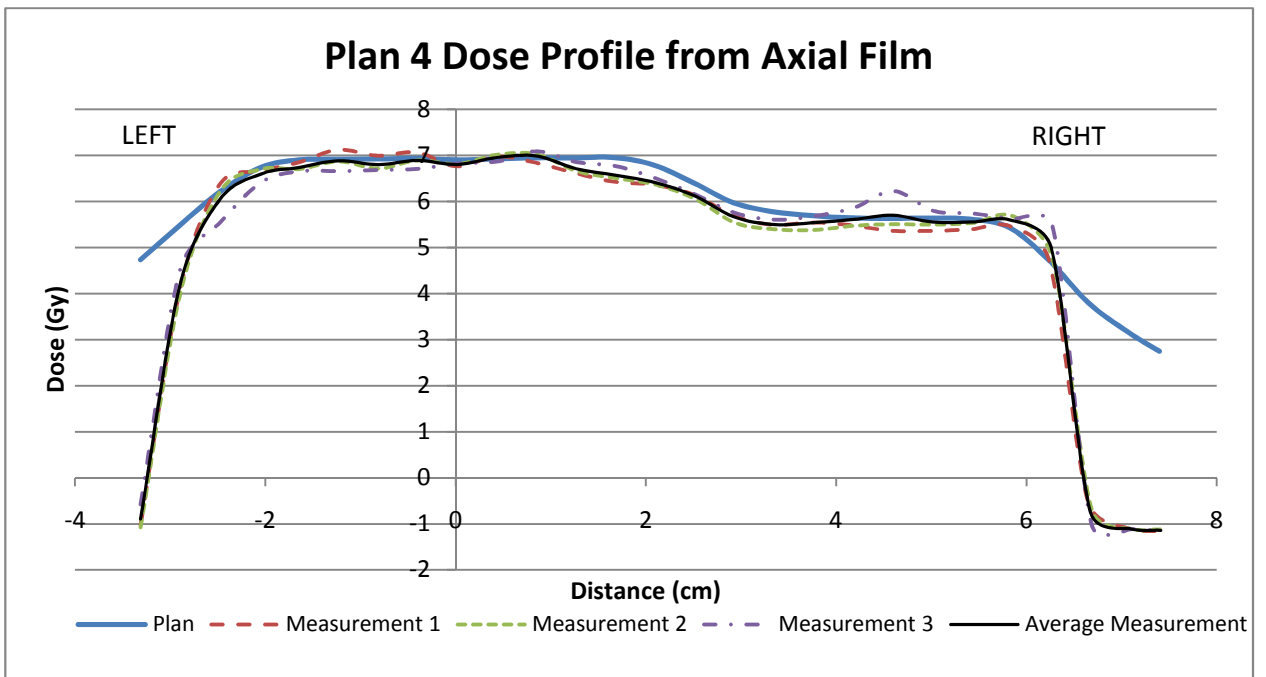
Figure 3.11 Lateral dose profile of Plan 4 as planned by the TPS and measured with the three axial films
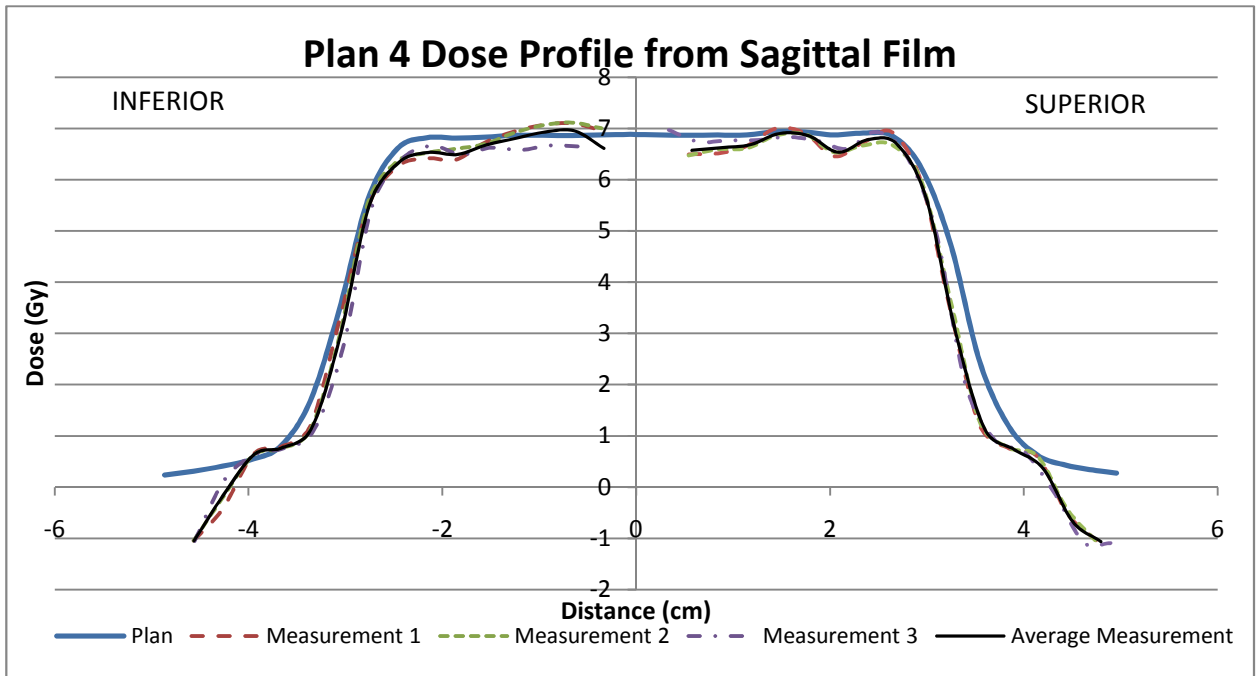
Figure 3.12 Inferior-to-superior dose profile of Plan 4 as planned by the TPS and measured by the three sagittal films

Roughness in the film measurements may be caused by dust or dents on the film or simply noise characteristic of the EBT2 film. This is the reason for the data smoothing performed. Some sagittal films do not line up exactly at the central axis and therefore a noticeable difference dose plateau on the inferior and superior halves may exist. This is likely caused by a small misalignment when the film is scanned. It can also be noticed that the measured profiles dip to negative values at each edge. This reflects the edge of the film.

To quantify the agreement between calculated and measured plans in a high dose gradient region, the distance-to-agreement (DTA) was found for each measurement on the axial film between the primary PTV and the OAR. The average DTA of the three measurements taken with each plan on the baseline machine as well as the standard deviation of these measurements are reported in Table 3.7. The average DTA of the three measurements taken with the baseline plan on the various machines and the incorrect beam model calculation as well as the standard deviation of these measurements are reported in Table 3.8. All average DTAs are positive and reflect the measured dose being to the right of the calculated dose as demonstrated by the arrow in Figure 3.13, indicating a steeper dose

45

gradient than calculated. All average DTA value are less than or equal to 3 mm and are therefore within the RPC criteria of ±4 mm. In Table 3.7 it can be seen that Plan 6 had the lowest average DTA and therefore the best agreement between delivery and calculation. This is interesting because Plan 6 also had the poorest TLD absolute dose agreement with expected doses. Also notice in Table 3.8 that the baseline machine had the largest DTA standard deviation of all machines and therefore poor agreement. Surprisingly, the measurements made on the baseline machine and compared to the treatment plan calculated with the incorrect beam model agreed better than the baseline machine with the original baseline plan with the treatment plan calculated as measured by average DTA. The Trilogy had the best DTA.
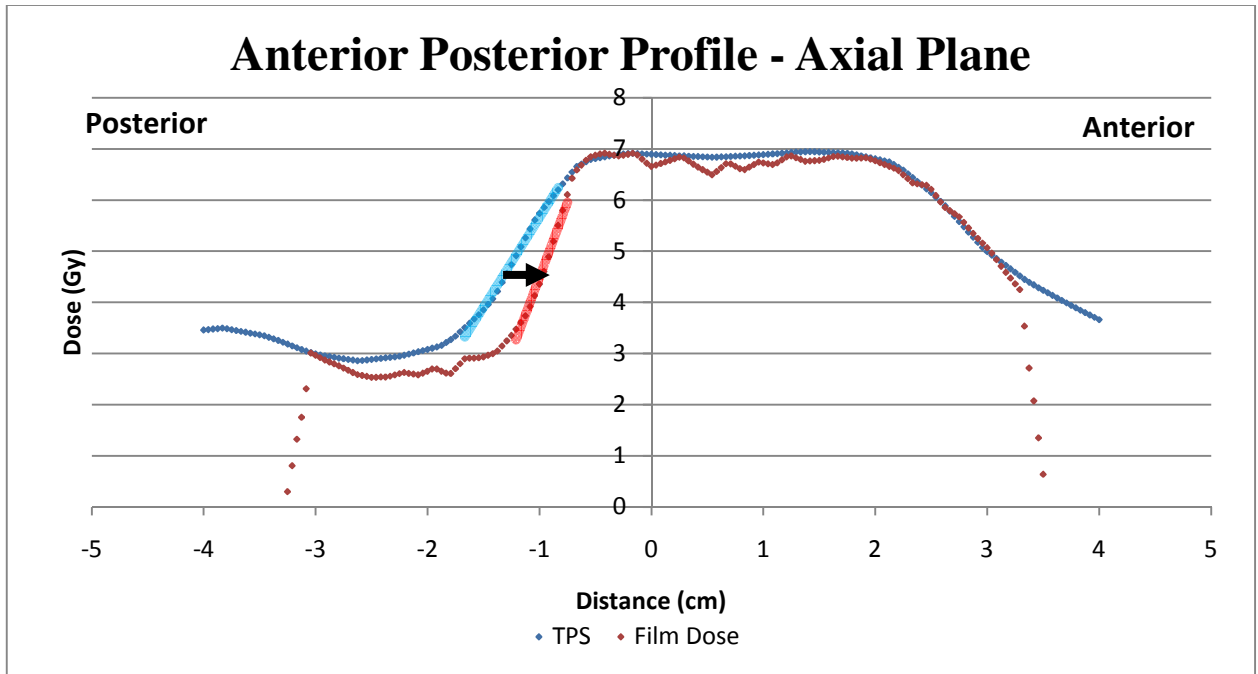
Figure 3.13 Posterior-to-anterior dose profile example demonstrated the measurement of distance-to-agreement

Plan Number	DTA (cm)	Standard Deviation
1	0.3	0.02
2	0.3	0.04
3	0.3	0.02
4	0.3	0.10
5	0.2	0.01
6	0.1	0.05
7	0.2	0.03
8	0.3	0.05

Table 3.7 Displacement (cm) of measurement from calculation and the standard deviation of the posterior penumbra between the primary PTV and the OAR for all eight treatment plans

Machine	DTA (cm)	Standard Deviation
Baseline	0.3	0.10
2100CD	0.2	0.02
21EX	0.2	0.02
Trilogy	0.1	0.02
6 EX	0.2	0.08

Table 3.8 Displacement (cm) of measurement from calculation and the standard deviation of the posterior penumbra between the primary PTV and the OAR for the baseline plan delivered on four matched machines and recalculated with an incorrect beam model

The distance-to-agreement values were compared to our three measures of complexity to evaluate possible dosimetric effects of increased treatment plan complexity. The average DTA values were graphed against each the MCS, number of MU, number of segments and minimum segment size and are shown in Figure 3.14, Figure 3.15, Figure 3.16, and Figure 3.17 respectively. None of these parameters have a clear relationship with planar dose distribution error demonstrated by DTA.
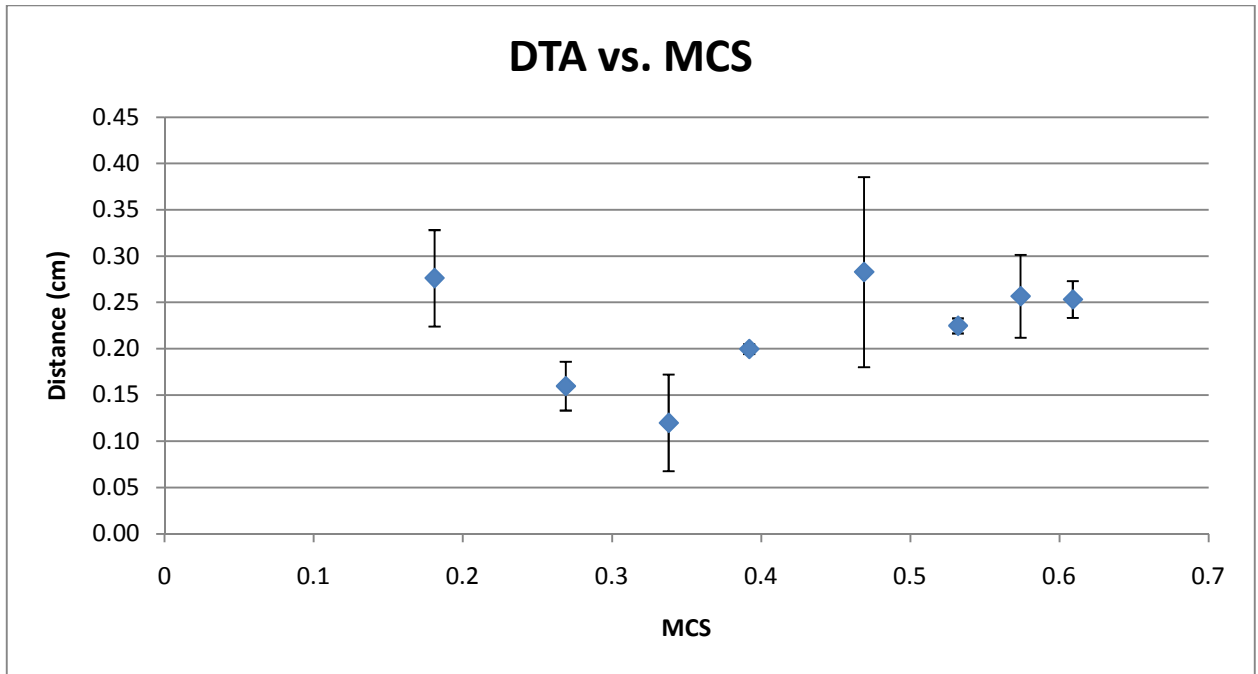
Figure 3.14 Displacement (cm) of measurement from calculation and the standard deviation of the posterior penumbra between the primary PTV and the OAR for all eight treatment plans according to MCS
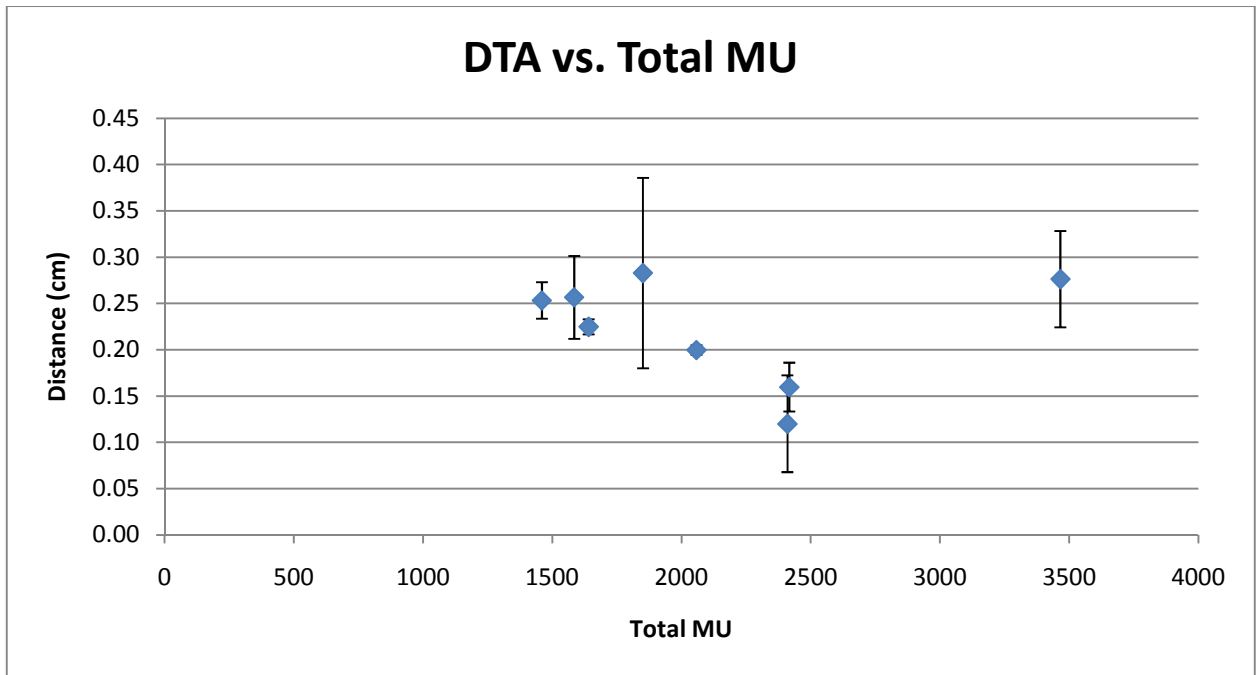
Figure 3.15 Displacement (cm) of measurement from calculation and the standard deviation of the posterior penumbra between the primary PTV and the OAR for all eight treatment plans according to total plan MU
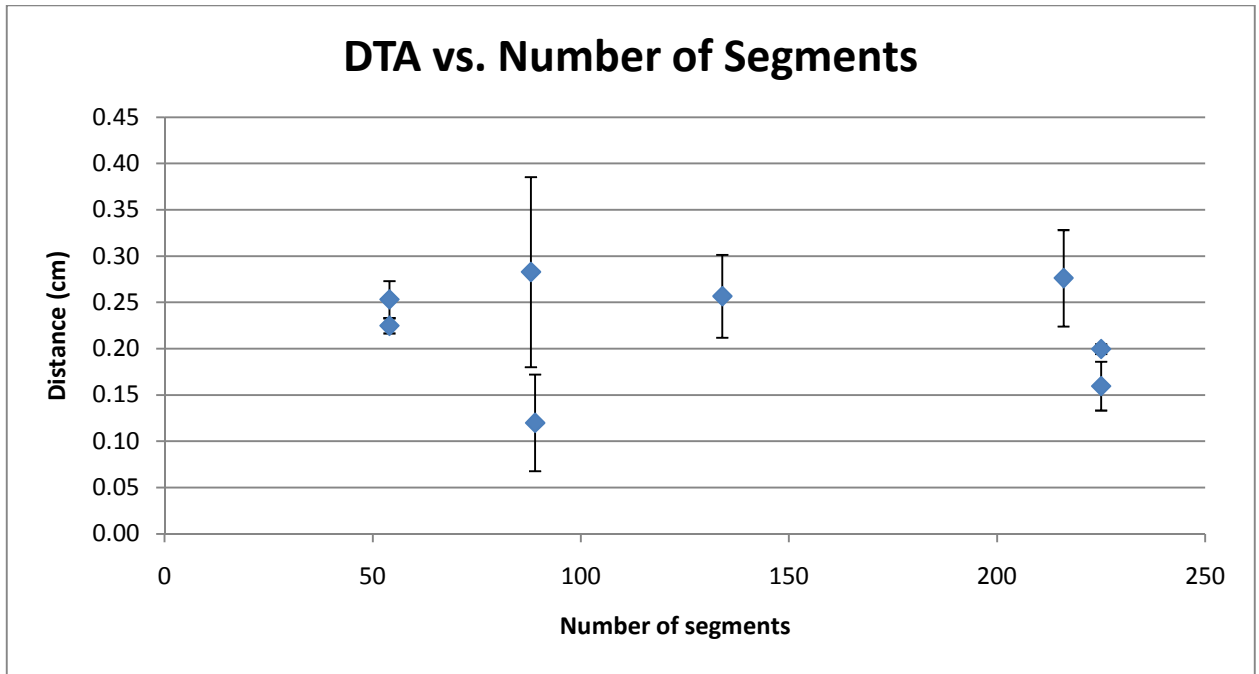
Figure 3.16 Displacement (cm) of measurement from calculation and the standard deviation of the posterior penumbra between the primary PTV and the OAR for all eight treatment plans according to total number of segments
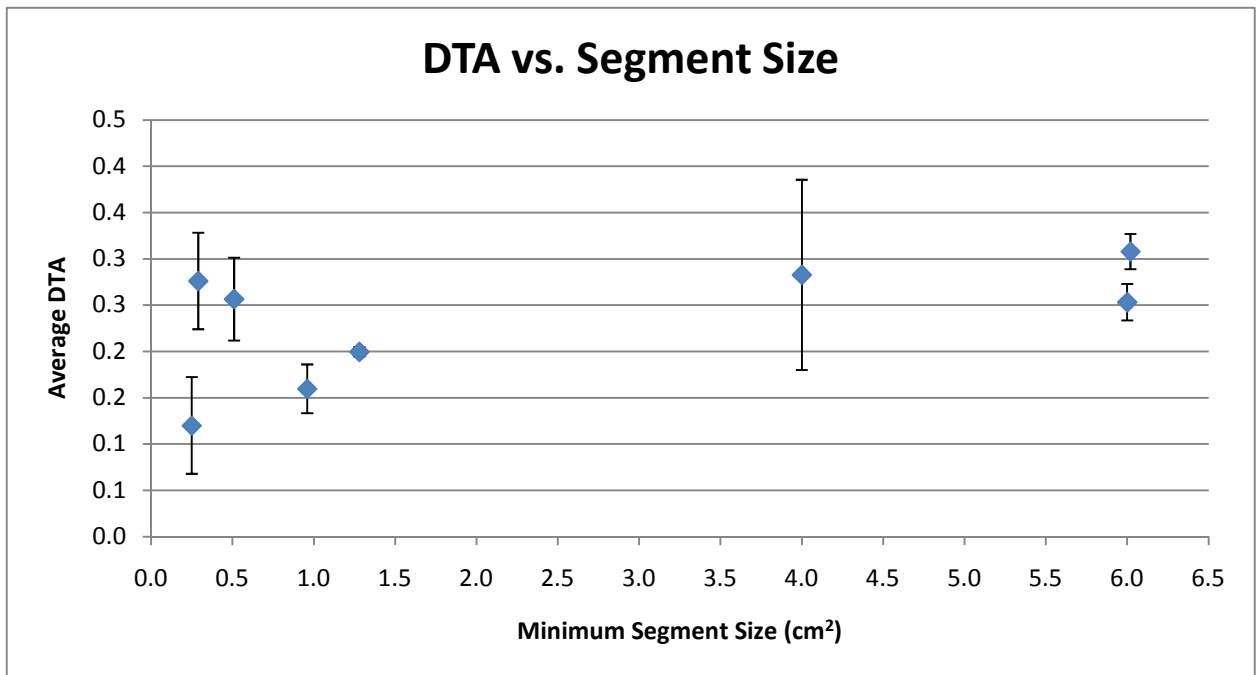
Figure 3.17 Displacement (cm) of measurement from calculation and the standard deviation of the posterior penumbra between the primary PTV and the OAR for all eight treatment plans according to minimum segment size (cm²)

49

3.3.3 Gamma Analysis

As our final measure of the agreement between calculated and delivered dose distributions, a gamma analysis was performed as described in Section 2.4.6. Table 3.9 contains the average percent of pixels passing a gamma analysis with 7%/4mm criteria of the primary PTV region of the axial films as shown in Figure 2.5 for each of the eight plans. All plans with the exception of Plan 3 had greater than 90% of pixels passing this analysis. For comparison, institutions irradiating the RPC's IMRT H&N phantom in 2010 had an average percent of pixels passing a gamma analysis performed by the RPC on the same region with the same criteria of 93 % ±11 %.

Plan	MCS	MU	# Seg	7%/4mm	Standard Deviation
1	0.609	1460	54	98.0%	4.7%
2	0.574	1585	134	96.8%	2.2%
3	0.532	1641	54	75.7%	12.7%
4	0.469	1851	88	90.8%	6.4%
5	0.392	2058	225	90.7%	3.6%
6	0.338	2410	89	94.7%	9.2%
7	0.269	2417	225	96.4%	3.7%
8	0.181	3466	216	91.7%	4.1%

Table 3.9 Percent of pixel passing gamma analysis of primary PTV axial film region with 7%/4mm criteria and standard deviation of all eight plans

Further gamma analysis was performed on more complete regions of the axial and sagittal films with criteria of 7%/4mm and 5%/3mm. The averages of the percent pixels passing for these gamma analyses for each of the eight treatment plans in axial and sagittal planes are presented below in Table 3.10 and Table 3.11, respectively. Similar to the gamma analysis performed on the primary PTV region, all films had near 90% agreement using criteria of 7%/4mm except for Plan 3. On the full sagittal film region, all plans had greater than 90% pixels passing the 7%/4mm criteria with the exception of Plan 3. Overall, Plan 3 had much lower average percent pixels passing for each of the criterion on each film region. These results are displayed in comparison to the MCS, number of MU, number of segments and minimum segment size in Figure 3.18, Figure 3.19, Figure 3.20, and Figure 3.21,

respectively. As with our evaluation of the effects of complexity on point doses and planar doses, there is no clear trend with complexity and percent of pixel passing gamma analysis.

Plan	7%/4mm	5%/3mm
1	97.8%	82.7%
2	94.7%	81.9%
3	73.6%	48.2%
4	90.7%	74.8%
5	88.9%	70.5%
6	95.3%	85.8%
7	97.6%	87.5%
8	89.3%	74.2%

Table 3.10 Average percent of pixels passing gamma analysis in the axial full film region for criteria of 7%/4mm and 5%/3mm for all eight plans

Plan	7%/4mm	5%/3mm
1	95.9%	86.3%
2	95.6%	86.2%
3	86.8%	73.4%
4	96.3%	86.1%
5	97.8%	92.1%
6	94.3%	89.7%
7	96.9%	90.4%
8	93.7%	81.3%

Table 3.11 Average percent of pixels passing gamma analysis in the sagittal full film region for criteria of 7%/4mm and 5%/3mm for all eight plans
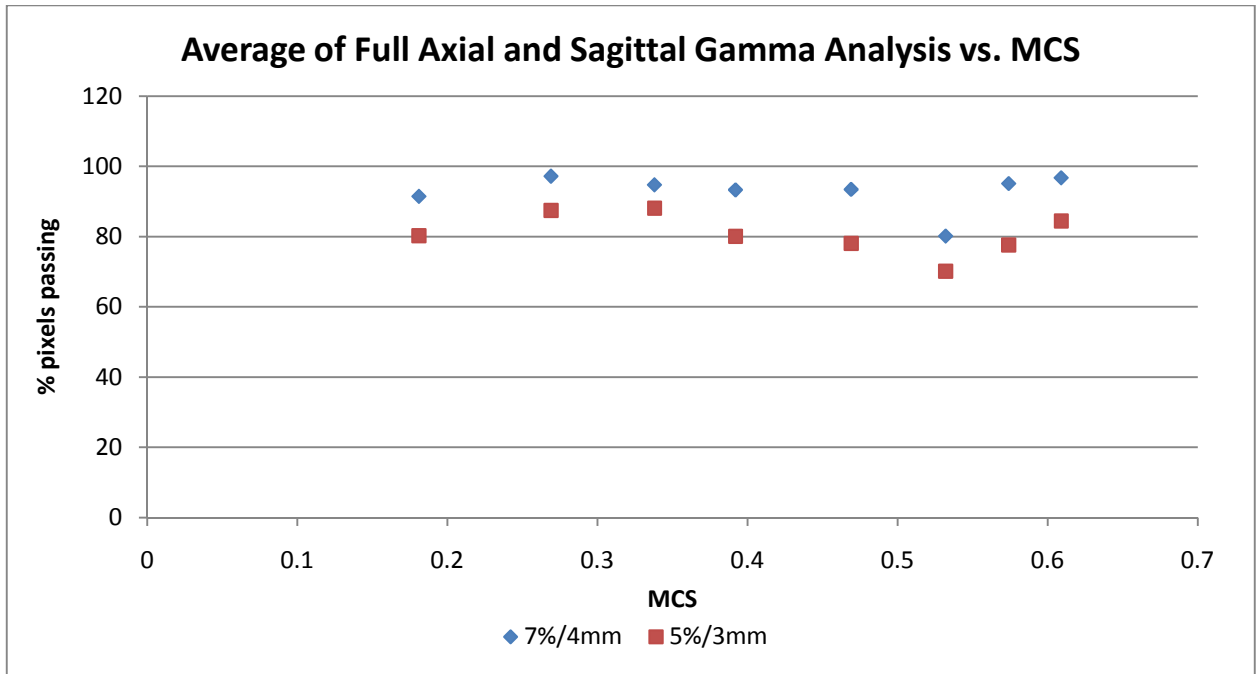
Figure 3.18 Average percent of pixels passing gamma analysis on the axial and sagittal full film regions for all eight plans according to MCS
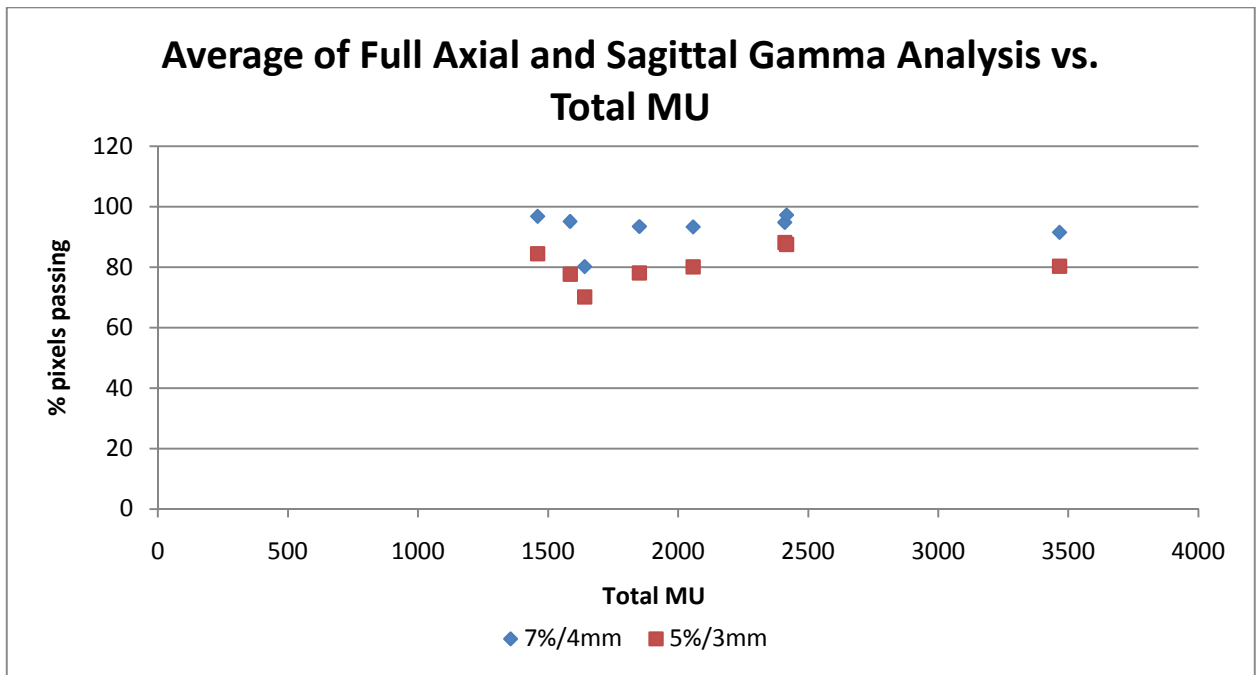
Figure 3.19 Average percent of pixels passing gamma analysis on the axial and sagittal full film regions for all eight plans according to total MU
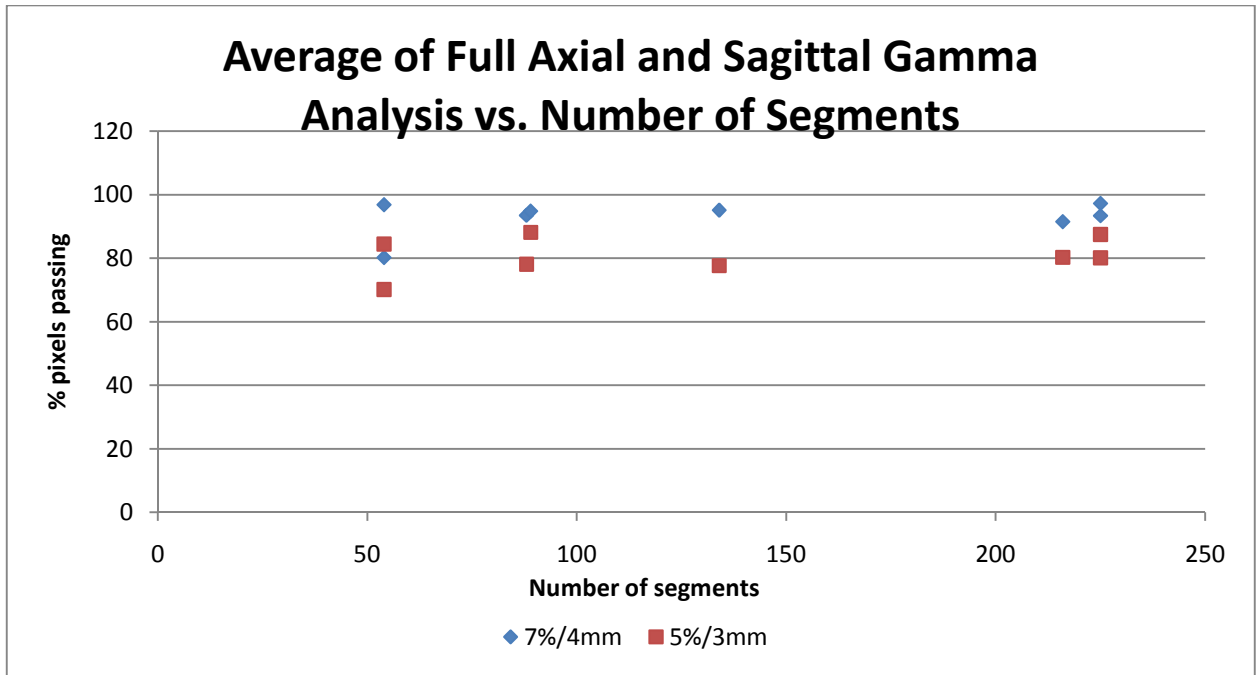
Figure 3.20 Average percent of pixels passing gamma analysis on the axial and sagittal full film regions for all eight plans according to total number of segments
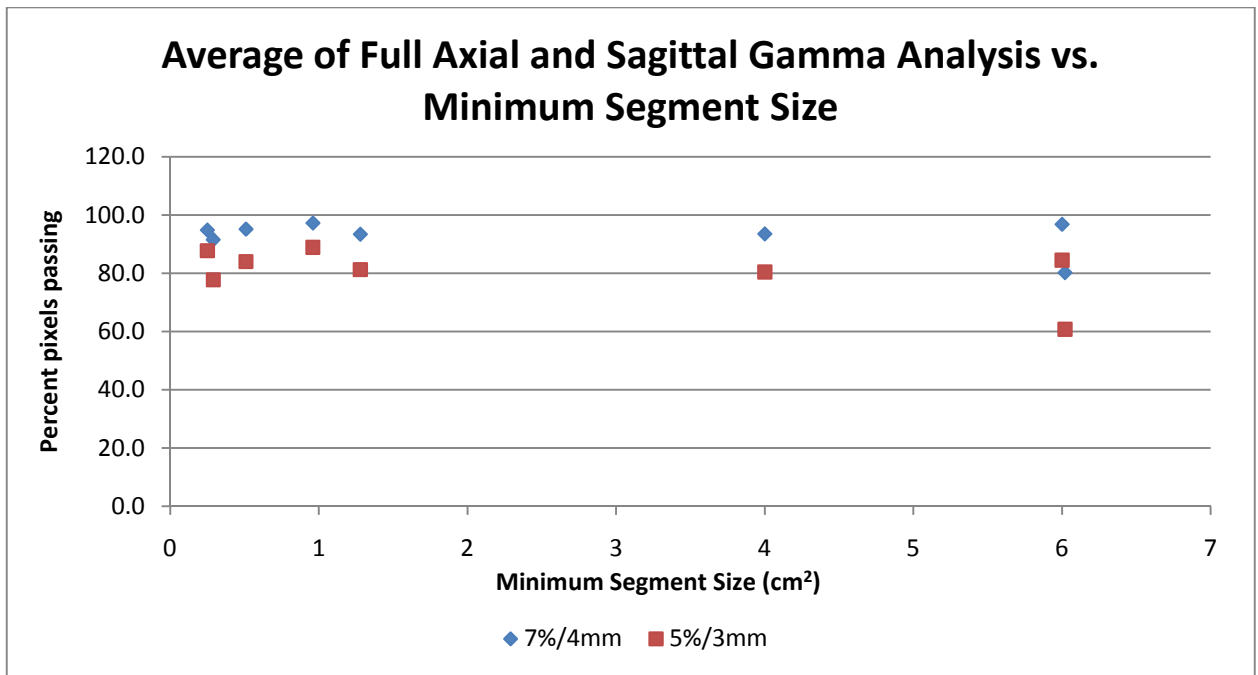
Figure 3.21 Average percent of pixels passing gamma analysis on the axial and sagittal full film regions for all eight plans according to the minimum segment size (cm²)

To further evaluate the gamma analysis we performed, three of the full film region results are presented below in Figure 3.22-Figure 3.33. Refer back to Figure 2.6 and Figure 2.7 for cross-sectional images of the phantom in the film planes. First, we looked at the baseline plan (Plan 4) results. It can be seen in Figure 3.22 and Figure 3.23 that the delivery of this plan begins to fail mainly posterior to the primary PTV around the OAR and laterally. This is also reflected in the sagittal gamma analysis shown in Figure 3.24 and Figure 3.25, where most of the failure occurs near the OAR TLD cut out. We next evaluated the gamma analysis of Plan 3, which was consistently low for no apparent reason. It can be seen in Figure 3.26 through Figure 3.29 that this plan delivery fails in the areas surrounding the PTVs and OAR, mainly low dose regions. Finally, we looked at the gamma analyses performed on Plan 6, which had the greatest TLD dose deviations. The failure seen in the Plan 6 axial gamma analysis, shown in Figure 3.30 and Figure 3.31 is similar to that of Plan 4. It is mainly in the area posterior to the primary PTV, around the OAR and lateral to the OAR. The sagittal gamma analysis of Plan 6 shown in Figure 3.32 and Figure 3.33 illustrates that the failure is located more in between then primary PTV and the OAR than directly on the OAR as it appears in Plan 4. The gamma analysis results for the remainder of the plans are presented in Appendix D Gamma Index Analyses Results.
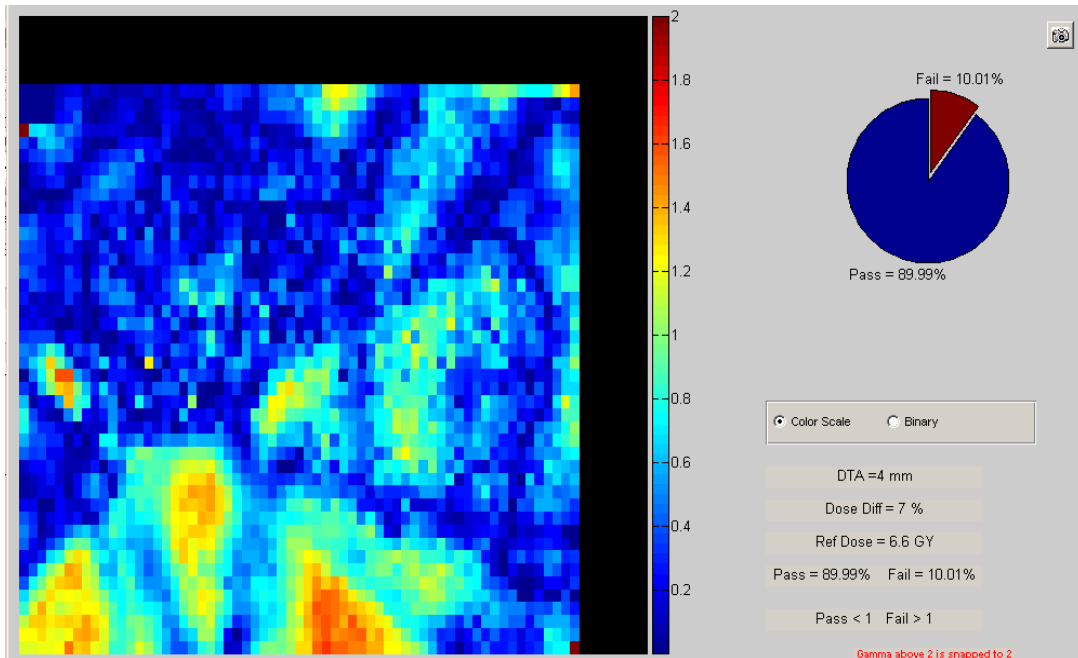
Figure 3.22 7%/4mm gamma analysis of full axial film region for one measurement of Plan 4 on the baseline machine
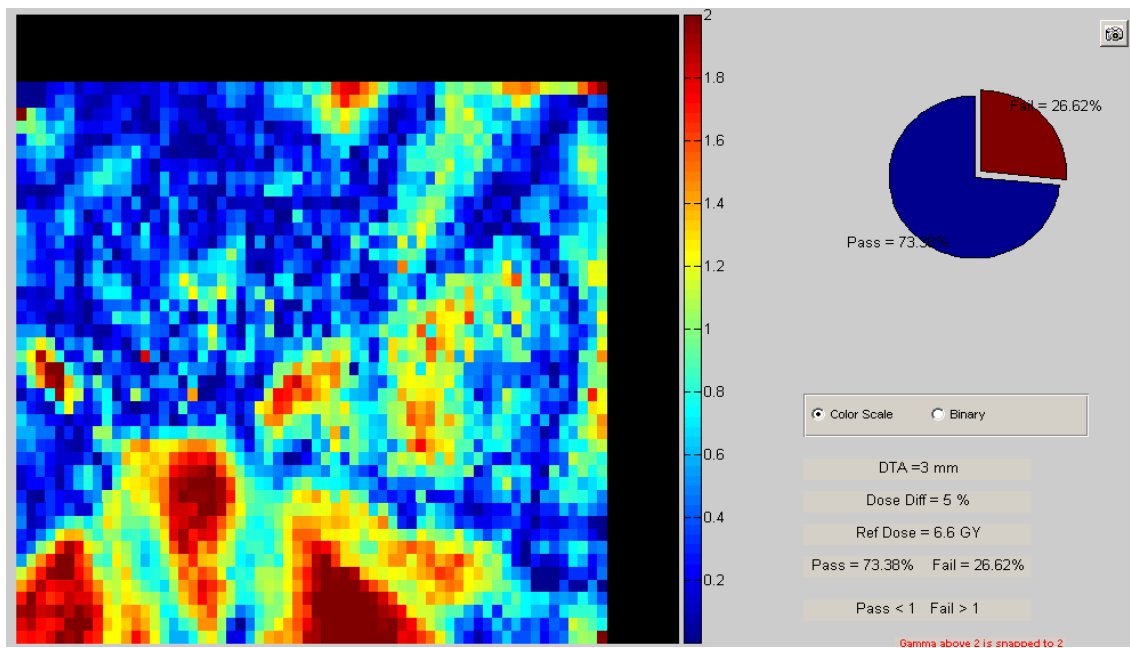
Figure 3.23 5%/3mm gamma analysis of full axial film region for one measurement made of Plan 4 on the baseline machine
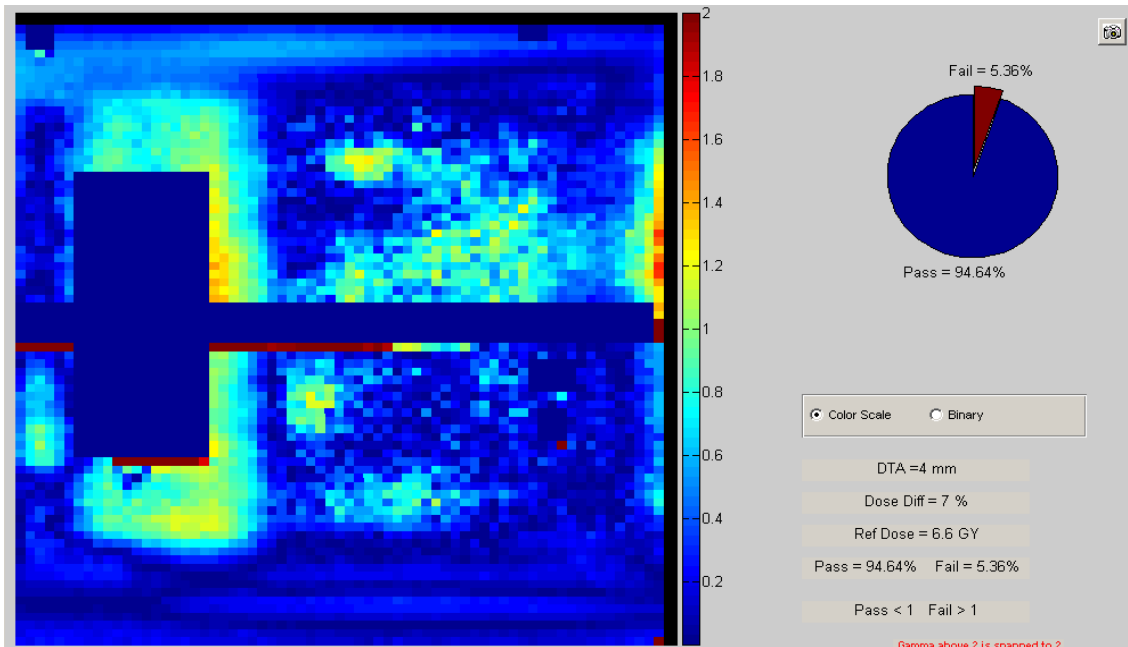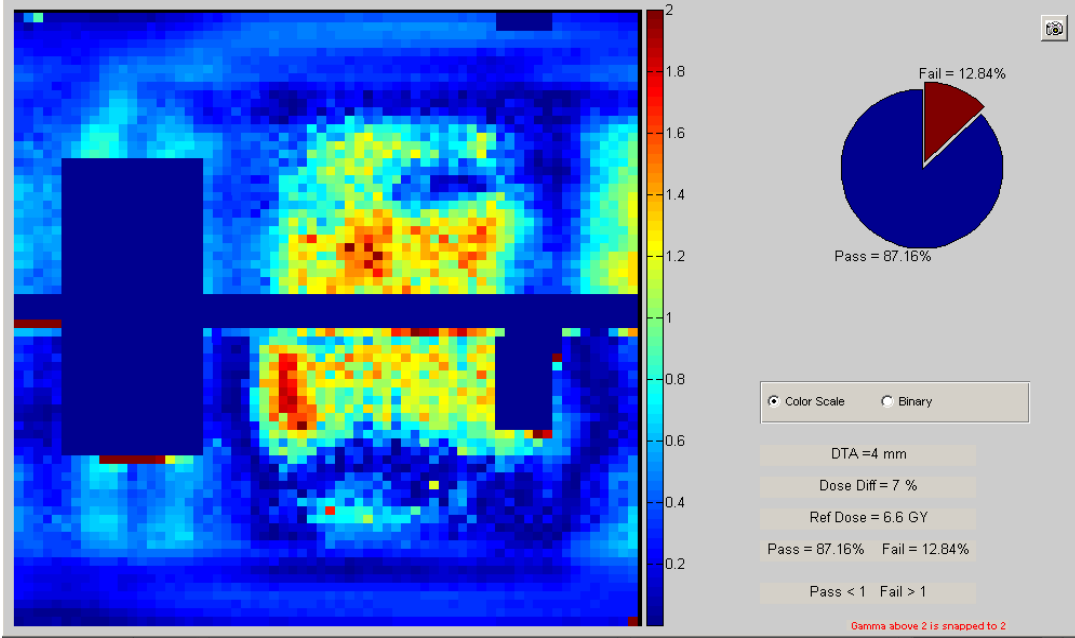
Figure 3.24 7%/4mm gamma analysis of full sagittal film region for one measurement made of Plan 4 on the baseline machine
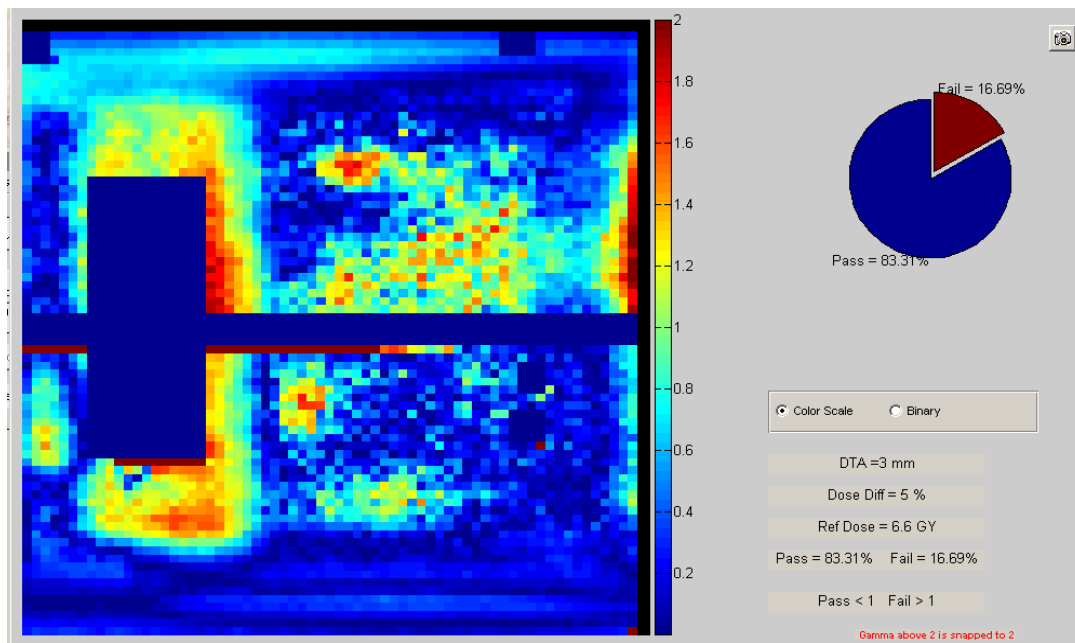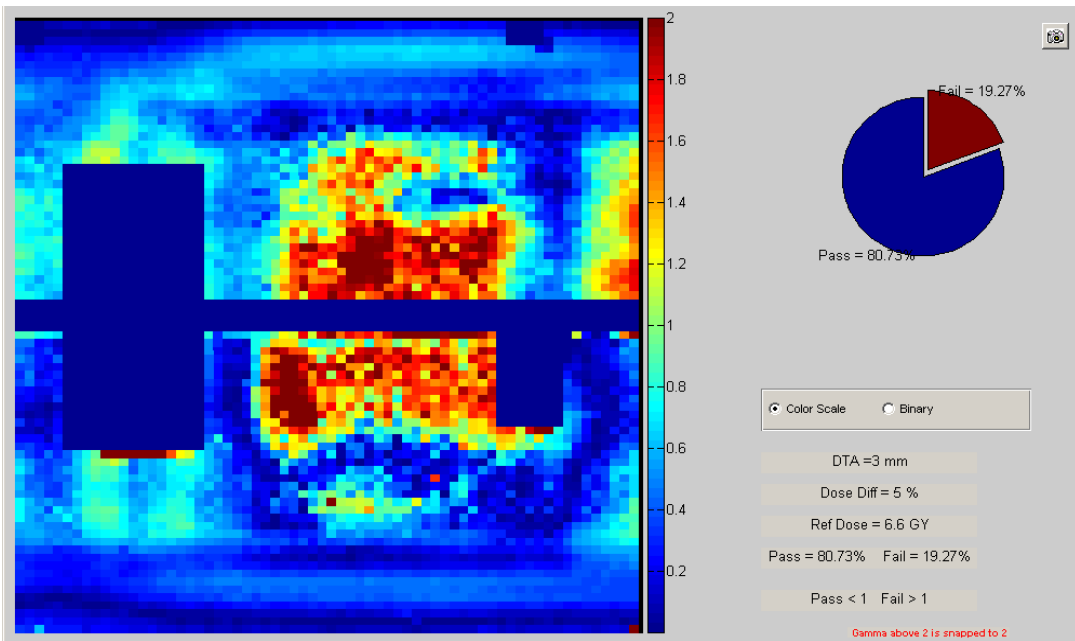

Figure 3.25 5%/3mm gamma analysis of full sagittal film region for one measurement made of Plan 4 on the baseline machine
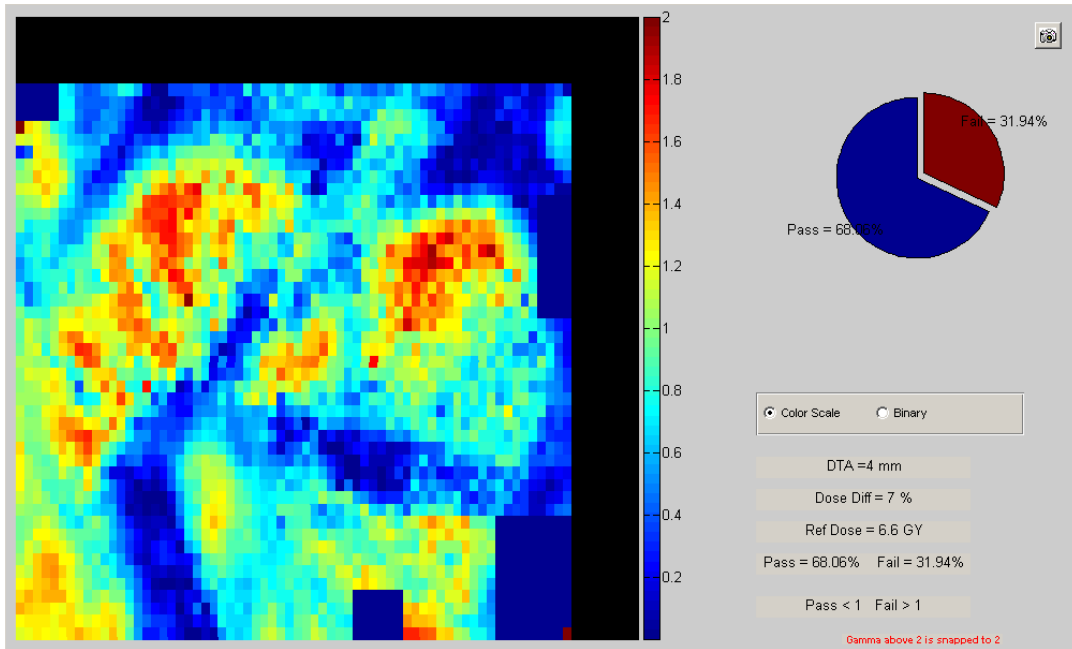
Figure 3.26 7%/4mm gamma analysis of full axial film region for one measurement made of Plan 3 on the baseline machine
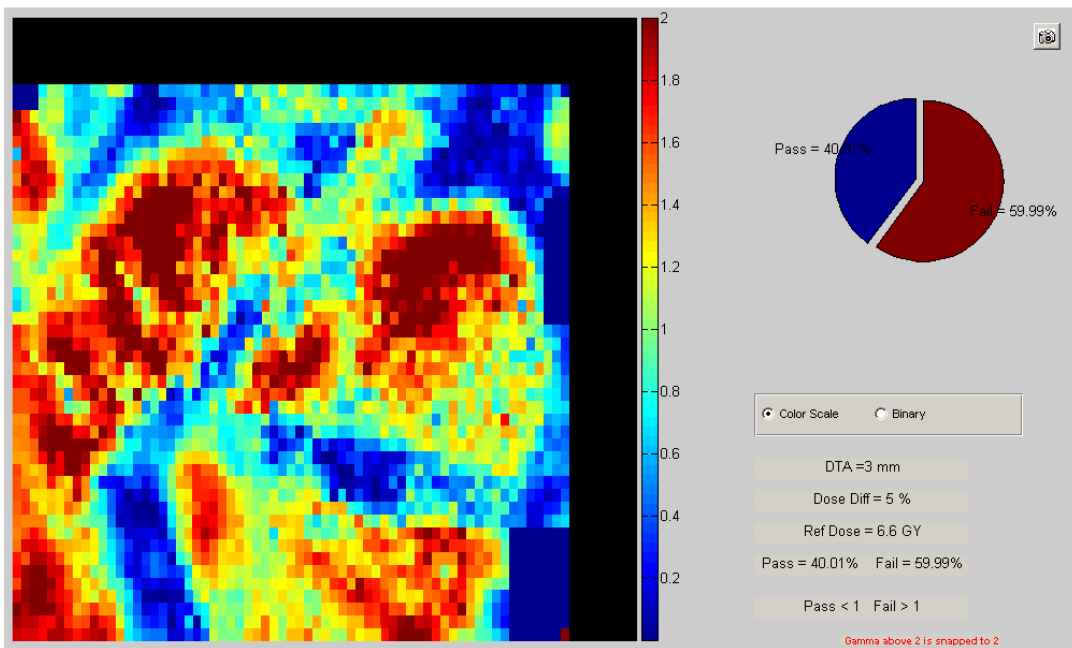
Figure 3.27 5%/3mm gamma analysis of full axial film region for one measurement made of Plan 3 on the baseline machine
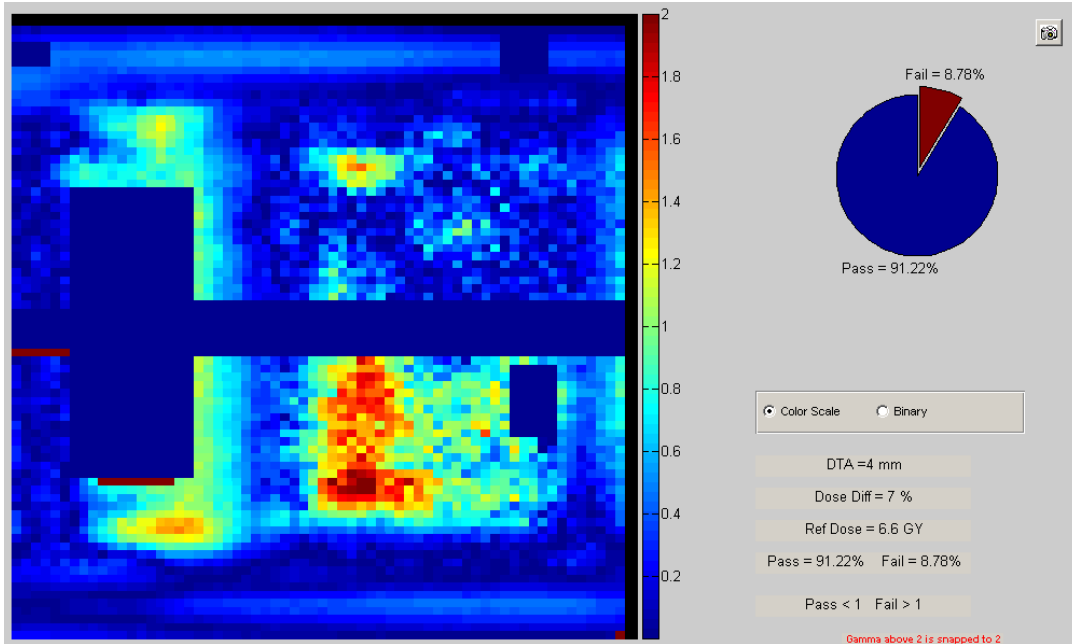
Figure 3.28 7%/4mm gamma analysis of full sagittal film region for one measurement made of Plan 3 on the baseline machine
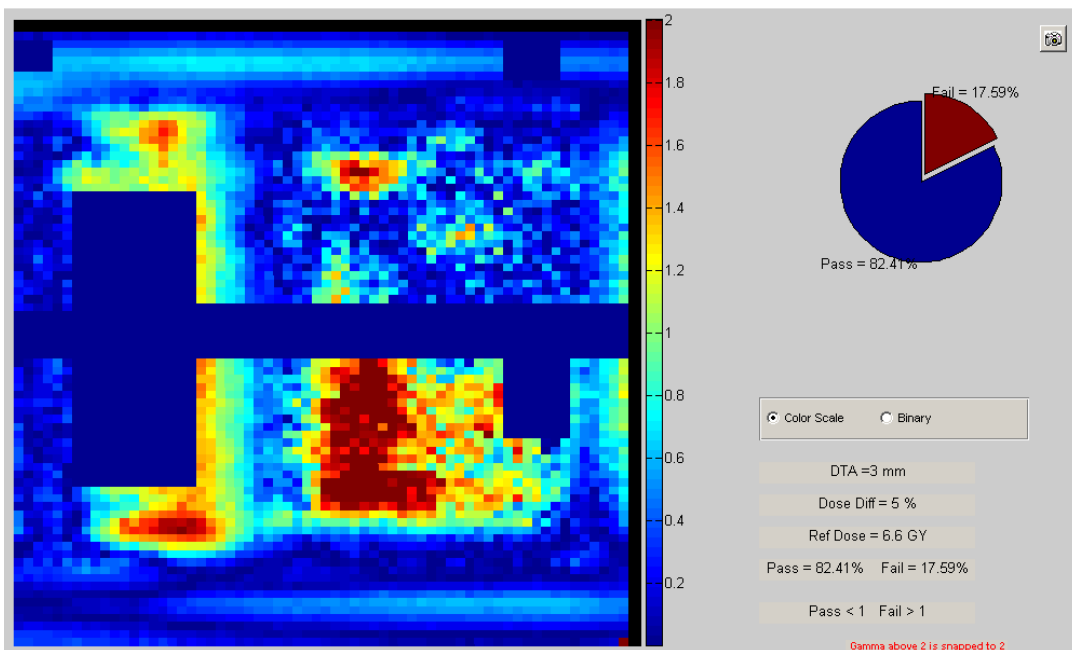
Figure 3.29 5%/3mm gamma analysis of full sagittal film region for one measurement made of Plan 3 on the baseline machine
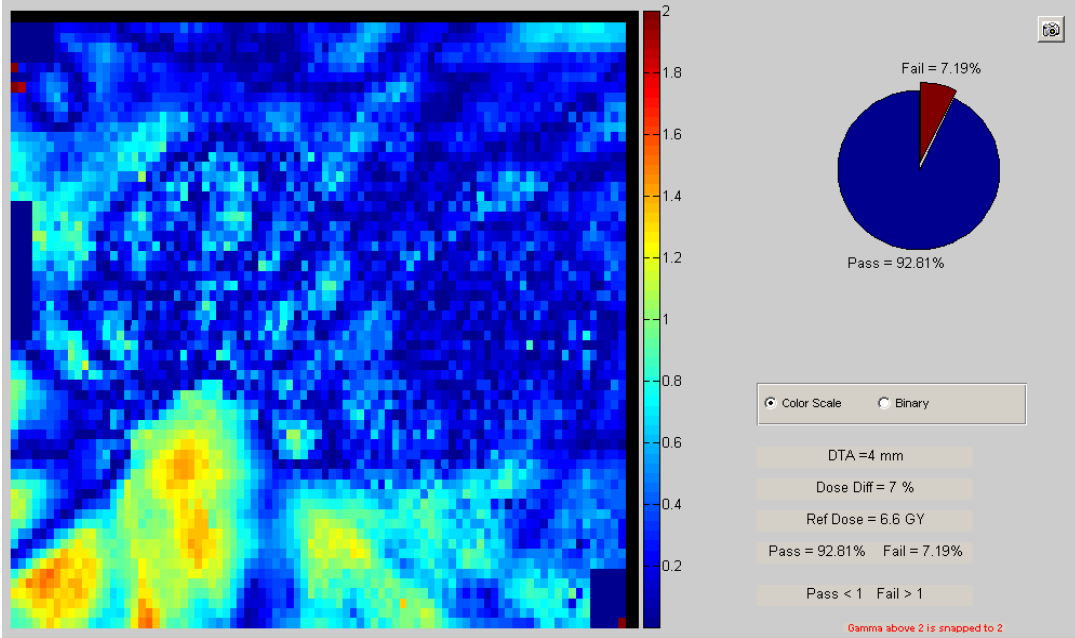
Figure 3.30 7%/4mm gamma analysis of full axial film region for one measurement made of Plan 6 on the baseline machine
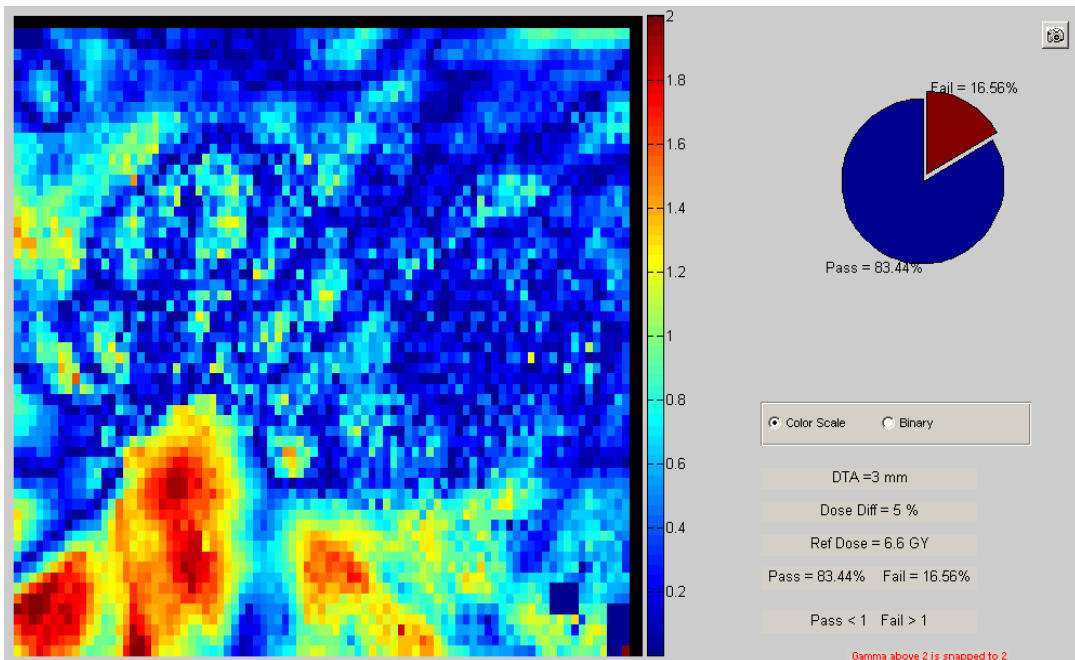
Figure 3.31 5%/3mm gamma analysis of full axial film region for one measurement made of Plan 6 on the baseline machine

Figure 3.32 7%/4mm gamma analysis of full sagittal film region for one measurement made of Plan 6 on the baseline machine

Figure 3.33 5%/3mm gamma analysis of full sagittal film region for one measurement made of Plan 6 on the baseline machine

The same gamma analysis was performed on the measurements taken with the baseline plan on the four different machines and on the calculation performed with the incorrect beam model. These results are displayed below in

Machine	7%/4mm	5%/3mm
Base	90.7%	74.8%
2100CD	96.8%	87.8%
21EX	95.8%	85.0%
Trilogy	95.6%	88.1%
6EX	92.0%	75.6%

Table 3.12, Table 3.13 and Figure 3.34. The average gamma analysis made on each machine with 7%/4mm criteria exceeded 90% pixels passing. There is no evidence that beam matching is affecting the accuracy of the dose calculation for these machines. The calculation intentionally performed with the incorrect beam model matched the measurement performed on the baseline machine just as well as the measurements performed on all the other machines.

Machine	7%/4mm	5%/3mm
Base	90.7%	74.8%
2100CD	96.8%	87.8%
21EX	95.8%	85.0%
Trilogy	95.6%	88.1%
6EX	92.0%	75.6%

Table 3.12 Average percent of pixels passing gamma analysis in the axial full film regions for criteria of 7%/4mm and 5%/3mmfor the baseline plan delivered on four matched machines and recalculated with the incorrect beam model (6EX)

Machine	7%/4mm	5%/3mm
Base	96.3%	86.1%
2100CD	93.5%	82.3%
21EX	96.7%	87.5%
Trilogy	90.9%	82.0%
6EX	97.9%	87.7%

Table 3.13 Average percent of pixels passing gamma analysis in the sagittal full film regions for criteria of 7%/4mm and 5%/3mmfor the baseline plan delivered on four matched machines and recalculated with the incorrect beam model (6EX)
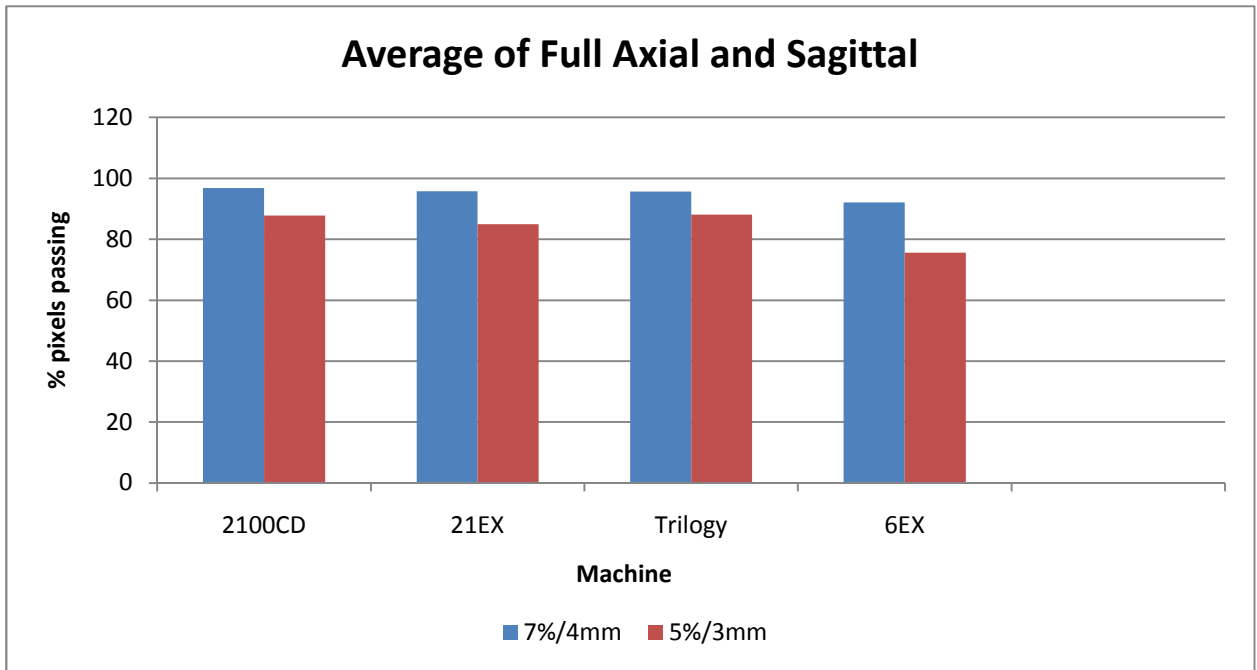
Figure 3.34 Average percent of pixels passing gamma analysis in both the axial and sagittal full film regions for criteria of 7%/4mm, 5%/3mm, and 3%/2mm for the baseline plan delivered on four matched machines and recalculated with the incorrect beam model (6EX)

Chapter 4 Discussion

4.1 General Discussion

The data presented in this study suggest that an increase in treatment plan complexity and the use of improperly matched beam dosimetry data do not lead to detectable errors in head and neck IMRT delivery that result in differences between the measured and planned dose distributions as measured by the RPC's IMRT head and neck phantom. Despite substantial increases in treatment plan complexity, as measured by the total number of MU, number of segments, and the MCS, all treatment plans delivered on the same treatment machine whose dosimetry data is used as the baseline dataset for the planning system, passed the RPC's criteria of 7% absolute point dose and 4 mm distance-to-agreement (DTA). In addition, a study of delivering the same IMRT treatments using four different matched linacs whose dosimetric parameters were matched to the baseline dataset as well as a the same plan recalculated using an intentionally incorrect beam model also all passed the 7% and 4 mm DTA criteria. Additionally, we did not identify any relationships between dosimetric accuracy and our measures of complexity or beam matching.

We performed TLD absolute point dose measurements and compared the results to the expected dose calculated by the TPS. While we found better than 7% agreement in all TLD within the PTVs, measurements made using Plan 3 and Plan 6 on the baseline machine had noticeably worse agreement than any other treatment delivery. Plan 3 is simpler than Plan 6, as demonstrated in Table 3.2, however, these two plans have the highest number of MU/segment with 28 and 32, respectively. The plan with the next largest number of MU/segment is Plan 1, with 27 MU/segment. Plan 1 did not have significantly different TLD results than any of the remaining plans, therefore we are unable to say definitively whether an increased number of MU/segment influenced the absolute point dose measurement agreement with calculation. Increased number of MU/segment would not intuitively decrease the accuracy of a dose calculation though, as it better resembles the field of a convention 3D conventional radiotherapy (CRT) treatment. However, it could be the case that particularly small segments that are prone to more inaccuracies are utilizing more MU, which could lead to differences between the measurement and calculation. However,

the smallest segment allowed in the optimization of Plan 3 was not particularly small at 2.45 X 2.45 cm^2. Increased MU with very small segments could decrease the accuracy of the dose calculation due to the increased MLC transmission and leakage and hence dependence on the TPS correction factors for each of these effects.

  We performed radiochromic film measurements to analyze the planar dose measurement to calculation agreement with dose profiles and DTA. From these two analyses, we could see that for each plan delivery of increasing complexity, the delivered dose had a visually steeper gradient between the primary PTV and the OAR than calculated through the center of the primary PTV. This was visually evident on the anterior-posterior dose profiles from the axial films and the positive average DTAs. The average DTA for each delivery was less than or equal to 3 mm, with Plan 6 having the smallest average DTA of 1 mm. This is interesting because Plan 6 had the poorest absolute dose agreement. The increased complexity appears to not lead to dosimetric errors, but can lead to sharper dose gradients that are planned on average. Another interesting observation resulting from the DTA measurements is that the baseline plan delivery measurement matched slightly better with the treatment plan recalculated using the incorrect beam model than with the calculation performed with the correct beam model. The Trilogy machine had the smallest DTA for the mismatched machine beam dosimetry data measurements of 1 mm. None of these planar dose measurements results indicate any trend.

  We also performed several gamma index analyses on each dose delivery to evaluate the overall agreement with the planned treatment dose distribution. All plans with the exception of Plan 3 performed well using a ±7%/4 mm gamma index analysis, with the percent of pixels meeting the criteria being approximately 90% or better in each case. As mentioned in Chapter 3, Plan 3 consistently had poor gamma analysis pass rates and in examining the distribution of gamma index values in Figure 3.26, Figure 3.27,Figure 3.28, and Figure 3.29, it can be seen that in addition to the area posterior to the primary PTV where most plans begin to fail, areas surrounding and within both the primary and secondary PTVs also failed. There is no obvious or simple explanation as to why the plan 3 irradiation resulted in poorer dosimetric accuracy than the other plans.

This work was based on the auditing and credentialing system used by the RPC, an internationally known group that audits over 1900 facilities. All of the phantom irradiations were performed following the same instructions given to institutions wishing to be credentialed for IMRT clinical trials. All of the above dosimetric analyses were performed in exactly the same manner as used by the RPC. This analysis process is well established and results have undergone extensive in-house QA and validation and are accurate and consistent. The impetus behind conducting this particular study was to try and understand some of the reasons why many institutions wishing to be credentialed to use IMRT in clinical trials fail the IMRT H&N phantom irradiation.

Although it has been speculated that increased complexity can degrade IMRT treatment plan delivery in several ways, this was not shown in our study. Increased fluence map complexity is suspected to have a significant effect on delivery accuracy. Giorgia et al demonstrated that less smooth fluence maps, i.e. more complex, have poorer agreement between calculation and delivery [3]. Mohan et al showed the increased dependence that more complex plans have on dose calculation corrections that are not entirely accurate. In addition, Mohan et al showed that sliding window IMRT plans with lower MU, i.e. more simple, had better agreement between calculation and delivery than those with higher [6]. There are many different parameters involved in the delivery of IMRT treatments that are machine, TPS, and user dependent. Because of these numerous dependencies, IMRT delivery can vary from institution to institution even though the sites might have similar machines and TPSs. A distinct possibility and reason that we did not observe any of the postulated errors in our experiment at MDACC is that the resources available at MDACC have minimized the potential errors, Performance of this same study at another institution or group of institutions might yield a very different result than what we observed. There are a plethora of factors that affect the delivery accuracy of an IMRT treatment and each of these may be regulated by different methods or held to different standards at different institutions. This is the nature of a user dependent dose delivery system.

As mentioned before, there are several steps within the IMRT treatment planning process and specifically dose calculation where possible errors can arise. Different dose calculations algorithms are utilized throughout the radiotherapy community and each may

implement a different approach to estimating the dose distribution delivered, bringing different levels of calculation accuracy. With increased treatment plan complexity, the certainty of the dose calculation can be decreased due to increased reliance on the MLC leakage and transmission factors as well as increased complexity of the buildup dose (Li)(Hsu).The resolution and size of a dose calculation grid can affect the accuracy of a dose calculation. Also of importance in the TPS is the beam model and how accurately it represents the true beam characteristics of the linac delivering the IMRT treatment. Specific points of question in the beam model include tongue-and-groove effects, MLC leakage and transmission, and penumbra modeling. Each TPS may use different information to form these beam models and judgment of different medical physicists as to the appropriateness of the resulting beam model may also differ between different institutions. Each institution is responsible for measuring and inputting this information correctly and ensuring that the beam model used for dose calculations represents their machines well. At MDACC, beam modeling is of paramount importance and extensive work is performed to ensure accuracy of beam modeling, matching, and consistency through verification measurements and independent dose calculations.

Another key component to achieve accurate dose delivery, in addition to the dose calculation, is the set up of the patient for an IMRT treatment due to the potential steep dose gradients the IMRT may create to deliver the high target doses while minimizing the doses to the surrounding normal tissues. Although the IMRT treatment process is simplified with the anthropomorphic phantom as compared to a live patient in several ways, specifically for set up due to the lack of intra- and inter-fractional external and internal motion and other issues, accurate set up of the phantom is nonetheless critical. To our knowledge and as demonstrated by the reproducibility of the phantom irradiations for each plan and the results of our experiments, our set up was consistent for each irradiation. Care was taken to align the phantom in the same way for each delivery. The alignment of the lasers with the true isocenter of the linac gantry was checked on several occasions. When a number of different individuals participate in dose delivery, variability in the set up of the phantom can be introduced whereas in this study the setup of each phantom was performed consistently by one person. In addition to the human factor, consistency and accuracy are required of the

mechanical features of the machine used to set up, including the lasers, optical distance indicator (ODI), couch position, etc. These are all possible factors that can contribute to why many institutions fail the IMRT H&N phantom irradiation test.

Most likely, one of the most important IMRT dose delivery components, that can contribute to an inaccurate IMRT dose delivery is the MLC. The uncertainty of deliverability of a treatment plan increases as the segments become smaller, more complex and greater in number, as in a more complex IMRT plan. Different institutions can have different linacs from different manufacturers and different MLC models. As mentioned before, the issue of dose calculation and beam modeling is important and the MLC are involved heavily in this. The effects of the leaf ends, tongue-and-groove, and transmission must be modeled correctly. Additionally, the positional accuracy of the MLC plays a large role in IMRT cases because numerous apertures are used and the MLC define not only the edges of the fields, but shape the non-uniform fluence map. MLC positional and dose delivery errors can be due to issues with the MLC controller and leaf motion errors are likely caused by limitations in the feedback control mechanism that controls the MLC and accelerator beam output [24]. If an institution does not maintain an appropriate preventive maintenance schedule or QA program for the MLCs then the possibility of inaccurate MLC positioning increases. Because of the importance of the MLC in IMRT delivery, its potential for contributing errors to dose delivery remains high.

Though comparable literature investigating IMRT dose delivery is limited, our study tends to agree with the few reported findings available. Other studies investigating the role of treatment plan complexity were detailed in earlier sections of this report, including those performed by McNiven *et al* and Giorgia *et al*. Similar to the results of the study by McNiven *et al.* in which the MCS was formulated, we did not find a direct relationship between MCS and gamma analysis results[2]. Giorgia *et al* utilized the modulation index (MI) created by Webb and found a threshold level of complexity that could ensure deliverability but again did not find a direct relationship between increasing complexity and treatment delivery accuracy[3].

Although it was not an objective of this study, we confirmed that treatment plans of comparable quality can have a wide range of levels of complexity. Craft *et al* observed that

while an inherent level of complexity is required to achieve conformal dose coverage with IMRT, generally the number of MU used can be significantly reduced without effects on the plan quality. Jiang *et al* saw that treatment plans may be created with nine segments per beam or less without reducing plan quality as compared to those with more, complimenting the idea that plans of similar quality can be achieved with various levels of complexity.

Limitations of this study mainly include the lack of variety in TPS, hardware, and linacs used to deliver IMRT. All treatments were planned with Pinnacle v.8m by the same individual. All treatments were delivered on Varian linacs with 120-leaf Millennium MLC at MDACC where consistent commissioning and QA is performed by experienced physicists. The set up was performed by the same individual for each irradiation. Therefore, the variability associated with the RPC's IMRT H&N phantom irradiation failure rate, does not exist within the irradiation conditions of this study.

Additional limitations to this study involve the measurement methodology. The RPC H&N IMRT phantom is anthropomorphic in shape and contains tissue equivalent structures that represent those in the human body. However, one must keep in mind that true human anatomy is much more complex and diverse than this phantom and therefore treatment plans for patient delivery may become even more complex than those seen in this study with the phantom. So, while this study reflects perfectly the conditions of those being credentialed by the RPC, it is important to remember that in the clinic these effects may be even greater. If we are seeing approximately a 20-30% failure rate on the simple geometry of a phantom, it is questionable and frightening what may be happening in the clinic.

4.1.1   Conclusions

In conclusion, our hypothesis that increased IMRT treatment plan complexity or the use of improperly matched accelerator dosimetry data can lead to errors in head and neck IMRT deliver, as measured with the RPC's H&N phantom, that result in differences between the measured and planned dose distributions was not supported. No variation in dosimetric accuracy with increased treatment plan complexity or with improper beam matching was seen. All deliveries of all treatment plans on each machine passed the RPC credentialing criteria. When compared to institutions passing the IMRT H&N credentialing, the average

percent of pixels passing the gamma analysis of all but one plan was within a standard deviation.

4.2 Future Work

The results of this study indicate a need for further research into the cause of failures in treatment delivery to the RPC's head and neck IMRT phantom. Further examination of the effects of increased treatment plan complexity and beam matching on IMRT delivery at other institutions under various is conditions warranted. IMRT is now a widely used technique and its inherent complexity demand increased attention to determine proper safety measures.

While it is intuitive that simple measures such as treatment plan complexity could identify treatment plans of higher sensitivity to errors of all sorts, it is crucial to investigate all components of possible error. AAPM Task Group 100 has performed a failure modes and effects analysis (FMEA) on IMRT at one institution and physical evaluation of many of the indicated failure modes would be very useful. An FMEA consists of identification of all components of a process (IMRT treatment), ways in which each component can fail, the likelihood and detectability of these failures, the consequences of these failures, and the severity of the consequences. While not all failure modes identified in the treatment of a patient may apply to that of a phantom, there are several cases that do. For example, for IMRT delivery there exists many possible failure modes that have been mentioned in this discussion. Linac hardware failure, such as incorrect beam output, can lead to consequences such as a wrong dose or wrong dose distribution. Inaccurate MLC motions and other factors considered in common QA procedures can lead to these same delivery issues. An FMEA based on expert experience and opinion can assist a particular institution identify the critical elements to accurate dose delivery hat need to be monitored frequently. Which of these processes is leading to failure in the RPC credentialing process? That is yet to be determined and it extremely important in order to continue not only consistent and comparable clinical trials, but also to identify possible causes of failure jeopardizing the safety of all patients.

Furthermore, IMRT QA was not performed on these treatment plans, but investigation into the ability of various IMRT QA methods to detect errors and predict failure of an audit with and RPC phantom would be useful. Investigation into any relationship between

treatment plan complexity and IMRT QA results would also be interesting and potentially useful in the creation of a standard IMRT QA method and acceptance criteria.

Plan 1

Objectives					IMRT Parameters	
ROI	Type	Target cGy	*% Volume*	Weight	Optimization Type	DMPO
PTV_66	UD	660		98	Allow jaw motion/Split beam?	No
PTV_54	UD	540		65	Max iterations	12
CORD	Max Dose	365		60	Convolution dose iteration	5
Normal tissue	Max DVH	245	18	20	Stopping tolerance	1.00E-05
Normal tissue	Max DVH	330	8	20	Min segment MUs	1
Normal tissue	Max DVH	450	2	20	Max number of segments	54
CORD expanded	Max Dose	490		45	Min segment area	6
PTV_66	Min Dose	660		100	Leaf/jaw overlap	1
					Overlap Distance	2

Plan 2

Objectives					IMRT Parameters	
ROI	Type	Target cGy	*% Volume*	Weight	Optimization Type	DMPO
PTV_66	UD	660		85	Allow jaw motion/Split beam?	Yes
PTV_54	UD	540		60	Max iterations	12
CORD	Max Dose	365		50	Convolution dose iteration	5
Normal tissue	Max DVH	245	18	20	Stopping tolerance	1.00E-05
Normal tissue	Max DVH	330	8	20	Min segment MUs	1
Normal tissue	Max DVH	450	2	20	Max number of segments	135
CORD expanded	Max Dose	495		45	Min segment area	0.5

ROI	Type	Target cGy	% Volume	Weight		
PTV_66	Min Dose	660		100	Leaf/jaw overlap	0.2
					Overlap Distance	2

Plan 3

Objectives					IMRT Parameters	
ROI	**Type**	**Target cGy**	**% Volume**	**Weight**	Optimization Type	DMPO
PTV_66	UD	660		94	Allow jaw motion/Split beam?	No
PTV_54	UD	540		60	Max iterations	25
CORD	Max Dose	370		55	Convolution dose iteration	4
Normal tissue	Max DVH	300	22	10	Stopping tolerance	1.00E-04
Normal tissue	Max DVH	385	10	10	Min segment MUs	5
Normal tissue	Max DVH	465	5	10	Max number of segments	54
CORD expanded	Max Dose	500		45	Min segment area	6
PTV_66	Min Dose	660		100	Leaf/jaw overlap	0.5
					Overlap Distance	2

Plan 4

Objectives					IMRT Parameters	
ROI	**Type**	**Target cGy**	**% Volume**	**Weight**	Optimization Type	DMPO
PTV_66	UD	660		87	Allow jaw motion/Split beam?	No
PTV_54	UD	540		60	Max iterations	20
CORD	Max Dose	365		50	Convolution dose iteration	5
Normal tissue	Max DVH	245	18	25	Stopping tolerance	0.00E+00
Normal tissue	Max DVH	330	8	25	Min segment MUs	1
Normal tissue	Max DVH	450	2	25	Max number of segments	90
CORD expanded	Max Dose	495		45	Min segment area	4

ROI	Type	Target cGy	% Volume	Weight	IMRT Parameters	
PTV_66	Min Dose	660		100	Leaf/jaw overlap	0.5
Hot Spot	Max Dose	725		50	Overlap Distance	2

Plan 5

Objectives					**IMRT Parameters**	
ROI	**Type**	**Target cGy**	*%* **Volume**	**Weight**	Optimization Type	DMPO
PTV_66	UD	660		95	Allow jaw motion/Split beam?	Yes
PTV_54	UD	540		70	Max iterations	50
CORD	Max Dose	365		65	Convolution dose iteration	12
Normal tissue	Max DVH	220	20	40	Stopping tolerance	0
Normal tissue	Max DVH	300	8	40	Min segment MUs	0.5
Normal tissue	Max DVH	430	2	40	Max number of segments	225
CORD expanded	Max Dose	470		53	Min segment area	0.5
PTV_66	Min Dose	660		100	Leaf/jaw overlap	0.2
Hot Spot12	Max Dose	690		85	Overlap Distance	2
Decrease Norm	Max Dose	570		20		

Plan 6						
Objectives					**IMRT Parameters**	
ROI	**Type**	**Target cGy**	*%* **Volume**	**Weight**	Optimization Type	DMPO
PTV_66	UD	660		100	Allow jaw motion/Split beam?	Yes
PTV_54	UD	540		75	Max iterations	50
CORD	Max Dose	350		85	Convolution dose iteration	12
Normal tissue	Max DVH	200	15	25	Stopping tolerance	0
Normal tissue	Max DVH	300	8	25	Min segment MUs	0.1

ROI	Type	Target cGy	% Volume	Weight	IMRT Parameters	
Normal tissue	Max DVH	400	2	25	Max number of segments	90
CORD expanded	Max Dose	480		60	Min segment area	0.1
PTV_66	Min Dose	660		100	Leaf/jaw overlap	0.5
PTV66 concave	Min Dose	665		30	Overlap Distance	2
Hot Spot 7	Max Dose	690		50	Dose Grid	0.3
Normal tissue	Max Dose	650		60		
PTV_66	Max Dose	710		50		
PTV54 Push	Min Dose	540		50		
DoseShape 6	Max Dose	500		25		
DoseShape 6	Max DVH	475	40	20		
Dose Shape7	Max Dose	550		20		
Dose Shape7	Max DVH	540	1	25		
Dose Shape8	Max DVH	540	1	20		
Dose Shape8	Max Dose	550		25		
Dose Shape8	Max DVH	500	10	20		
Push662	Min Dose	660		90		
Hot Spot8	Max Dose	690		50		

Plan 7						
Objectives					**IMRT Parameters**	
ROI	**Type**	**Target cGy**	**% Volume**	**Weight**	Optimization Type	DMPO
PTV_66	UD	660		100	Allow jaw motion/Split beam?	Yes
PTV_54	UD	540		80	Max iterations	200
CORD	Max	355		70	Convolution dose	24

ROI	Type	Target cGy	% Volume	Weight		
	Dose				iteration	
Normal tissue	Max DVH	155	18	50	Stopping tolerance	0
Normal tissue	Max DVH	240	8	50	Min segment MUs	0.1
Normal tissue	Max DVH	330	2	50	Max number of segments	225
CORD expanded	Max Dose	460		55	Min segment area	0.25
PTV_66	Min Dose	660		100	Leaf/jaw overlap	0.2
Normal Tissue	Max Dose	600		50	Overlap Distance	2
Hot Spot Kry	Max Dose	690		50	Dose Grid	0.3
Bonus 7	Max DVH	550	2	20		
Bonus 7	Max DVH	450	10	1		

Plan 8						
Objectives					**IMRT Parameters**	
ROI	**Type**	**Target cGy**	**% Volume**	**Weight**	Optimization Type	DMPO
PTV_66	UD	660		100	Allow jaw motion/Split beam?	Yes
PTV_54	UD	540		75	Max iterations	200
CORD	Max Dose	355		85	Convolution dose iteration	12
Normal tissue	Max DVH	245	18	25	Stopping tolerance	1.00E-05
Normal tissue	Max DVH	330	8	25	Min segment MUs	0.1
Normal tissue	Max DVH	450	2	25	Max number of segments	216
CORD expanded	Max Dose	480		75	Min segment area	0.1
PTV_66	Min Dose	660		100	Leaf/jaw overlap	0.5
Hot Spot	Max Dose	695		70	Overlap Distance	2
Hot Spot 2	Max Dose	695		70		

PTV66 concave	Min Dose	665		50
Hot Spot 4	Max Dose	690		45
Extra	Max Dose	200		20
Extra	Max DVH	150	70	20
Extra2	Max Dose	210		20
Extra2	Max DVH	182	63	18
Extra3	Max DVH	160	68	22
Extra3	Max DVH	100	85	15
Dose Shape3	Max DVH	540	10	18
Dose Shape4	Max DVH	525	5	20
Dose Shape4	Max Dose	560		21
Dose Shape5	Max DVH	660	12	18
Dose Shape5	Max Dose	670		22
Extra4	Max Dose	200		26
Hot Spot 7	Max Dose	690		35
Push66	Min Dose	660		28
Dose Shape 6	Max Dose	500		20
Dose Shape 6	Max DVH	400	50	20
Dose Shape 7	Max DVH	525	2	18
Dose Shape7	Max Dose	550		25
PTV54 Push	Min Dose	540		35
Push 66 2	Min Dose	660		35

Hot Spot8	Max Dose	690		20
Hot Spot 12	Max Dose	690		22
Dose Shape9	Max DVH	540	20	20

Appendix B Absolute Point Dose Measurements

TLD #	TLD position
1	Primary PTV Superior Anterior
2	Primary PTV Inferior Anterior
3	Primary PTV Superior Posterior
4	Primary PTV Inferior Posterior
5	Secondary PTV Superior
6	Secondary PTV Inferior
7	OAR Superior
8	OAR Inferior

Table B.1 TLD position numbering

Plan 1							
	Measured Dose			**Average (cGy)**	**Planned Dose (cGy)**	**% Difference**	**Std Dev**
TLD #	**1 (cGy)**	**2 (cGy)**	**3 (cGy)**				
1	674.5	652.6	682.7	669.9	688.7	2.7%	2.3%
2	681.9	663.6	652.6	666.0	687.1	3.1%	2.2%
3	680.7	684.1	697.6	687.5	686.9	-0.1%	1.3%
4	692.5	686.3	677.0	685.3	684.6	-0.1%	1.1%
5	555.5	548.3	548.5	550.8	564.2	2.4%	0.7%
6	559.7	549.7	546.4	552.0	564.5	2.2%	1.2%
7	313.1	316.3	323.9	317.8	347.6	8.6%	1.6%
8	309.9	310.4	305.3	308.5	343.6	10.2%	0.8%

Table B.2 Absolute doses measured with eight TLD for three deliveries of treatment Plan 1 on the baseline machine, corresponding doses calculated with the TPS and the percent difference

Plan 2						
TLD #	Measured Dose			Average (cGy)	Planned Dose (cGy)	% Difference	Std Dev
	1 (cGy)	2 (cGy)	3 (cGy)				
1	678.0	671.4	668.7	672.7	690.3	2.5%	0.7%
2	676.4	667.0	656.1	666.5	689.8	3.4%	1.5%
3	684.6	688.8	681.1	684.8	680.5	-0.6%	0.6%
4	694.2	679.8	680.1	684.7	678.8	-0.9%	1.2%
5	556.5	533.5	535.1	541.7	563.4	3.9%	2.3%
6	566.4	550.1	544.7	553.7	566	2.2%	2.0%
7	336.4	344.5	340.9	340.6	364.6	6.6%	1.1%
8	342.7	335.4	333.8	337.3	362.3	6.9%	1.3%

Table B.3 Absolute doses measured with eight TLD for three deliveries of treatment Plan 2 on the baseline machine, corresponding doses calculated with the TPS and the percent difference

Plan 3						
TLD #	Measured Dose			Average (cGy)	Planned Dose (cGy)	% Difference	Std Dev
	1 (cGy)	2 (cGy)	3 (cGy)				
1	649.4	641.7	653.0	648.0	687.2	5.7%	0.8%
2	653.4	642.3	635.7	643.8	687.2	6.3%	1.3%
3	685.0	665.7	672.2	674.3	691.9	2.5%	1.4%
4	681.4	659.0	659.5	666.6	691.2	3.6%	1.9%
5	534.2	523.8	523.6	527.2	562.4	6.3%	1.1%
6	542.2	526.8	532.6	533.9	564.7	5.5%	1.4%
7	280.3	282.8	278.2	280.4	316	11.3%	0.7%
8	272.5	267.3	261.9	267.2	302.6	11.7%	1.8%

Table B.4 Absolute doses measured with eight TLD for three deliveries of treatment Plan 3 on the baseline machine, corresponding doses calculated with the TPS and the percent difference

Plan 4							
TLD #	**Measured Dose**			**Average (cGy)**	**Planned Dose (cGy)**	**% Difference**	**Std Dev**
	1 (cGy)	**2 (cGy)**	**3 (cGy)**				
1	657.4	664.1	688.1	669.9	685.5	2.3%	2.4%
2	674.2	672.1	657.8	668.0	689.2	3.1%	1.3%
3	692.8	686.7	679.4	686.3	689	0.4%	1.0%
4	709.1	708.3	678.5	698.6	689.9	-1.3%	2.5%
5	553.4	546.6	546.3	548.8	564.5	2.8%	0.7%
6	556.3	552.5	554.4	554.4	563.1	1.5%	0.3%
7	284.4	285.8	328.1	299.5	317.7	5.7%	7.8%
8	273.4	267.7	298.0	279.7	299.4	6.6%	5.4%

Table B.5 Absolute doses measured with eight TLD for three deliveries of treatment Plan 4 on the baseline machine, corresponding doses calculated with the TPS and the percent difference

Plan 5							
TLD #	**Measured Dose**			**Average (cGy)**	**Planned Dose (cGy)**	**% Difference**	**Std Dev**
	1 (cGy)	**2 (cGy)**	**3 (cGy)**				
1	663.5	654.7	661.5	659.9	659.2	-0.1%	0.7%
2	669.5	672.5	637.5	659.8	658.8	-0.2%	2.9%
3	683.3	678.8	682.0	681.4	663.4	-2.7%	0.3%
4	690.3	685.1	664.5	680.0	662.7	-2.6%	2.1%
5	553.2	543.5	548.6	548.4	539.1	-1.7%	0.9%
6	557.4	546.1	543.8	549.1	541.3	-1.4%	1.3%
7	256.8	253.2	263.9	258.0	303	14.9%	1.8%
8	274.2	273.1	275.1	274.1	290.1	5.5%	0.3%

Table B.6 Absolute doses measured with eight TLD for three deliveries of treatment Plan 5 on the baseline machine, corresponding doses calculated with the TPS and the percent difference

Plan 6							
	Measured Dose			**Average (cGy)**	**Planned Dose (cGy)**	**% Difference**	**Std Dev**
TLD #	**1 (cGy)**	**2 (cGy)**	**3 (cGy)**				
1	658.8	652.6	649.6	653.7	686.4	4.8%	0.7%
2	657.7	631.6	627.0	638.8	683.2	6.5%	2.4%
3	668.0	649.4	663.6	660.3	699.8	5.6%	1.4%
4	670.9	651.3	649.7	657.3	698.7	5.9%	1.7%
5	544.7	529.6	527.2	533.8	560.3	4.7%	1.7%
6	547.2	533.0	522.2	534.1	560.6	4.7%	2.2%
7	249.5	247.8	253.1	250.1	275.7	9.3%	1.0%
8	235.3	236.1	237.7	236.4	262.1	9.8%	0.4%

Table B.7 Absolute doses measured with eight TLD for three deliveries of treatment Plan 6 on the baseline machine, corresponding doses calculated with the TPS and the percent difference

Plan 7							
	Measured Dose			**Average (cGy)**	**Planned Dose (cGy)**	**% Difference**	**Std Dev**
TLD #	**1 (cGy)**	**2 (cGy)**	**3 (cGy)**				
1	637.9	631.0	635.7	634.9	660.6	3.9%	0.5%
2	644.2	640.2	624.7	636.4	655.7	2.9%	1.6%
3	659.1	648.2	650.4	652.6	666.9	2.1%	0.9%
4	655.7	658.3	636.9	650.3	671.4	3.1%	1.7%
5	536.5	533.7	531.0	533.7	542.3	1.6%	0.5%
6	530.1	531.1	536.8	532.7	549.6	3.1%	0.7%
7	212.1	218.8	218.7	216.6	250.8	13.6%	1.5%
8	217.1	218.7	217.0	217.6	248.1	12.3%	0.4%

Table B.8 Absolute doses measured with eight TLD for three deliveries of treatment Plan 7 on the baseline machine, corresponding doses calculated with the TPS and the percent difference

Plan 8							
	Measured Dose			**Average (cGy)**	**Planned Dose (cGy)**	**% Difference**	**Std Dev**
TLD #	**1 (cGy)**	**2 (cGy)**	**3 (cGy)**				
1	657.5	665.3	677.2	666.6	684.9	2.7%	1.4%
2	701.3	681.0	672.7	685.0	683.8	-0.2%	2.2%
3	698.5	705.4	707.3	703.7	689	-2.1%	0.7%
4	706.6	711.4	699.0	705.7	688.2	-2.5%	0.9%
5	564.9	553.2	549.8	555.9	565.8	1.7%	1.4%
6	538.1	522.1	515.9	525.4	545.8	3.7%	2.1%
7	218.9	212.2	214.2	215.1	261.7	17.8%	1.3%
8	213.1	203.1	204.2	206.8	248.7	16.9%	2.2%

Table B.9 Absolute doses measured with eight TLD for three deliveries of treatment Plan 8 on the baseline machine, corresponding doses calculated with the TPS and the percent difference

2100 CD							
	Measured Dose			**Average (cGy)**	**Planned Dose (cGy)**	**% Difference**	**Std Dev**
TLD #	**1 (cGy)**	**2 (cGy)**	**3 (cGy)**				
1	661.6	657.9	677.9	665.8	685.5	2.9%	1.5%
2	666.3	679.3	692.4	679.3	689.2	1.4%	1.9%
3	677.5	684.9	698.3	686.9	689	0.3%	1.5%
4	700.5	692.0	708.5	700.3	689.9	-1.5%	1.2%
5	540.5	541.4	554.8	545.6	564.5	3.4%	1.4%
6	548.6	557.0	564.8	556.8	563.1	1.1%	1.4%
7	300.1	299.0	301.8	300.3	317.7	5.5%	0.4%
8	283.4	286.6	283.9	284.6	299.4	4.9%	0.6%

Table B.10 Absolute doses measured with eight TLD for three deliveries of treatment Plan 4 on another Varian 2100CD, corresponding doses calculated with the TPS and the percent difference

21EX							
TLD #	**Measured Dose**			Average (cGy)	Planned Dose (cGy)	% Difference	Std Dev
	1 (cGy)	2 (cGy)	3 (cGy)				
1	674.9	683.9	675.1	678.0	685.5	1.1%	0.8%
2	677.1	675.7	683.0	678.6	689.2	1.5%	0.6%
3	696.2	702.8	698.4	699.1	689	-1.5%	0.5%
4	708.5	713.8	699.4	707.2	689.9	-2.5%	1.1%
5	545.3	540.2	548.8	544.8	564.5	3.5%	0.8%
6	569.5	560.4	556.7	562.2	563.1	0.2%	1.2%
7	296.1	295.1	292.7	294.6	317.7	7.3%	0.5%
8	279.3	273.9	280.9	278.0	299.4	7.1%	1.2%

Table B.11 Absolute doses measured with eight TLD for three deliveries of treatment Plan 4 on a Varian 21EX, corresponding doses calculated with the TPS and the percent difference

Trilogy							
TLD #	**Measured Dose**			Average (cGy)	Planned Dose (cGy)	% Difference	Std Dev
	1 (cGy)	2 (cGy)	3 (cGy)				
1	693.8	692.9	688.9	691.9	685.5	-0.9%	0.4%
2	696.3	700.0	695.4	697.2	689.2	-1.2%	0.4%
3	699.2	707.2	712.4	706.3	689	-2.5%	1.0%
4	684.8	702.9	712.7	700.1	689.9	-1.5%	2.1%
5	557.9	559.0	557.4	558.1	564.5	1.1%	0.1%
6	564.9	572.5	567.5	568.3	563.1	-0.9%	0.7%
7	317.1	307.2	313.5	312.6	317.7	1.6%	1.6%
8	297.0	285.8	288.9	290.5	299.4	3.0%	1.9%

Table B.12 Absolute doses measured with eight TLD for three deliveries of treatment Plan 4 on another Varian Trilogy, corresponding doses calculated with the TPS and the percent difference

6 EX Beam Model							
TLD #	Measured Dose			Average (cGy)	Planned Dose (cGy)	% Difference	Std Dev
	1 (cGy)	2 (cGy)	3 (cGy)				
1	657.4	664.1	688.1	669.9	686.6	2.4%	2.4%
2	674.2	672.1	657.8	668.0	688.0	2.9%	1.3%
3	692.8	686.7	679.4	686.3	687.8	0.2%	1.0%
4	709.1	708.3	678.5	698.6	687.7	-1.6%	2.5%
5	553.4	546.6	546.3	548.8	562.9	2.5%	0.7%
6	556.3	552.5	554.4	554.4	561.5	1.3%	0.3%
7	284.4	285.8	328.1	299.5	313.4	4.5%	7.9%
8	273.4	267.7	298.0	279.7	295.0	5.2%	5.5%

Table B.13 Absolute doses measured with eight TLD for three deliveries of treatment Plan 4 on the baseline machine, corresponding doses calculated with the Varian 6EX beam model and the percent difference

Appendix C Dose Profiles
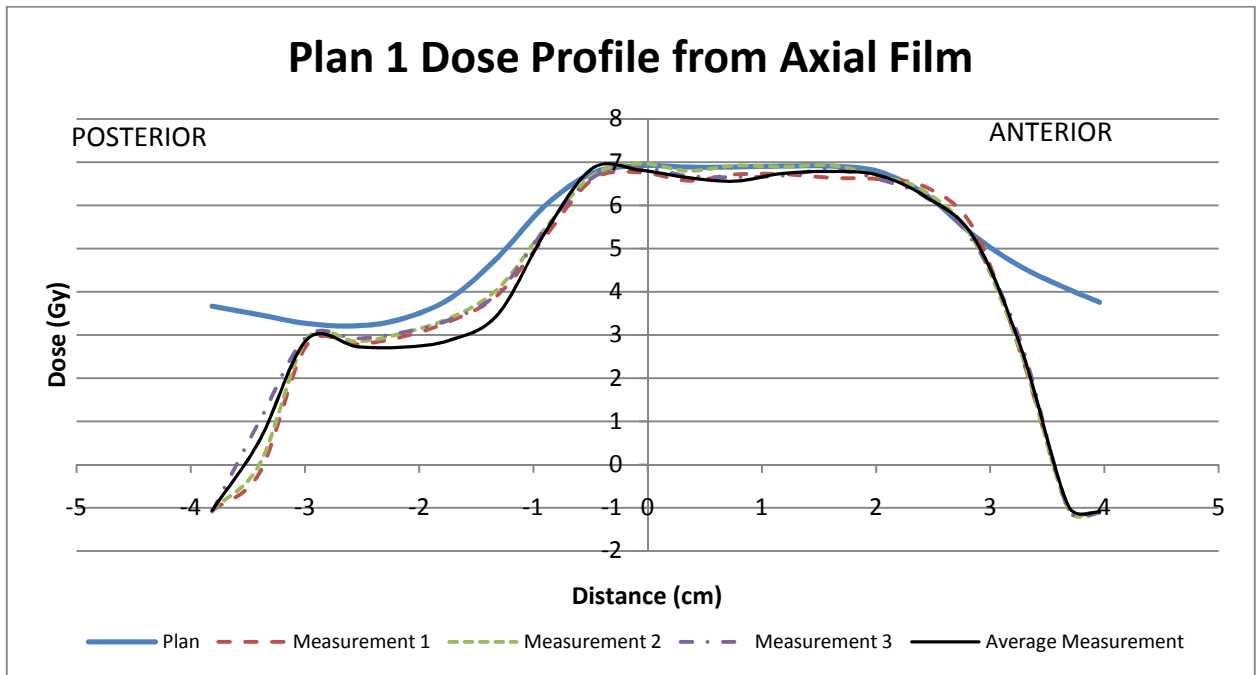
Figure C.1 Posterior-to-anterior dose profile of Plan 1 as planned by the TPS and measured with the three axial films
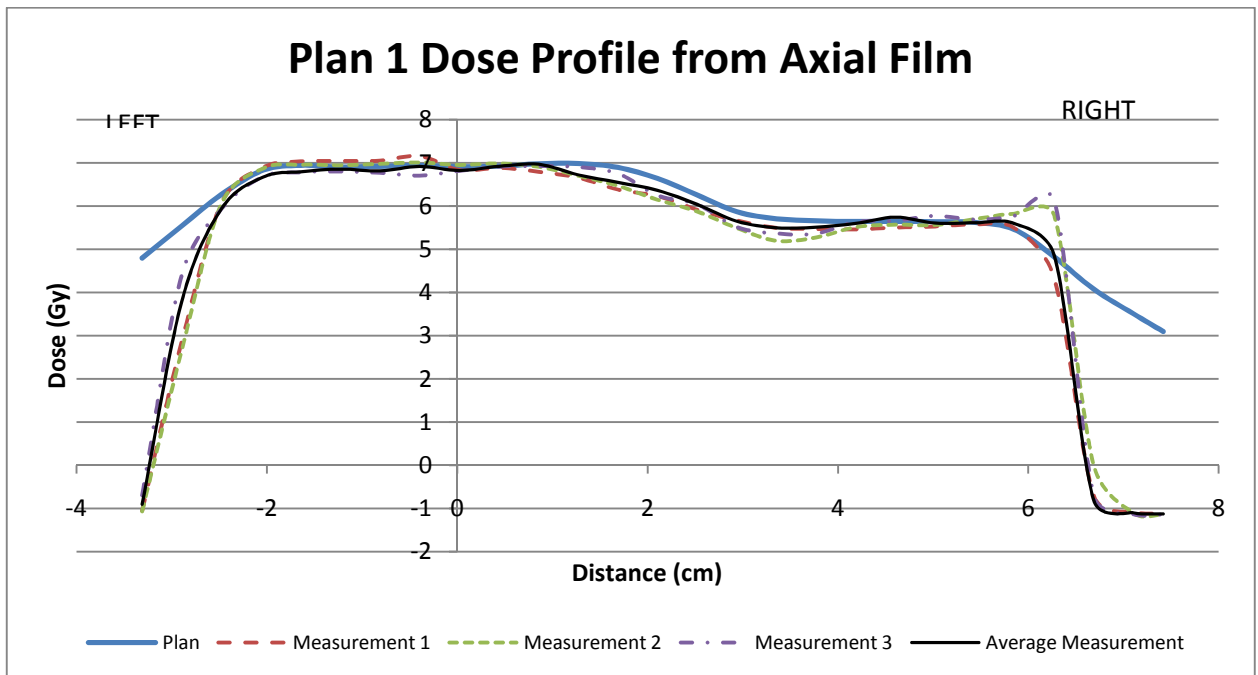
Figure C.2 Left-to-right dose profile of Plan 1 as planned by the TPS and measured by the three axial films

Plan 1 Dose Profile from Sagittal Film

INFERIOR

SUPERIOR

Y-axis: Dose (Gy)

X-axis: Distance (cm)

Plan — Measurement 1 — Measurement 2 — Measurement 3 — Average Measurement
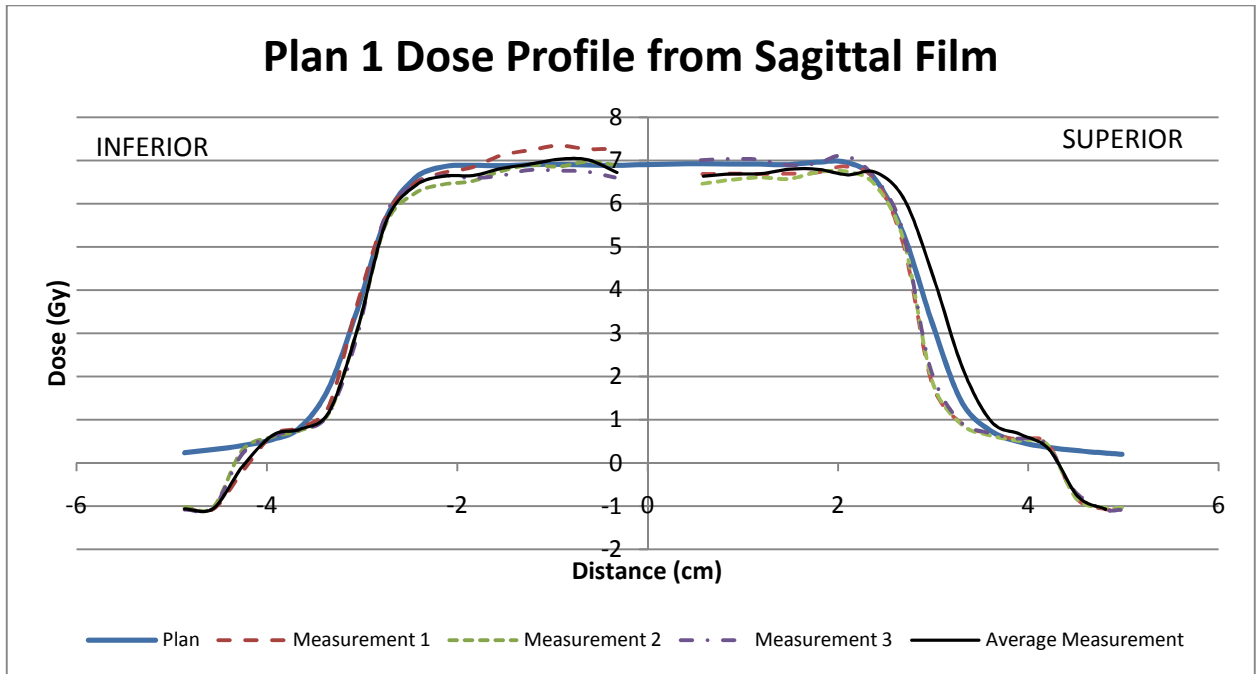
Figure C.3 Inferior-to-superior dose profile of Plan 1 as planned by the TPS and measured by the three sagittal films

Plan 2 Dose Profile from Axial Film

POSTERIOR

ANTERIOR

Y-axis: Dose (Gy)

X-axis: Distance (cm)

Plan — Measurement 1 — Measurement 2 — Measurement 3 — Average Measurement
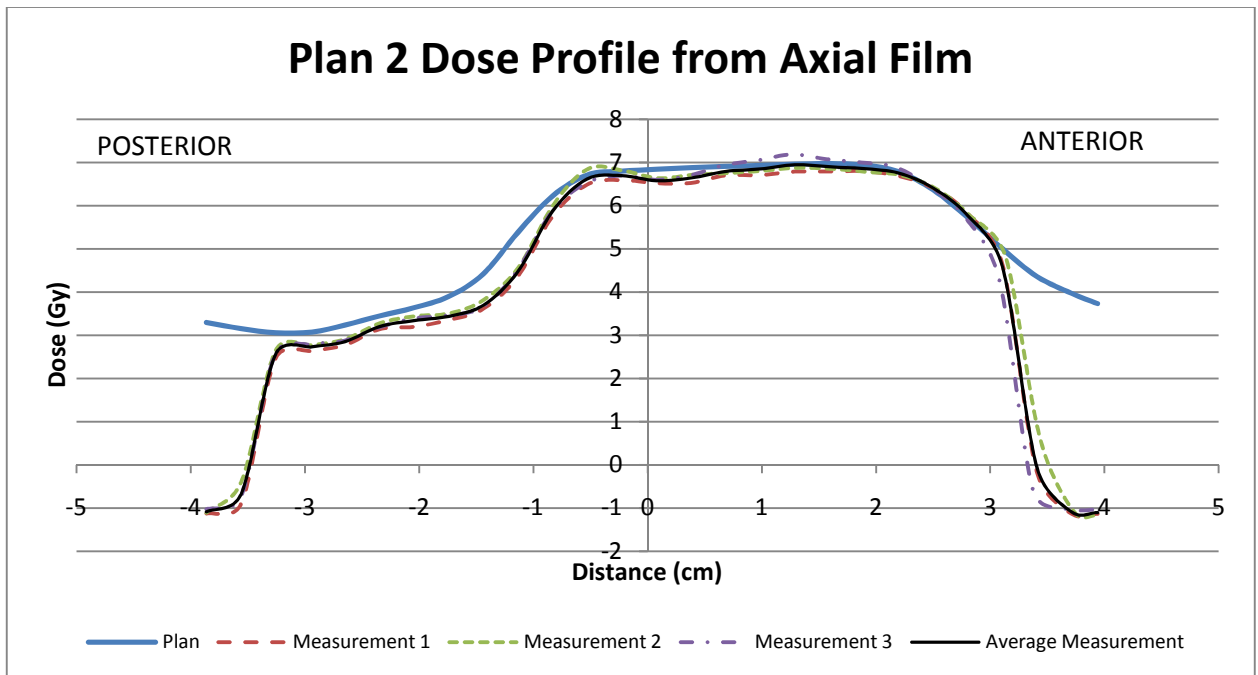
Figure C.4 Posterior-to-anterior dose profile of Plan 2 as planned by the TPS and measured with the three axial films

86
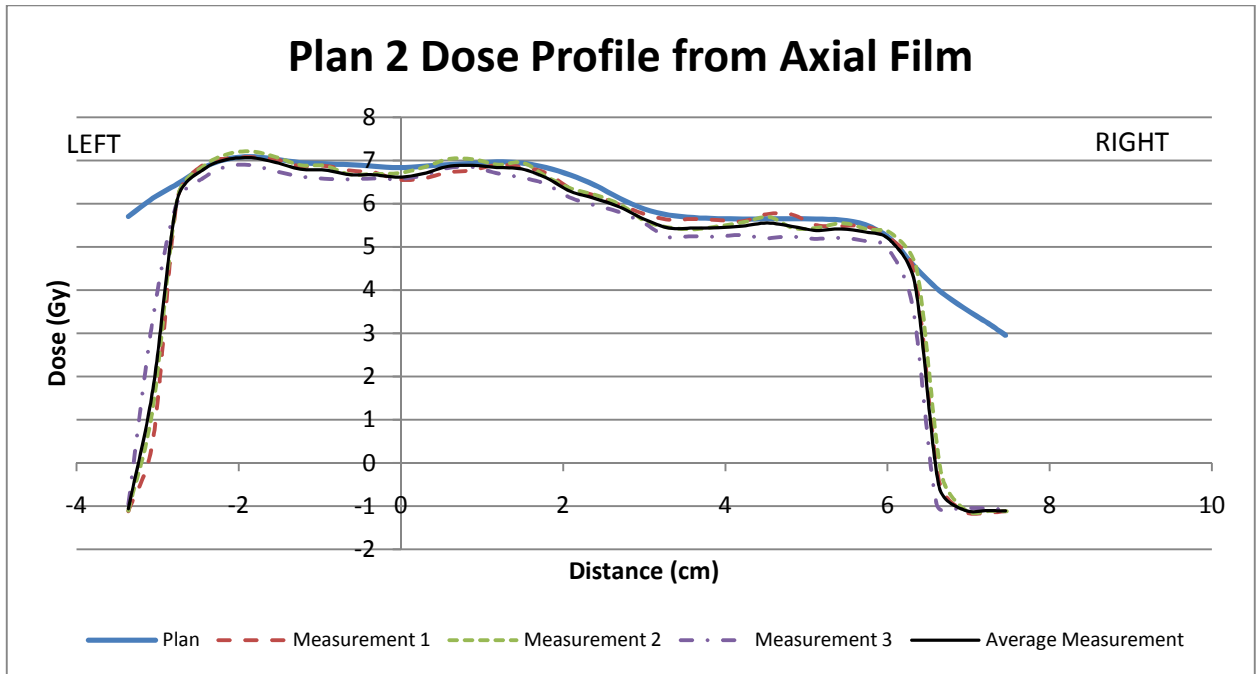
Figure C.5 Left-to-right dose profile of Plan 2 as planned by the TPS and measured by the three axial films
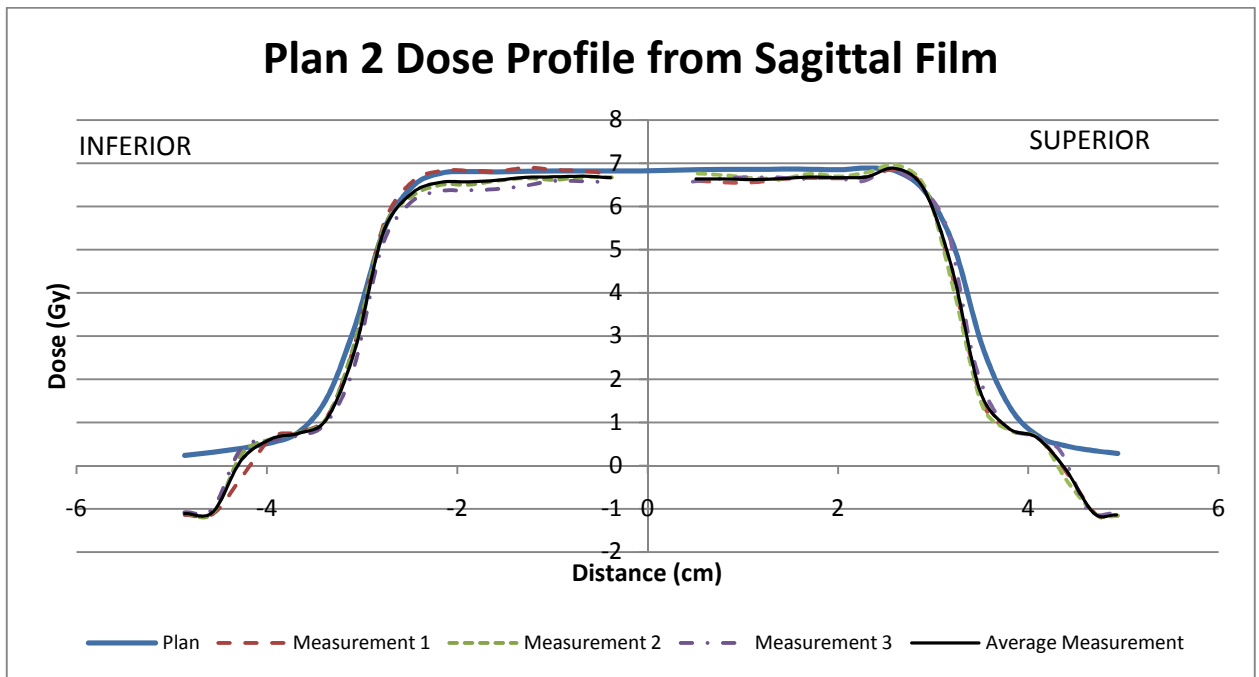
Figure C.6 Inferior-to-superior dose profile of Plan 2 as planned by the TPS and measured by the three sagittal films
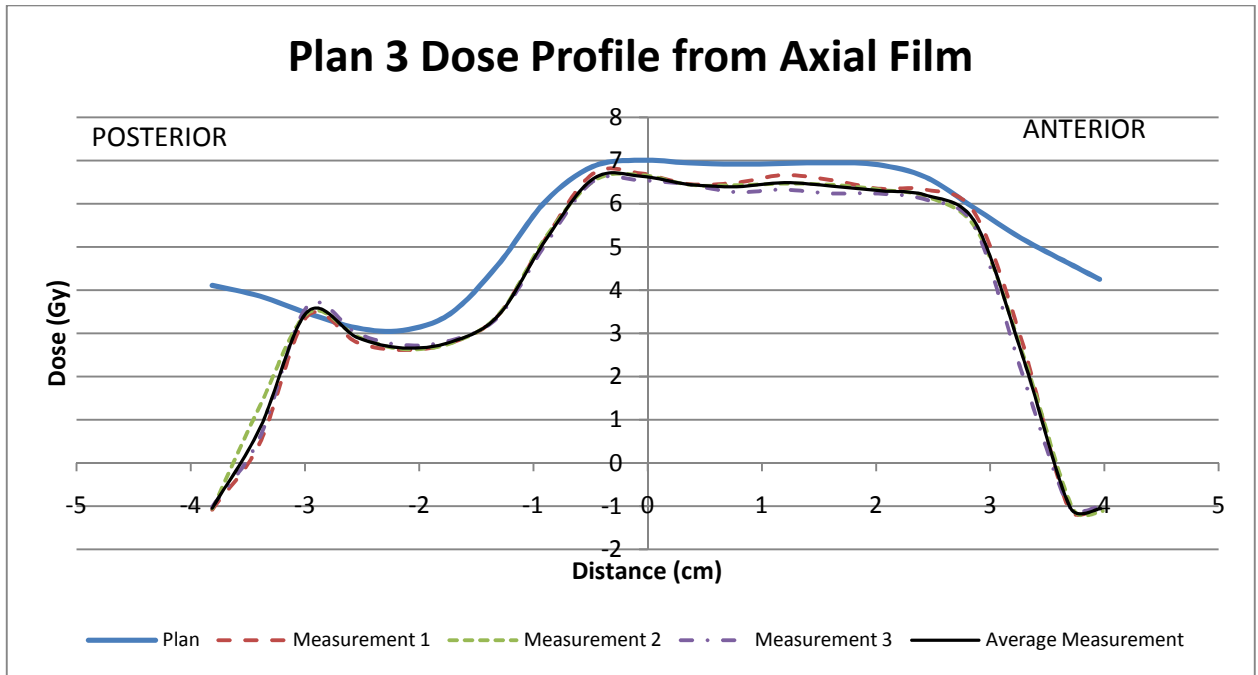
Figure C.7 Posterior-to-anterior dose profile of Plan 3 as planned by the TPS and measured with the three axial films
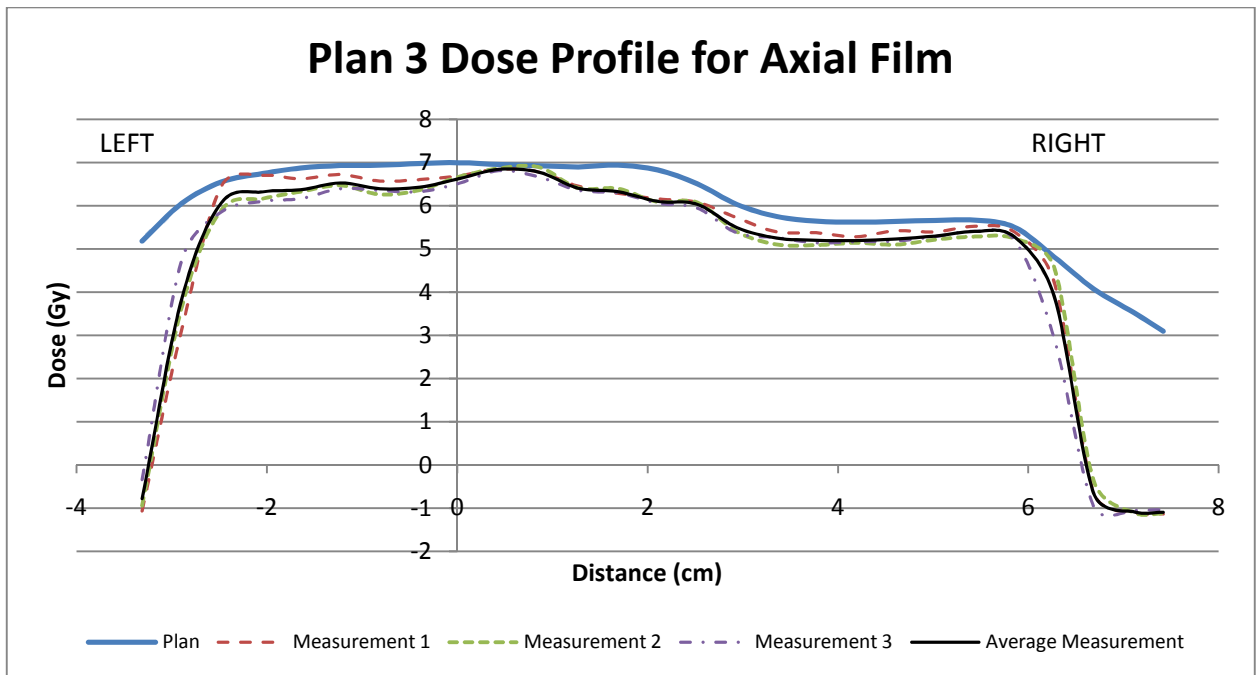
Figure C.8 Left-to-right dose profile of Plan 3 as planned by the TPS and measured by the three axial films
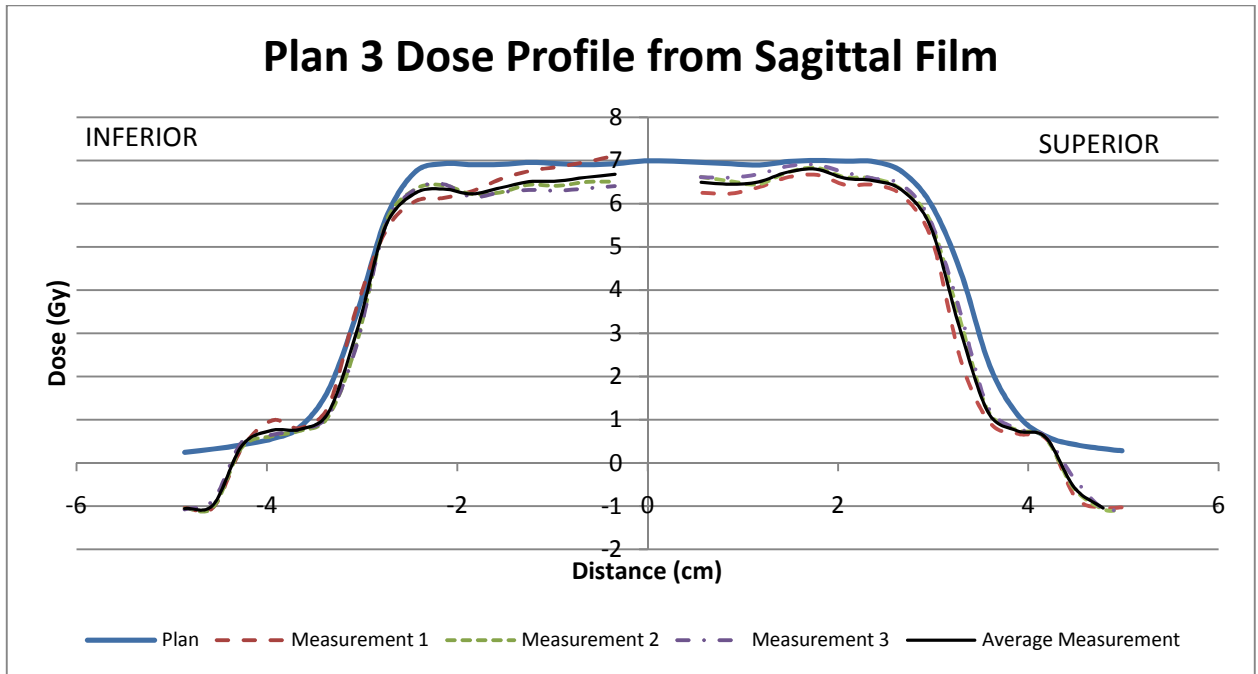
Figure C.9 Inferior-to-superior dose profile of Plan 3 as planned by the TPS and measured by the three sagittal films
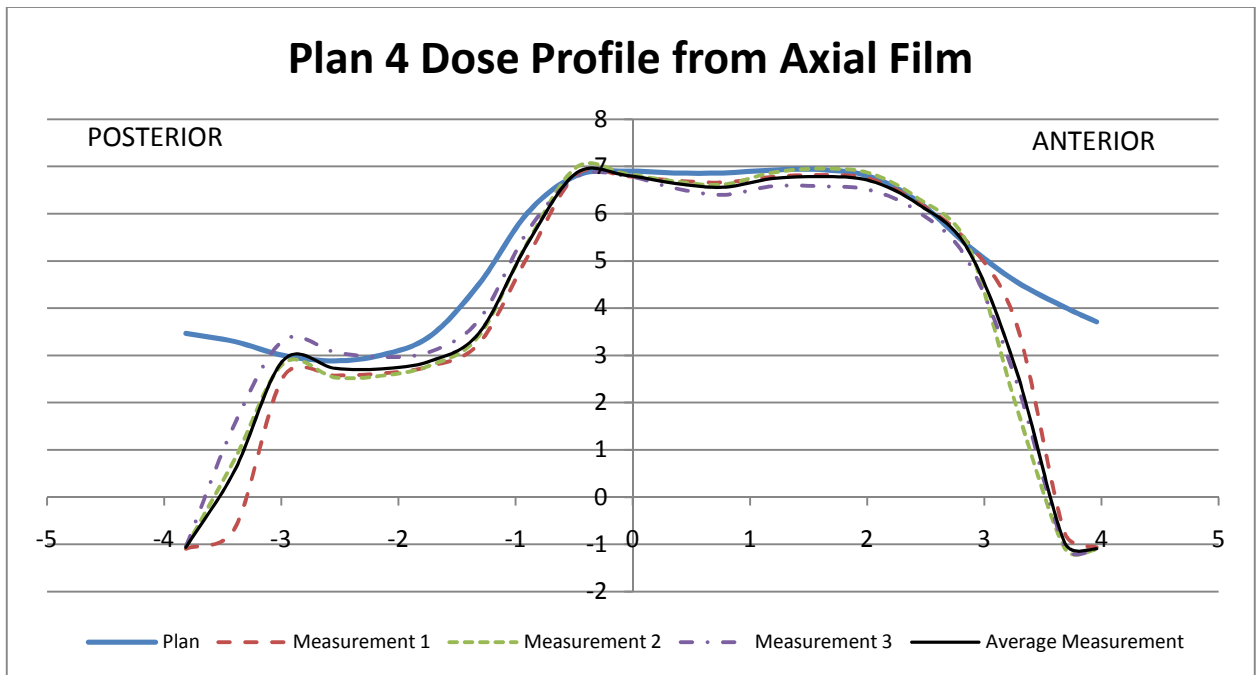
Figure C.10 Posterior-to-anterior dose profile of Plan 4 as planned by the TPS and measured with the three axial films

Plan 4 Dose Profile from Axial Film

LEFT

RIGHT

Dose (Gy)

Distance (cm)

Plan — Measurement 1 — Measurement 2 — Measurement 3 — Average Measurement
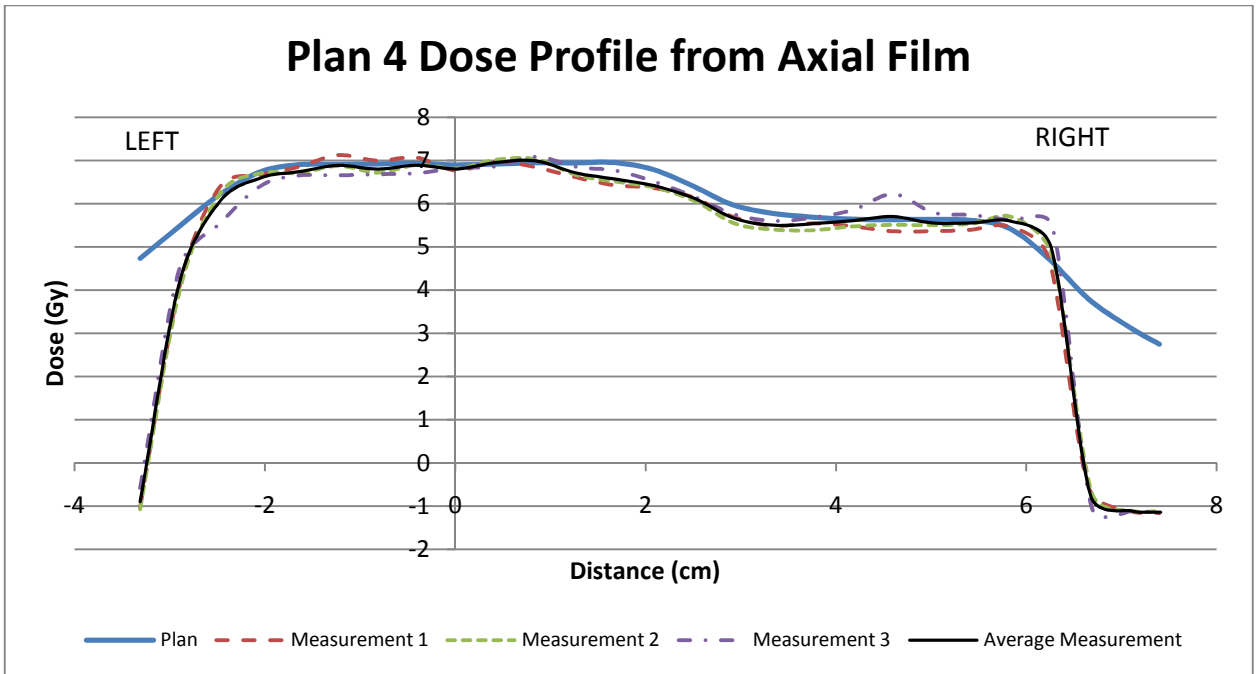
Figure C.11 Left-to-right dose profile of Plan 4 as planned by the TPS and measured by the three axial films

Plan 4 Dose Profile from Sagittal Film

INFERIOR

SUPERIOR

Dose (Gy)

Distance (cm)

Plan — Measurement 1 — Measurement 2 — Measurement 3 — Average Measurement
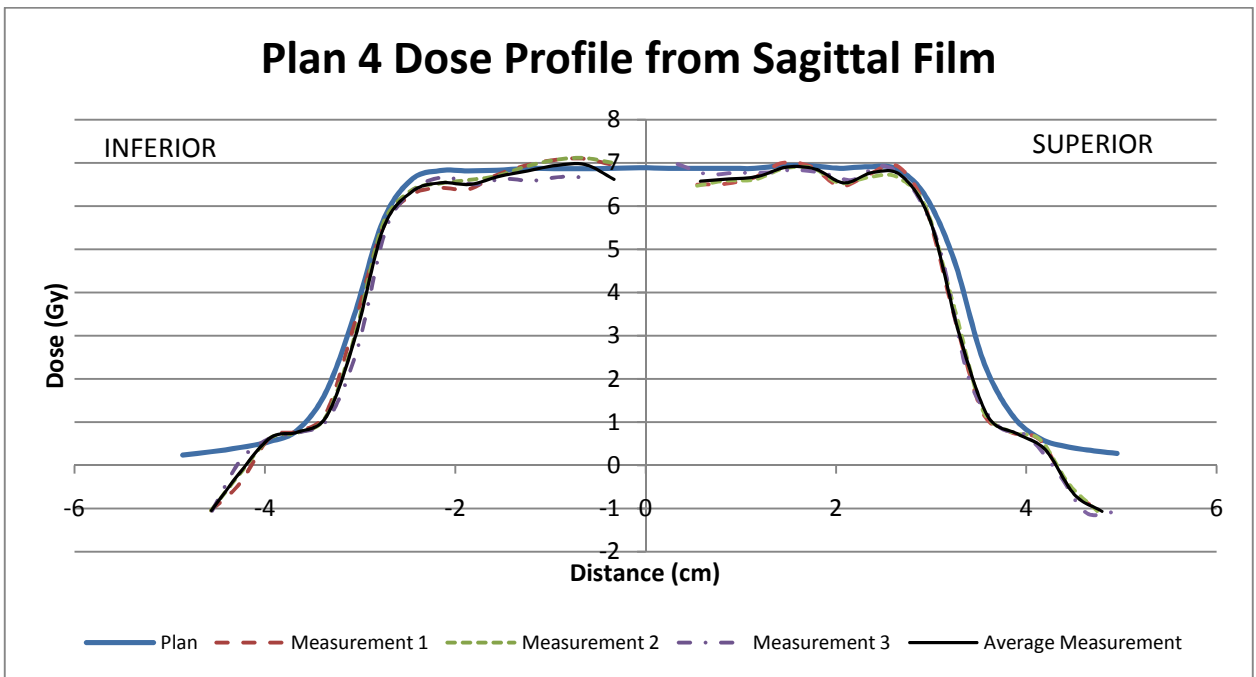
Figure C.12 Inferior-to-superior dose profile of Plan 4 as planned by the TPS and measured by the three sagittal films
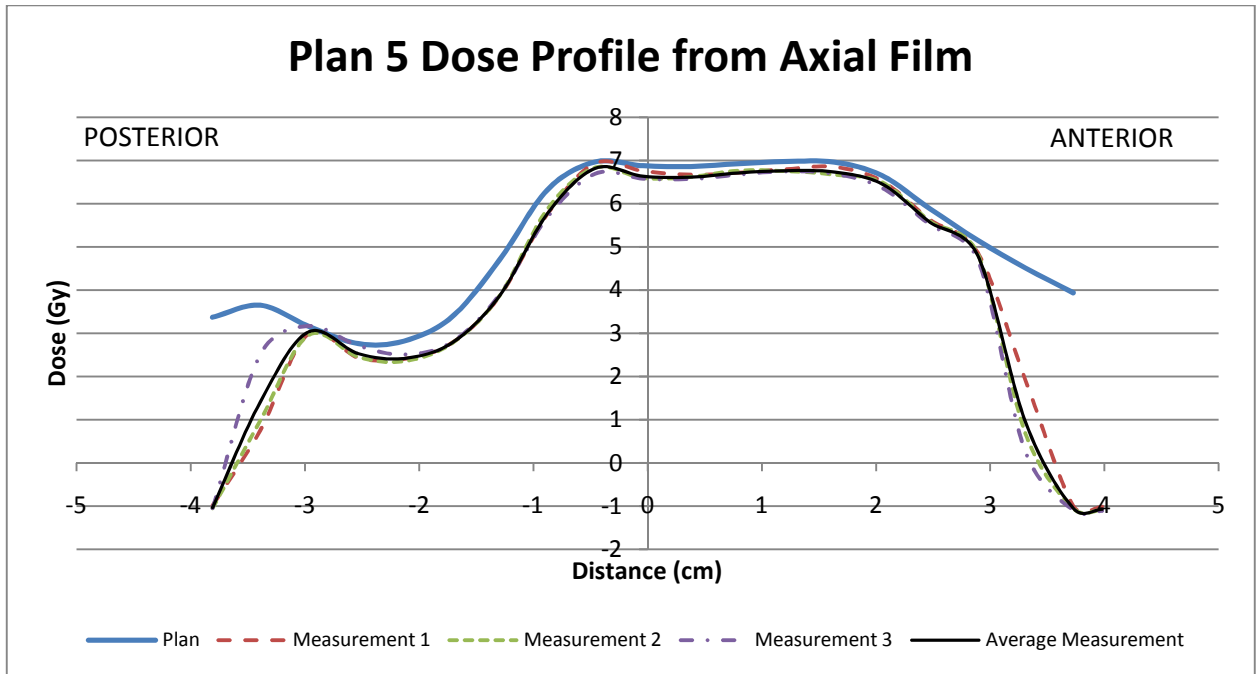
Figure C.13 Posterior-to-anterior dose profile of Plan 5 as planned by the TPS and measured with the three axial films
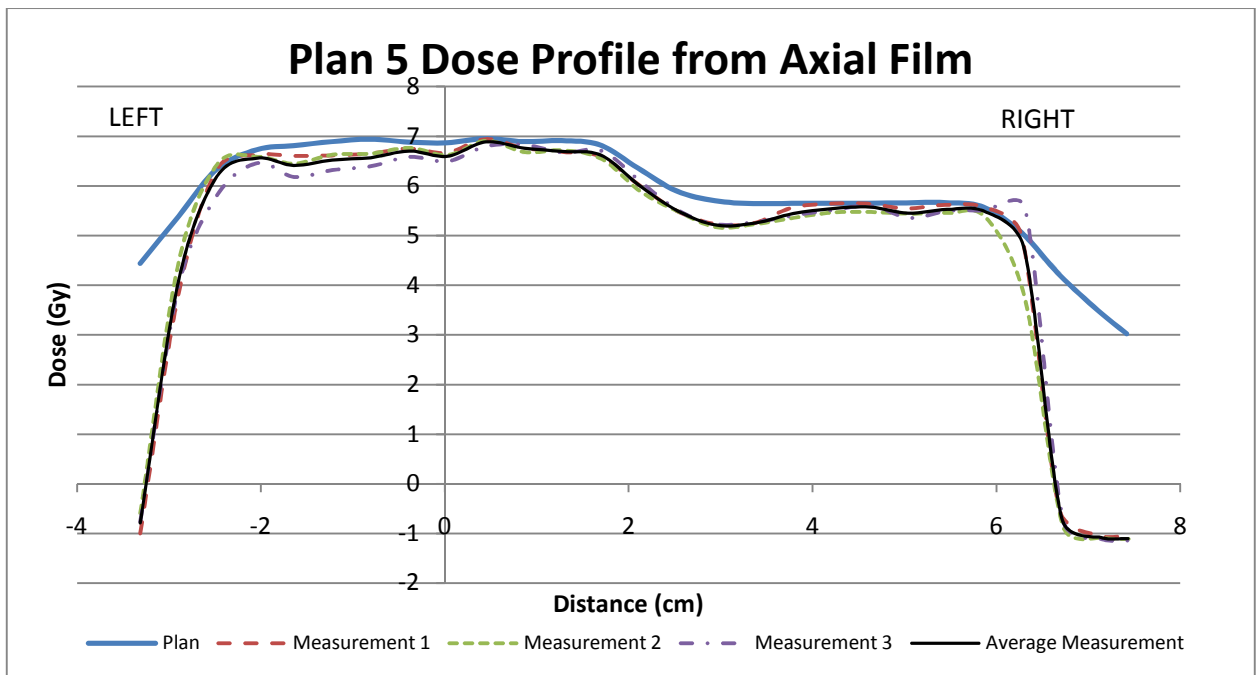
Figure C.14 Left-to-right dose profile of Plan 5 as planned by the TPS and measured by the three axial films

Plan 5 Dose Profile from Sagittal Film

INFERIOR

SUPERIOR

Dose (Gy)

Distance (cm)

Plan — Measurement 1 — Measurement 2 — Measurement 3 — Average Measurement
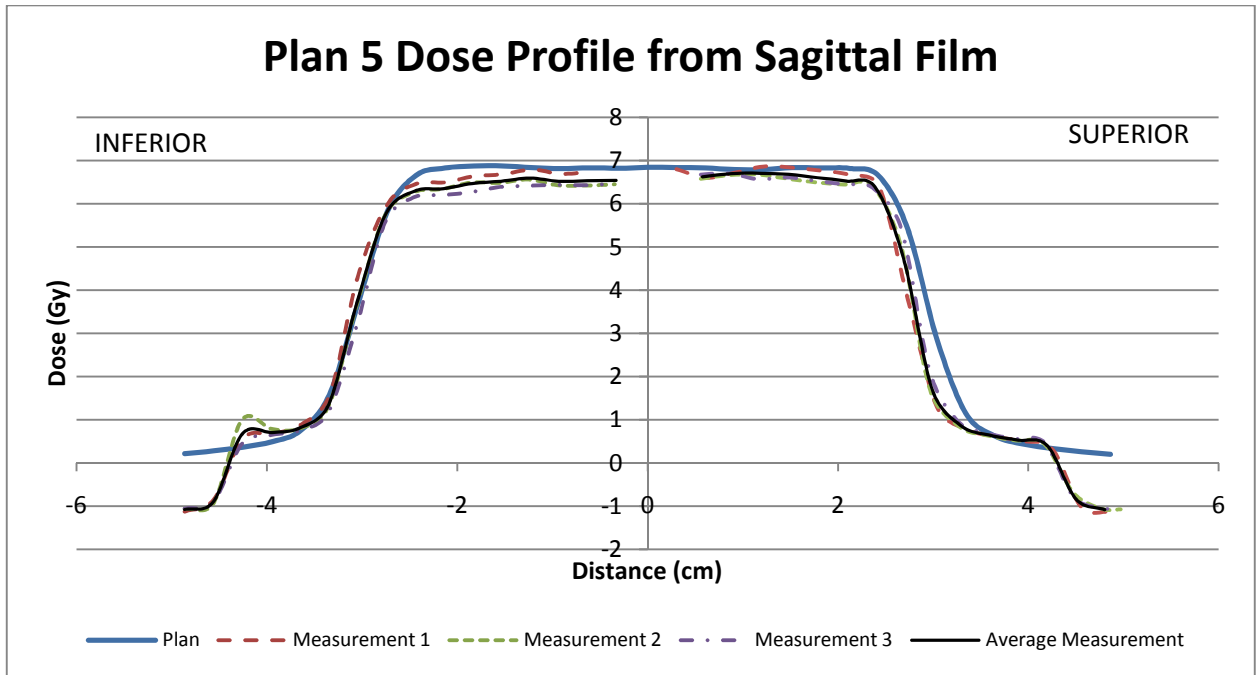
Figure C.15 Inferior-to-superior dose profile of Plan 5 as planned by the TPS and measured by the three sagittal films

Plan 6 Dose Profile from Axial Film

POSTERIOR

ANTERIOR

Dose (Gy)

Distance (cm)

Plan — Measurement 1 — Measurement 2 — Measurement 3 — Average Measurement
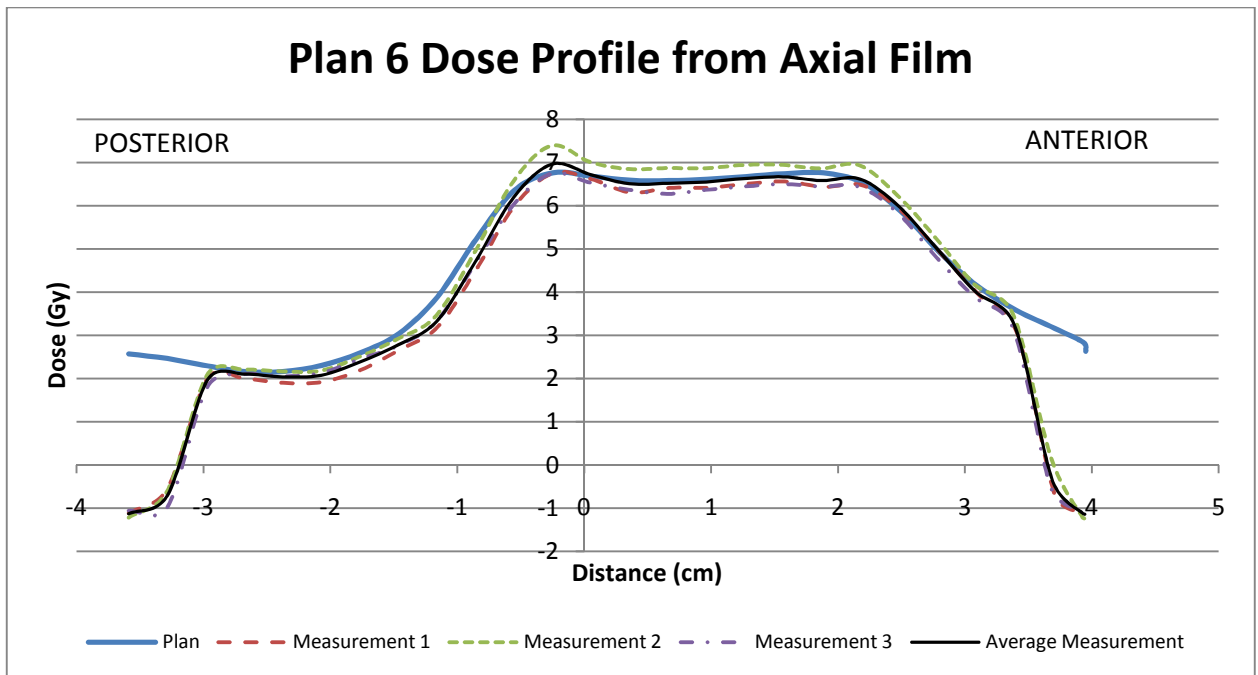
Figure C.16 Posterior-to-anterior dose profile of Plan 6 as planned by the TPS and measured with the three axial films

Plan 6 Dose Profile from Axial Film
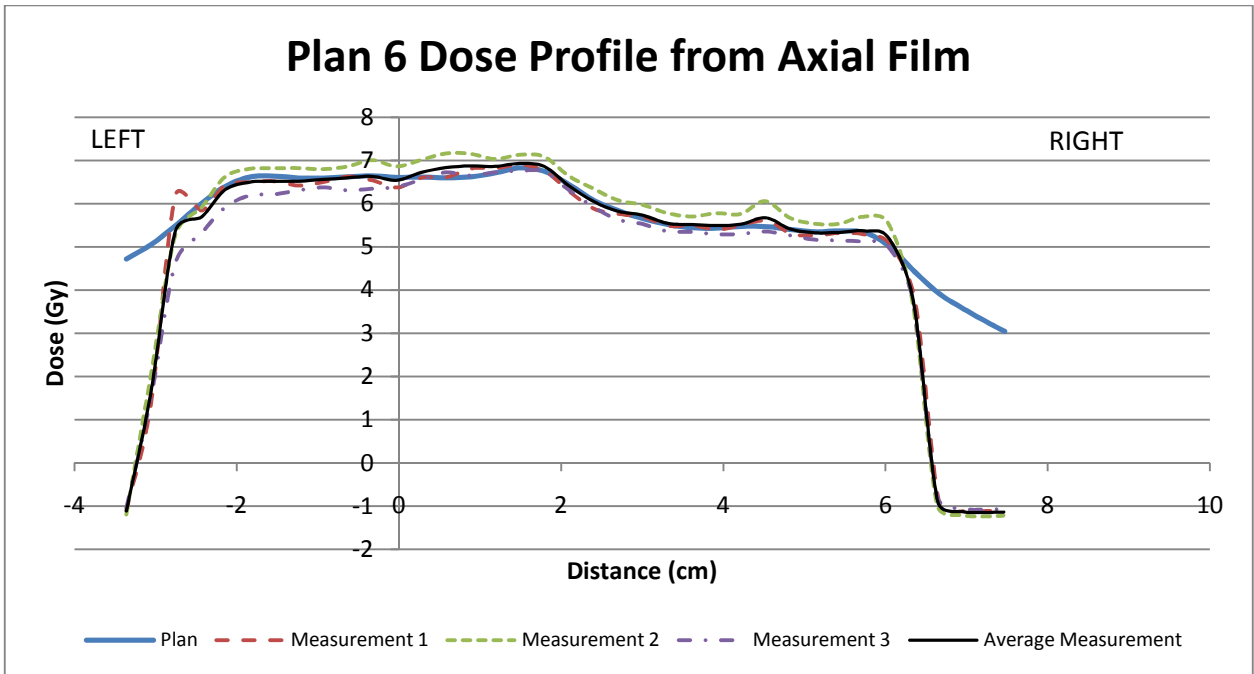
Figure C.17 Left-to-right dose profile of Plan 6 as planned by the TPS and measured by the three axial films

Plan 6 Dose Profile from Sagittal Film
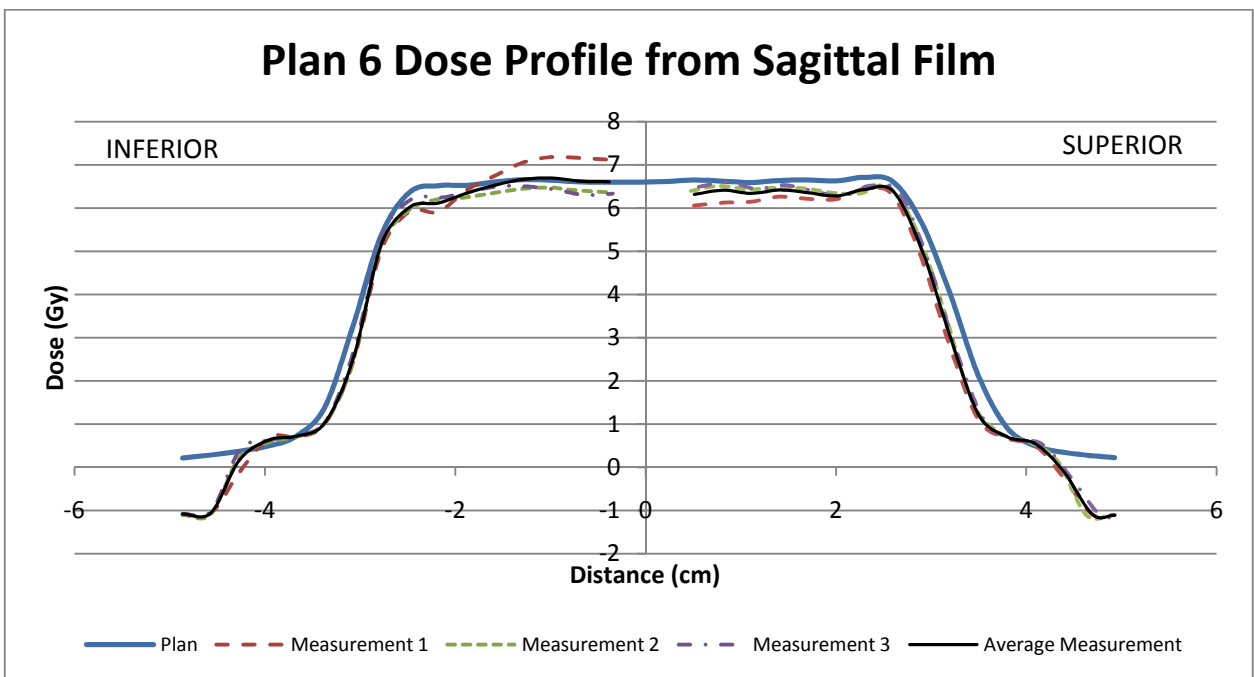
Figure C.18 Inferior-to-superior dose profile of Plan 6 as planned by the TPS and measured by the three sagittal films
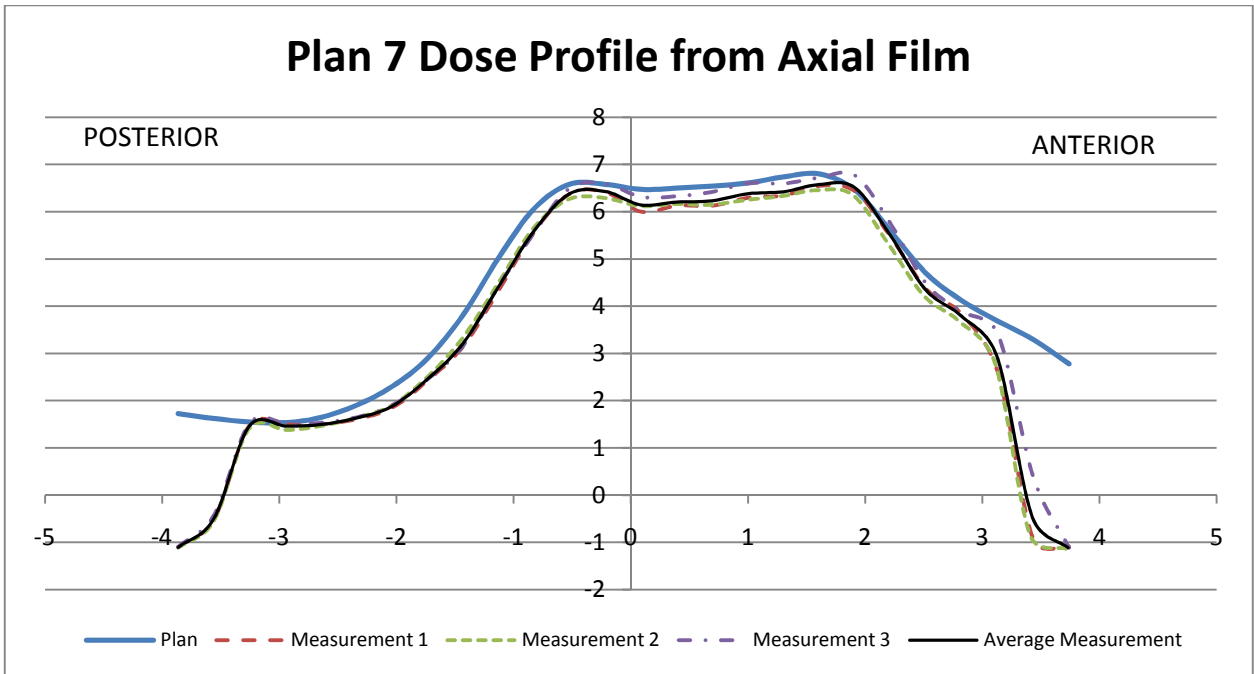
Figure C.19 Posterior-to-anterior dose profile of Plan 7 as planned by the TPS and measured with the three axial films
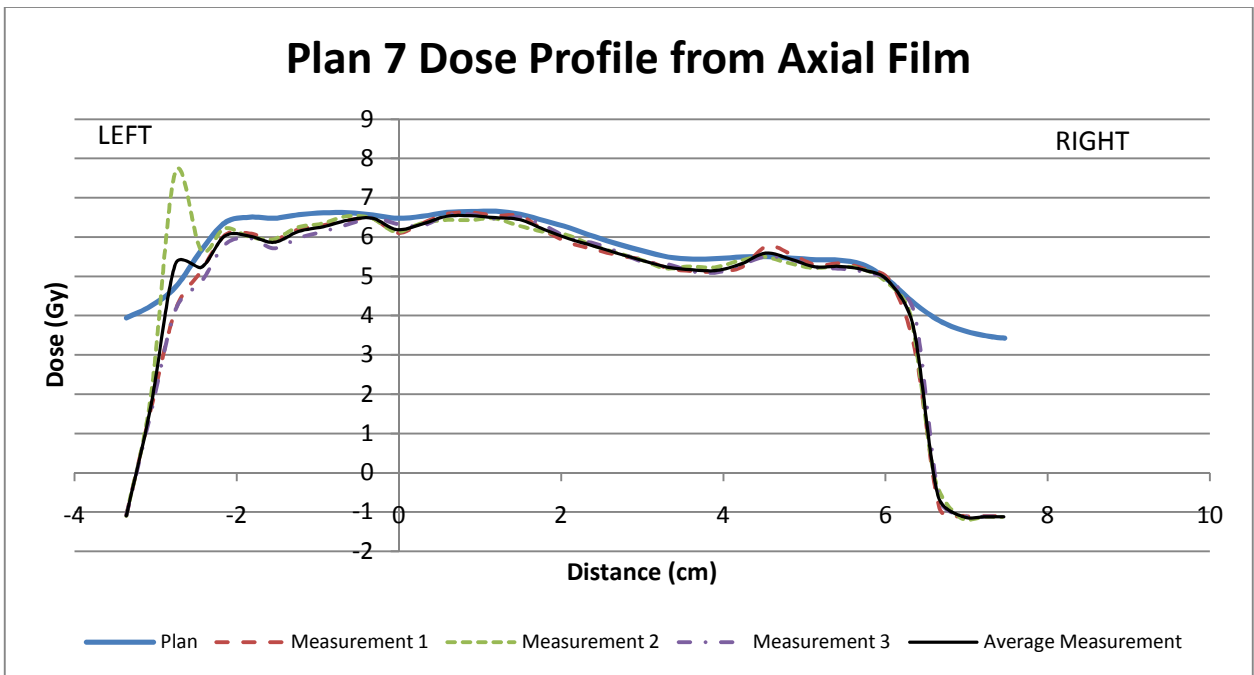
Figure C.20 Left-to-right dose profile of Plan 7 as planned by the TPS and measured by the three axial films

Plan 7 Dose Profile from Sagittal Film

INFERIOR

SUPERIOR

Dose (Gy)

Distance (cm)

Plan — Measurement 1 — Measurement 2 — · — Measurement 3 — Average Measurement
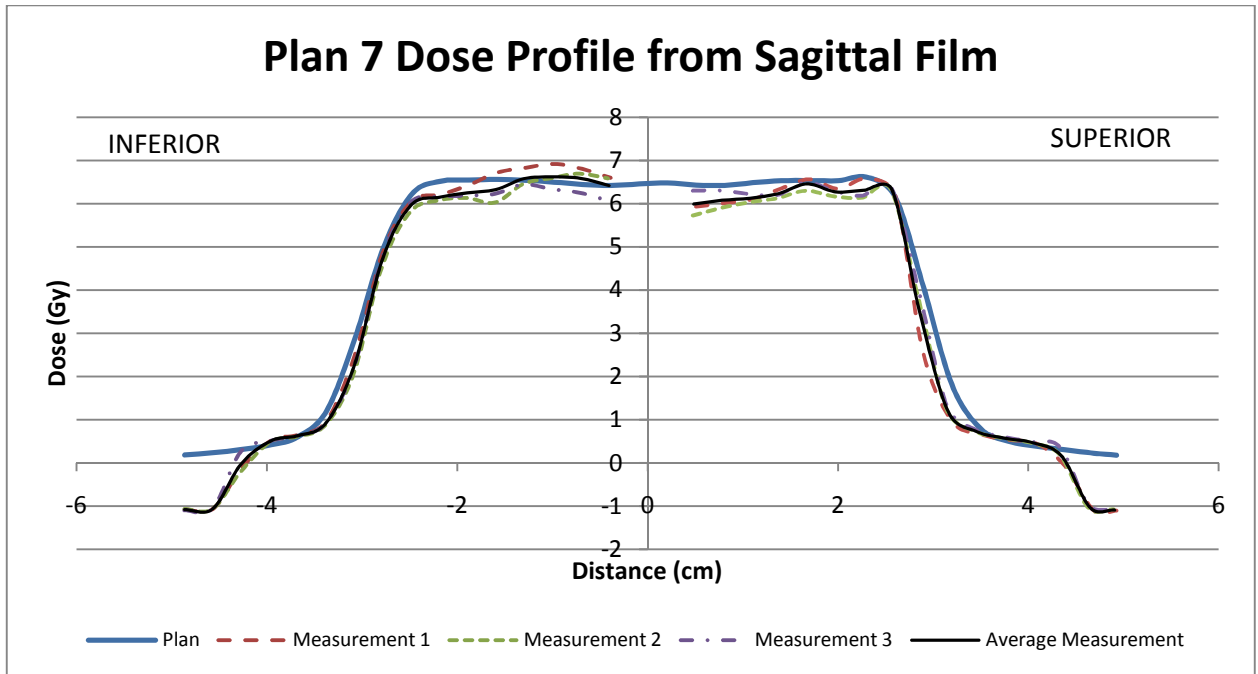
Figure C.21 Inferior-to-superior dose profile of Plan 7 as planned by the TPS and measured by the three sagittal films

Plan 8 Dose Profile from Axial Film

POSTERIOR

ANTERIOR

Dose (Gy)

Distance (cm)

Plan — Measurement 1 — Measurement 2 — · — Measurement 3 — Average Measurement
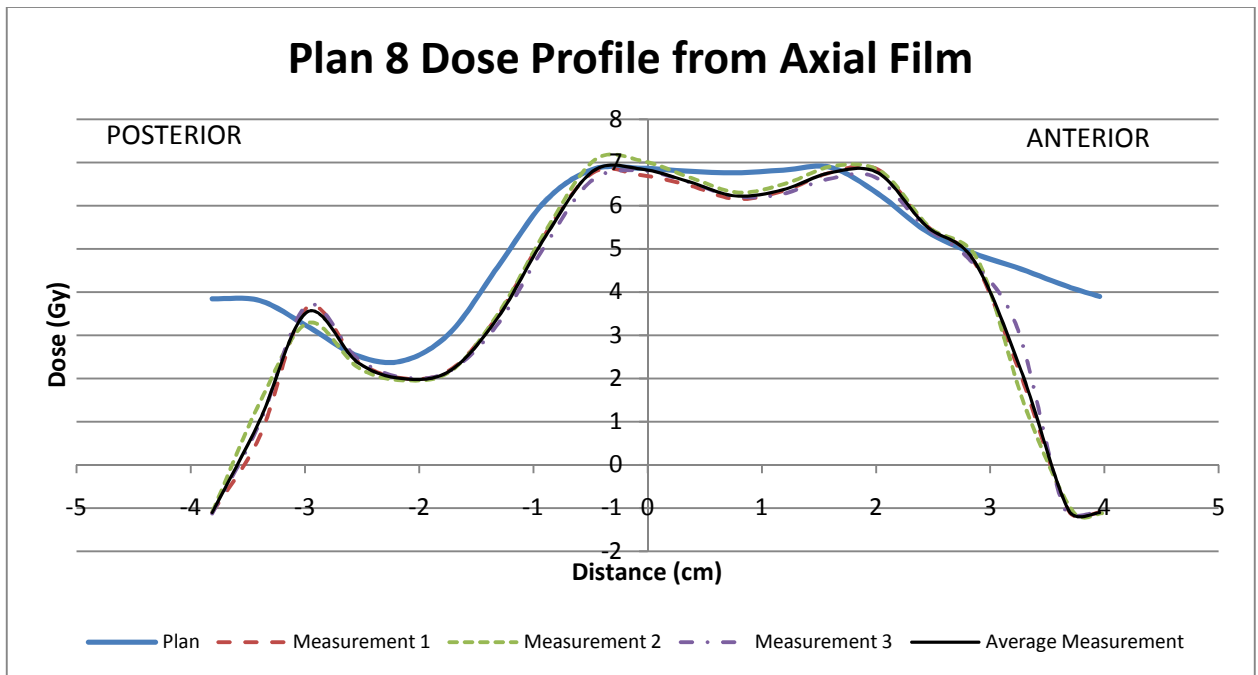
Figure C.22 Posterior-to-anterior dose profile of Plan 8 as planned by the TPS and measured with the three axial films
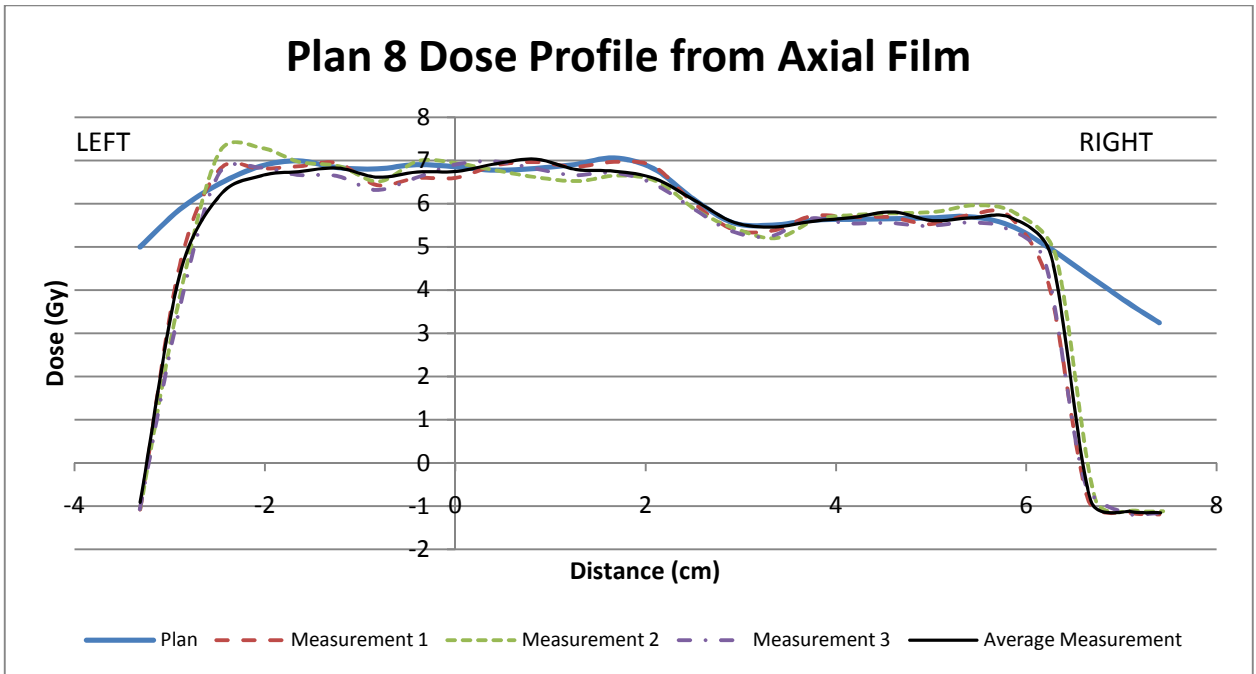
Figure C.23 Left-to-right dose profile of Plan 8 as planned by the TPS and measured by the three axial films
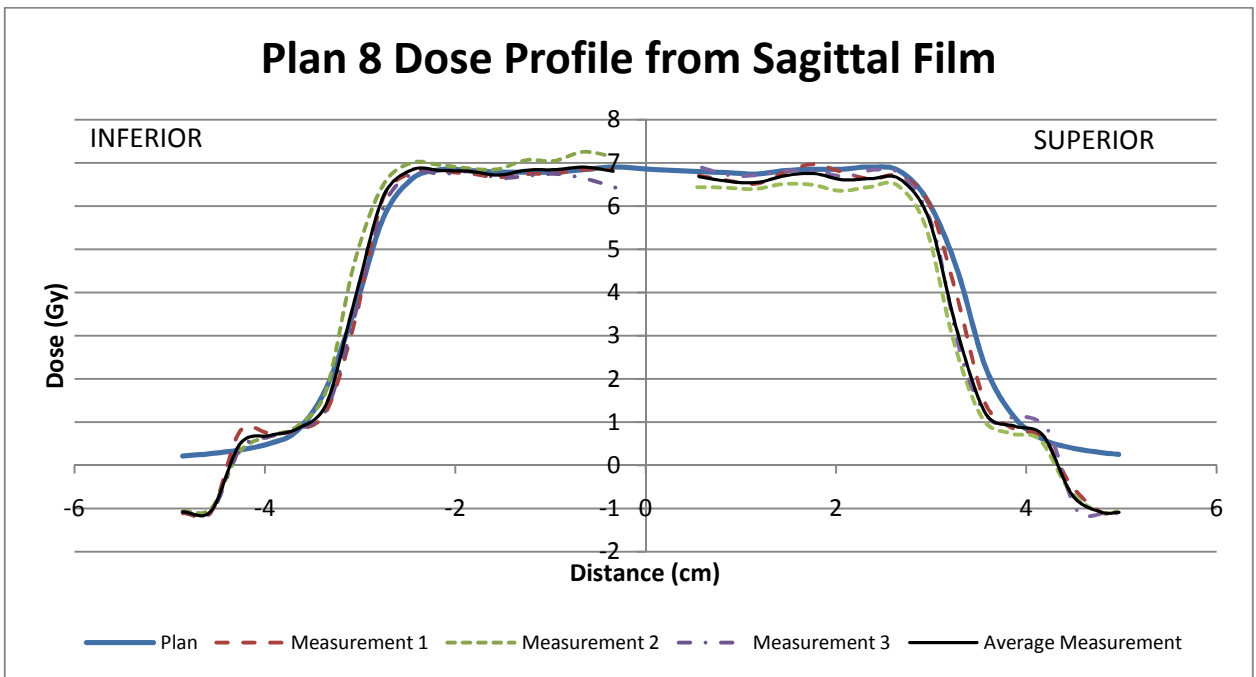
Figure C.24 Inferior-to-superior dose profile of Plan 8 as planned by the TPS and measured by the three sagittal films
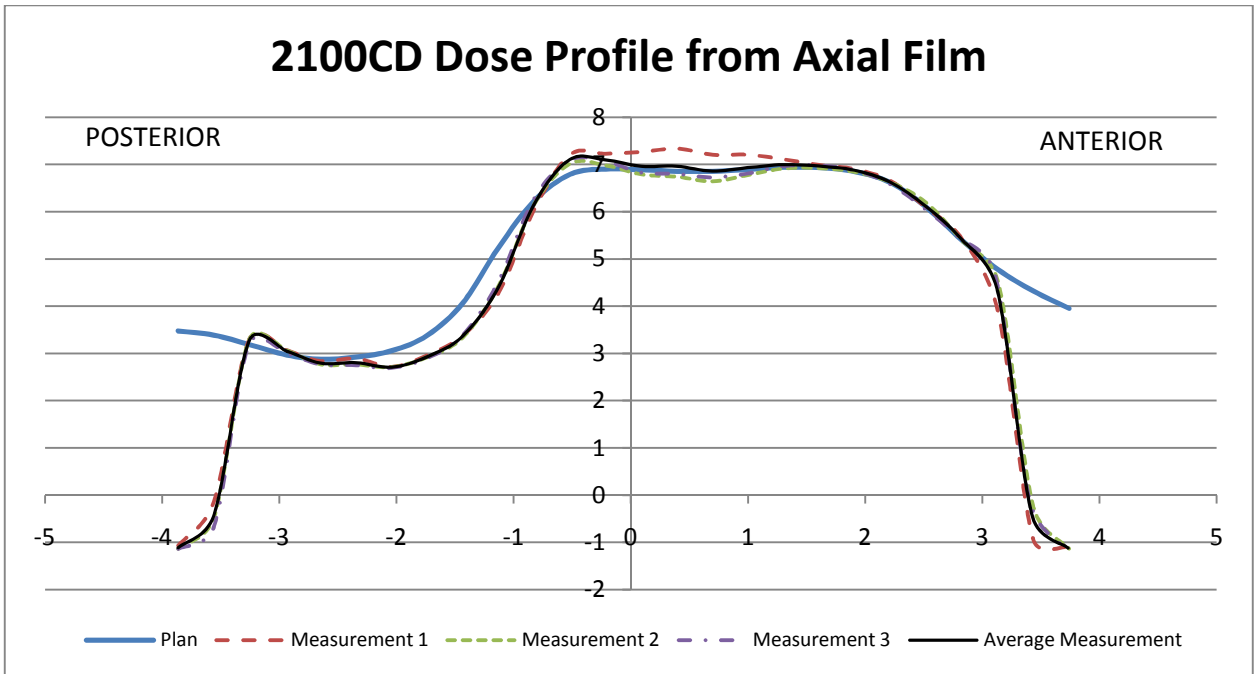
Figure C.25 Posterior-to-anterior dose profile of Plan 4 delivered on the second 2100CD machine as planned by the TPS and measured with the three axial films
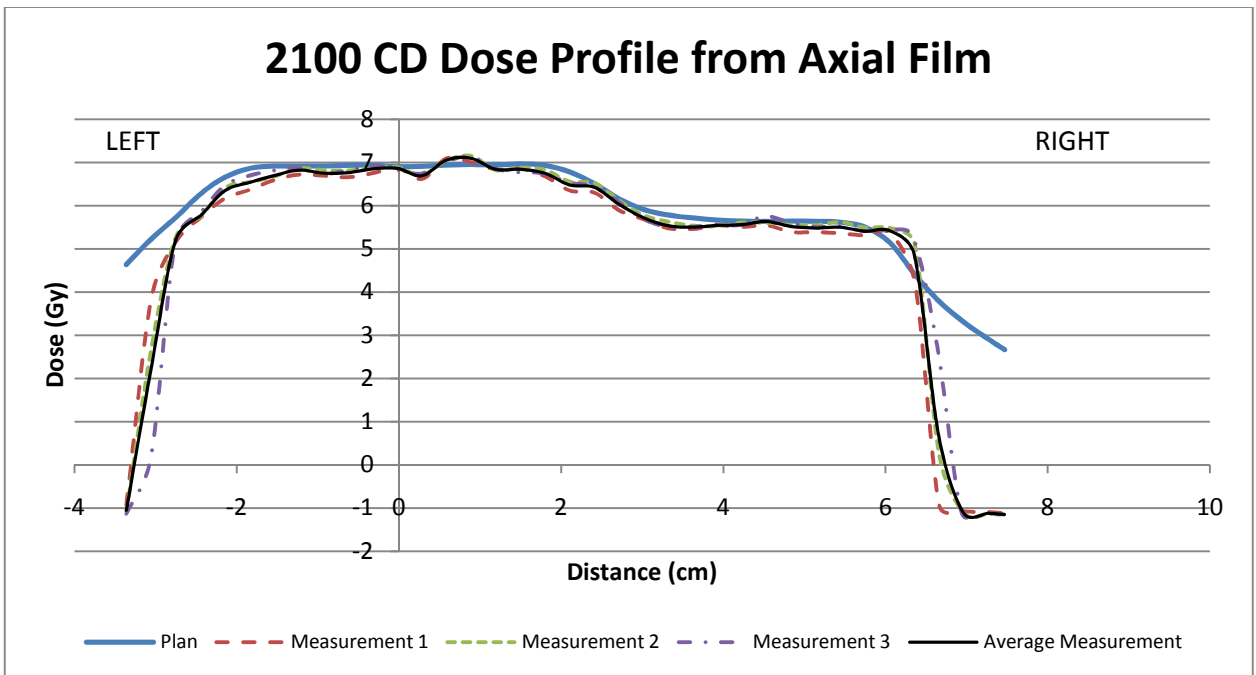
Figure C.26 Left-to-right dose profile of Plan 4 delivered on the second 2100CD machine as planned by the TPS and measured by the three axial films
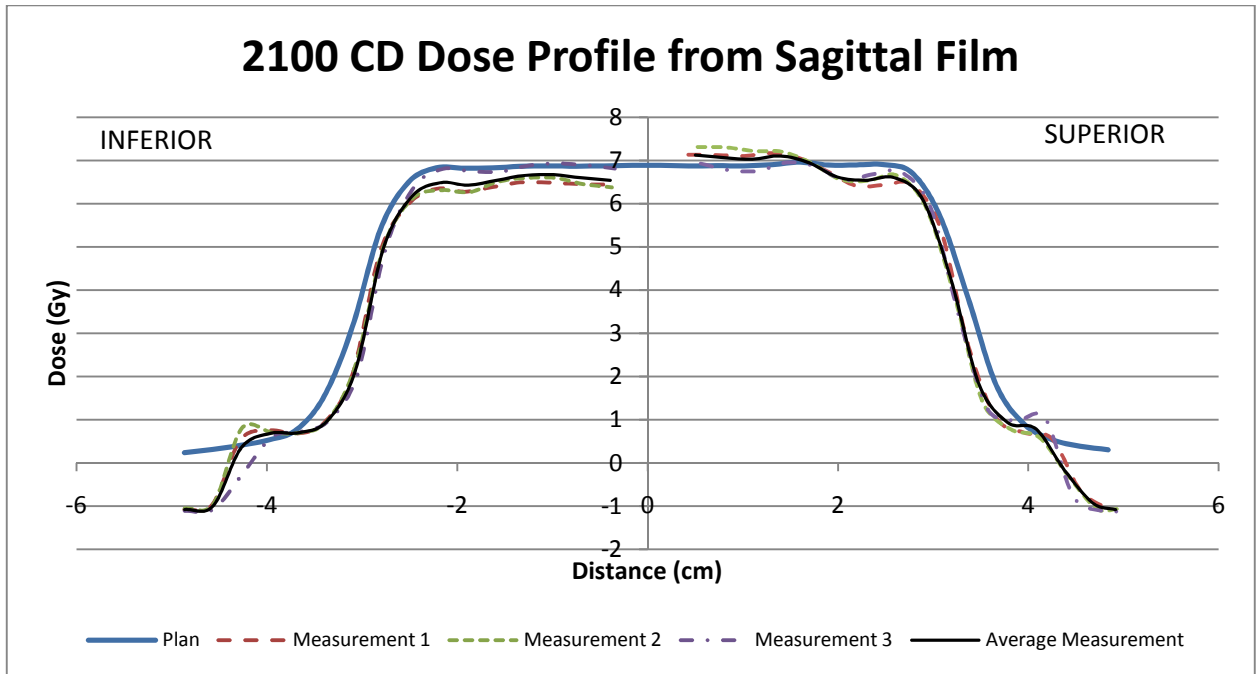
Figure C.27 Inferior-to-superior dose profile of Plan 4 delivered on the second 2100CD machine as planned by the TPS and measured by the three sagittal films
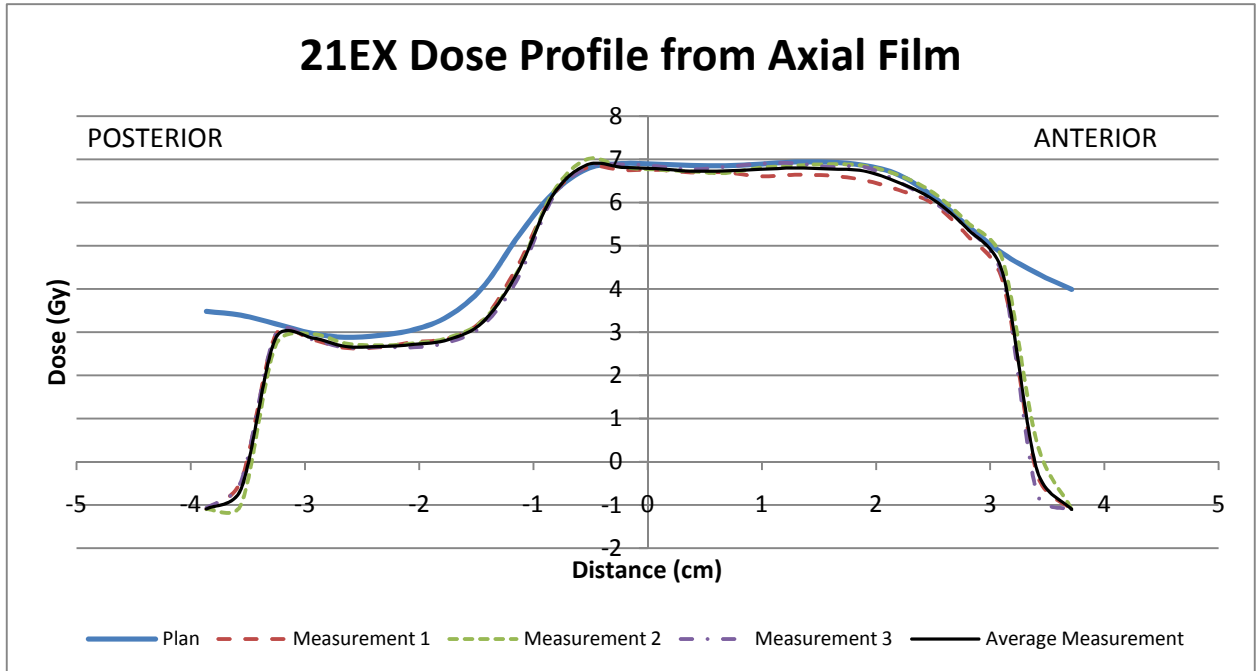
Figure C.28 Posterior-to-anterior dose profile of Plan 4 delivered on the 21EX machine as planned by the TPS and measured with the three axial films
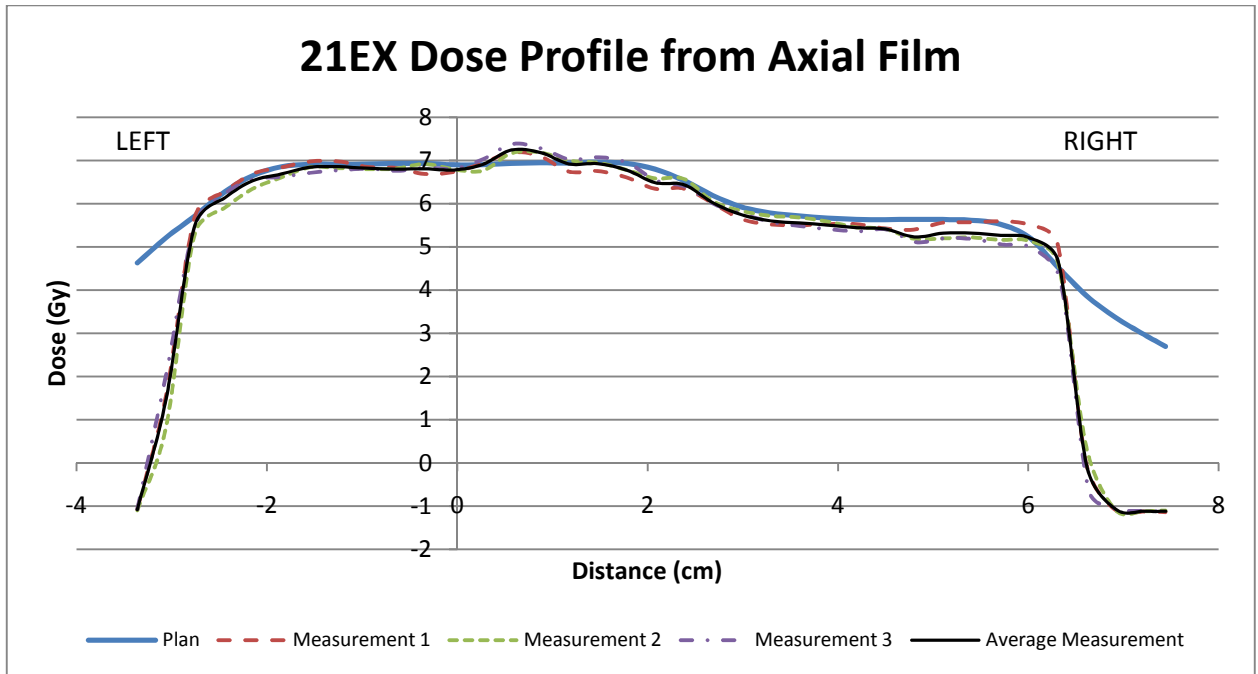
Figure C.29 Left-to-right dose profile of Plan 4 delivered on the 21EX machine as planned by the TPS and measured by the three axial films
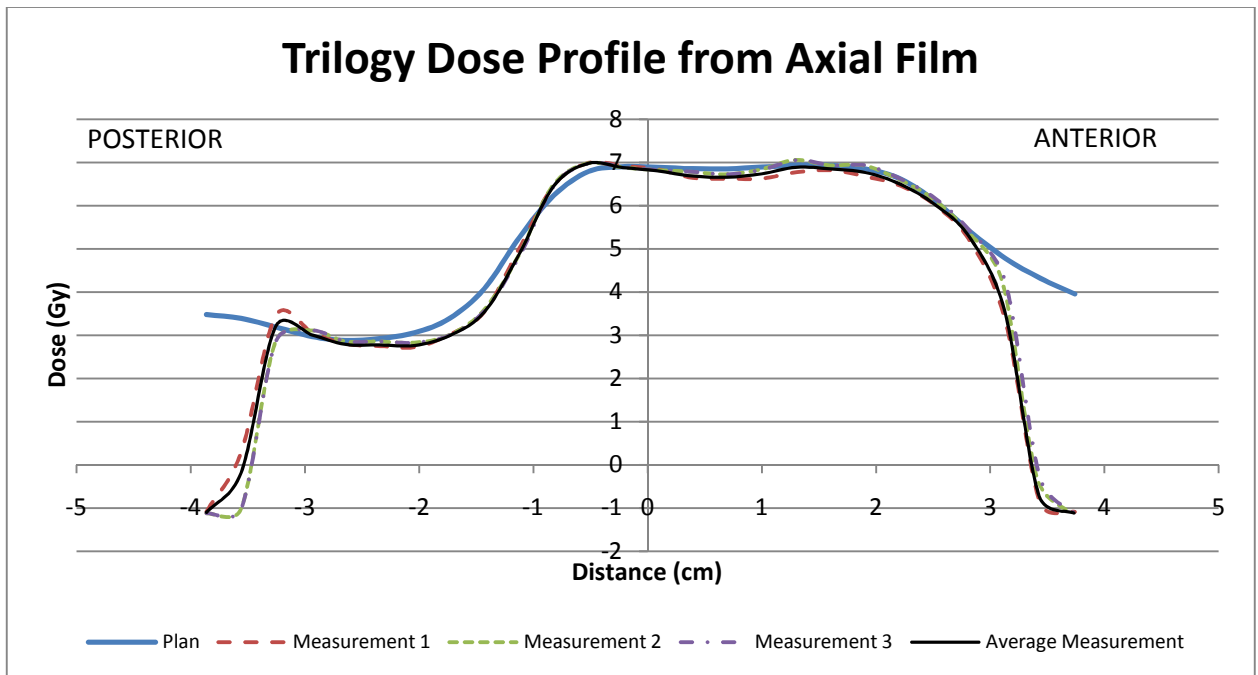
Figure C.30 Posterior-to-anterior dose profile of Plan 4 delivered on the second Trilogy machine as planned by the TPS and measured with the three axial films
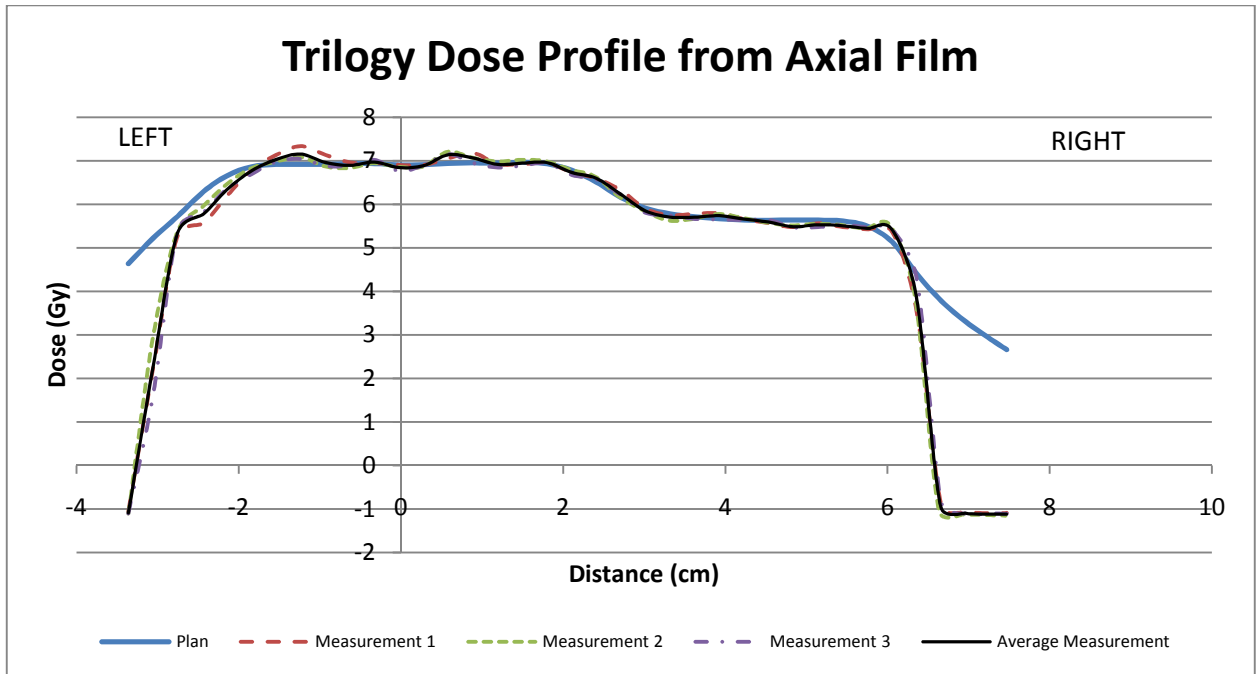
Figure C.31 Left-to-right dose profile of Plan 4 delivered on the Trilogy machine as planned by the TPS and measured by the three axial films
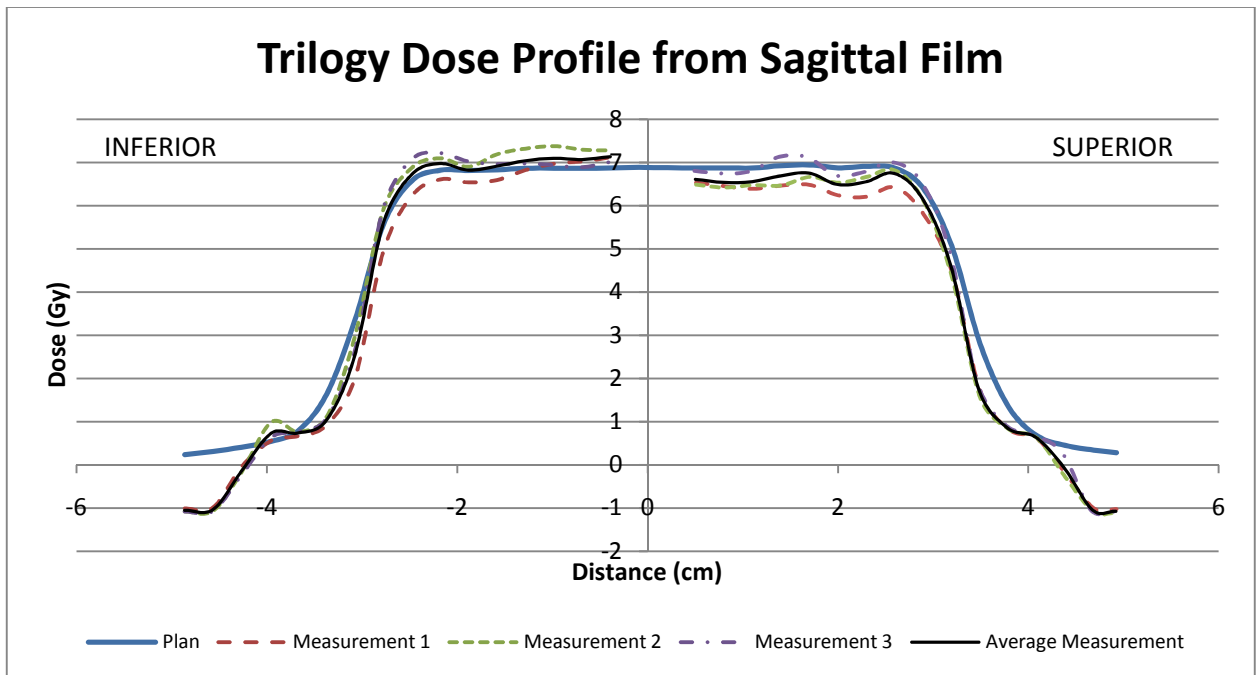
Figure C.32 Inferior-to-superior dose profile of Plan 4 delivered on the Trilogy machine as planned by the TPS and measured by the three sagittal films
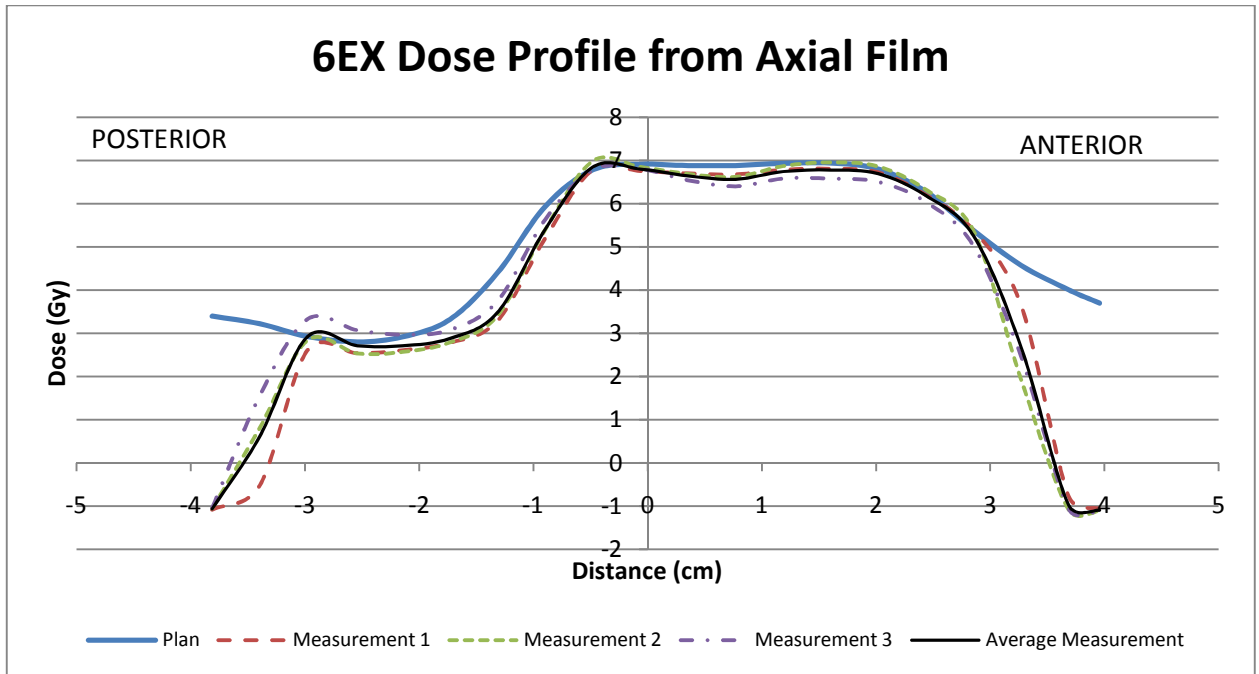
Figure C.33 Posterior-to-anterior dose profile of Plan 4 delivered on the baseline machine as compared to the dose calculated with the incorrect beam model measured with the three axial films
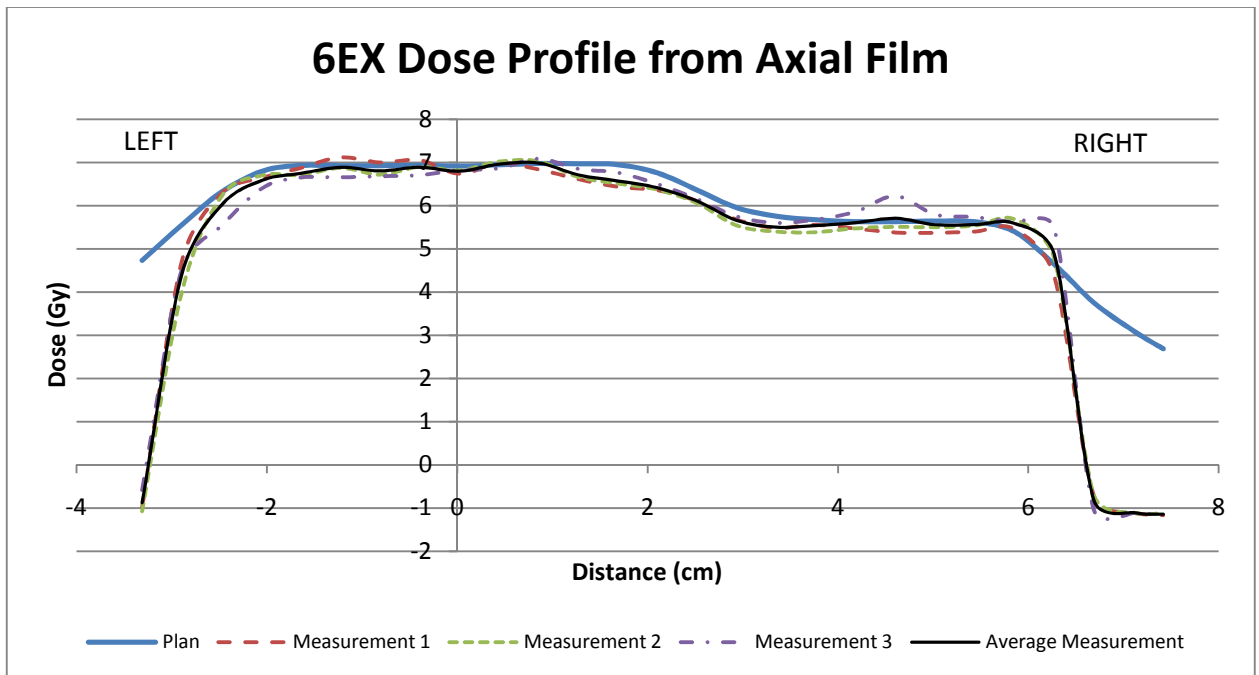
Figure C.34 Left-to-right dose profile of Plan 4 delivered on the baseline machine as compared to the dose calculated with the incorrect beam model measured with the three axial films

6EX Dose Profile from Sagittal Film

INFERIOR

SUPERIOR

Dose (Gy)

Distance (cm)

Plan — Measurement 1 — Measurement 2 — Measurement 3 — Average Measurement
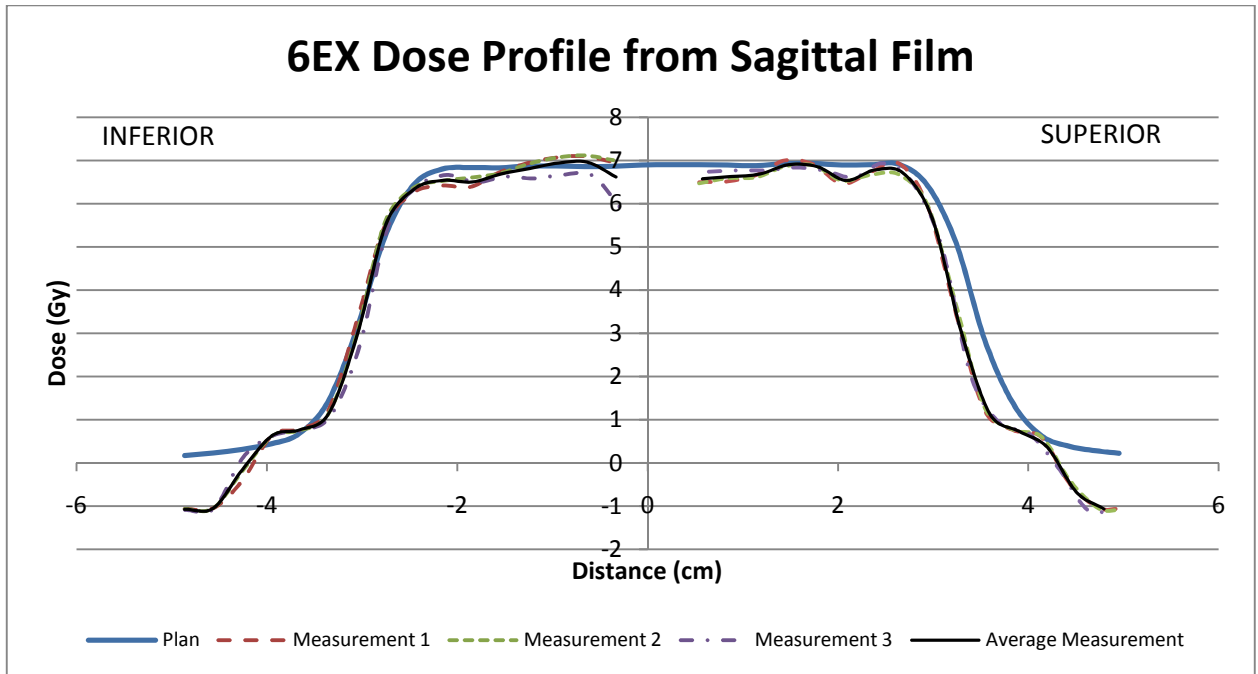
Figure C.35 Inferior-to-superior dose profile of Plan 4 delivered on the baseline machine as compared to the dose calculated with the incorrect beam model measured by the three sagittal films

Appendix D Gamma Index Analyses Results
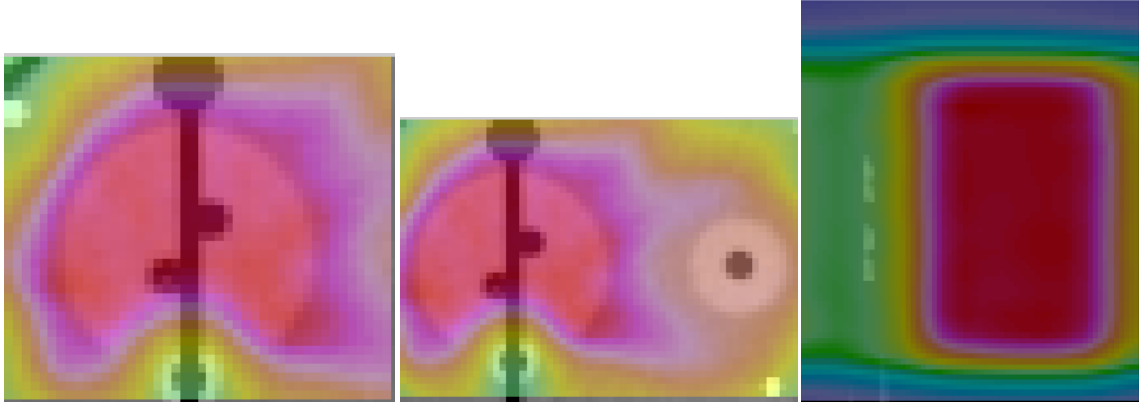
Figure D.36 Regions used for the gamma index analysis: Axial primary PTV (right), axial full (center), sagittal full (left)

Plan 1 Results
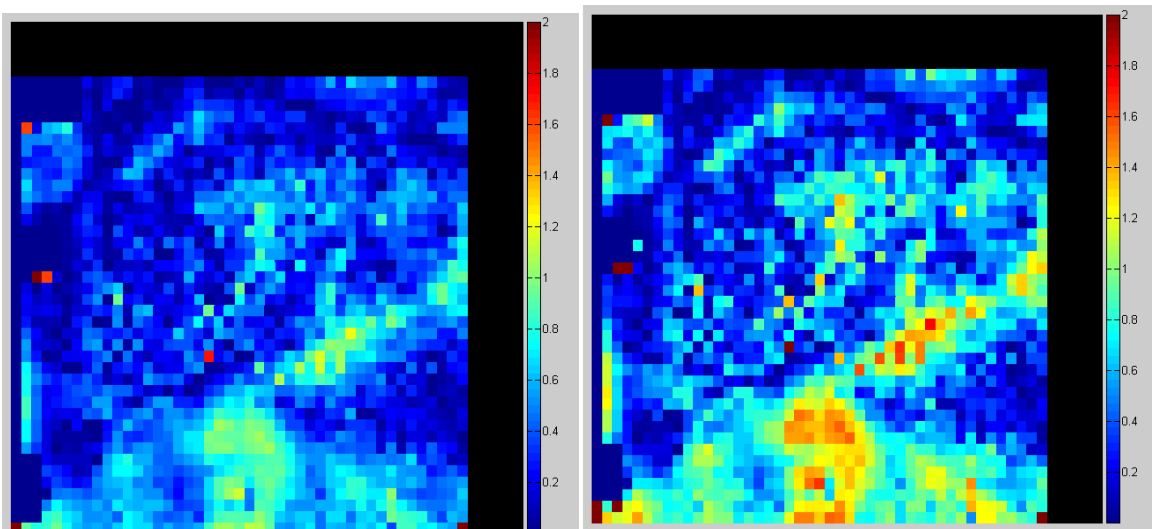
Figure D.37 Plan 1 measurement 1 axial PTV region, 7%/4mm with 98.54% pixels passing (left) and 5%/3mm with 87.7% pixels passing (right)
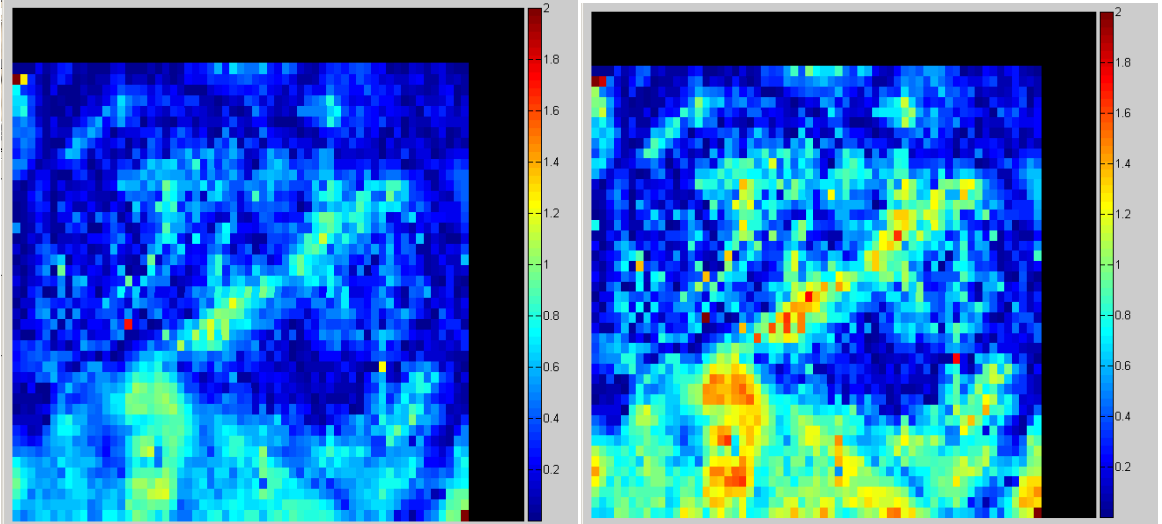
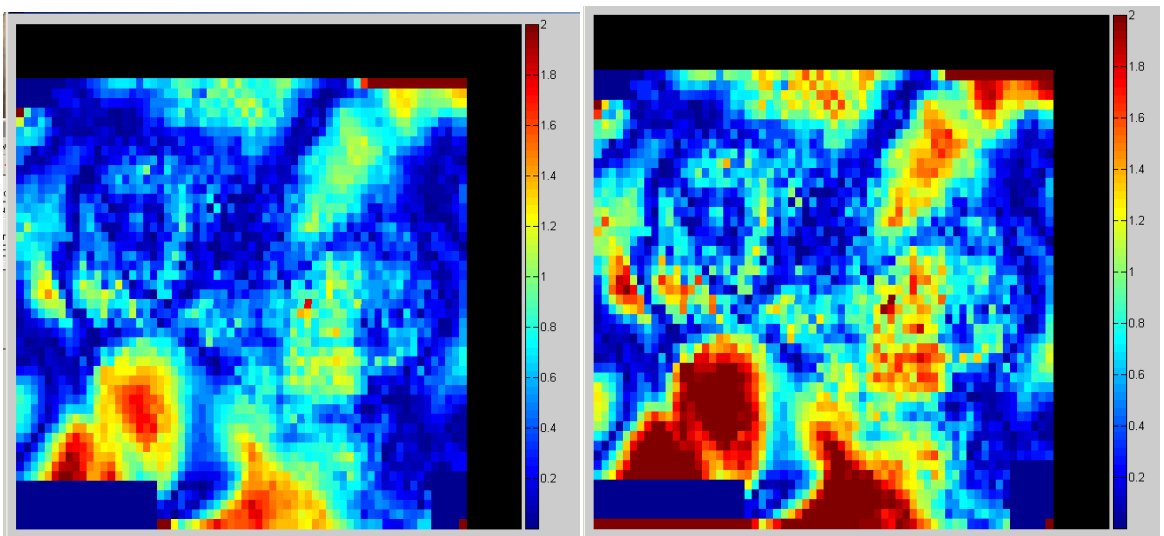**Figure D.38 Plan 1 measurement 1 full axial region, 7%/4mm with 98.89% pixels passing (left) and 5%/3mmwith 86.76% pixels passing (right)**
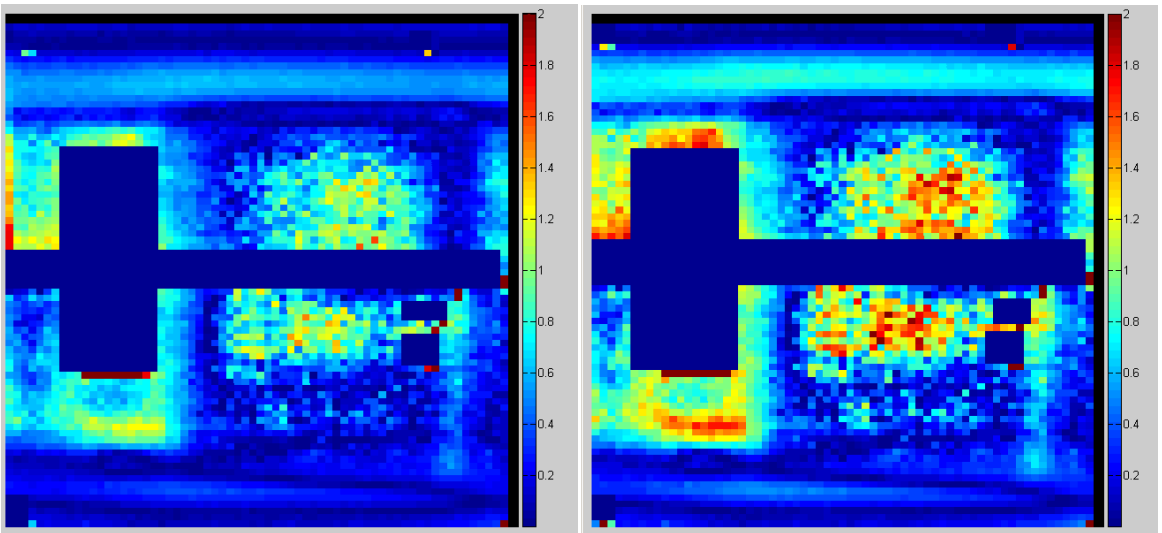
Figure D.39 Plan 1 measurement 1 full sagittal region, 7%/4mmwith 94.9% pixels passing (left) and 5%/3mmwith 85.13% pixels passing (right)
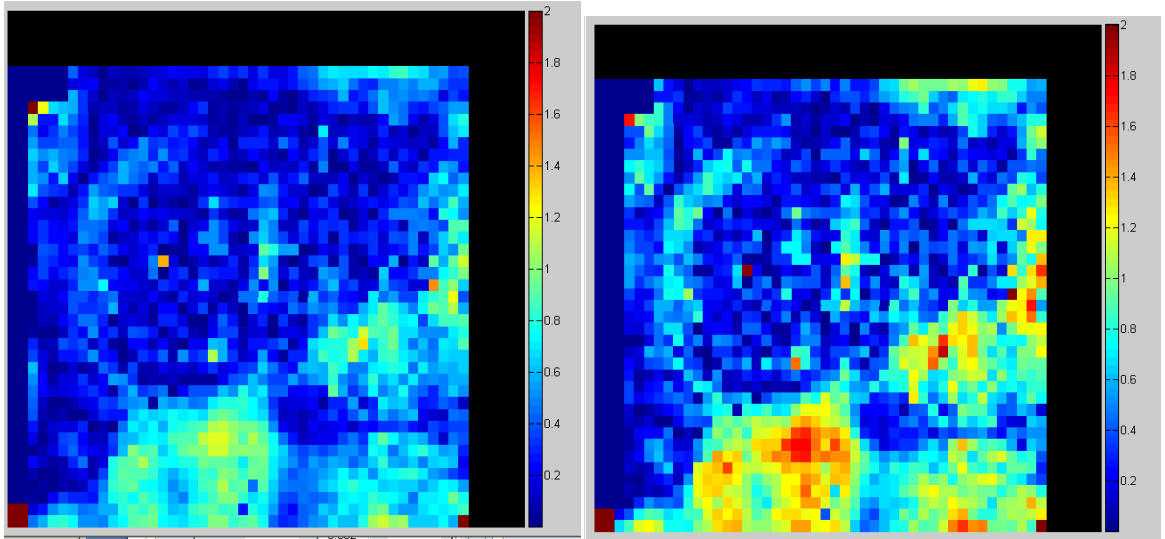
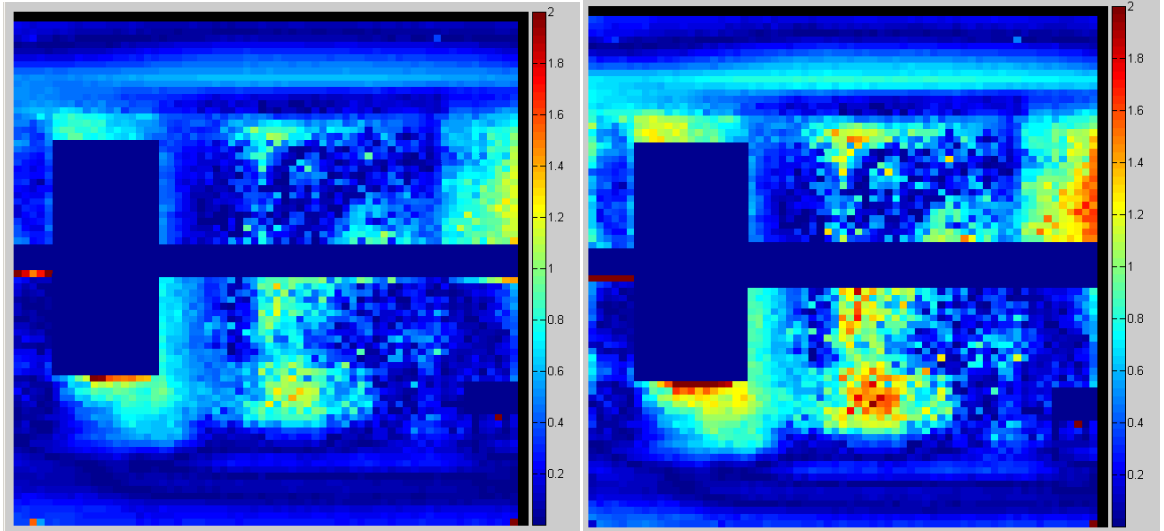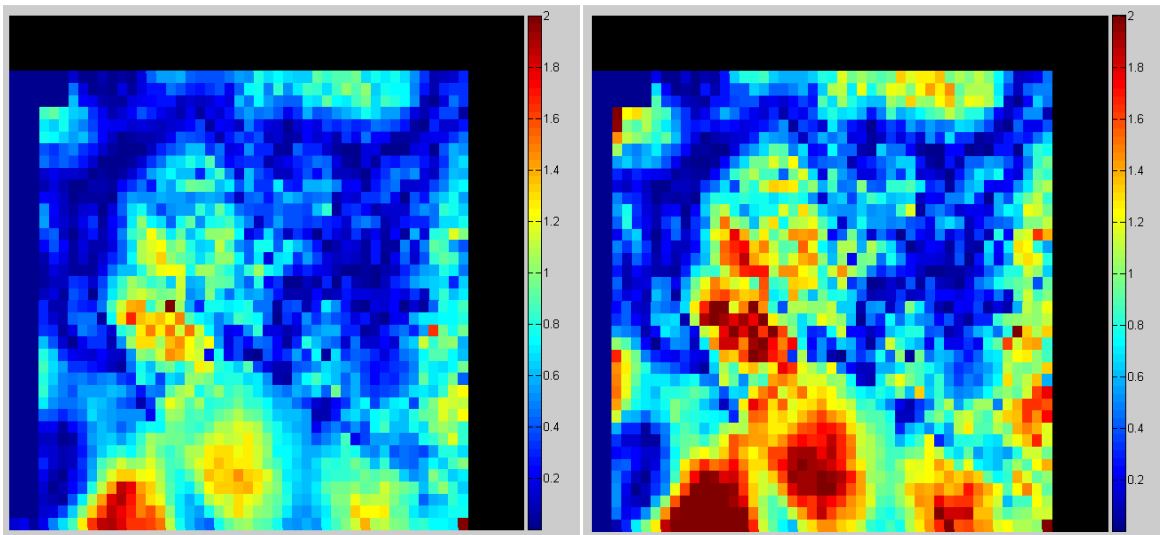**Figure D.40 Plan 1 measurement 2 axial PTV region, 7%/4mm with 97.89% pixels passing (left) and 5%/3mm with 82.74% pixels passing (right)**
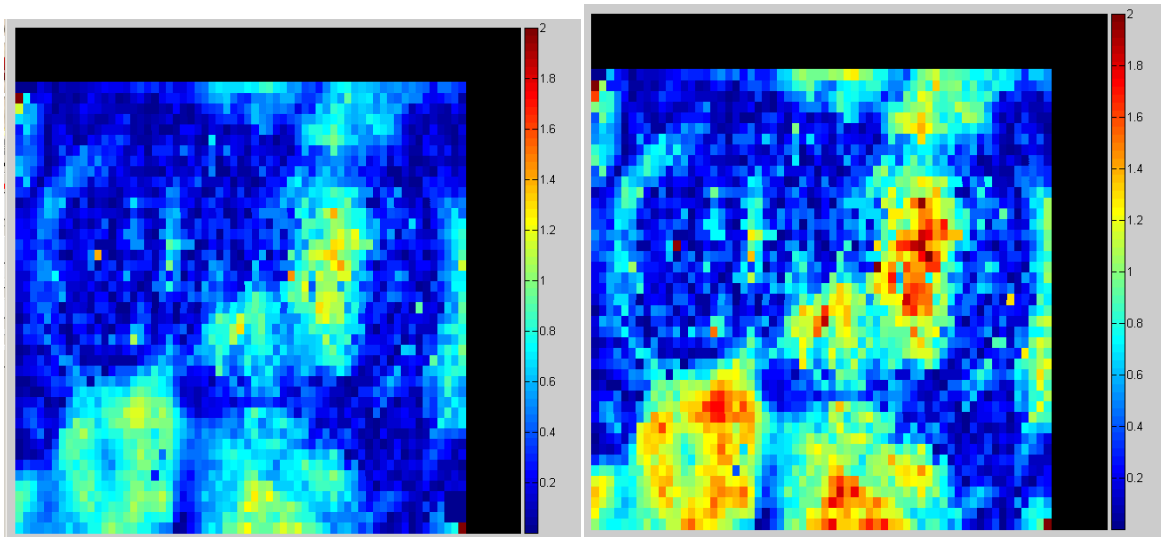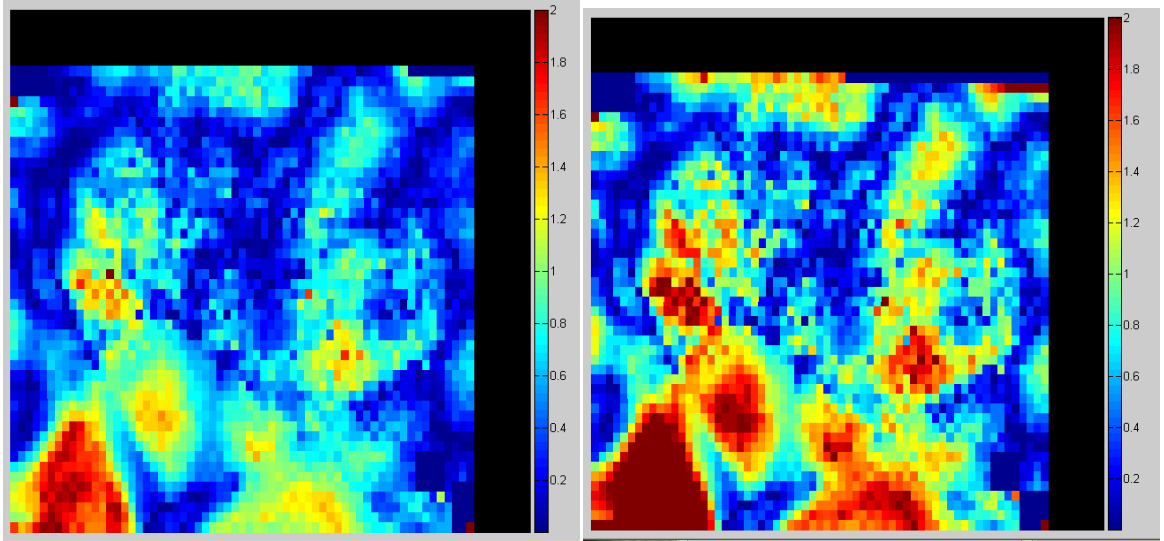

Figure D.41 Plan 1 measurement 2 full axial region, 7%/4mm with 96.44% pixels passing (left) and 5%/3mm with 79.69% pixels passing(right)
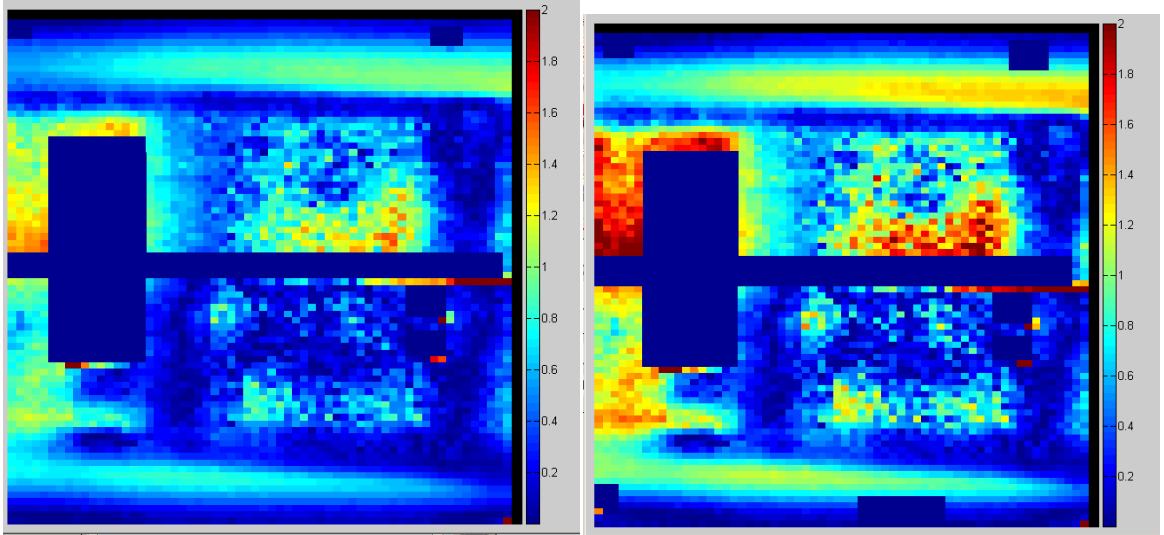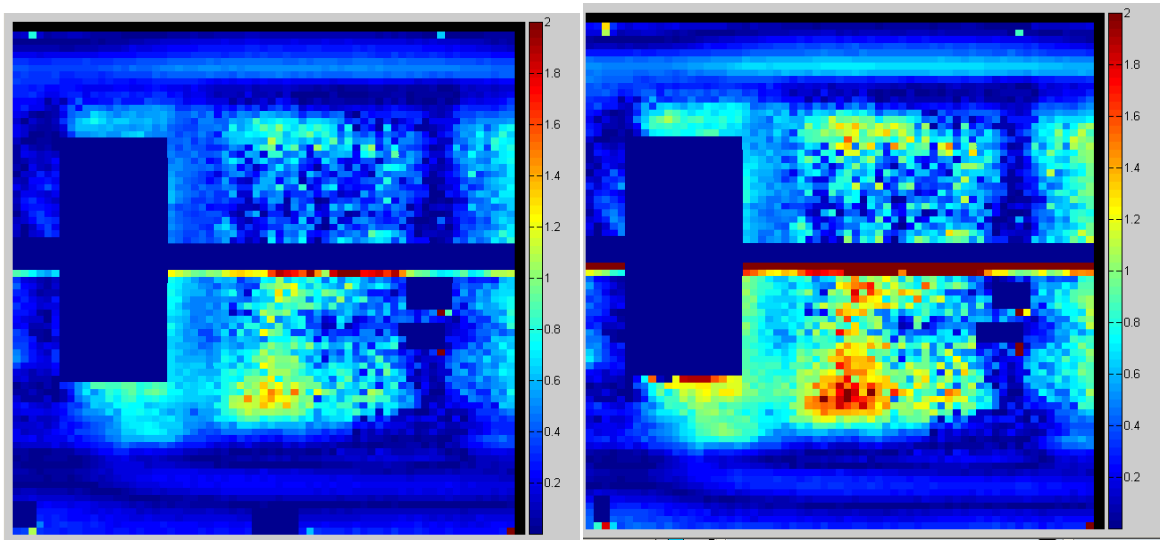
Figure D.42 Plan 1 measurement 2 full sagittal region, 7%/4mm with 93.12% pixels passing (left) and 5%/3mm with 77.48% pixels passing (right)
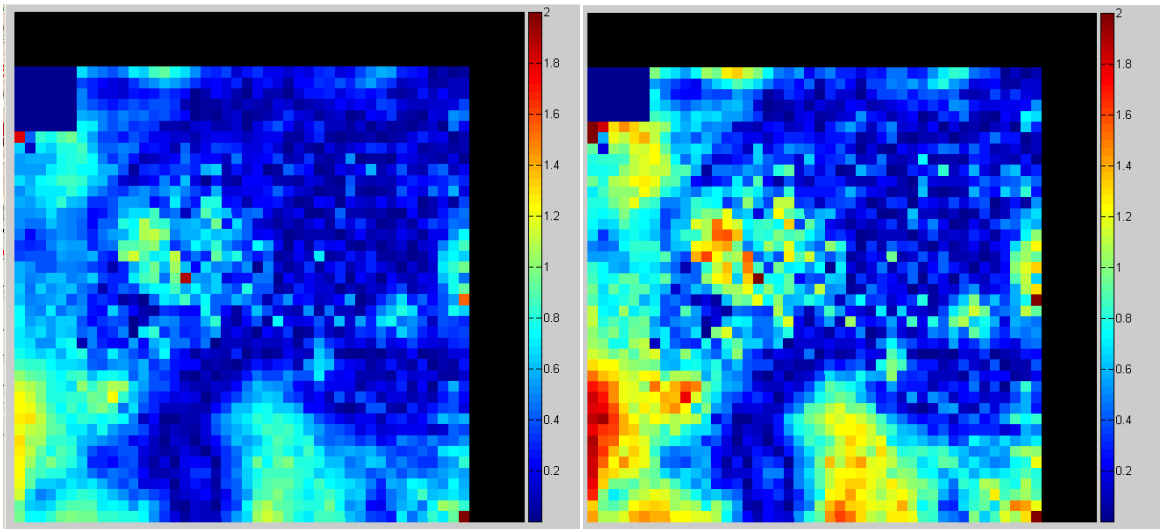
Figure D.43 Plan 1 measurement 3 axial PTV region, 7%/4mm with 97.57% pixels passing (left) and 5%/3mm with 81.68% pixels passing (right)
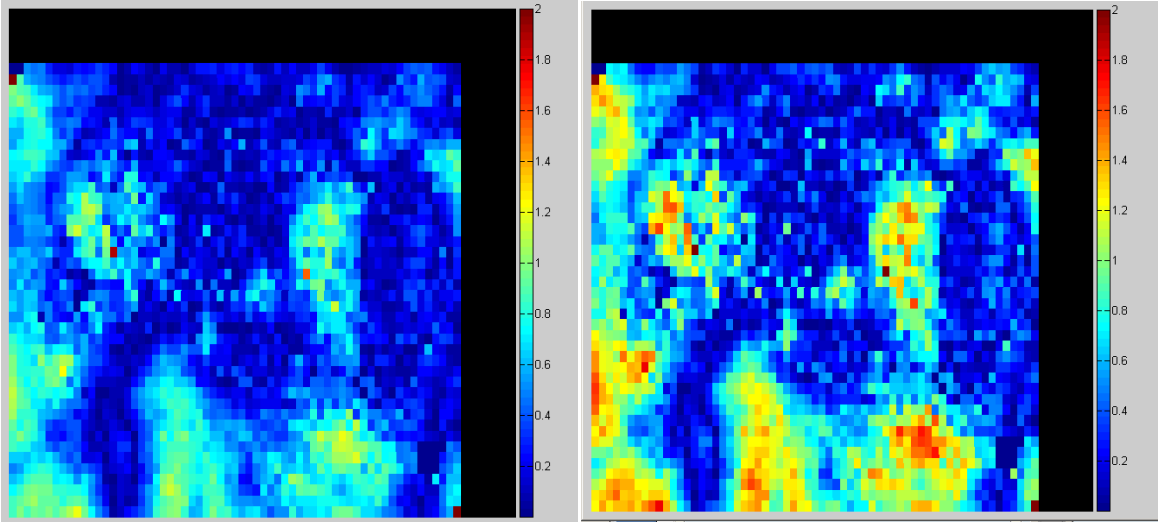
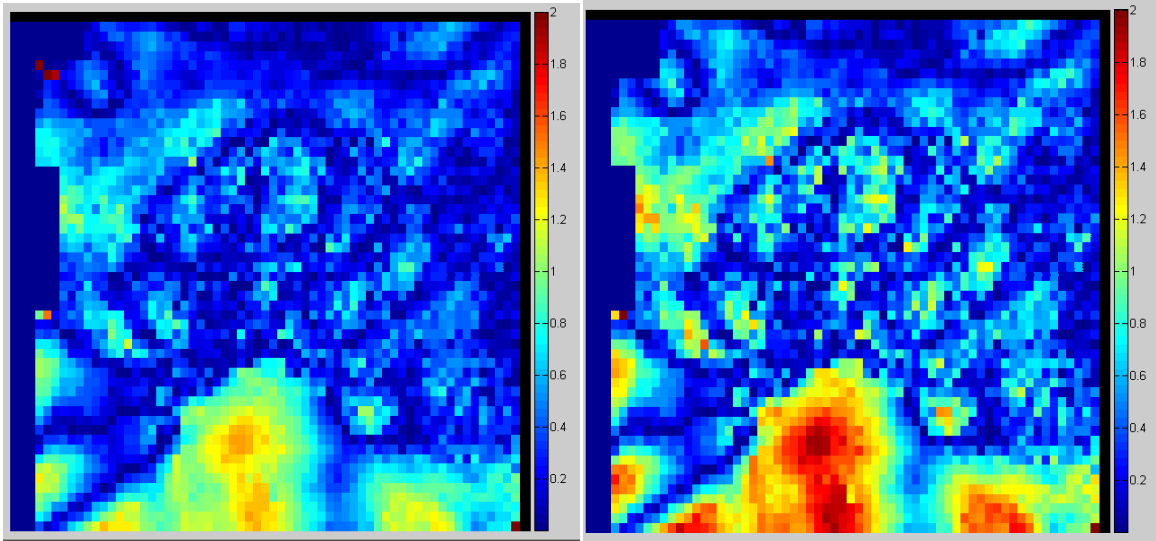**Figure D.44 Plan 1 measurement 3 full axial region, 7%/4mm with 97.95% pixels passing (left) and 5%/3mm with 81.59% pixels passing (right)**
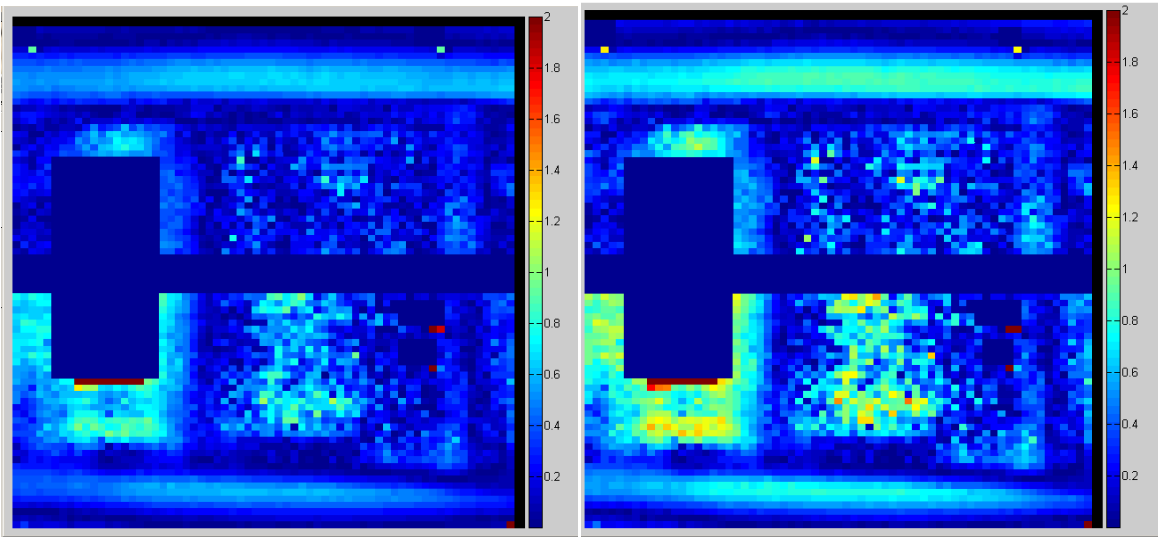
Figure D.45 Plan 1 measurement 3 full sagittal region, 7%/4mm with 99.54% pixels passing (left) and 5%/3mm with 96.38% pixels passing (right)

Plan 2 Results
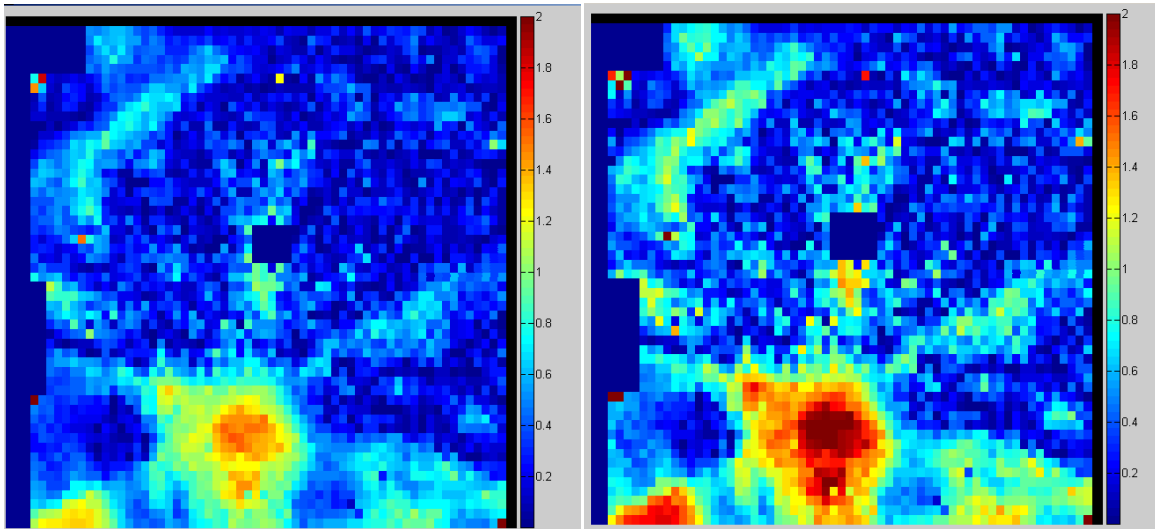
Figure D.46 Plan 2 measurement 1 axial PTV region, 7%/4mm with 93.74% pixels passing (left) and 5%/3mm with 86.38% pixels passing (right)
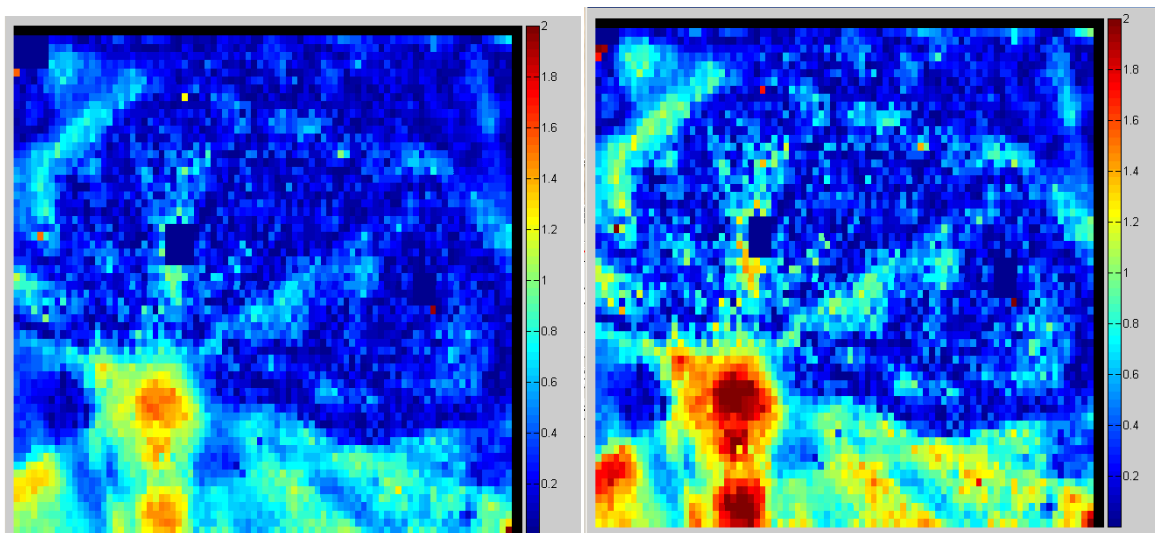
Figure D.47 Plan 2 measurement 1 full axial region, 7%/4mm with 94.54% pixels passing (left) and 5%/3mm with 85.24% pixels passing (right)
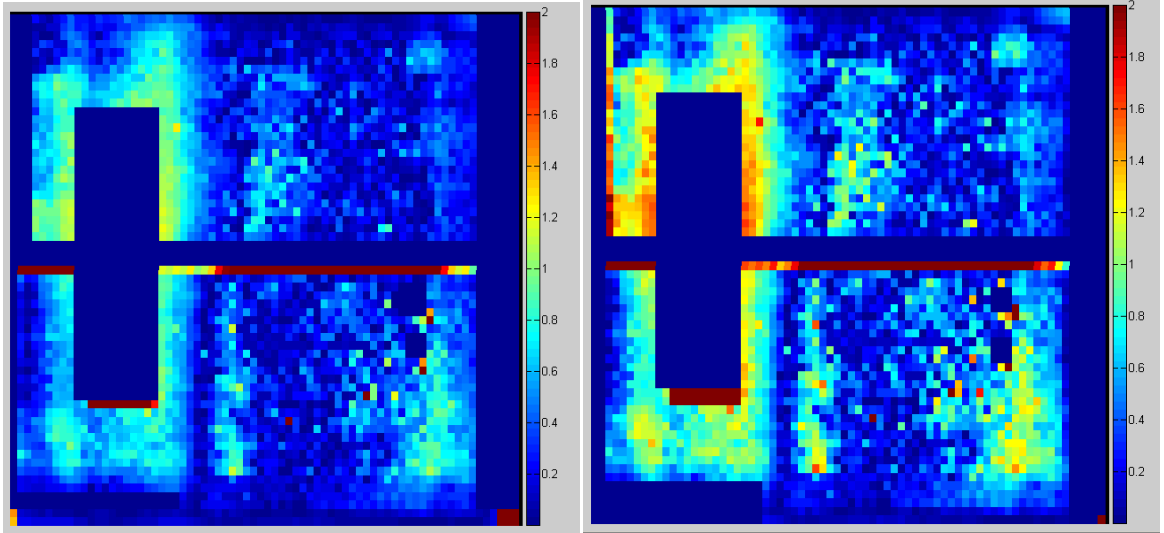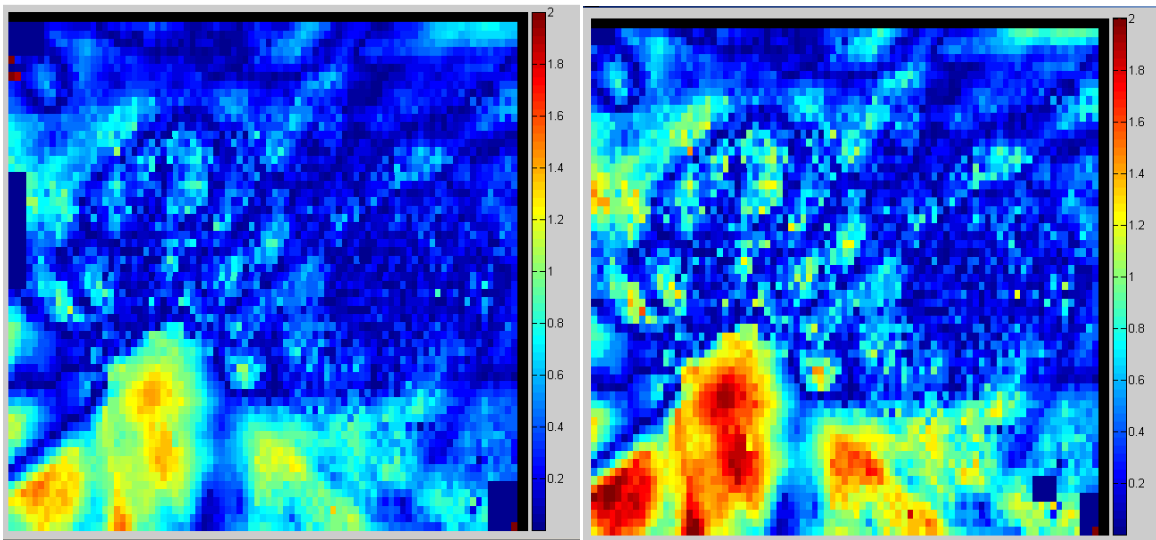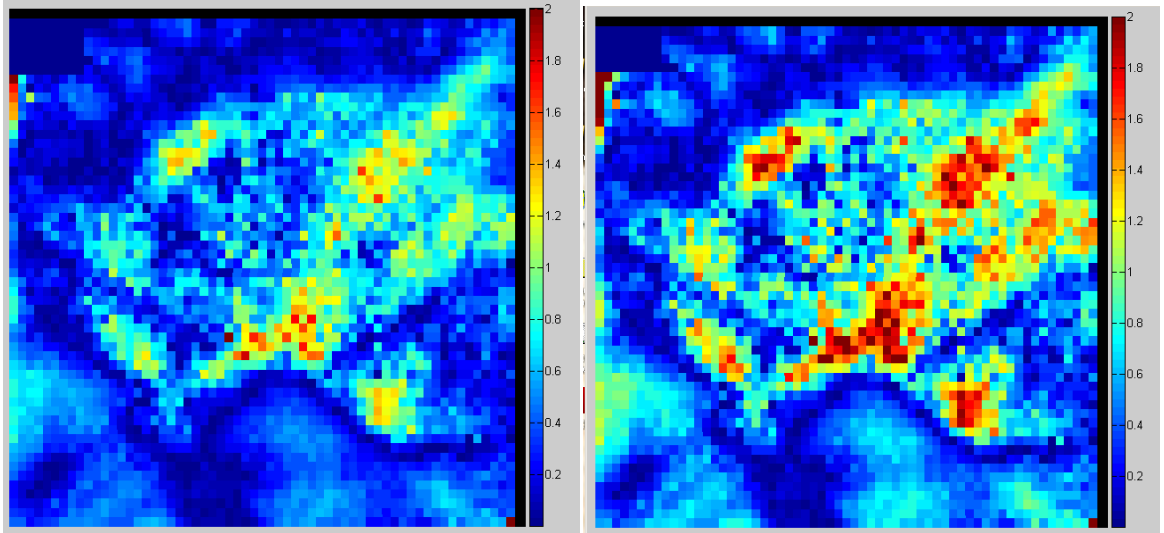
Figure D.48 Plan 2 measurement 1 full sagittal region, 7%/4mm with 96.15% pixels passing (left) and 5%/3mm with 85.55% pixels passing (right)
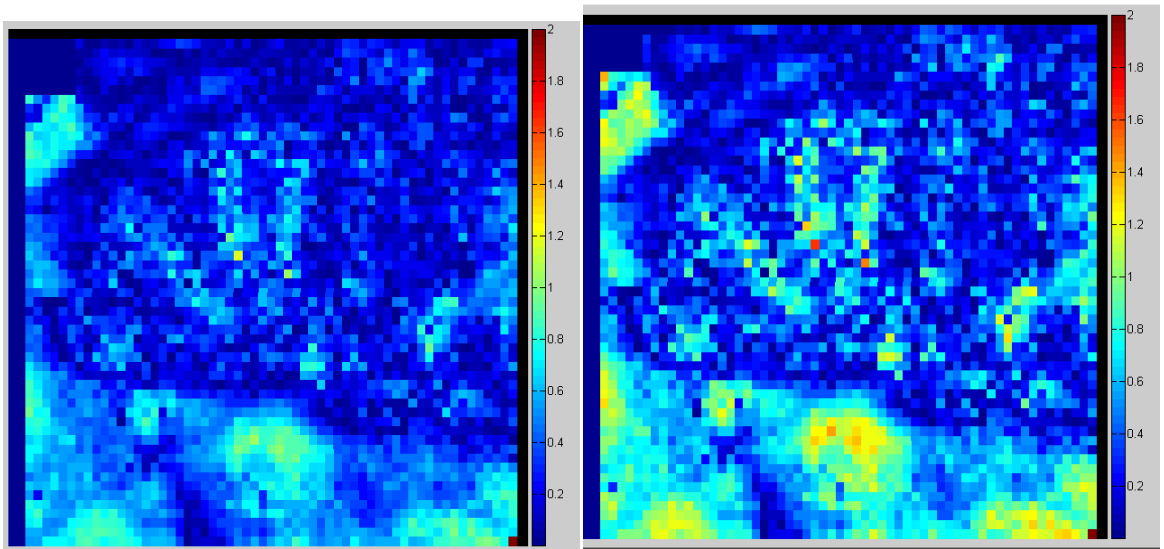
Figure D.49 Plan 2 measurement 2 axial PTV region, 7%/4mm with 99.84% pixels passing (left) and 5%/3mm with 94% pixels passing (right)
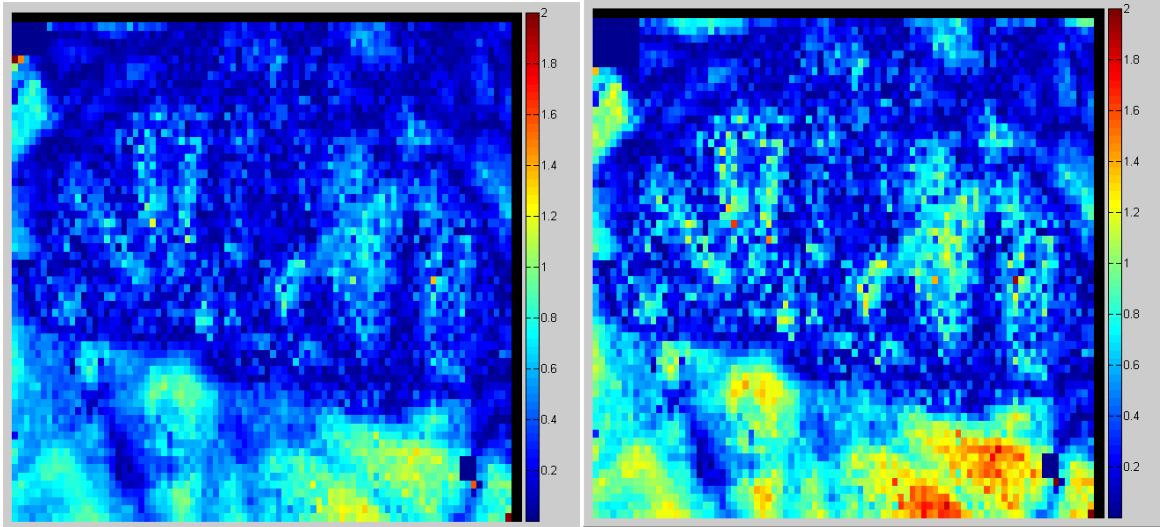
Figure D.50 Plan 2 measurement 2 full axial region, 7%/4mm with 98.24% pixels passing (left) and 5%/3mm with 89.9% pixels passing (right)
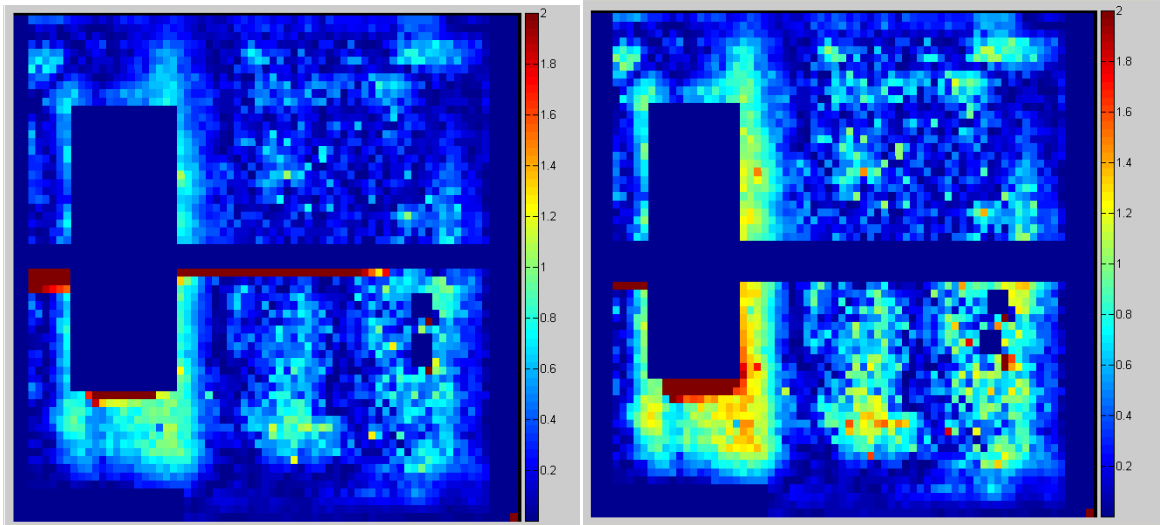
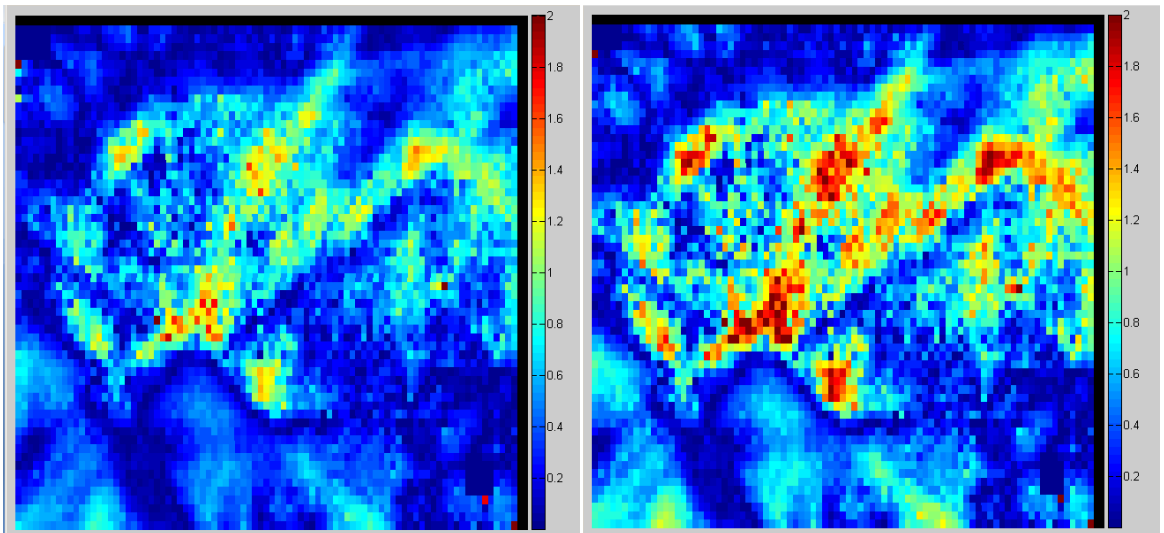**Figure D.51 Plan 2 measurement 2 full sagittal region, 7%/4mm with 97.17% pixels passing (left) and 5%/3mm with 90.43% pixels passing (right)**
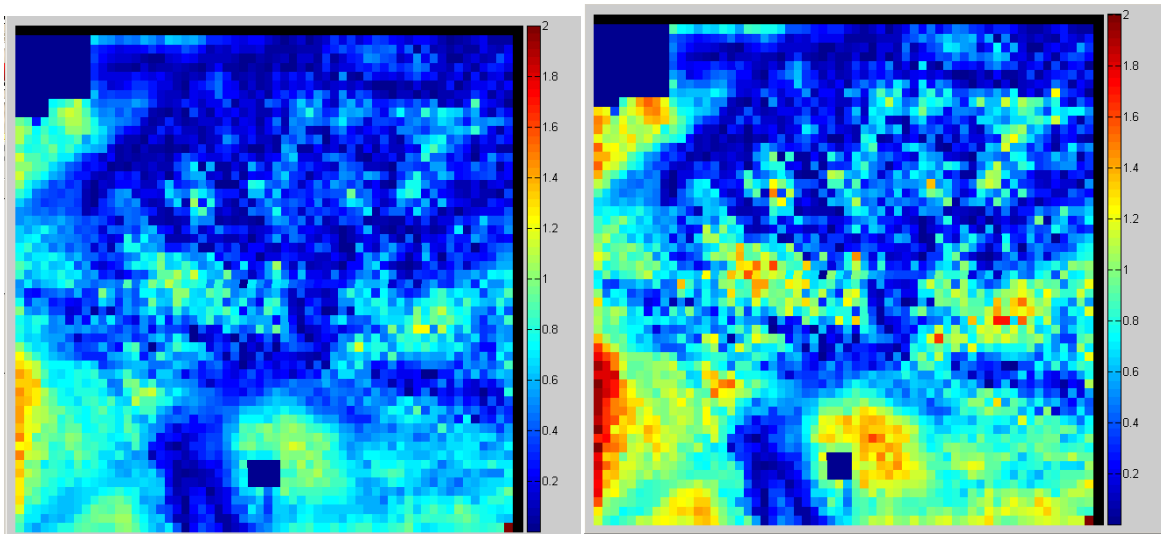
Figure D.52 Plan 2 measurement 3 axial PTV region, 7%/4mm with 96.83% pixels passing (left) and 5%/3mm with 81.22% pixels passing (right)
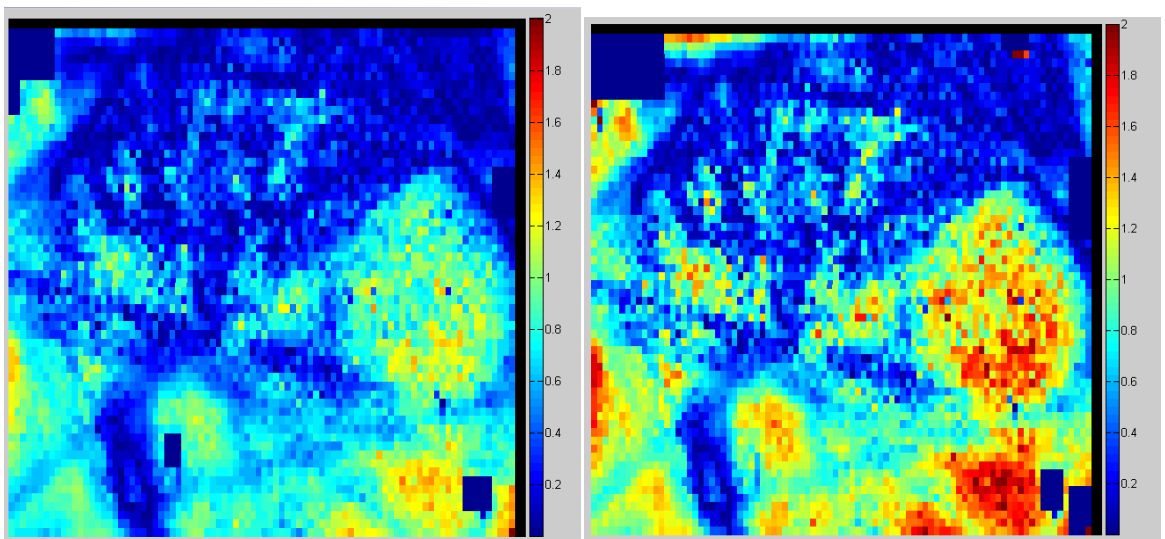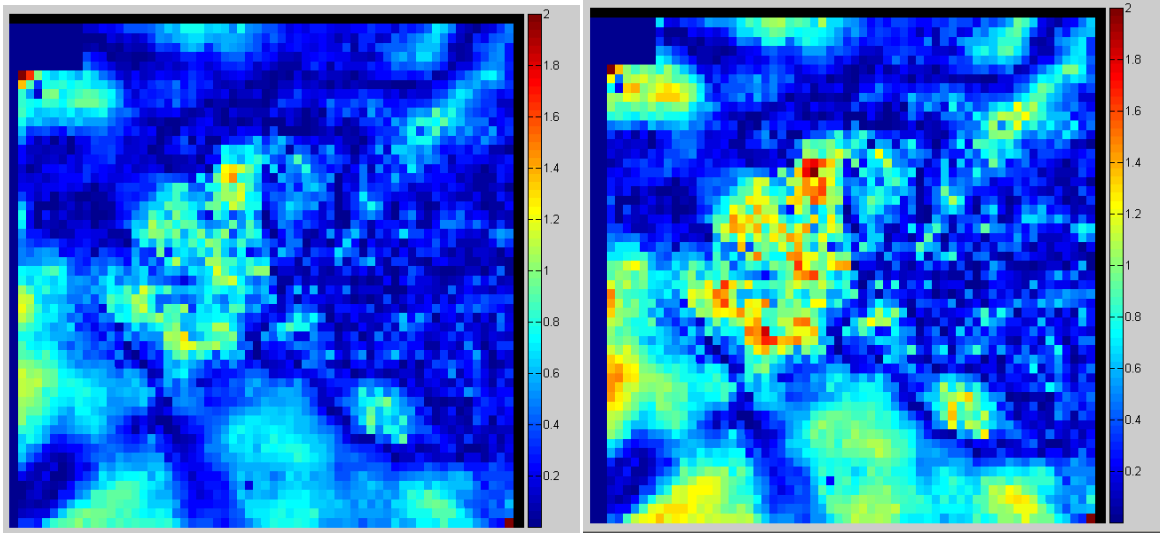

Figure D.53 Plan 2 measurement 3 full axial region, 7%/4mm with 91.32% pixels passing (left) and 5%/3mm with 70.51% pixels passing (right)
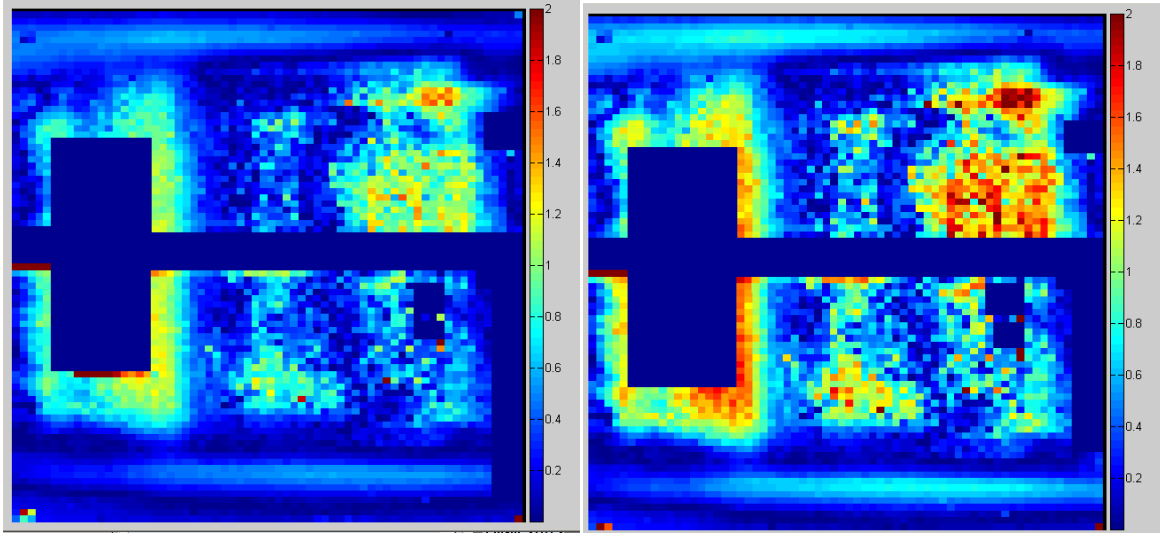
Figure D.54 Plan 2 measurement 3 full sagittal region, 7%/4mm with 93.33% pixels passing (left) and 5%/3mm with 82.57% pixels passing (right)

Plan 3 Results
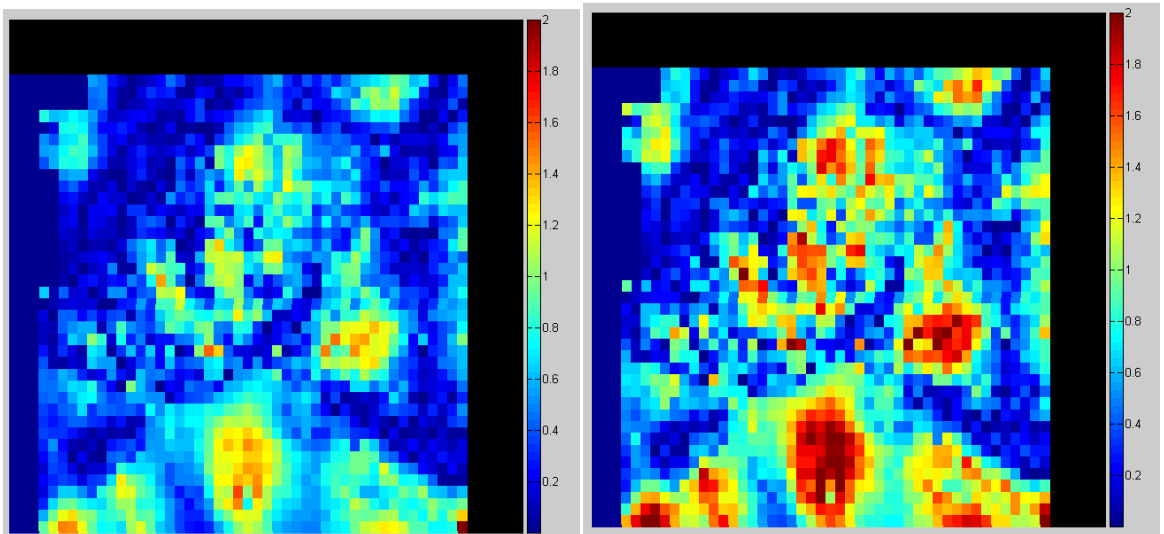
Figure D.55 Plan 3 measurement 1 axial PTV region, 7%/4mm gamma index analysis with 90.3% pixels passing (left) and 5%/3mm with 71.62% pixels passing (right)
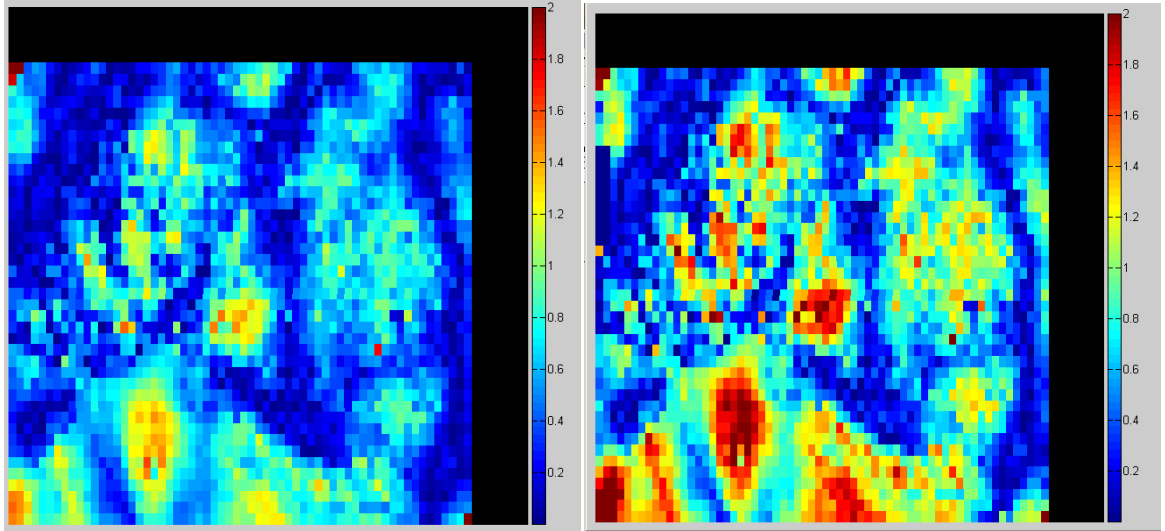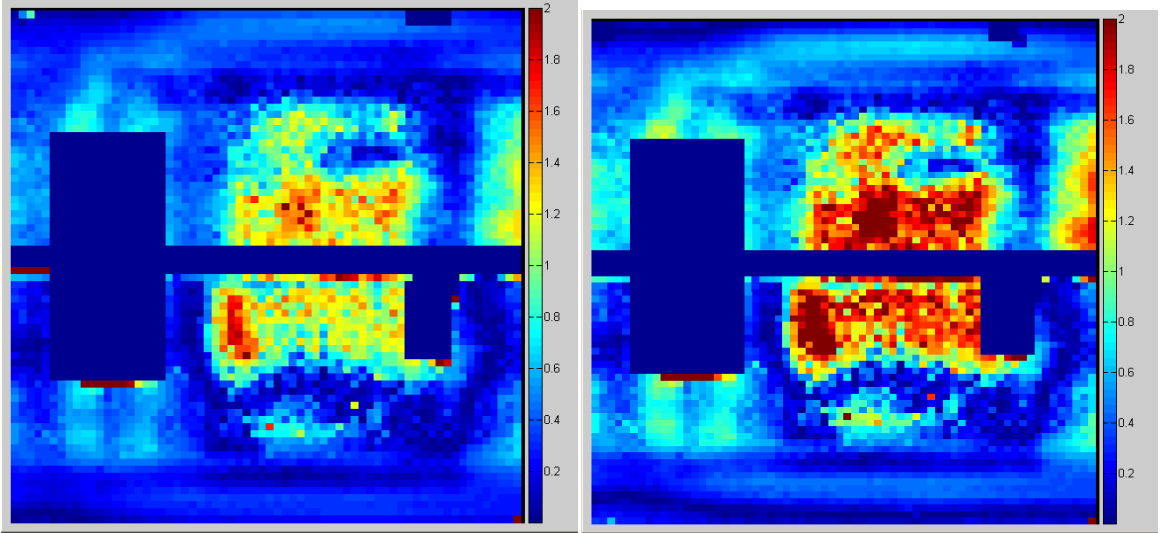
Figure D.56 Plan 3 measurement 1 full axial region, 7%/4mm gamma index analysis with 92.09% pixels passing (left) and 5%/3mm with 70.34% pixels passing (right)
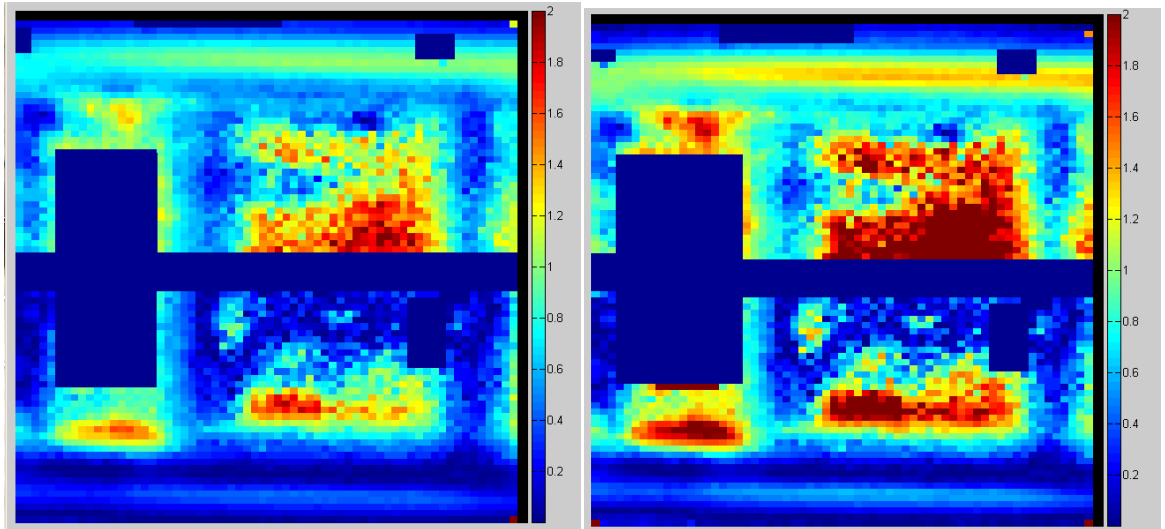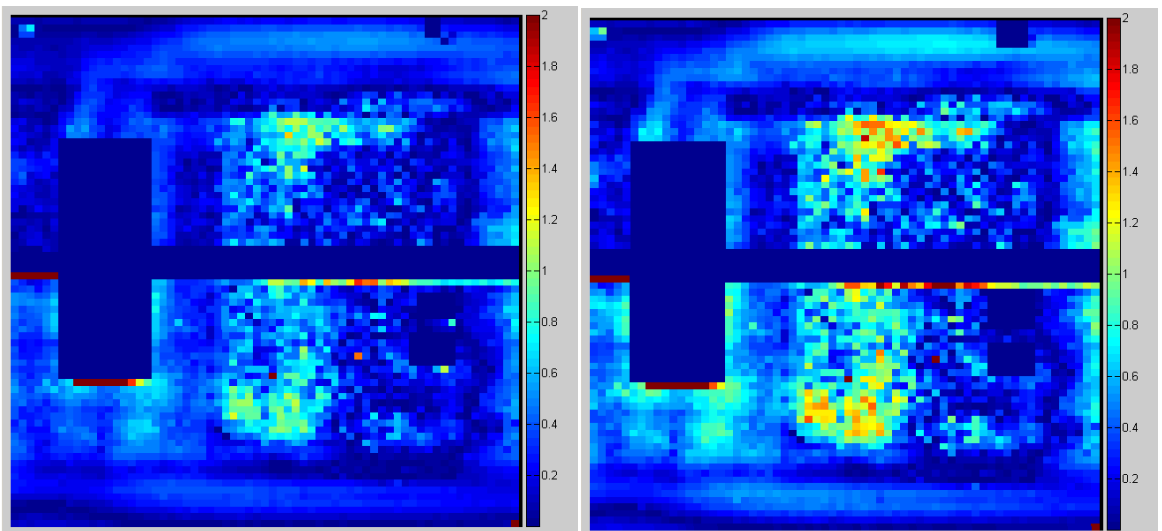

Figure D.57 Plan 3 measurement 1 full sagittal region, 7%/4mm gamma index analysis with 83.72% pixels passing (left) and 5%/3mm with 68.17% pixels passing (right)
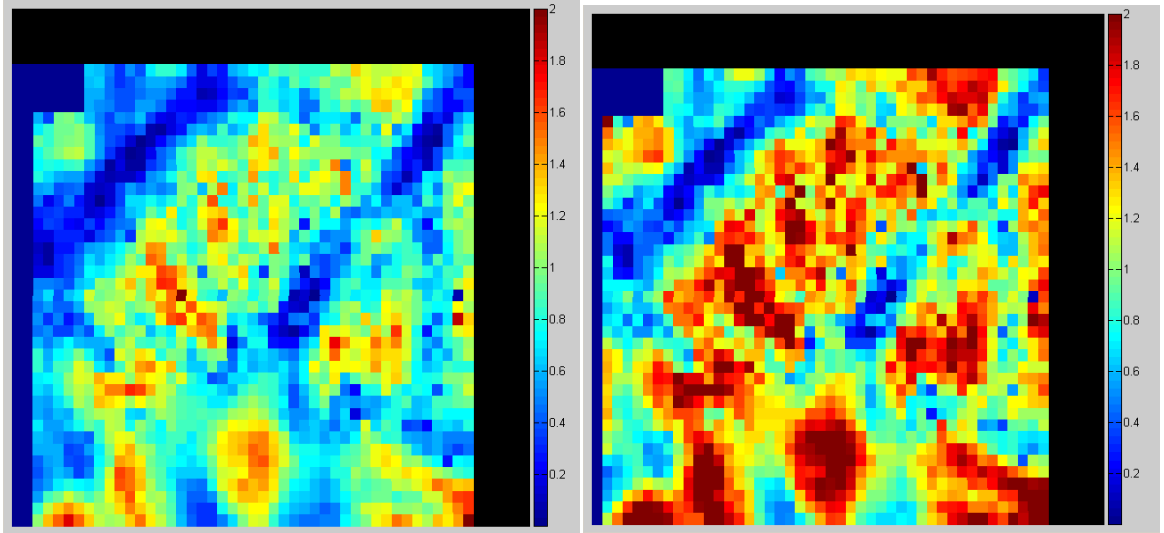
Figure D.58 Plan 3 measurement 2 axial PTV region, 7%/4mm gamma index analysis with 69.34% pixels passing (left) and 5%/3mm with 37.12% pixels passing (right)
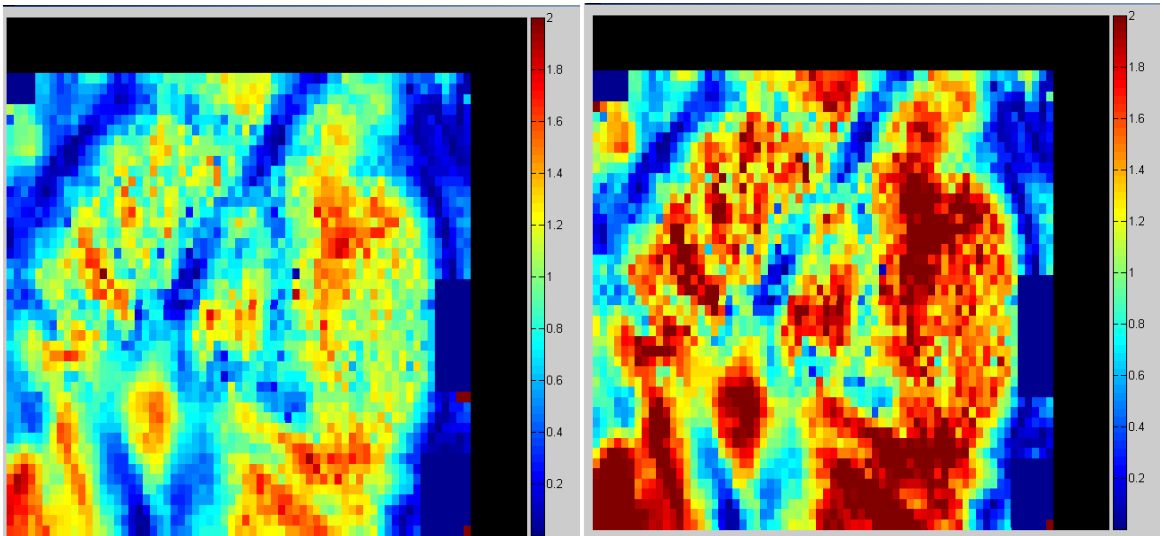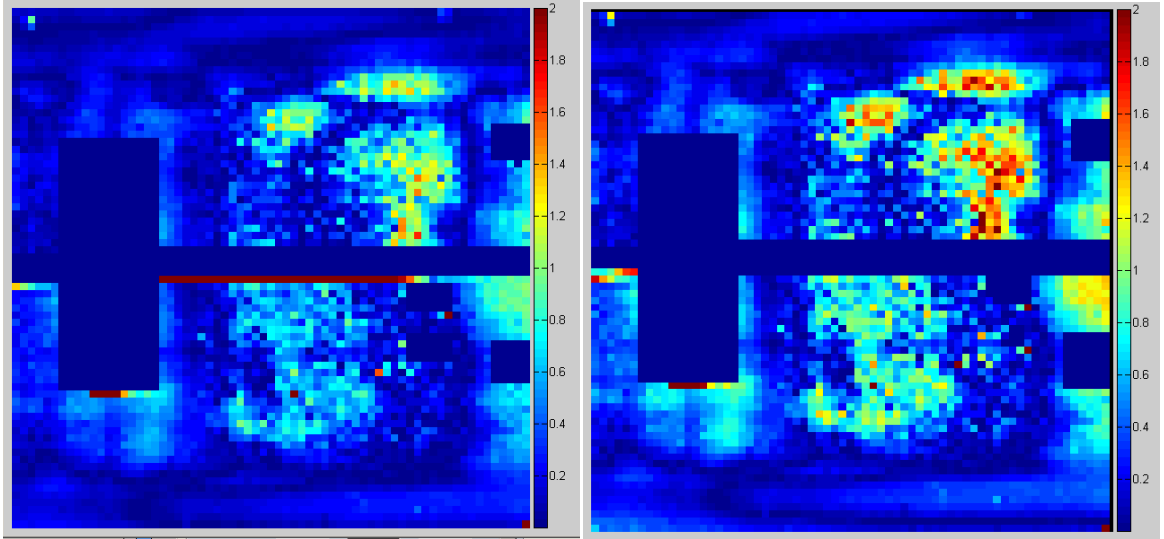

Figure D.59 Plan 3 measurement 2 full axial region, 7%/4mm gamma index analysis with 60.54% pixels passing (left) and 5%/3mm with 34.34% pixels passing (right)
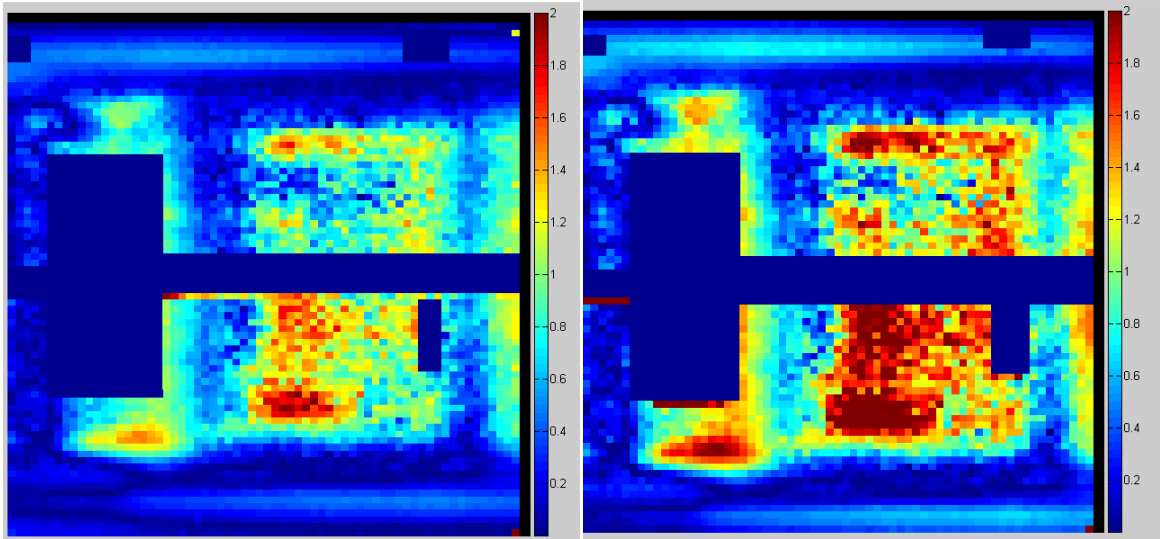
Figure D.60 Plan 3 measurement 2 full sagittal region, 7%/4mm gamma index analysis with 85.33% pixels passing (left) and 5%/3mm with 69.57% pixels passing (right)
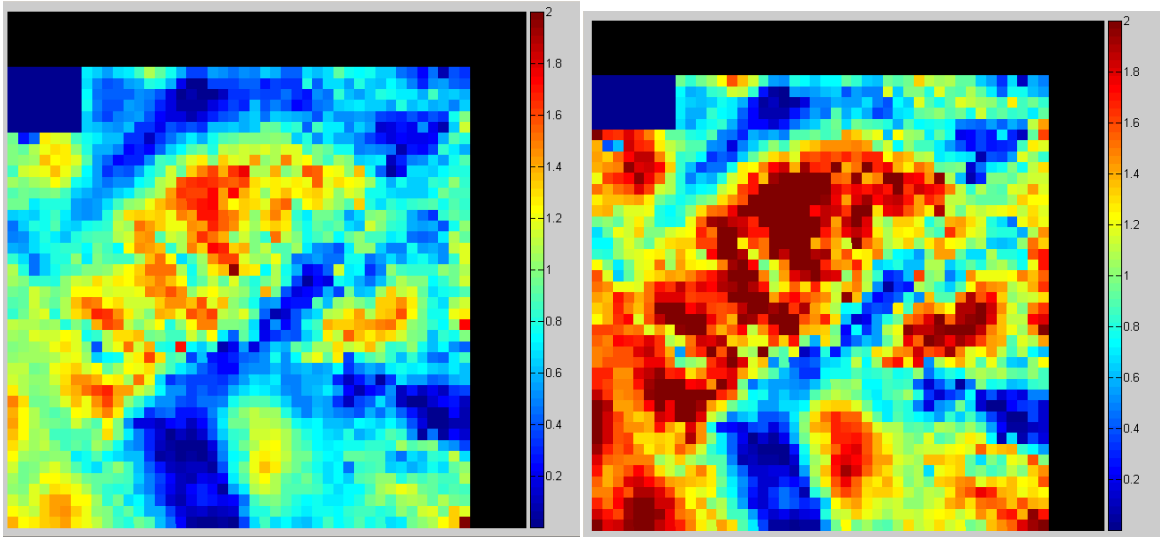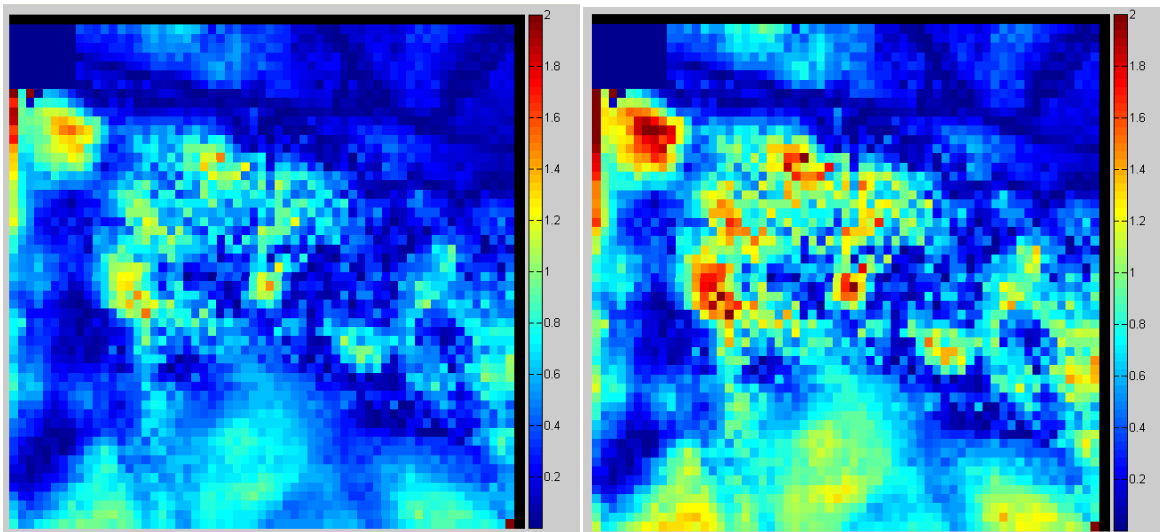

Figure D.61 Plan 3 measurement 3 axial PTV region, 7%/4mm gamma index analysis with 67.33% pixels passing (left) and 5%/3mm with 37.11% pixels passing (right)
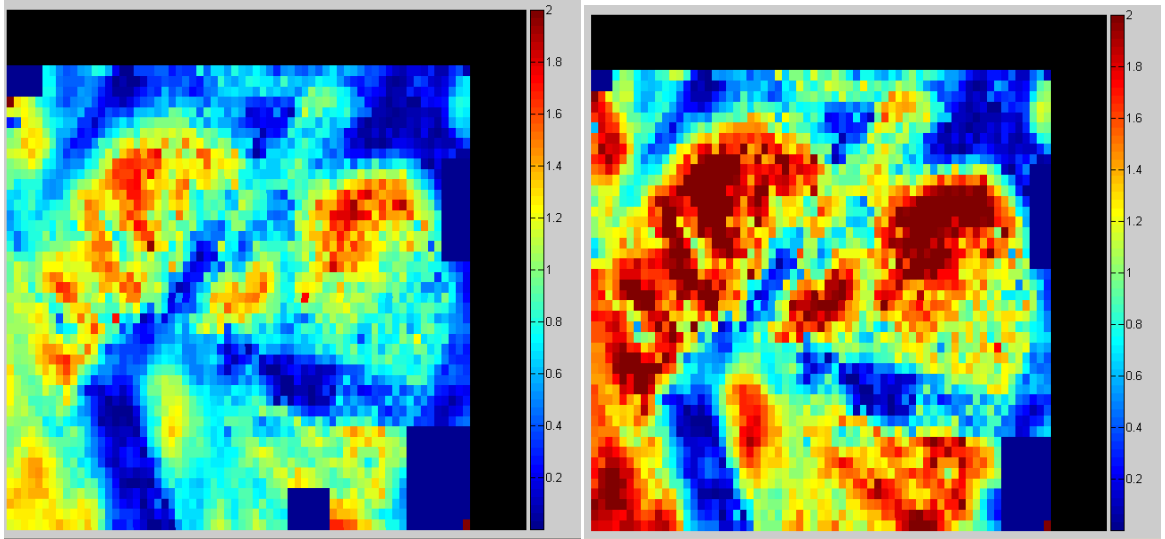
Figure D.62 Plan 3 measurement 3 full axial region, 7%/4mm gamma index analysis with 68.06% pixels passing (left) and 5%/3mm with 40.01% pixels passing (right)
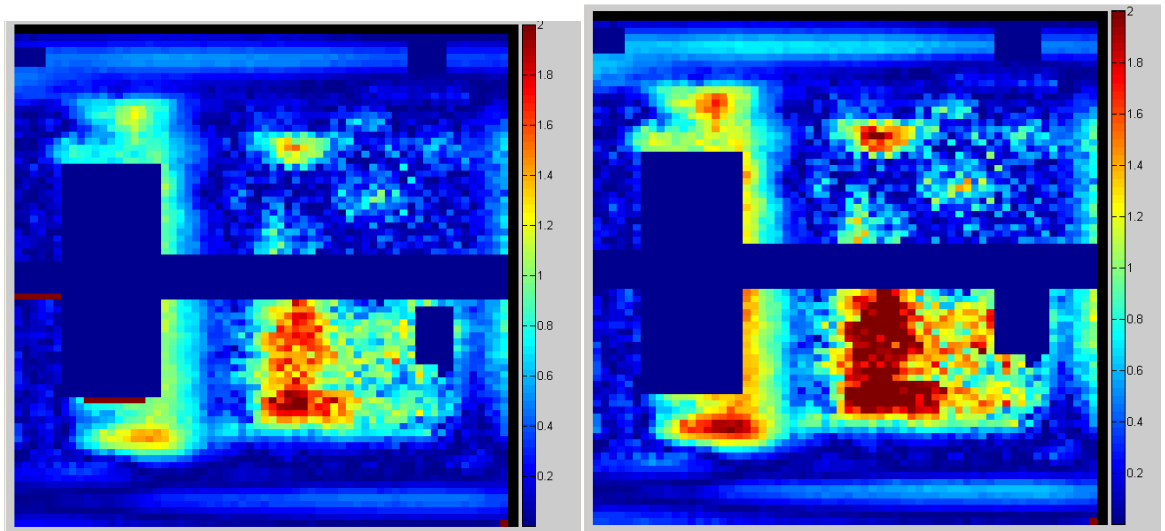
Figure D.63 Plan 3 measurement 3 full sagittal region, 7%/4mm gamma index analysis with 91.22% pixels passing (left) and 5%/3mm with 82.41% pixels passing (right)
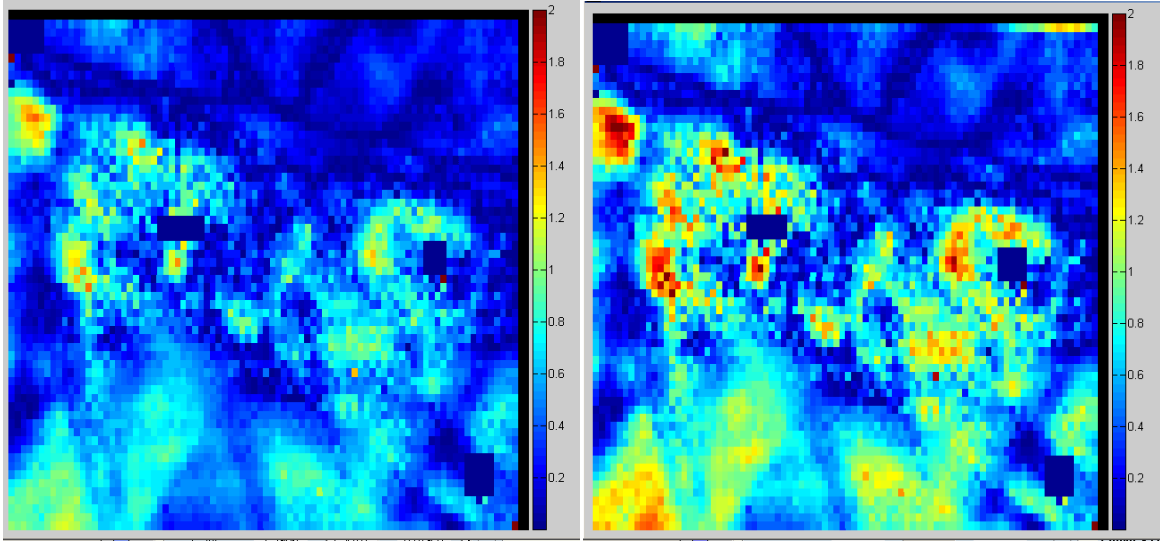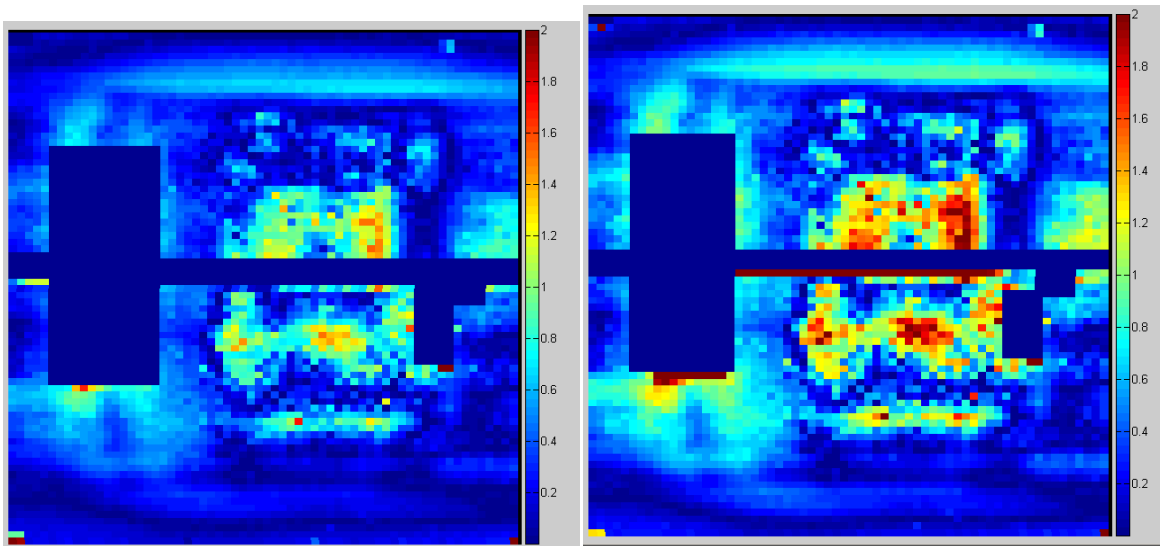
Plan 4 Results
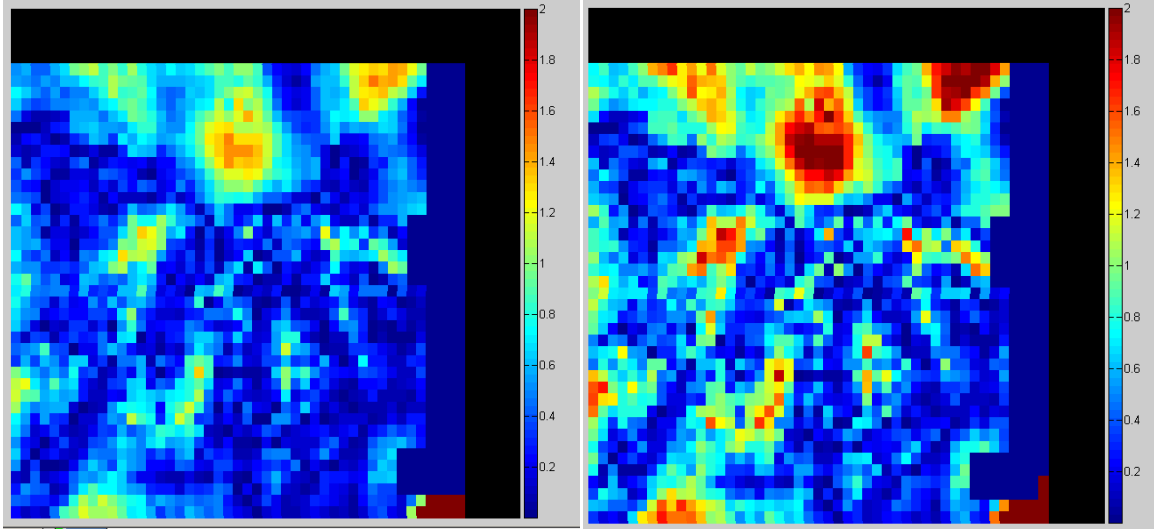
Figure D.64 Plan 4 measurement 1 axial PTV region, 7%/4mm gamma index analysis with 92.66% pixels passing (left) and 5%/3mm with 81.07% pixels passing (right)
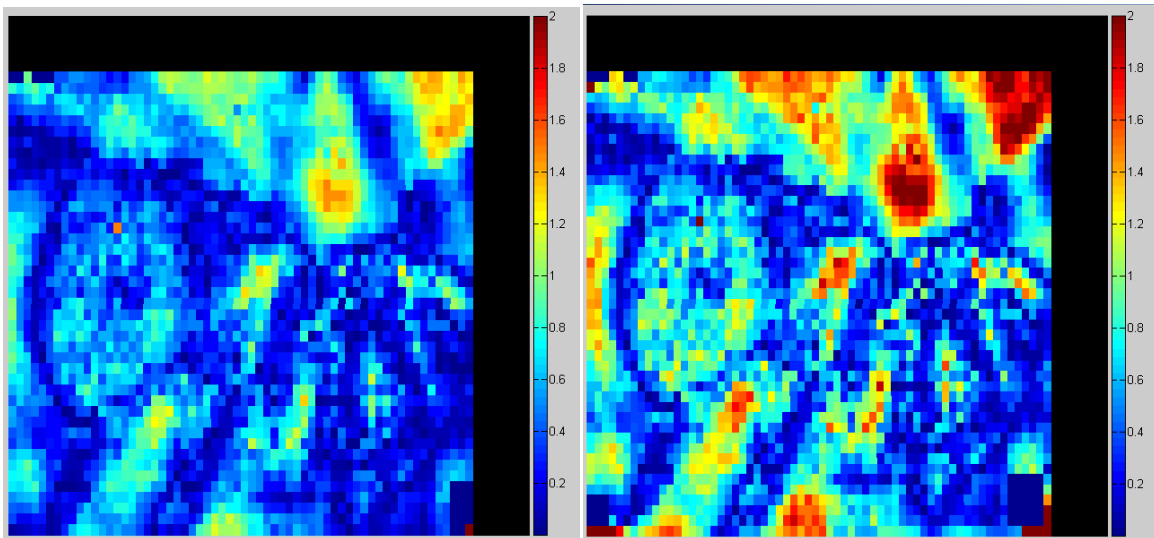
Figure D.65 Plan 4 measurement 1 full axial region, 7%/4mm gamma index analysis with 93.2% pixels passing (left) and 5%/3mm with 77.79% pixels passing (right)
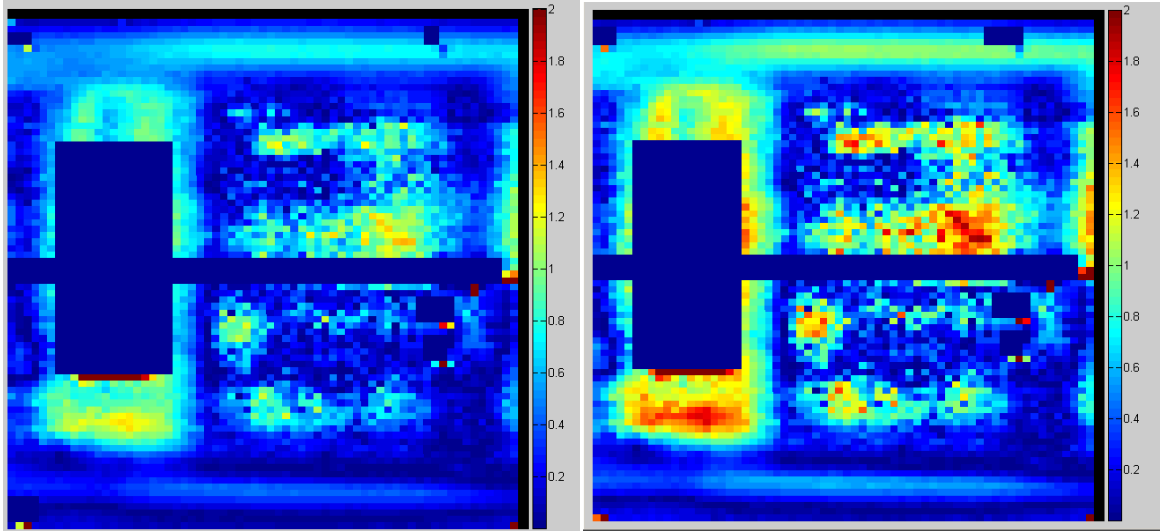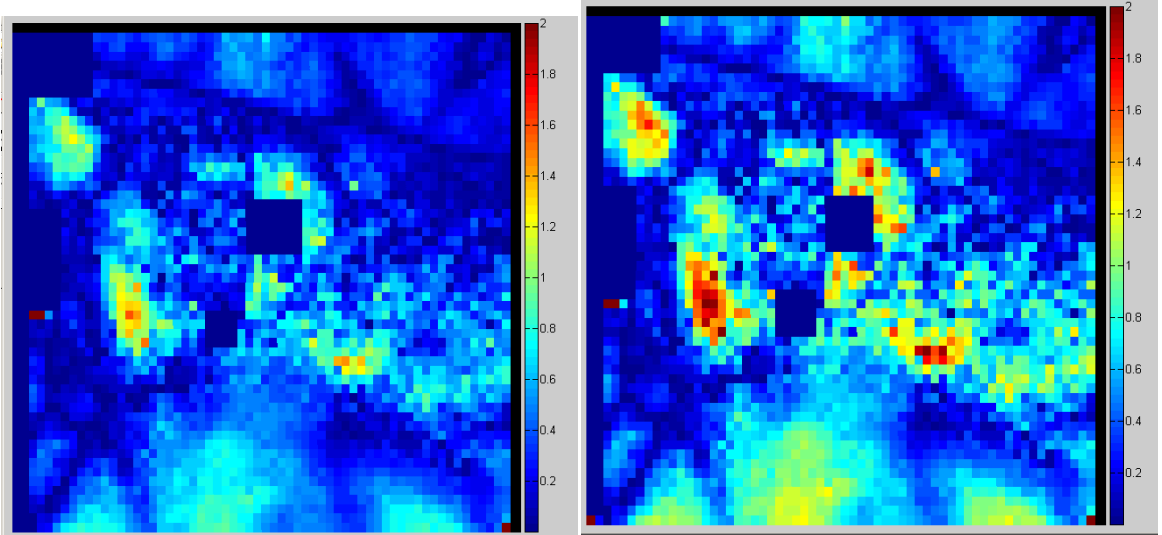
Figure D.66 Plan 4 measurement 1 full sagittal region, 7%/4mm gamma index analysis with 96.34% pixels passing (left) and 5%/3mm with 84.43% pixels passing (right)
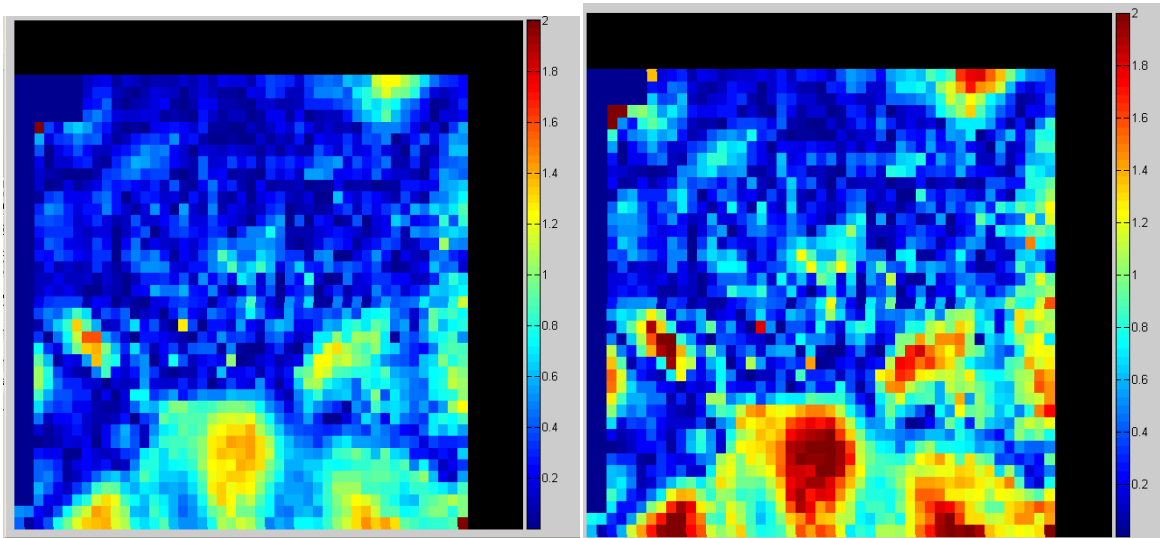
Figure D.67 Plan 4 measurement 2 axial PTV region, 7%/4mm gamma index analysis with 92.35% pixels passing (left) and 5%/3mm with 77.73% pixels passing (right)
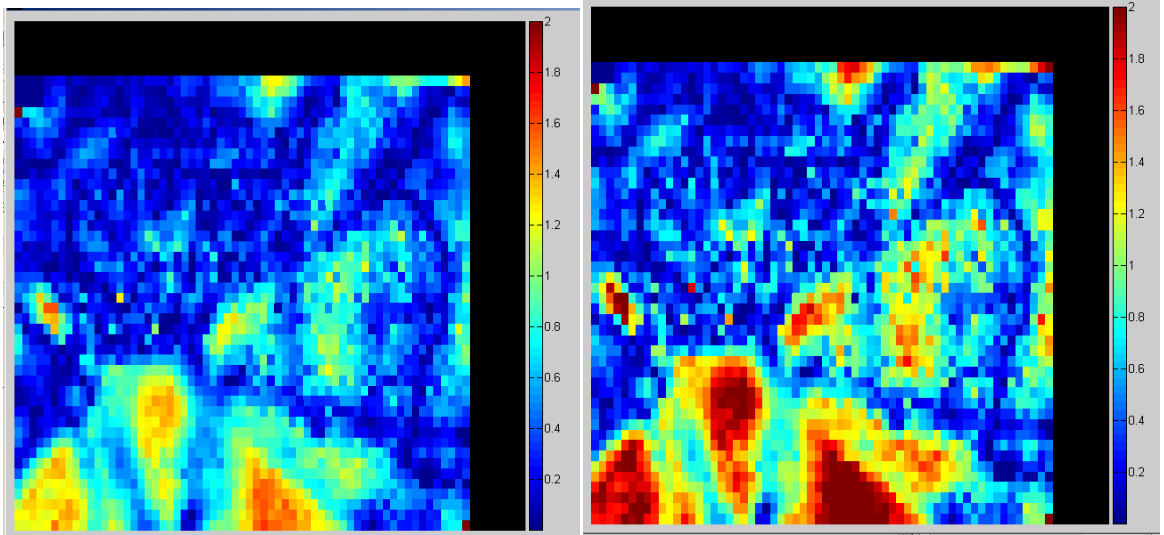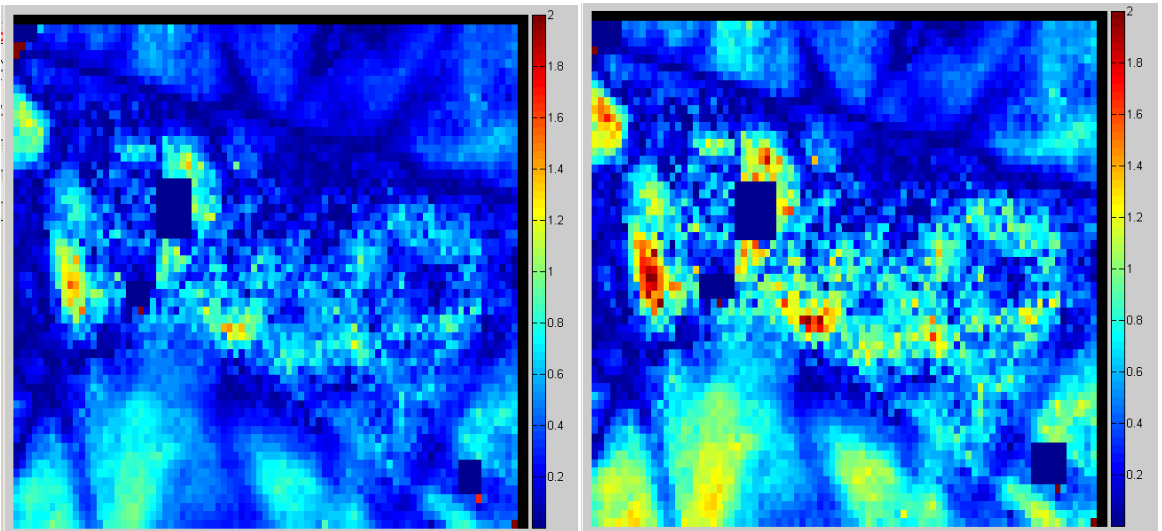
Figure D.68 Plan 4 measurement 2 full axial region, 7%/4mm gamma index analysis with 89.99% pixels passing (left) and 5%/3mm with 73.38% pixels passing (right)
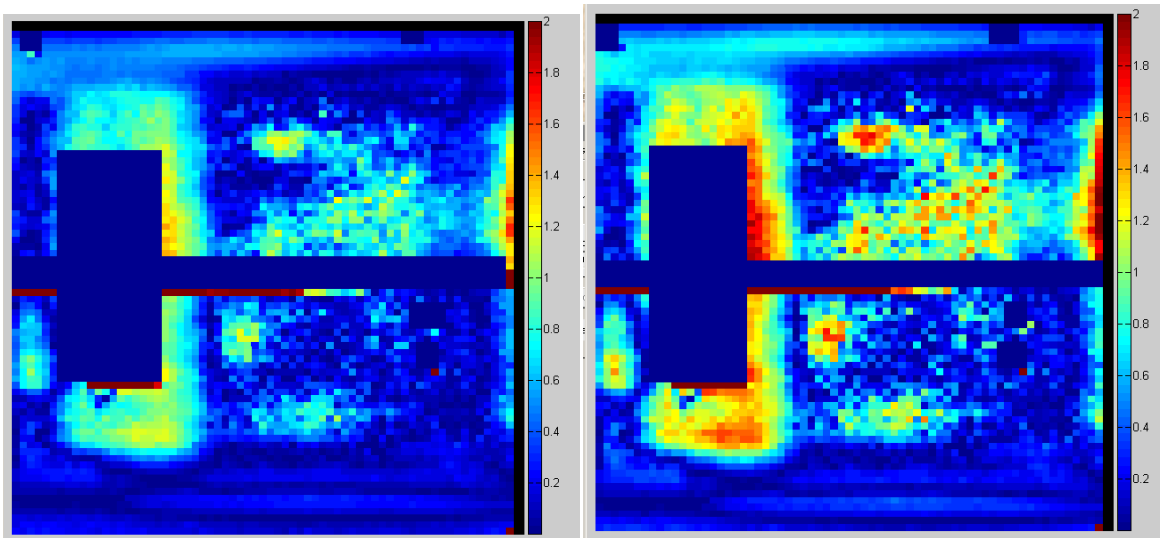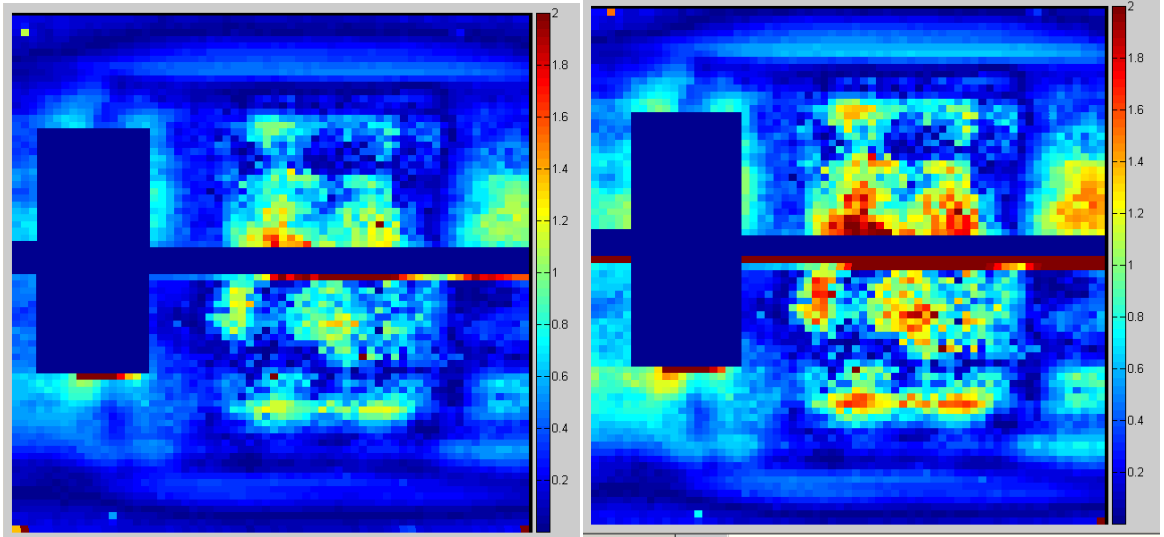

Figure D.69 Plan 4 measurement 2 full sagittal region, 7%/4mm gamma index analysis with 94.64% pixels passing (left) and 5%/3mm with 83.31% pixels passing (right)
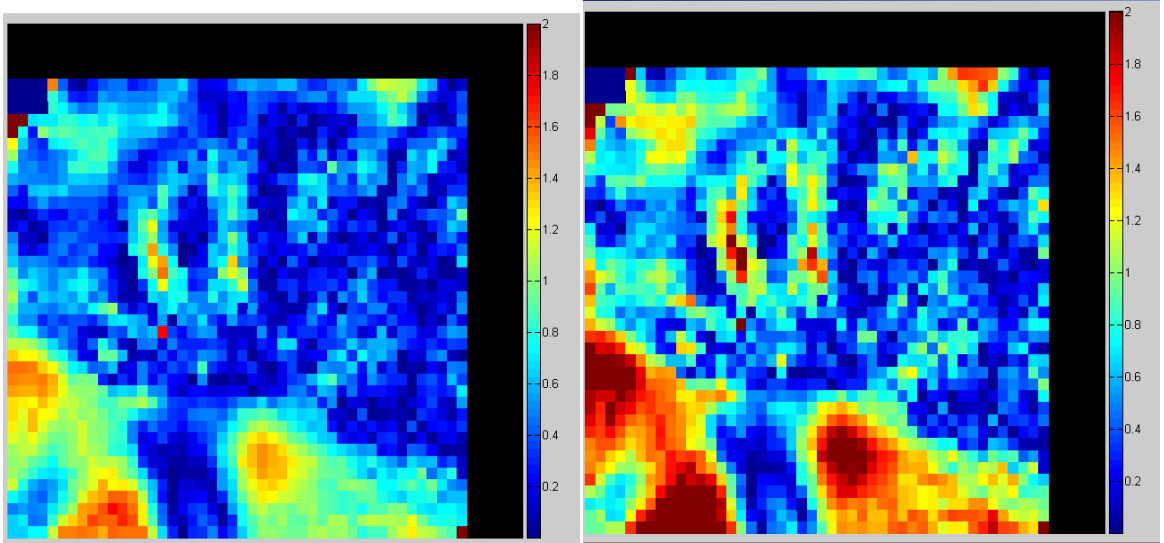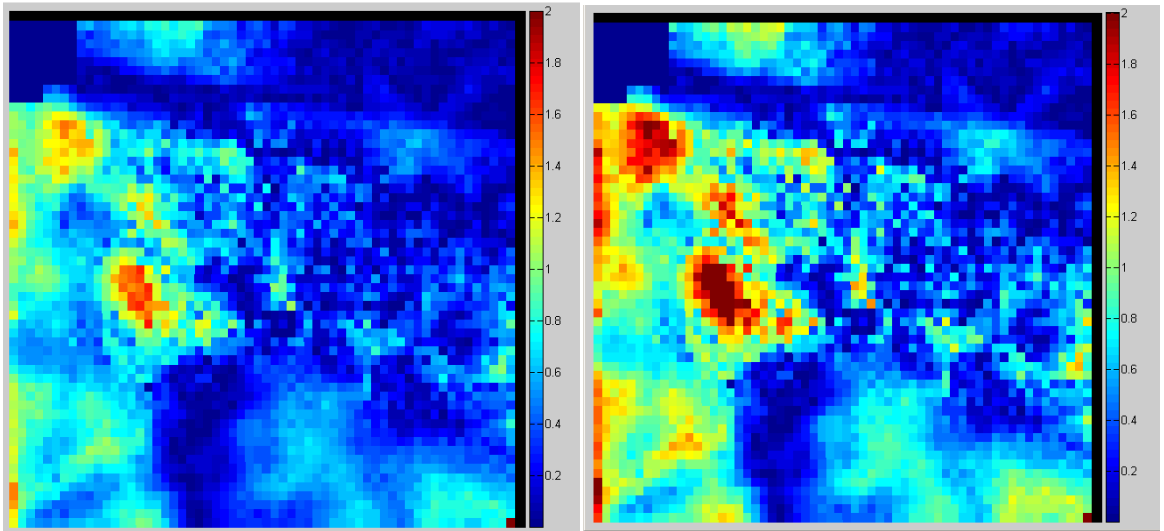
Figure D.70 Plan 4 measurement 3 axial PTV region, 7%/4mm gamma index analysis with 87.32% pixels passing (left) and 5%/3mm with 71.83% pixels passing (right)
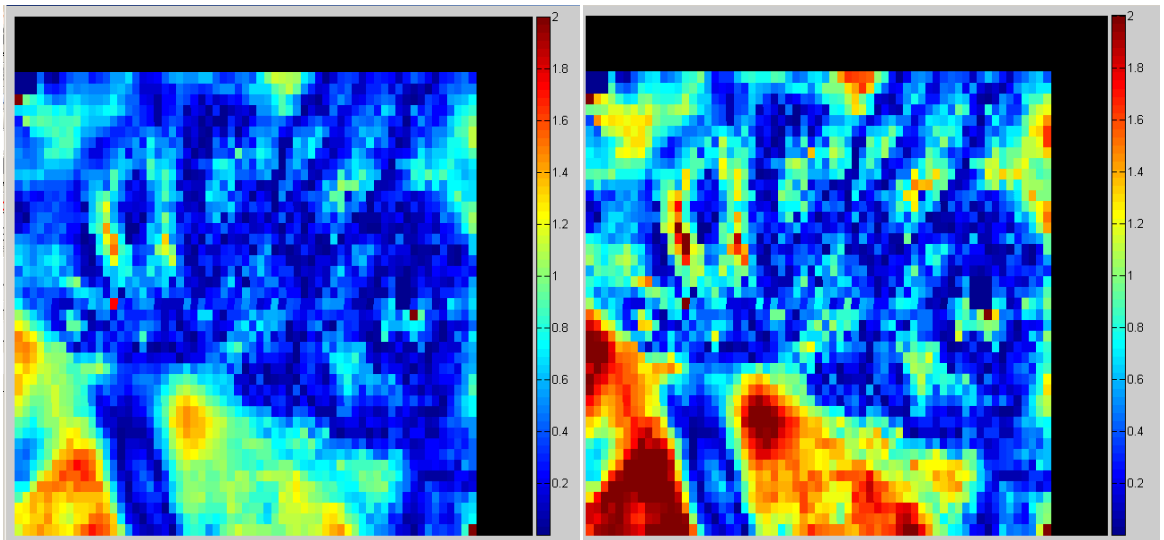
Figure D.71 Plan 4 measurement 3 full axial region, 7%/4mm gamma index analysis with 88.77% pixels passing (left) and 5%/3mm with 73.69% pixels passing (right)
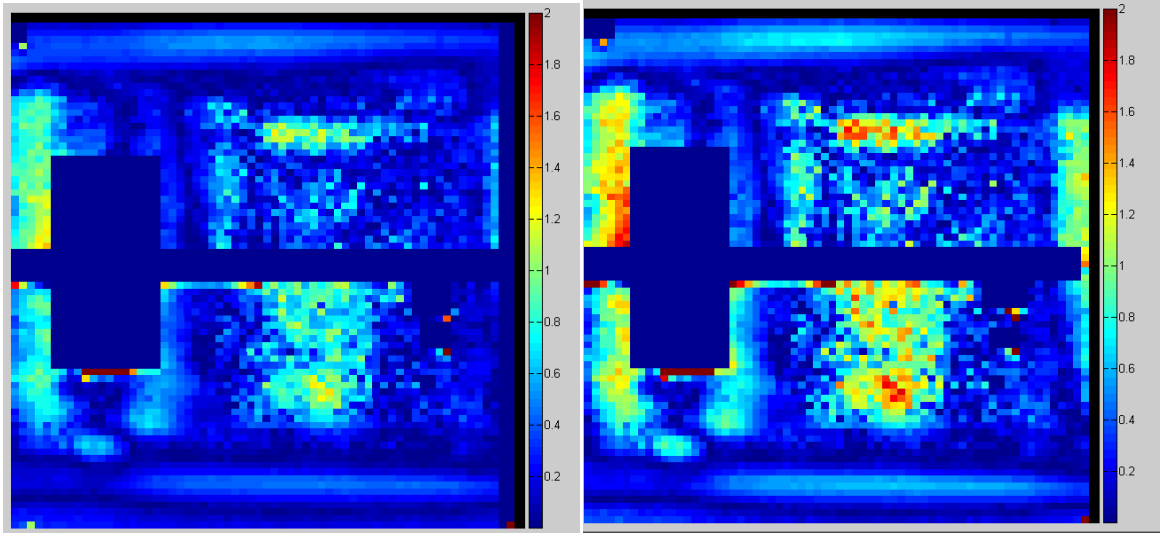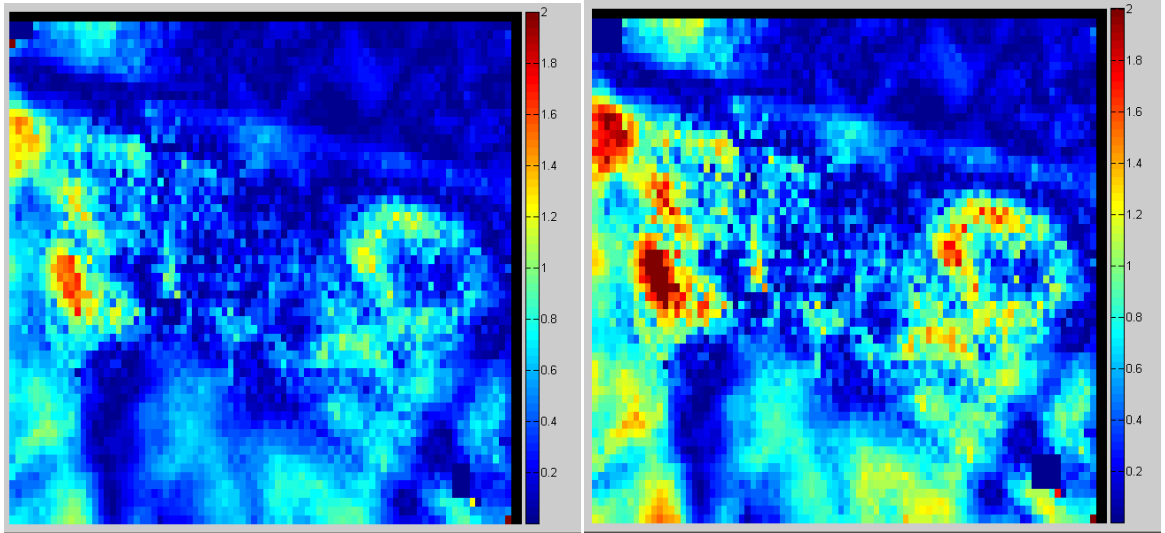
Figure D.72 Plan 4 measurement 3 full sagittal region, 7%/4mm gamma index analysis with 97.81% pixels passing (left) and 5%/3mm with 90.6% pixels passing (right)

Plan 5 Results
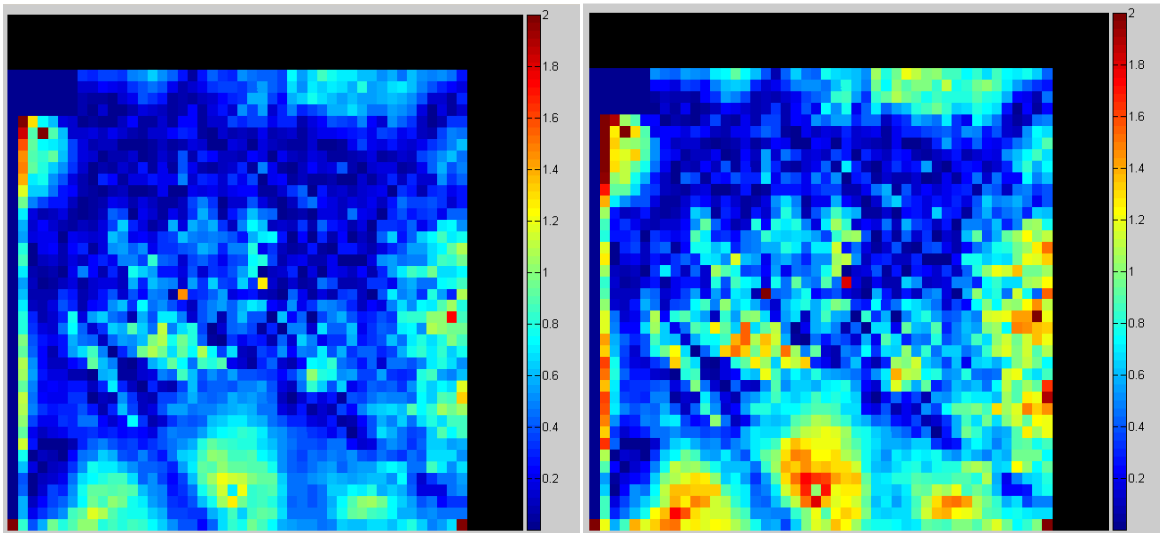
Figure D.73 Plan 5 measurement 1 axial PTV region, 7%/4mm gamma index analysis with 97.02% pixels passing (left) and 5%/3mm with 83.49% pixels passing (right)
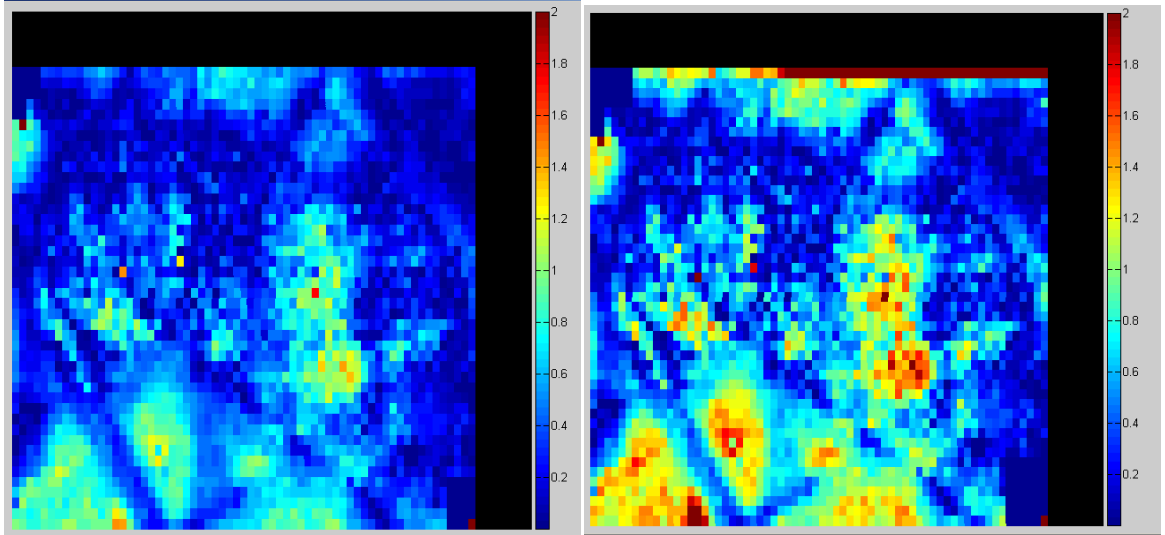
Figure D.74 Plan 5 measurement 1 full axial region, 7%/4mm gamma index analysis with 97.49% pixels passing (left) and 5%/3mm with 81.82% pixels passing (right)
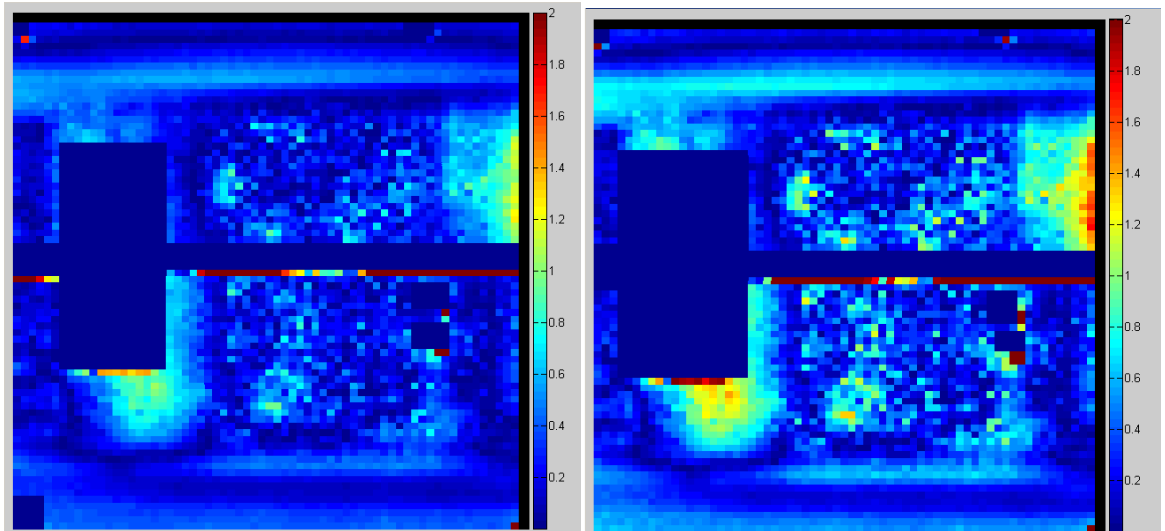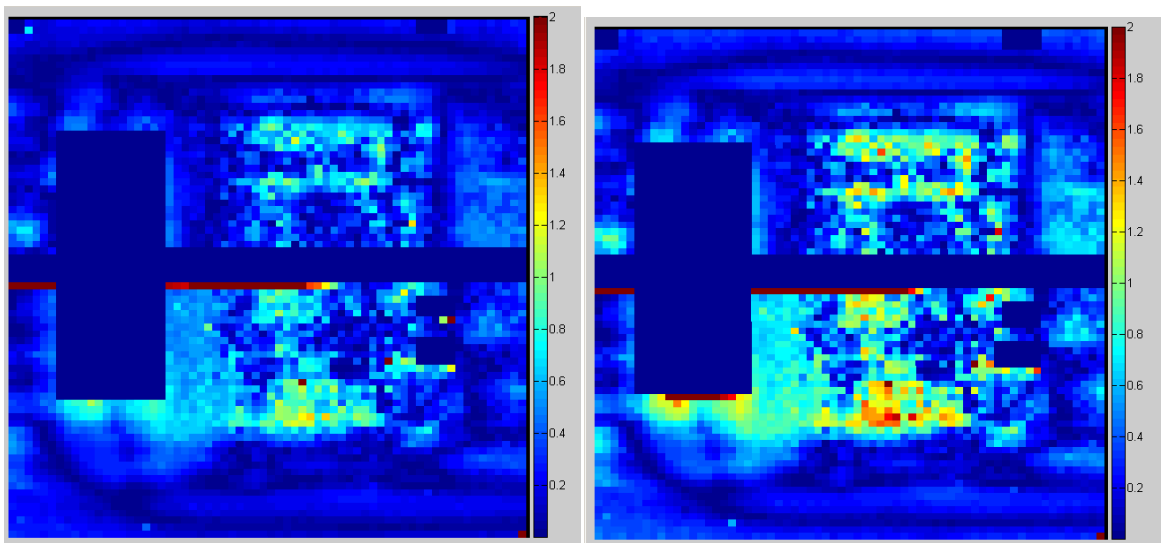

Figure D.75 Plan 5 measurement 1 full sagittal region, 7%/4mm gamma index analysis with 98.28% pixels passing (left) and 5%/3mm with 95.39% pixels passing (right)
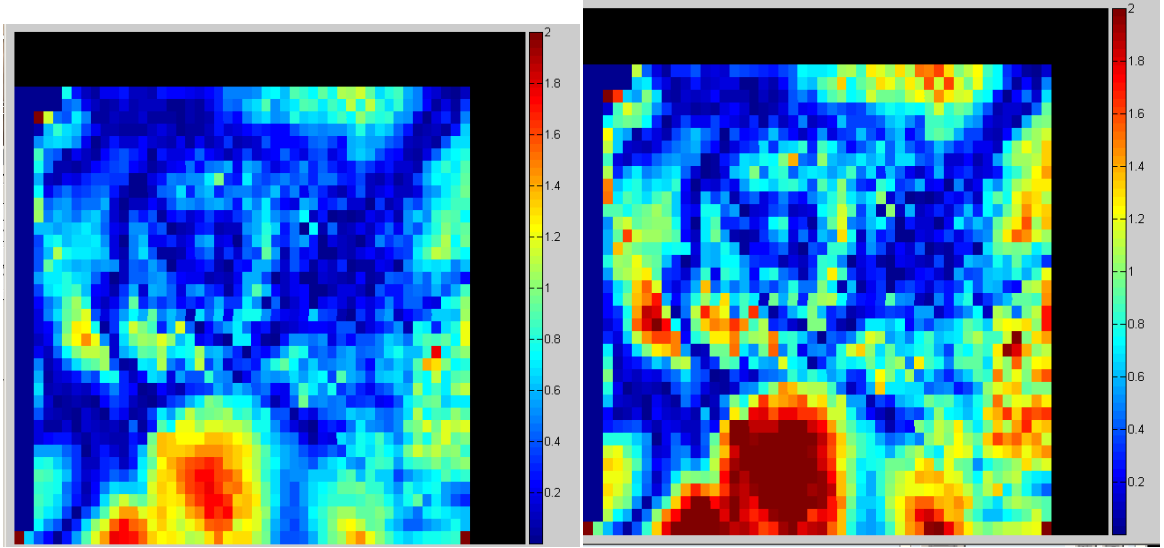
Figure D.76 Plan 5 measurement 2 axial PTV region, 7%/4mm gamma index analysis with 87.81% pixels passing (left) and 5%/3mm with 70.61% pixels passing (right)
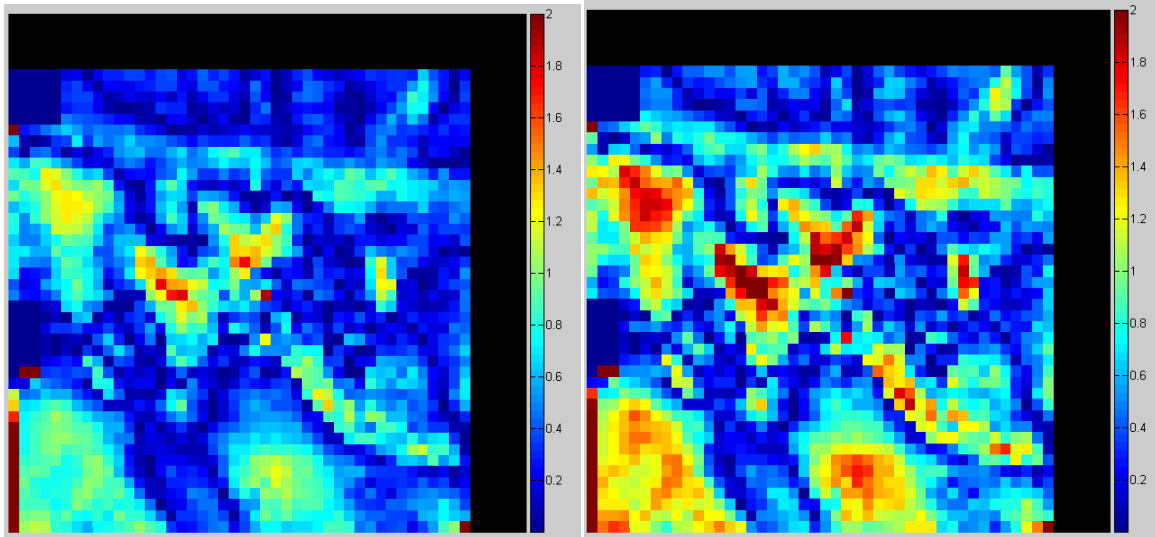

Figure D.77 Plan 5 measurement 2 full axial region, 7%/4mm gamma index analysis with 84.74% pixels passing (left) and 5%/3mm with 66.46% pixels passing (right)
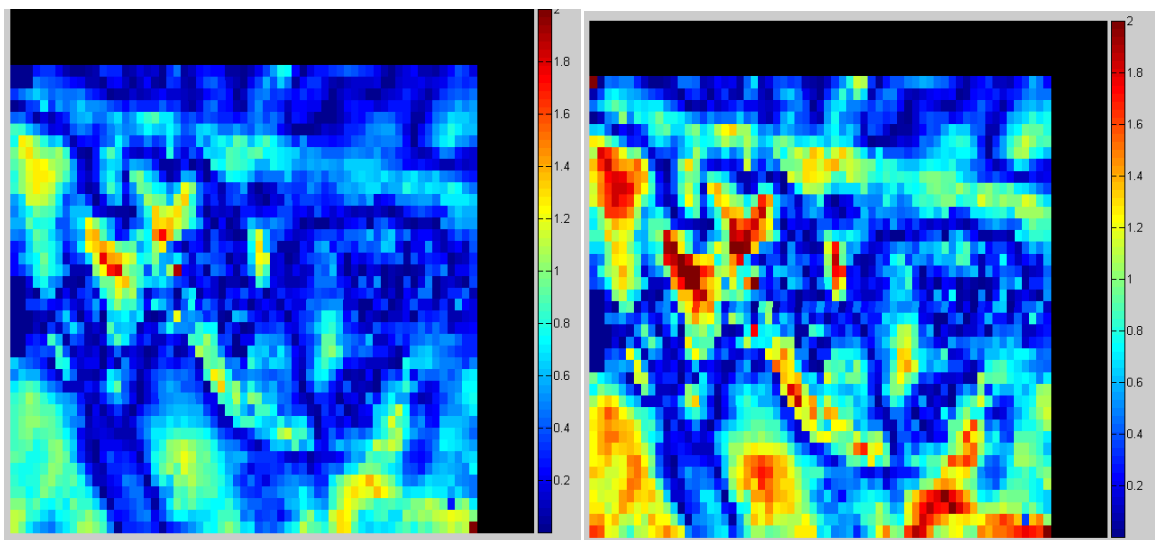
Figure D.78 Plan 5 measurement 2 full sagittal region, 7%/4mm gamma index analysis with 97.67% pixels passing (left) and 5%/3mm with 91.33% pixels passing (right)
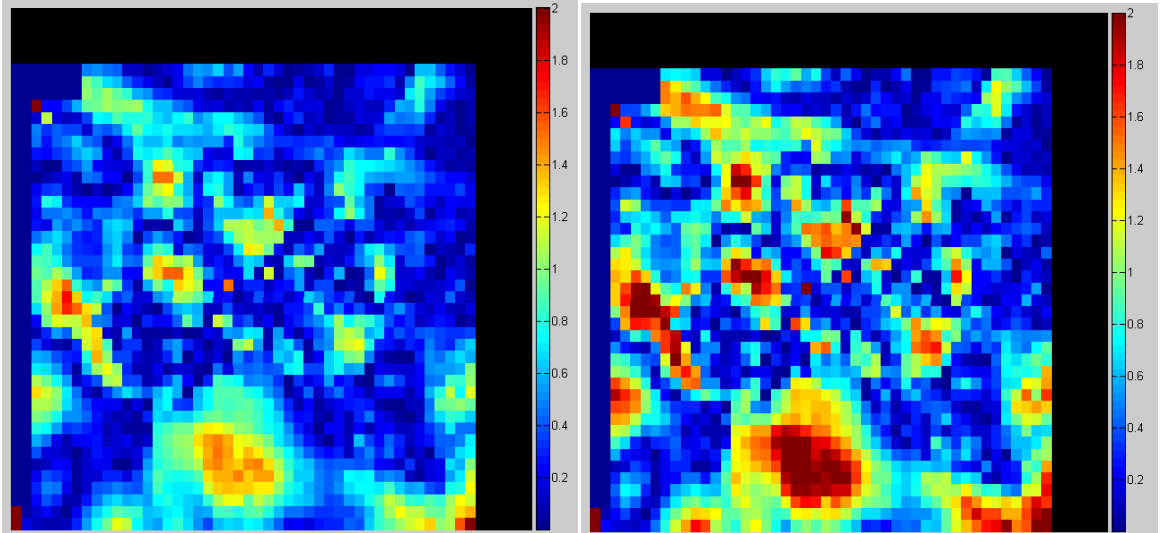

Figure D.79 Plan 5 measurement 3 axial PTV region, 7%/4mm gamma index analysis with 87.21% pixels passing (left) and 5%/3mm with 65.67% pixels passing (right)

Figure D.80 Plan 5 measurement 3 full axial region, 7%/4mm gamma index analysis with 84.46% pixels passing (left) and 5%/3mm with 63.2% pixels passing (right)

Figure D.81 Plan 5 measurement 3 full sagittal region, 7%/4mm gamma index analysis with 97.43% pixels passing (left) and 5%/3mm with 89.48% pixels passing (right)
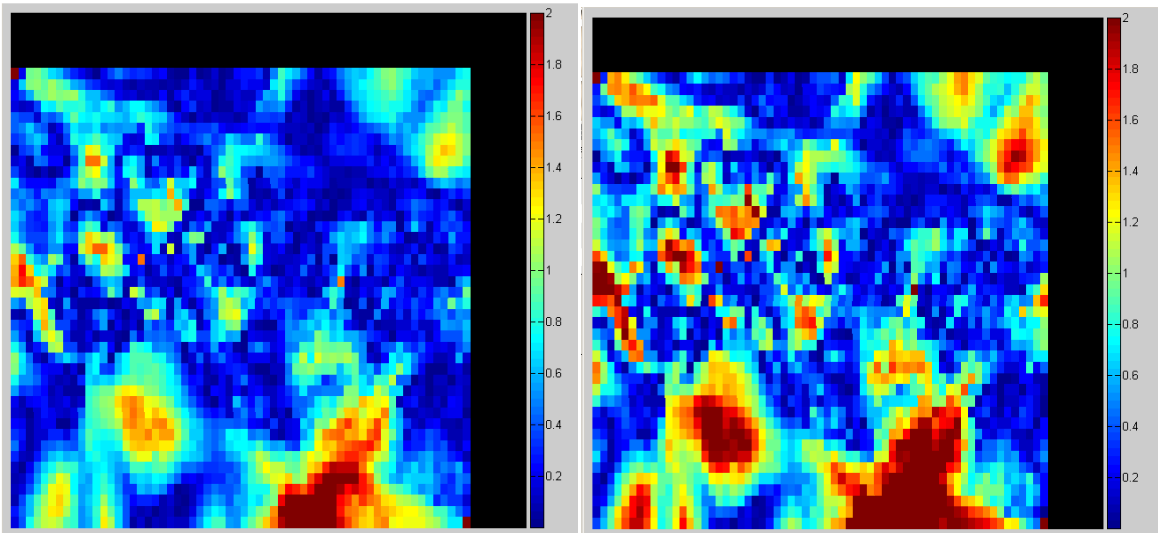
Plan 6 Results

Figure D.82 Plan 6 measurement 1 axial PTV region, 7%/4mm gamma index analysis with 92.67% pixels passing (left) and 5%/3mm with 83.32% pixels passing (right)
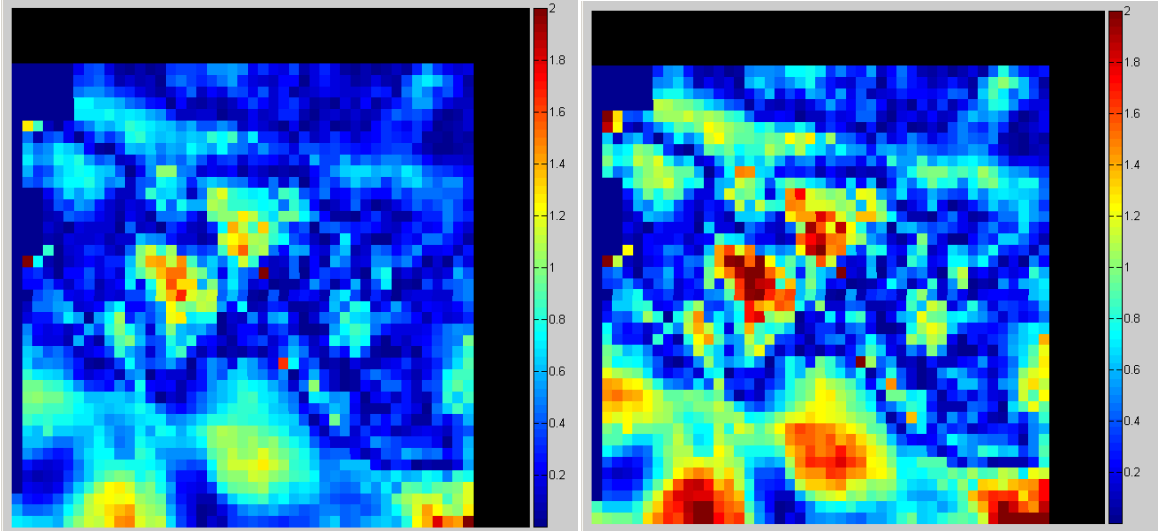

Figure D.83 Plan 6 measurement 1 full axial region, 7%/4mm gamma index analysis with 92.81% pixels passing (left) and 5%/3mm with 83.44% pixels passing (right)
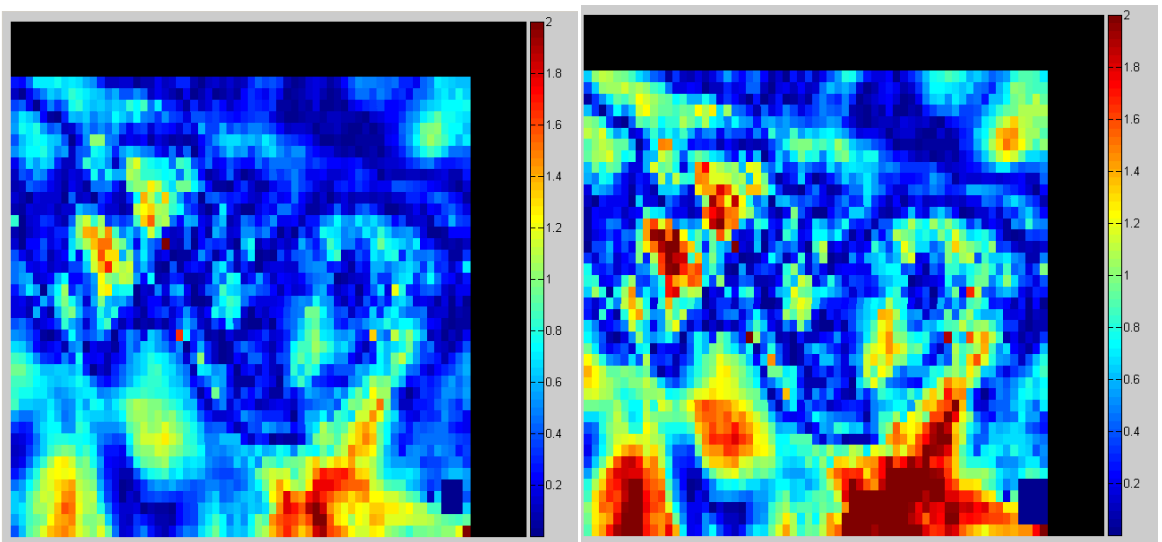
Figure D.84 Plan 6 measurement 2 axial PTV region, 7%/4mm gamma index analysis with 93.46% pixels passing (left) and 5%/3mm with 81.84% pixels passing (right)
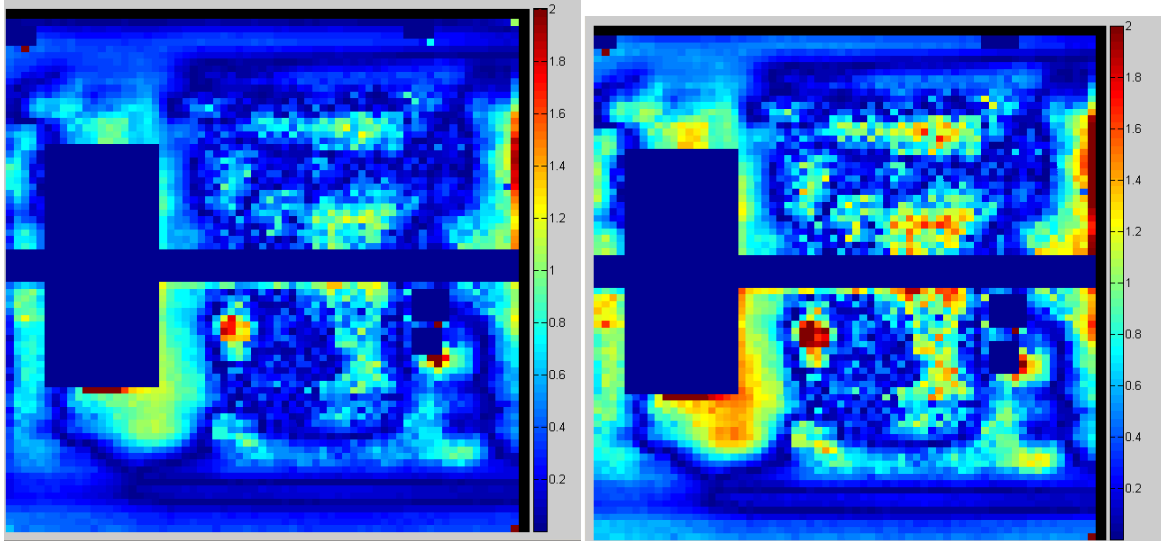

Figure D.85 Plan 6 measurement 2 full axial region, 7%/4mm gamma index analysis with 94.54% pixels passing (left) and 5%/3mm with 83.23% pixels passing (right)

Figure D.86 Plan 6 measurement 3 axial PTV region, 7%/4mm gamma index analysis with 98.06% pixels passing (left) and 5%/3mm with 88.79% pixels passing (right)
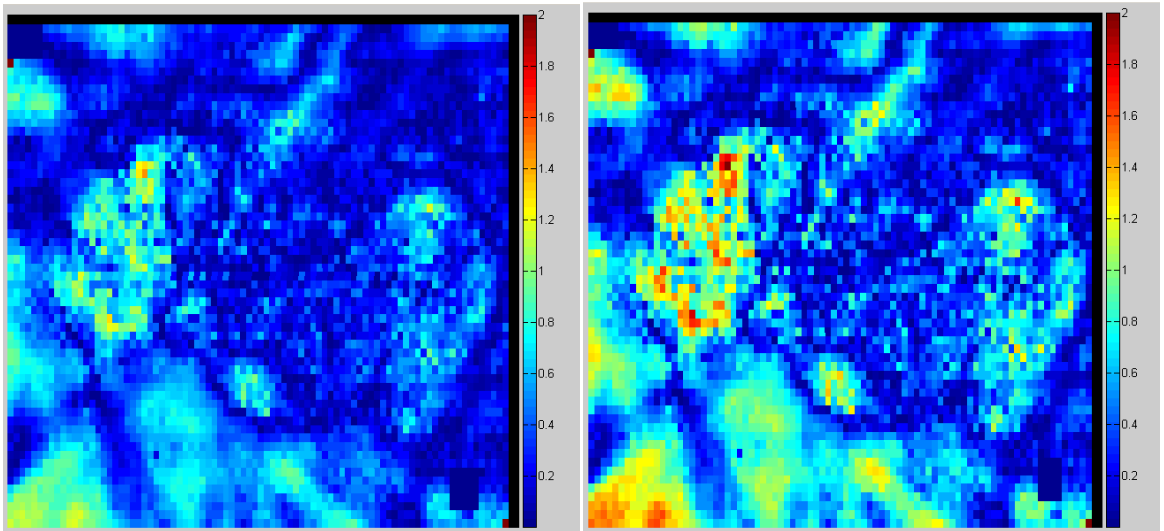
Figure D.87 Plan 6 measurement 3 full axial region, 7%/4mm gamma index analysis with 98.47% pixels passing (left) and 5%/3mm with 90.83% pixels passing (right)
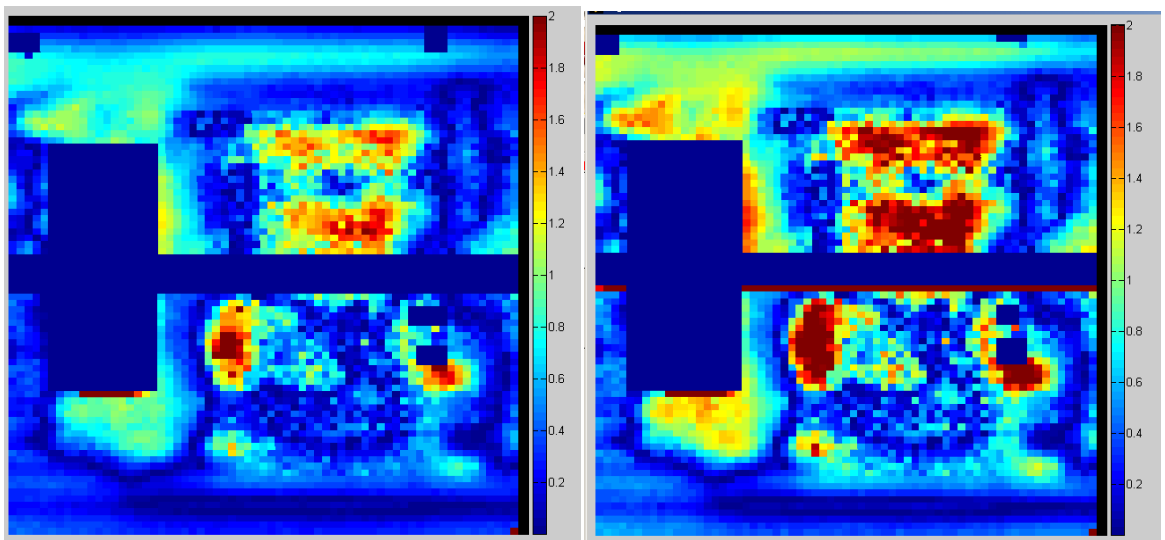
Figure D.88 Plan 6 measurement 1 full sagittal region, 7%/4mm gamma index analysis with 87.16% pixels passing (left) and 5%/3mm with 80.73% pixels passing (right)

Figure D.89 Plan 6 measurement 2 full sagittal region, 7%/4mm gamma index analysis with 98.59% pixels passing (left) and 5%/3mm with 95.48% pixels passing (right)
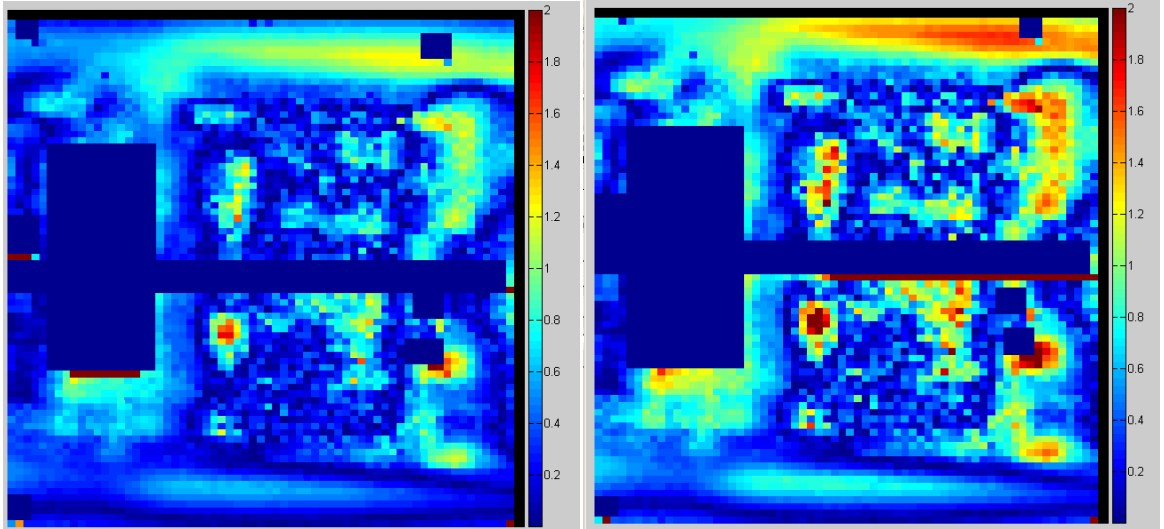
Figure D.90 Plan 6 measurement 3 full sagittal region, 7%/4mm gamma index analysis with 97.16% pixels passing (left) and 5%/3mm with 92.85% pixels passing (right)

Plan 7 Results

Figure D.91 Plan 7 measurement 1 axial PTV region, 7%/4mm gamma index analysis with 96.64% pixels passing (left) and 5%/3mm with 84.9% pixels passing (right)

Figure D.92 Plan 7 measurement 1 full axial region, 7%/4mm gamma index analysis with 97.26% pixels passing (left) and 5%/3mm with 85.15% pixels passing (right)
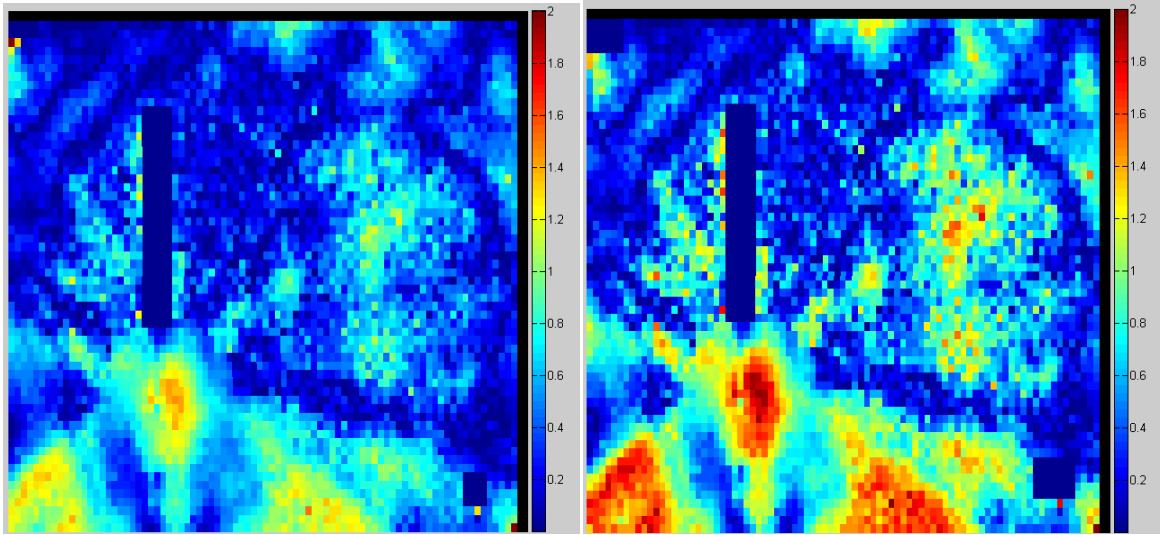

Figure D.93 Plan 7 measurement 1 full sagittal region, 7%/4mm gamma index analysis with 96.58% pixels passing (left) and 5%/3mm with 88.9% pixels passing (right)
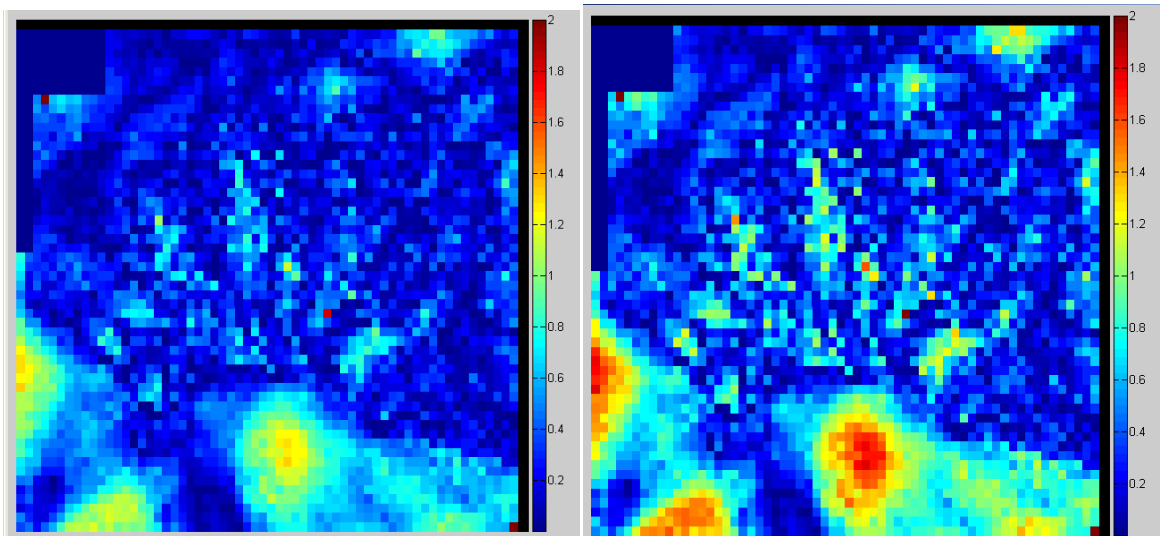
Figure D.94 Plan 7 measurement 2 axial PTV region, 7%/4mm gamma index analysis with 98.12% pixels passing (left) and 5%/3mm with 90.36% pixels passing (right)

Figure D.95 Plan 7 measurement 2 full axial region, 7%/4mm gamma index analysis with 98.7% pixels passing (left) and 5%/3mm with 91% pixels passing (right)

Figure D.96 Plan 7 measurement 2 full sagittal region, 7%/4mm gamma index analysis with 95.55% pixels passing (left) and 5%/3mm with 87.21% pixels passing (right)
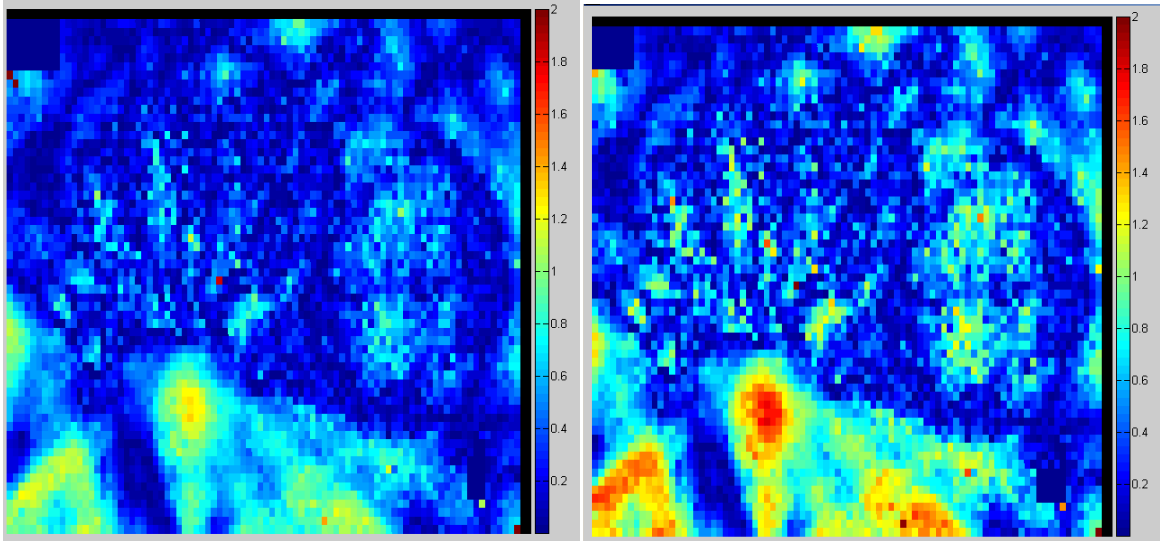

Figure D.97 Plan 7 measurement 3 axial PTV region, 7%/4mm gamma index analysis with 94.36% pixels passing (left) and 5%/3mm with 82.24% pixels passing (right)
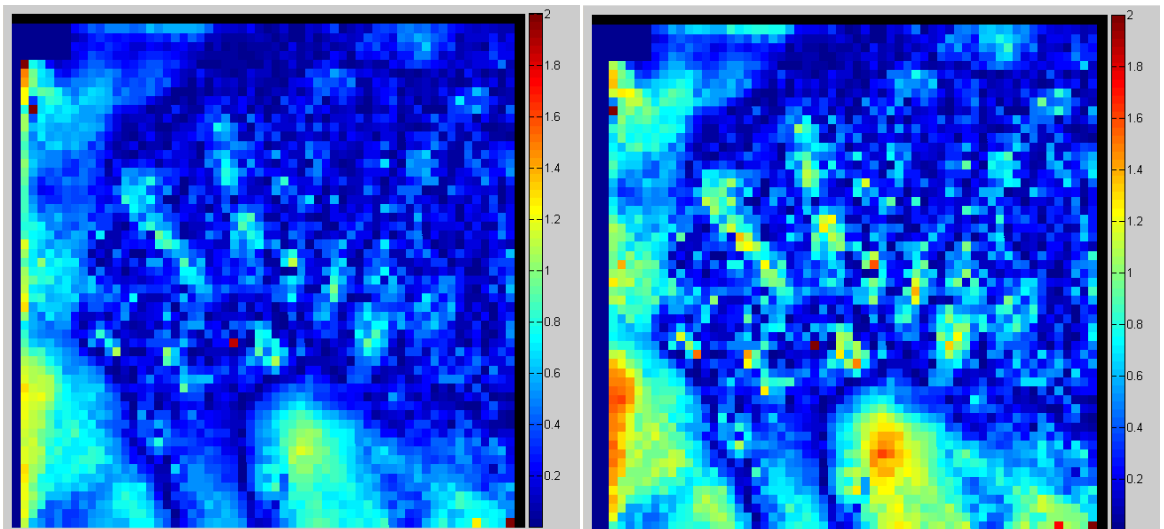
Figure D.98 Plan 7 measurement 3 full axial region, 7%/4mm gamma index analysis with 96.88% pixels passing (left) and 5%/3mm with 86.21% pixels passing (right)

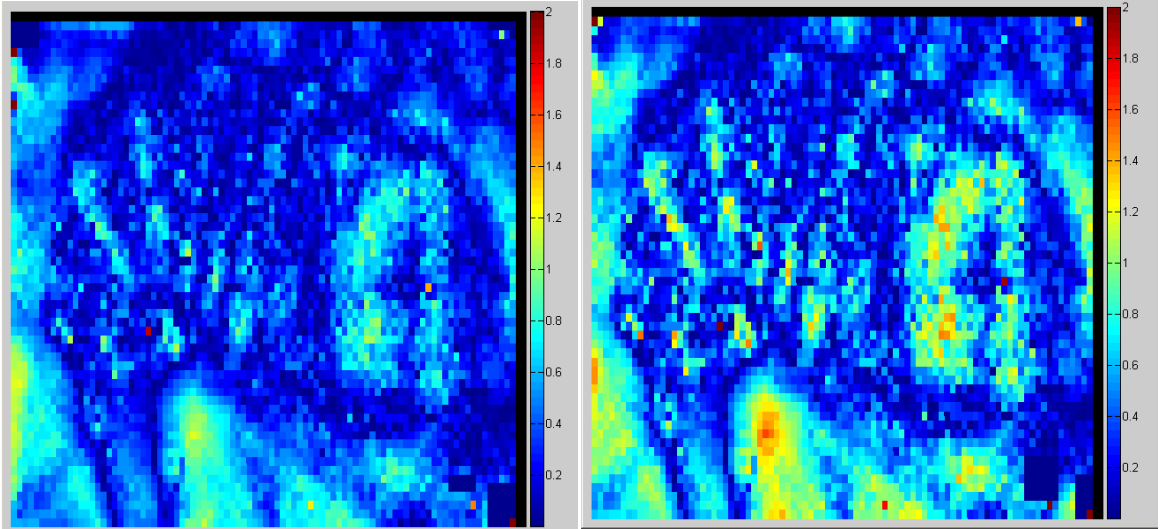**Figure D.99 Plan 7 measurement 3 full sagittal region, 7%/4mm gamma index analysis with 98.54% pixels passing (left) and 5%/3mm with 94.19% pixels passing (right)**

Plan 8 Results

Figure D.100 Plan 8 measurement 1 axial PTV region, 7%/4mm gamma index analysis with 92.74% pixels passing (left) and 5%/3mm with 73.85% pixels passing (right)
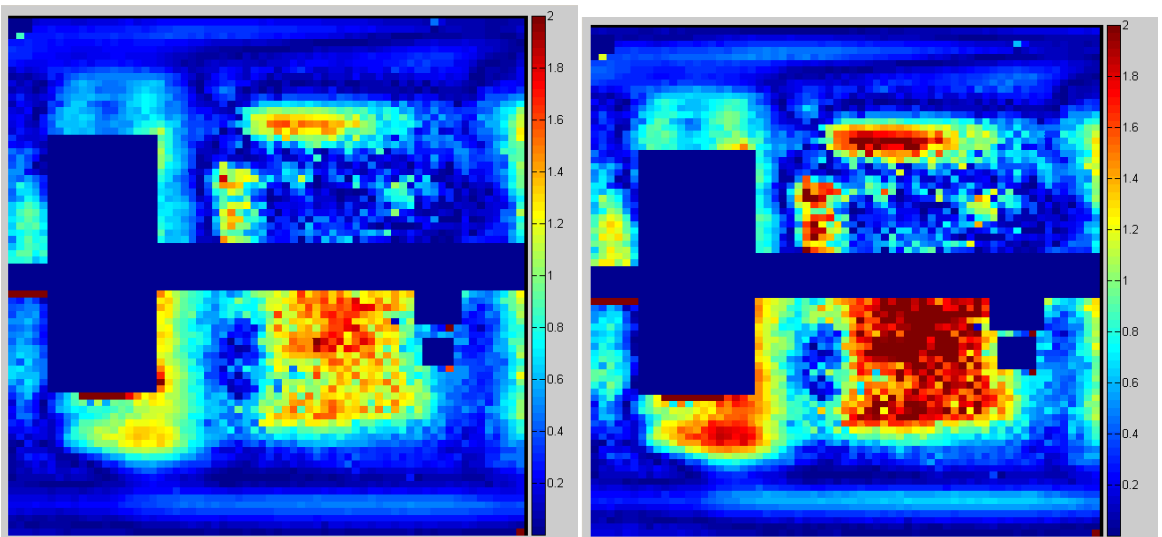

Figure D.101 Plan 8 measurement 1 full axial region, 7%/4mm gamma index analysis with 93.32% pixels passing (left) and 5%/3mm with 77% pixels passing (right)

Figure D.102 Plan 8 measurement 2 axial PTV region, 7%/4mm gamma index analysis with 89.44% pixels passing (left) and 5%/3mm with 74.13% pixels passing (right)

Figure D.103 Plan 8 measurement 2 full axial region, 7%/4mm gamma index analysis with 89.44% pixels passing (left) and 5%/3mm with 74.13% pixels passing (right)
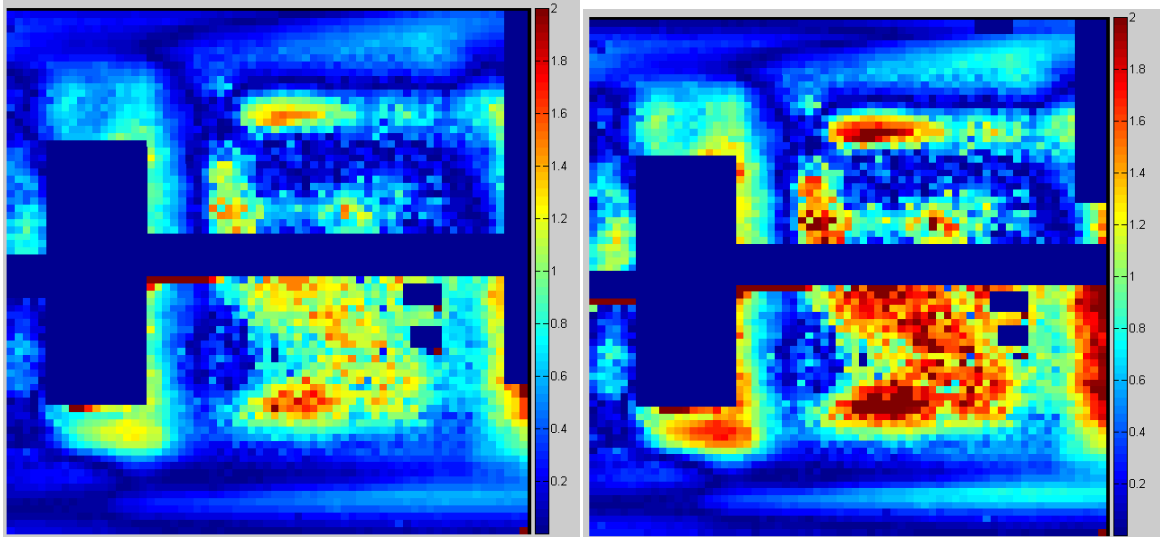
Figure D.104 Plan 8 measurement 3 axial PTV region, 7%/4mm gamma index analysis with 92.77% pixels passing (left) and 5%/3mm with 77.82% pixels passing (right)

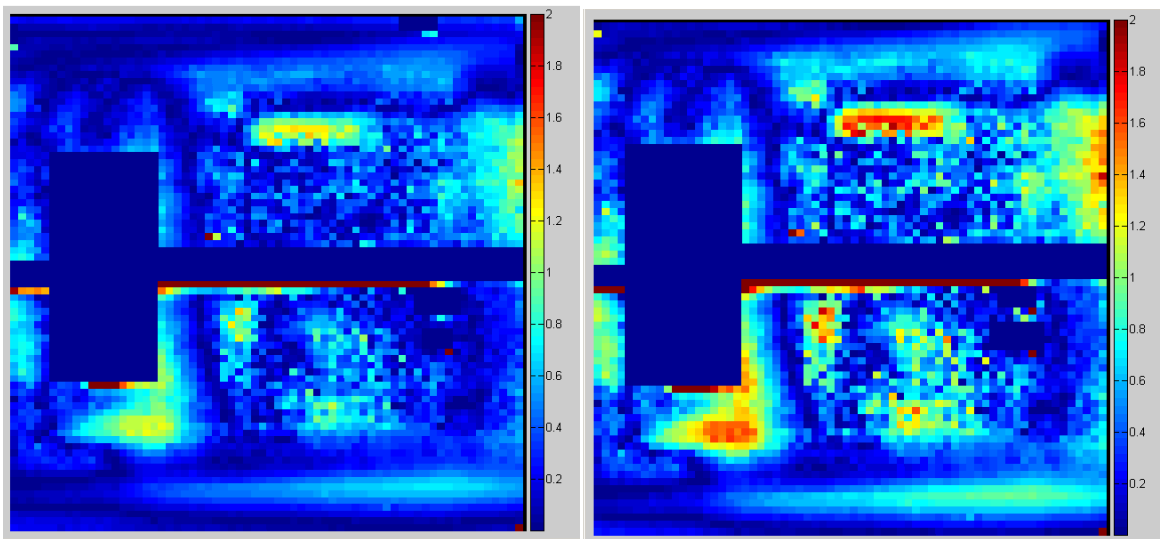**Figure D.105 Plan 8 measurement 3 full axial region, 7%/4mm gamma index analysis with 88.48% pixels passing (left) and 5%/3mm with 73.59% pixels passing (right)**

Figure D.106 Plan 8 measurement 1 full sagittal region, 7%/4mm gamma index analysis with 96.2% pixels passing (left) and 5%/3mm with 86.22% pixels passing (right)

Figure D.107 Plan 8 measurement 2 full sagittal region, 7%/4mm gamma index analysis with 90.36% pixels passing (left) and 5%/3mm with 74.89% pixels passing (right)

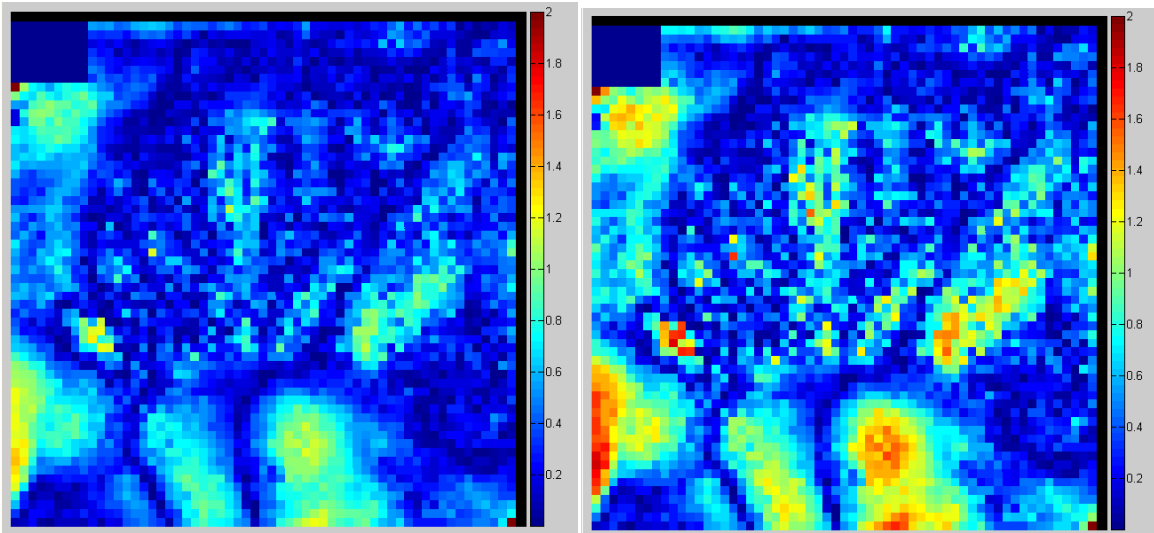**Figure D.108 Plan 8 measurement 3 full sagittal region, 7%/4mm gamma index analysis with 94.59% pixels passing (left) and 5%/3mm with 82.9% pixels passing (right)**

2100 CD Results
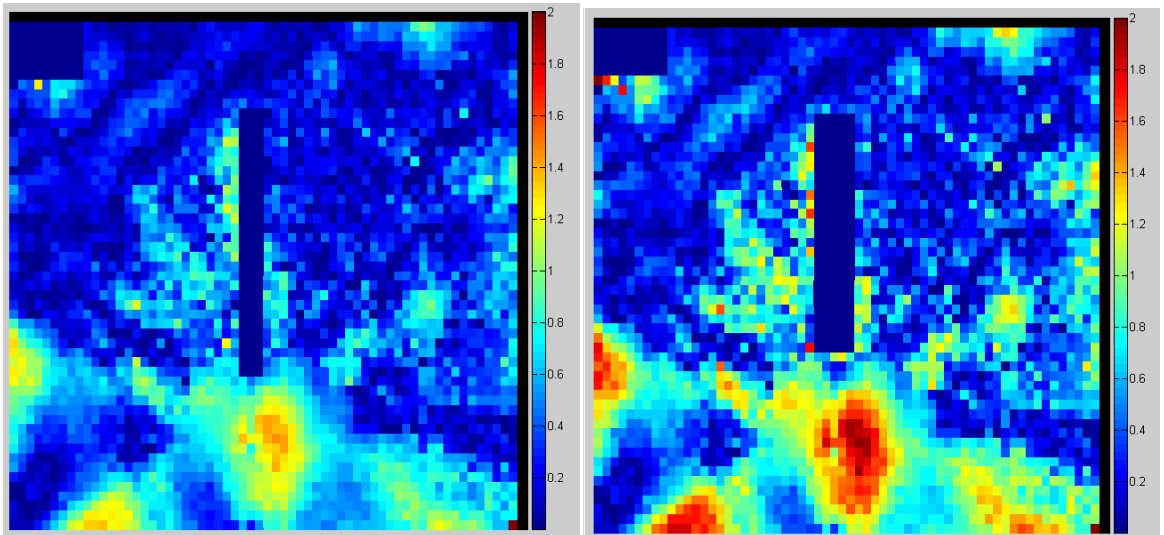
Figure D.109 Plan 4 (baseline) delivery on 2100 CD measurement 1 axial PTV region, 7%/4mm gamma index analysis with 95.58% pixels passing (left) and 5%/3mm with 85.82% pixels passing (right)
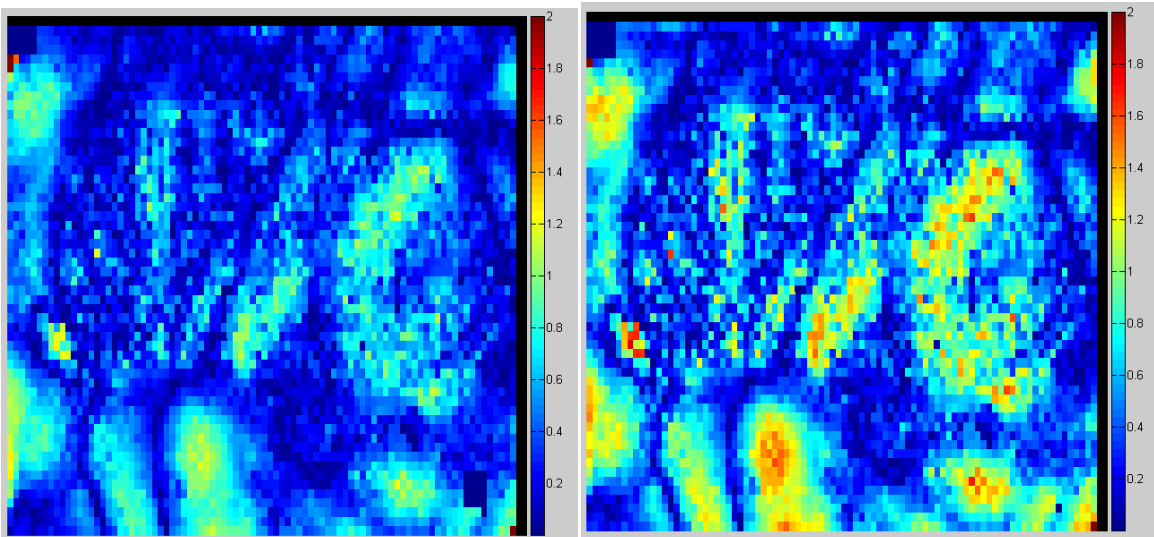
Figure D.110 Plan 4 (baseline) delivery on 2100 CD measurement 1 full axial region, 7%/4mm gamma index analysis with 94.21% pixels passing (left) and 5%/3mm with 81.81% pixels passing (right)
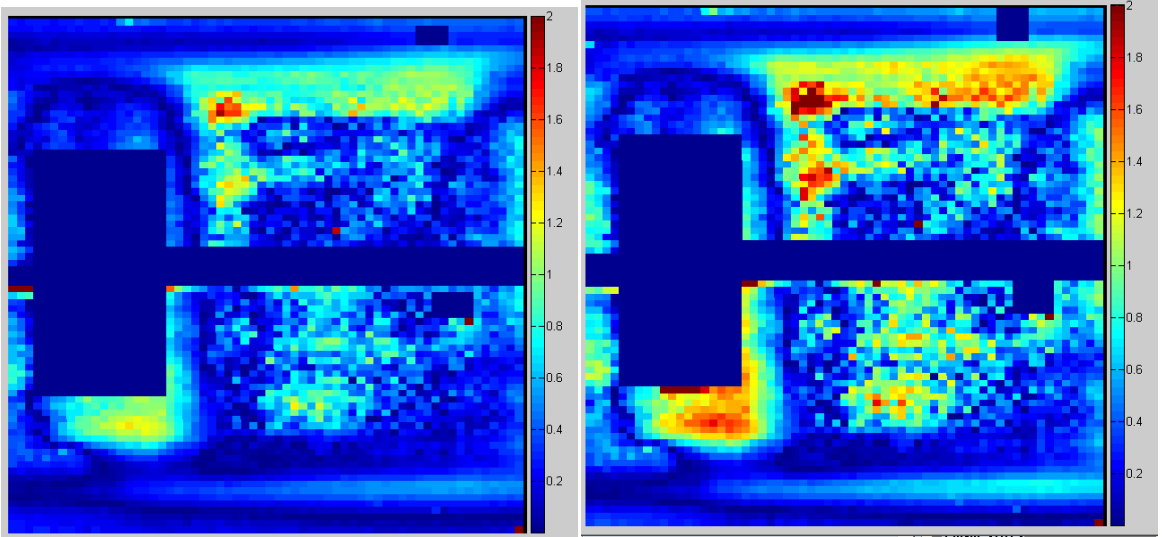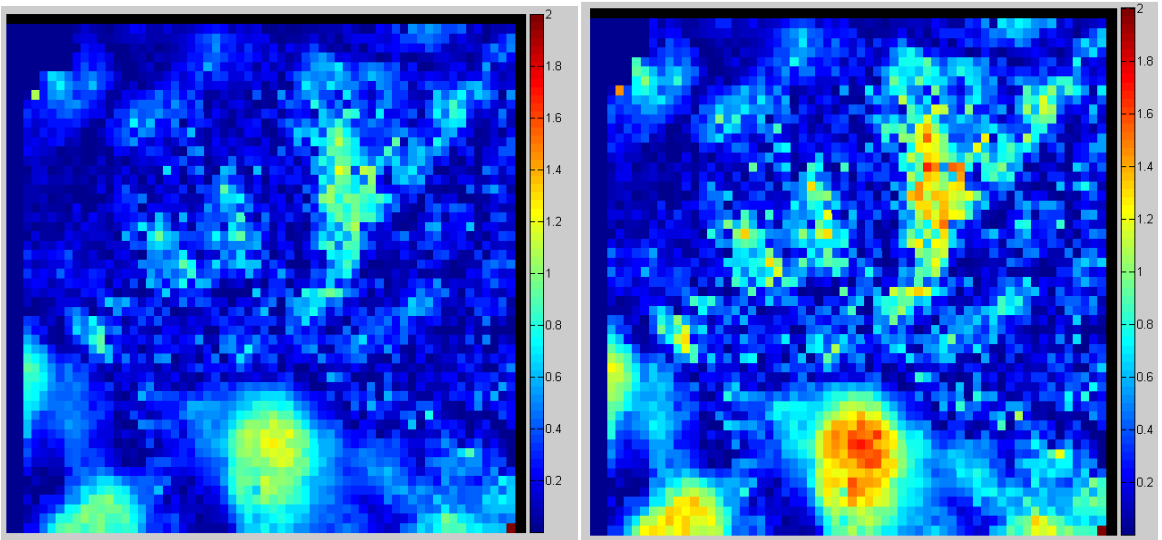

Figure D.111 Plan 4 (baseline) delivery on 2100 CD measurement 2 axial PTV region, 7%/4mm gamma index analysis with 97.1% pixels passing (left) and 5%/3mm with 90.25% pixels passing (right)

Figure D.112 Plan 4 (baseline) delivery on 2100 CD measurement 2 full axial region, 7%/4mm gamma index analysis with 97.39% pixels passing (left) and 5%/3mm with 89.23% pixels passing (right)

Figure D.113 Plan 4 (baseline) delivery on 2100 CD measurement 3 axial PTV region, 7%/4mm gamma index analysis with 97.5% pixels passing (left) and 5%/3mm with 91.54% pixels passing (right)
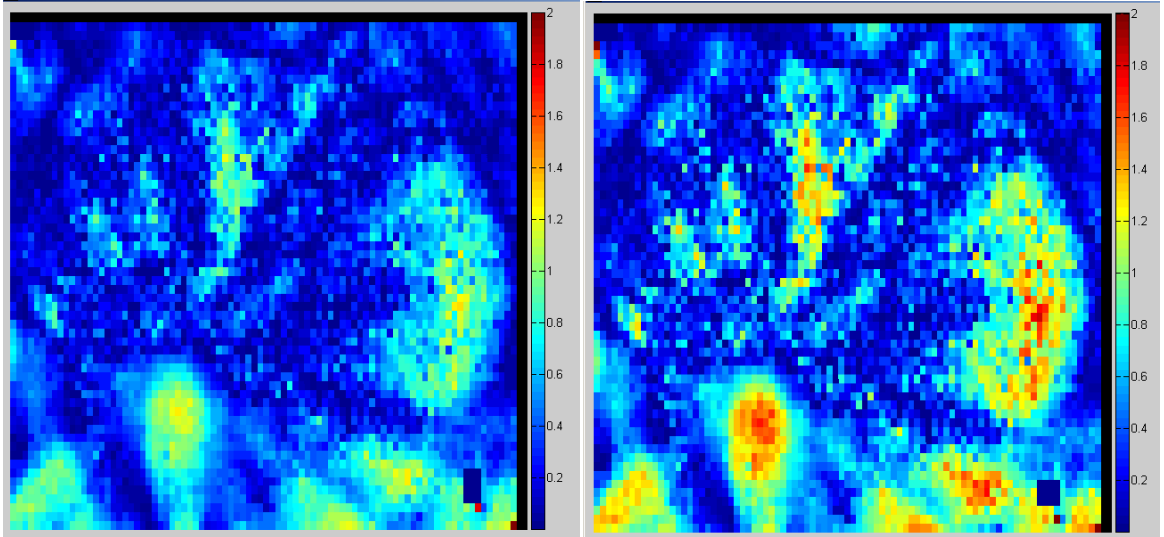
Figure D.114 Plan 4 (baseline) delivery on 2100 CD measurement 3 full axial region, 7%/4mm gamma index analysis with 98.86% pixels passing (left) and 5%/3mm with 92.47% pixels passing (right)
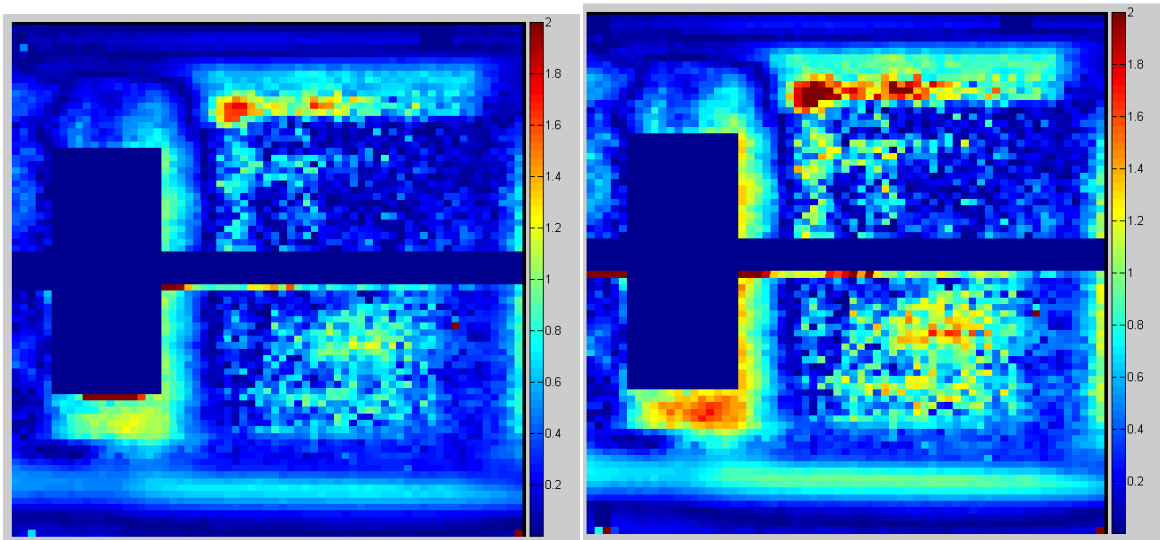

Figure D.115 Plan 4 (baseline) delivery on 2100 CD measurement 1 full sagittal region, 7%/4mm gamma index analysis with 86.02% pixels passing (left) and 5%/3mm with 79.34% pixels passing (right)

Figure D.116 Plan 4 (baseline) delivery on 2100 CD measurement 2 full sagittal region, 7%/4mm gamma index analysis with 87.61% pixels passing (left) and 5%/3mm with 76.62% pixels passing (right)

Figure D.117 Plan 4 (baseline) delivery on 2100 CD measurement 3 full sagittal region, 7%/4mm gamma index analysis with 96.91% pixels passing (left) and 5%/3mm with 90.84% pixels passing (right)

21EX Results

Figure D.118 Plan 4 (baseline) delivery on 21EX measurement 1 axial PTV region, 7%/4mm gamma index analysis with 97.65% pixels passing (left) and 5%/3mm with 87.79% pixels passing (right)
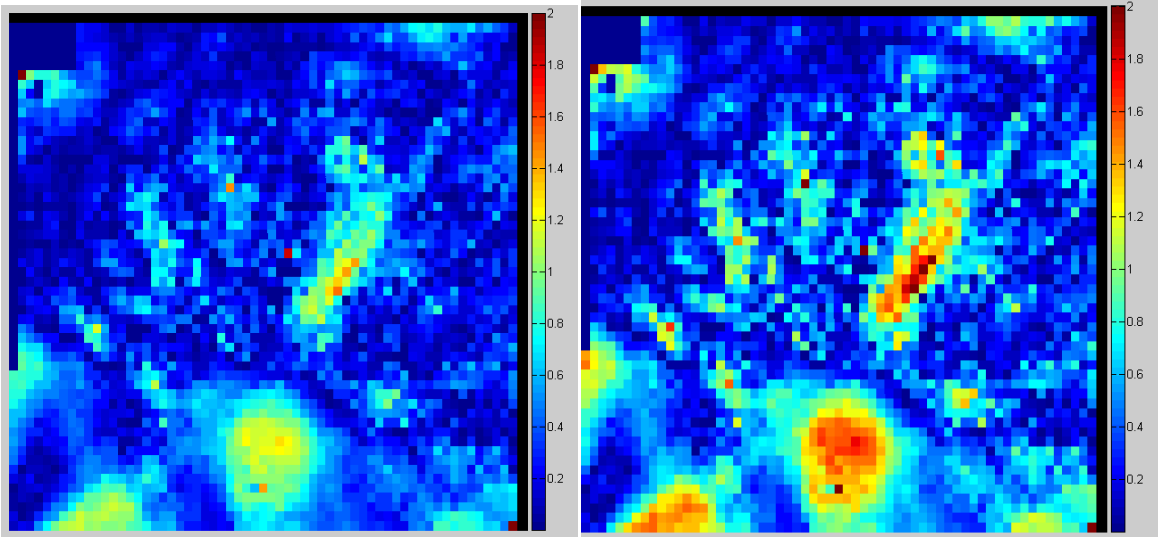

Figure D.119 Plan 4 (baseline) delivery on 21EX measurement 1 full axial region, 7%/4mm gamma index analysis with 98.27% pixels passing (left) and 5%/3mm with 87.73% pixels passing (right)
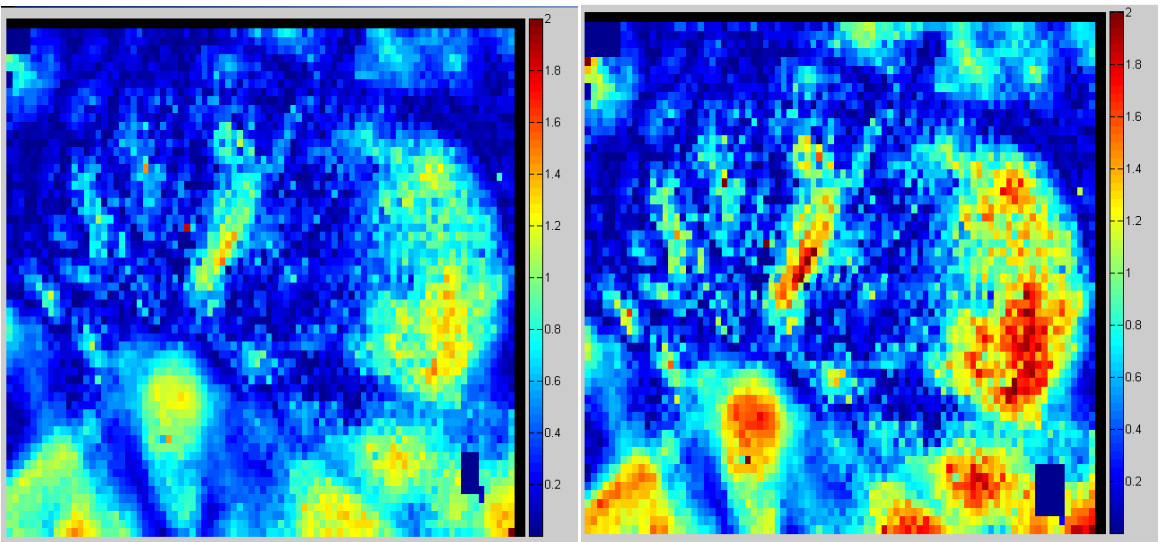
Figure D.120 Plan 4 (baseline) delivery on 21EX measurement 1 full sagittal region, 7%/4mm gamma index analysis with 96.32% pixels passing (left) and 5%/3mm with 85.53% pixels passing (right)
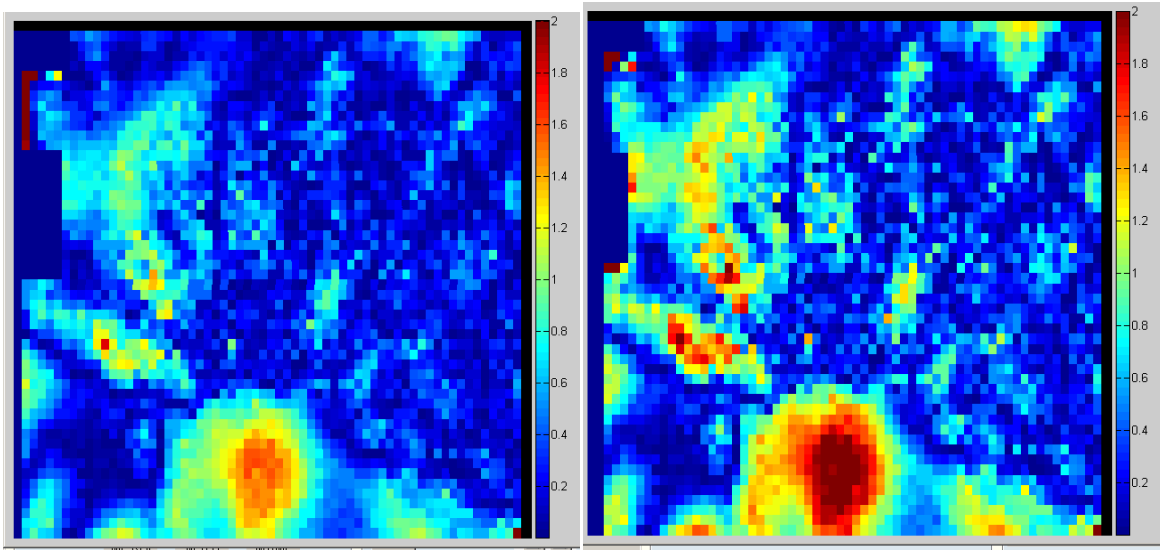

Figure D.121 Plan 4 (baseline) delivery on 21EX measurement 2 axial PTV region, 7%/4mm gamma index analysis with 98.38% pixels passing (left) and 5%/3mm with 92.21% pixels passing (right)
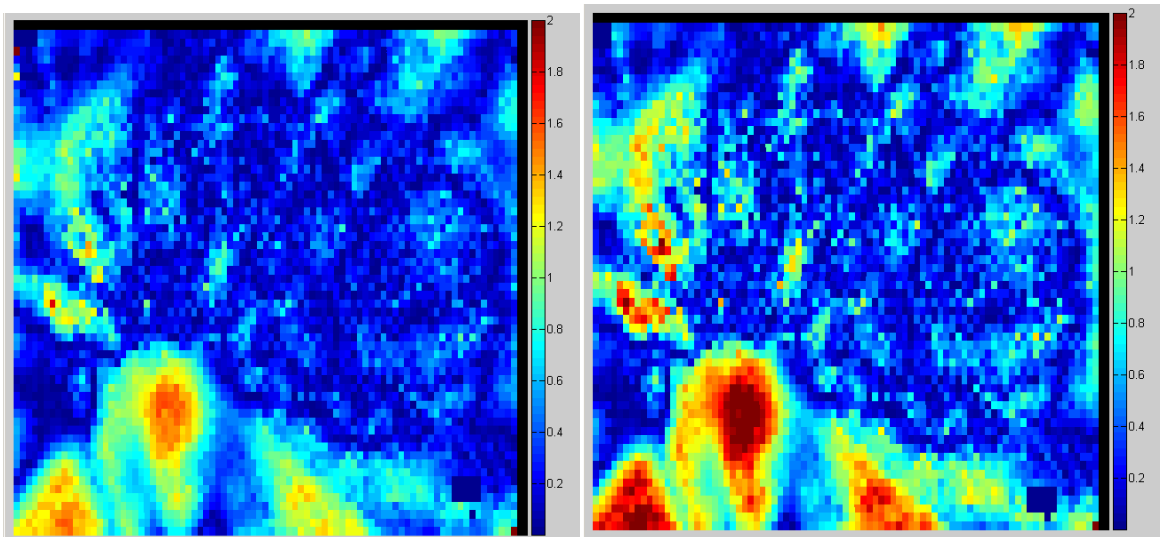
Figure D.122 Plan 4 (baseline) delivery on 21EX measurement 2 full axial region, 7%/4mm gamma index analysis with 97.32% pixels passing (left) and 5%/3mm with 87.56% pixels passing (right)
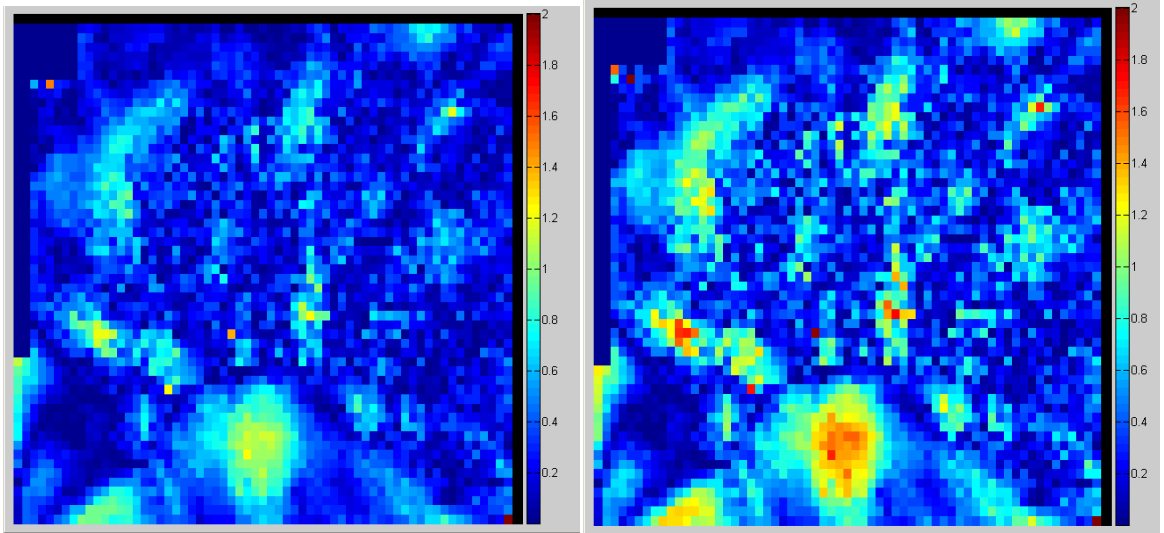

Figure D.123 Plan 4 (baseline) delivery on 21EX measurement 2 full sagittal region, 7%/4mm gamma index analysis with 97.11% pixels passing (left) and 5%/3mm with 89.45% pixels passing (right)

Figure D.124 Plan 4 (baseline) delivery on 21EX measurement 3 axial PTV region, 7%/4mm gamma index analysis with 97.02% pixels passing (left) and 5%/3mm with 89.97% pixels passing (right)

Figure D.125 Plan 4 (baseline) delivery on 21EX measurement 3 full axial region, 7%/4mm gamma index analysis with 91.66% pixels passing (left) and 5%/3mm with 79.66% pixels passing (right)
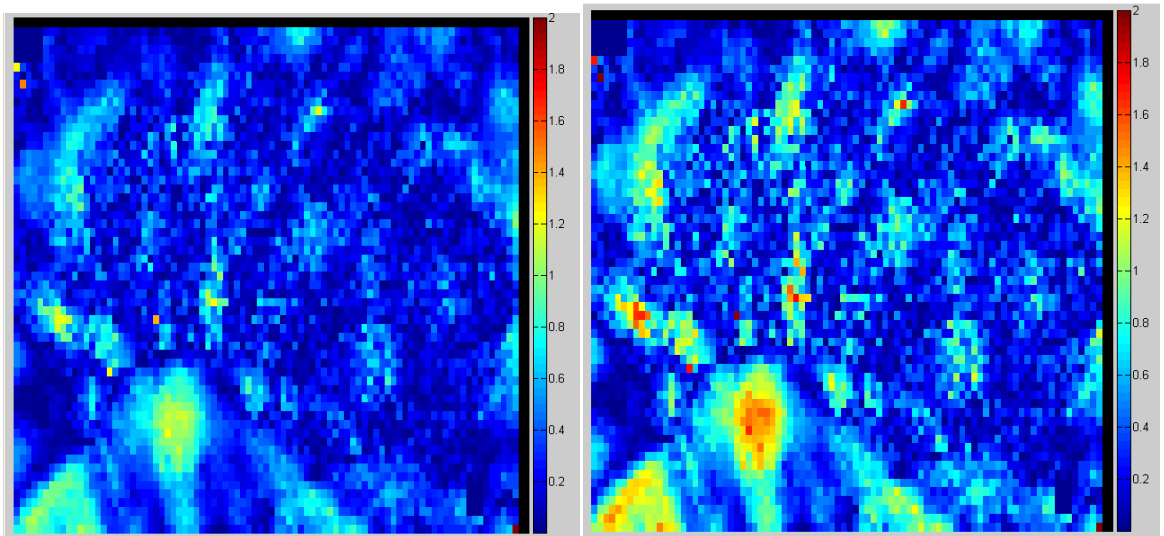
Trilogy Results

Figure D.126 Plan 4 (baseline) delivery on Trilogy measurement 1 axial PTV region, 7%/4mm gamma index analysis with 93.95% pixels passing (left) and 5%/3mm with 84.1% pixels passing (right)
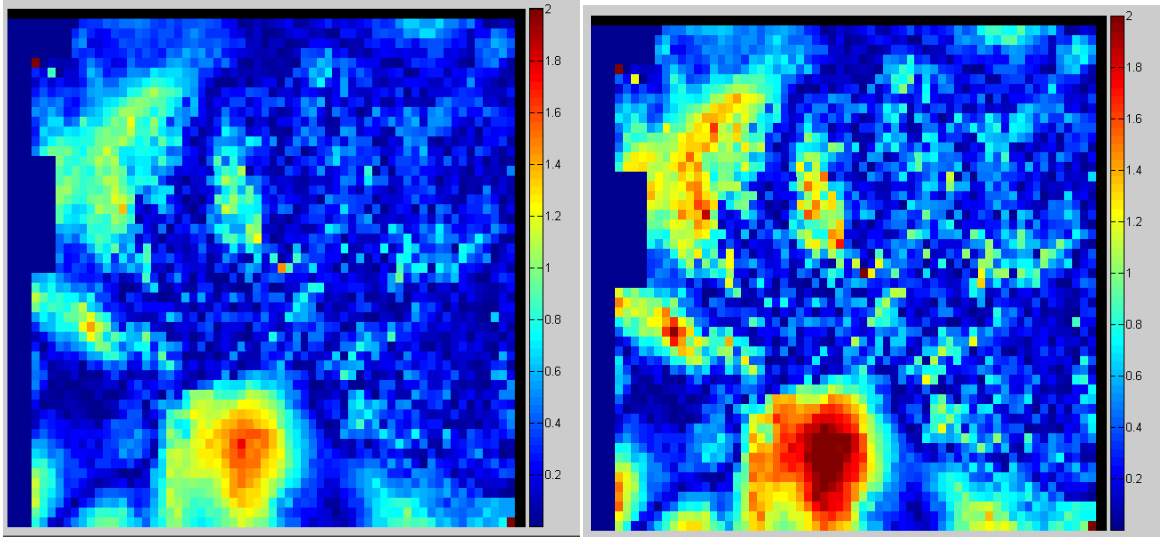

Figure D.127 Plan 4 (baseline) delivery on Trilogy measurement 1 full axial region, 7%/4mm gamma index analysis with 92.93% pixels passing (left) and 5%/3mm with 84.03% pixels passing (right)
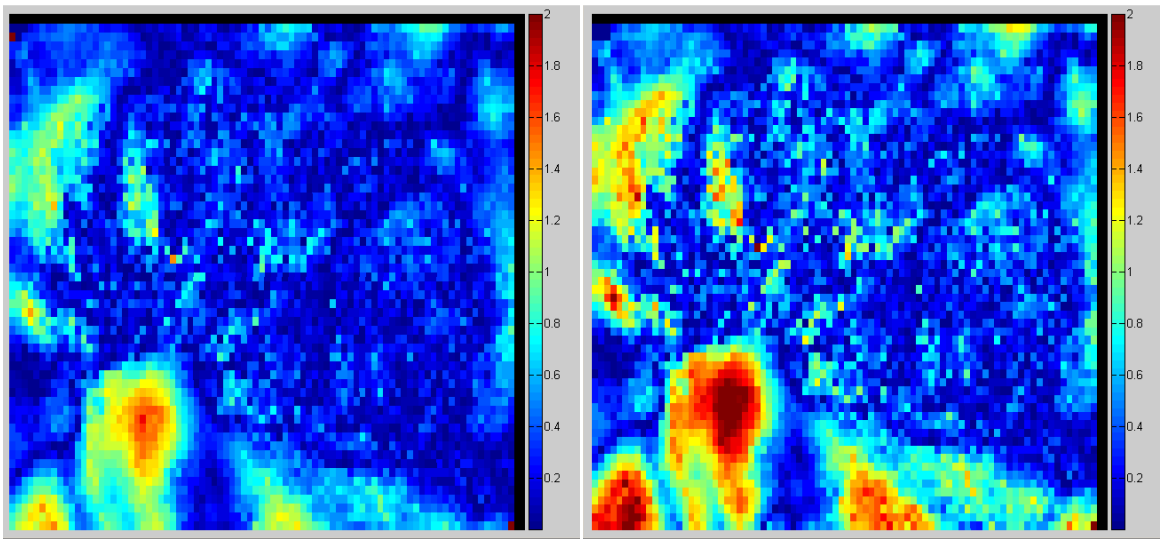
Figure D.128 Plan 4 (baseline) delivery on Trilogy measurement 2 axial PTV region, 7%/4mm gamma index analysis with 98.82% pixels passing (left) and 5%/3mm with 93.96% pixels passing (right)
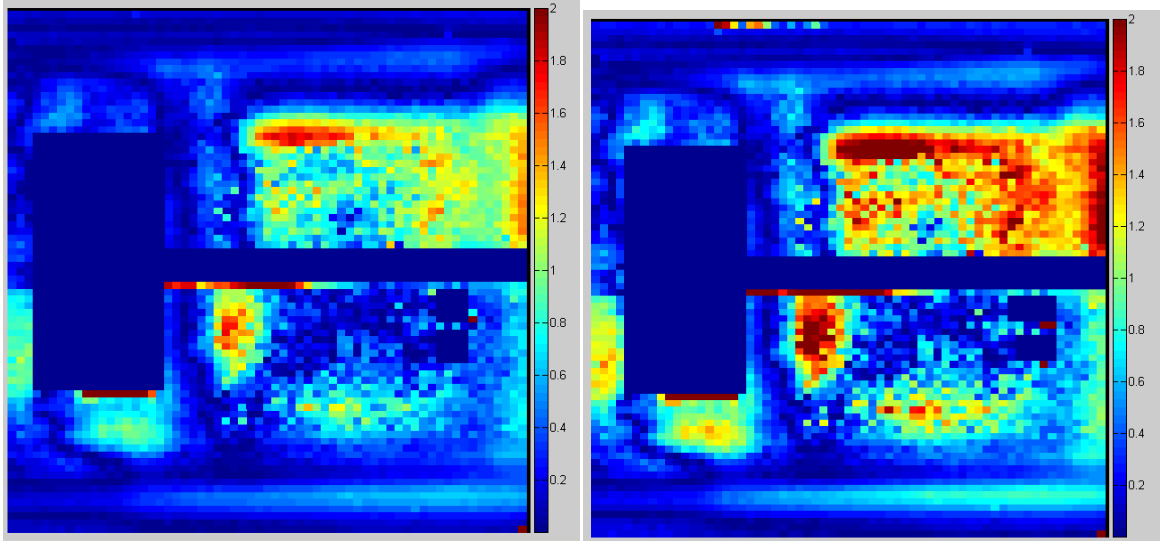

Figure D.129 Plan 4 (baseline) delivery on Trilogy measurement 2 full axial region, 7%/4mm gamma index analysis with 99.1% pixels passing (left) and 5%/3mm with 94.87% pixels passing (right)
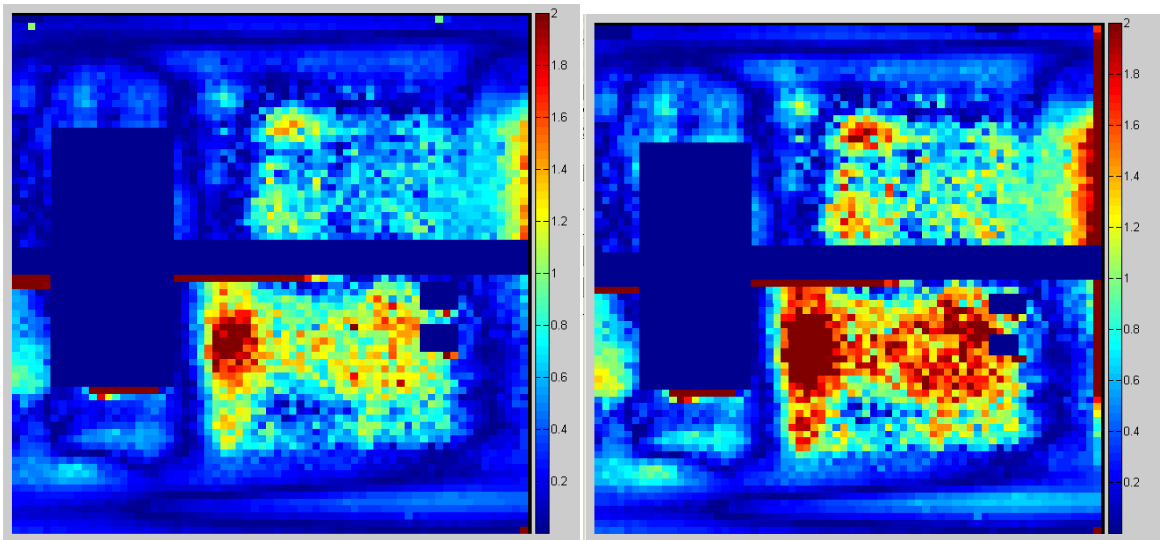
Figure D.130 Plan 4 (baseline) delivery on Trilogy measurement 3 axial PTV region, 7%/4mm gamma index analysis with 93.74% pixels passing (left) and 5%/3mm with 83.54% pixels passing (right)
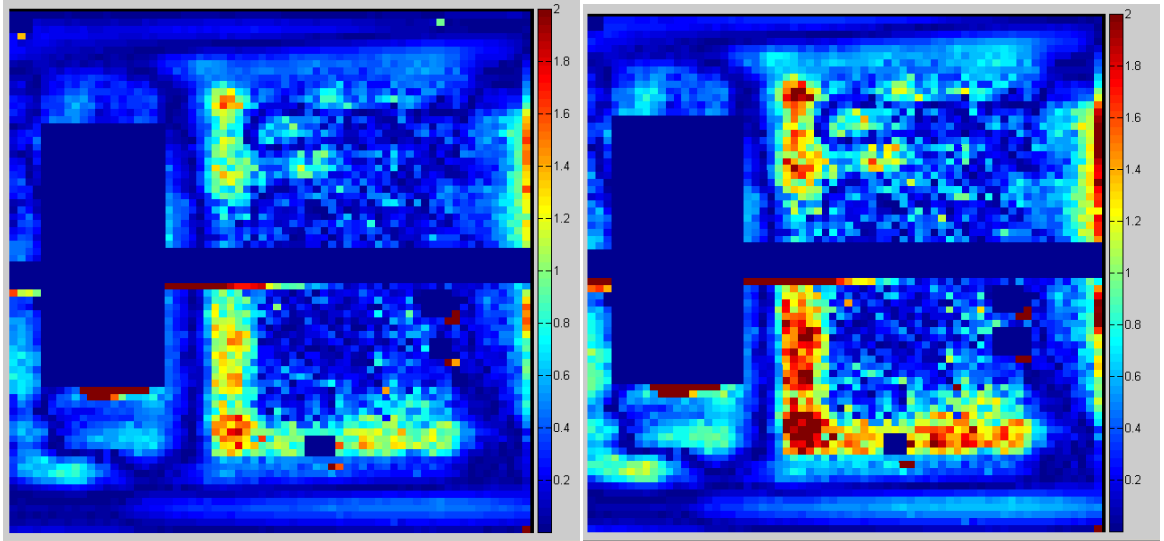

Figure D.131 Plan 4 (baseline) delivery on Trilogy measurement 3 full axial region, 7%/4mm gamma index analysis with 94.9% pixels passing (left) and 5%/3mm with 85.48% pixels passing (right)

Figure D.132 Plan 4 (baseline) delivery on Trilogy measurement 1 full sagittal region, 7%/4mm gamma index analysis with 89.81% pixels passing (left) and 5%/3mm with 79.75% pixels passing (right)

Figure D.133 Plan 4 (baseline) delivery on Trilogy measurement 2 full sagittal region, 7%/4mm gamma index analysis with 88.56% pixels passing (left) and 5%/3mm with 78.37% pixels passing (right)
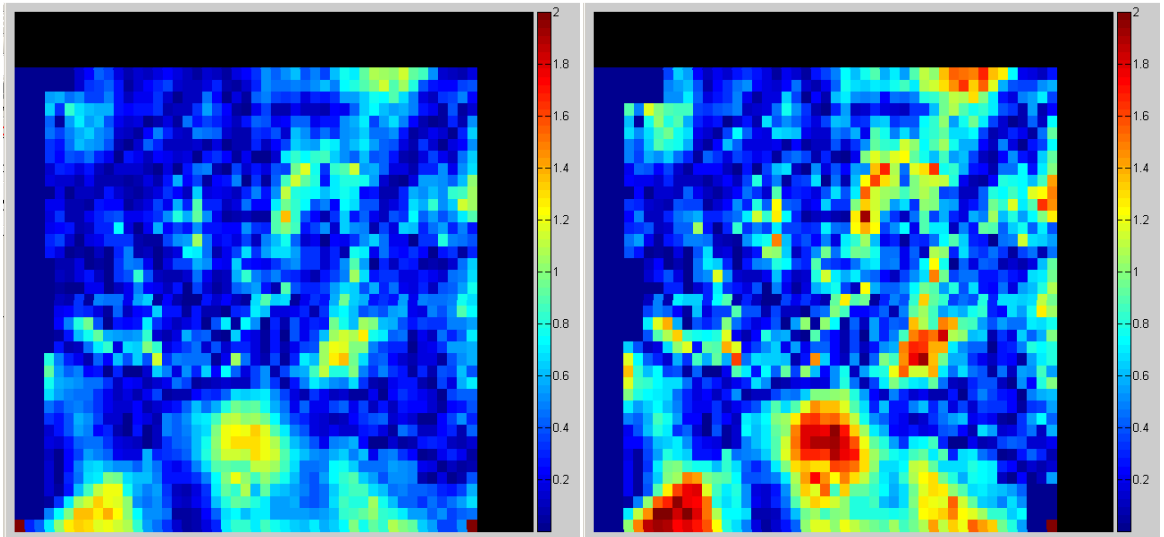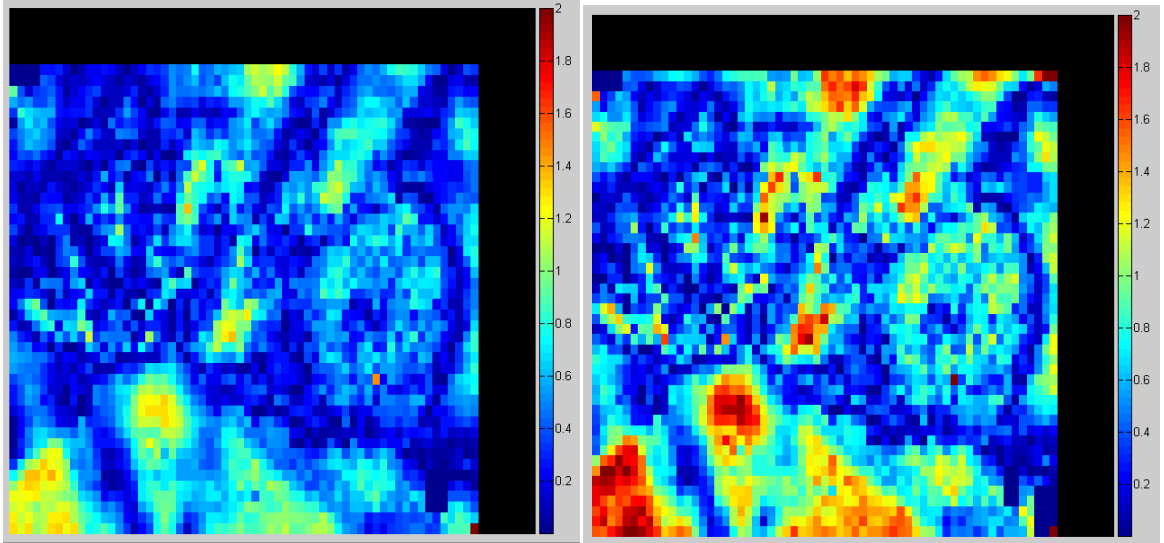
Figure D.134 Plan 4 (baseline) delivery on Trilogy measurement 3 full sagittal region, 7%/4mm gamma index analysis with 94.37% pixels passing (left) and 5%/3mm with 87.92% pixels passing (right)
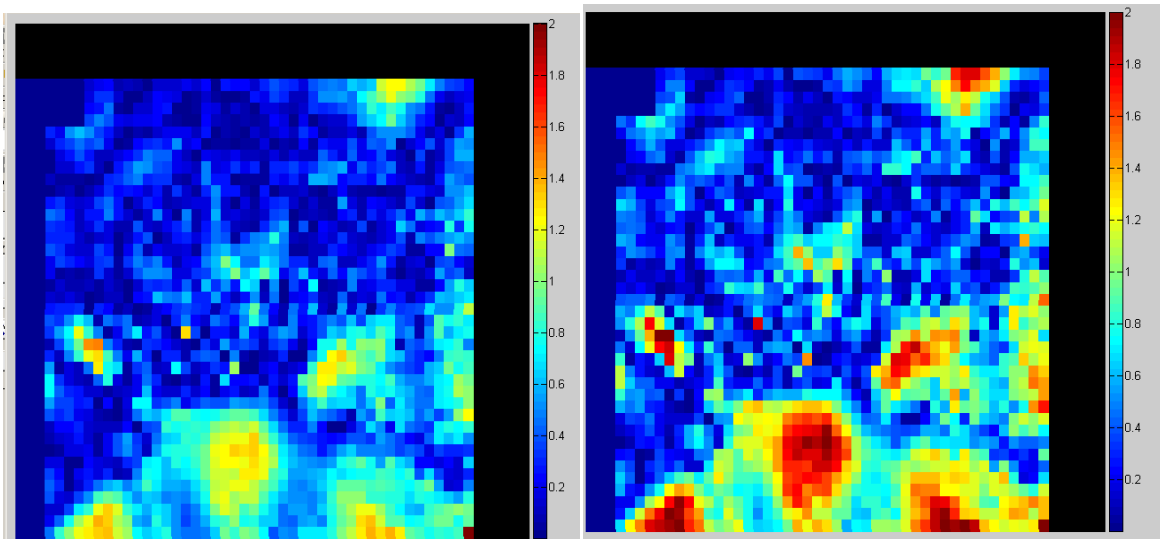
6EX Results

Figure D.135 Plan 4 (baseline) recalculated with the 600 series beam model and compared to the baseline machine delivery measurement 1 axial PTV region, 7%/4mm gamma index analysis with 94.84% pixels passing (left) and 5%/3mm with 83.56% pixels passing (right)

Figure D.136 Plan 4 (baseline) recalculated with the 600 series beam model and compared to the baseline machine delivery measurement 1 full axial region, 7%/4mm gamma index analysis with 94.87% pixels passing (left) and 5%/3mm with 80.22% pixels passing (right)
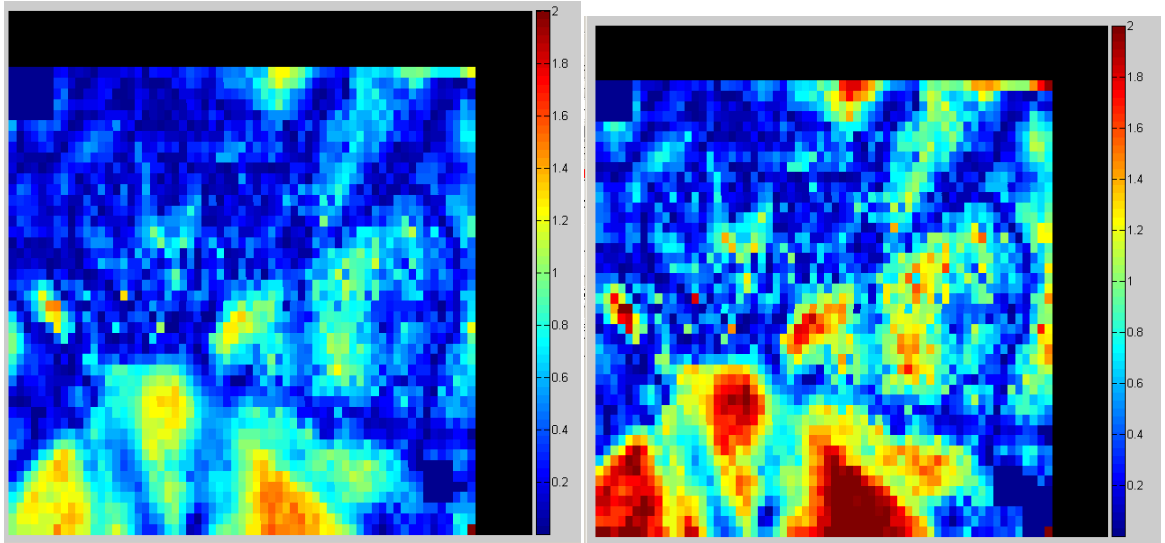

Figure D.137 Plan 4 (baseline) recalculated with the 600 series beam model and compared to the baseline machine delivery measurement 2 axial PTV region, 7%/4mm gamma index analysis with 93.35% pixels passing (left) and 5%/3mm with 78.76% pixels passing (right)
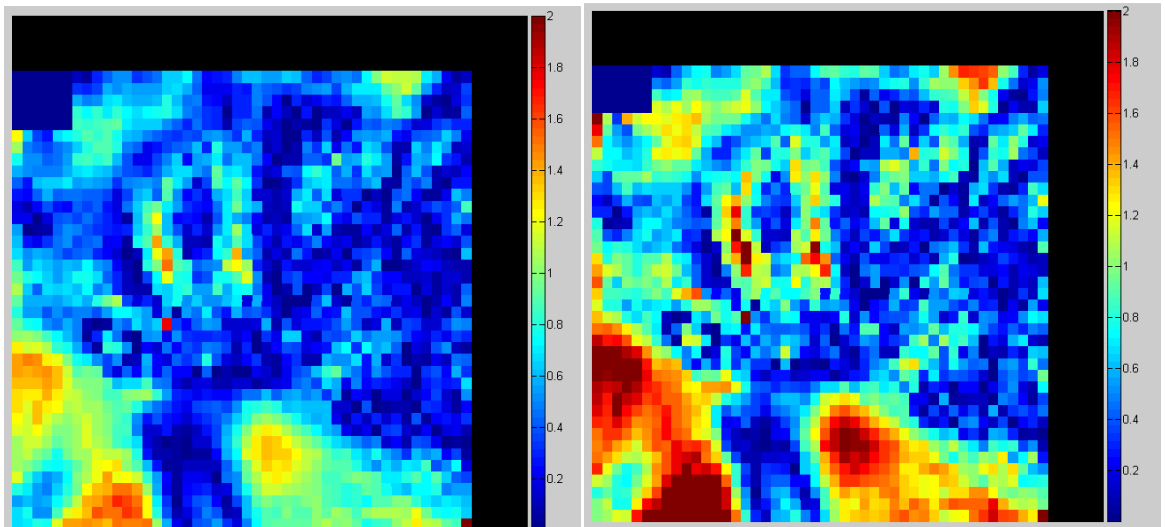
Figure D.138 Plan 4 (baseline) recalculated with the 600 series beam model and compared to the baseline machine delivery measurement 2 full axial region, 7%/4mm gamma index analysis with 91.12% pixels passing (left) and 5%/3mm with 73.97% pixels passing (right)

Figure D.139 Plan 4 (baseline) recalculated with the 600 series beam model and compared to the baseline machine delivery measurement 3 axial PTV region, 7%/4mm gamma index analysis with 88.49% pixels passing (left) and 5%/3mm with 71.56% pixels passing (right)
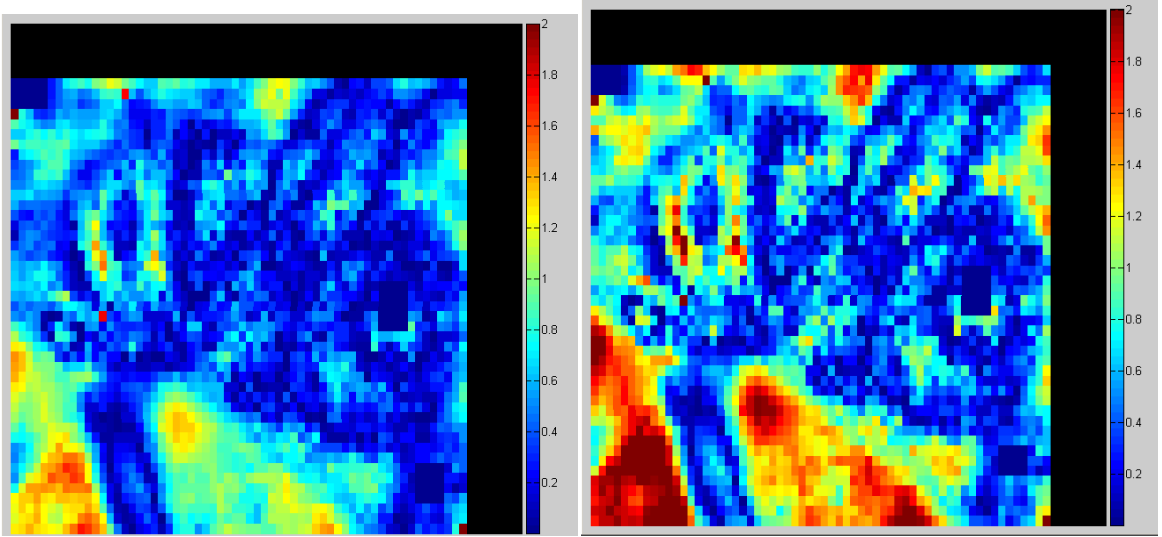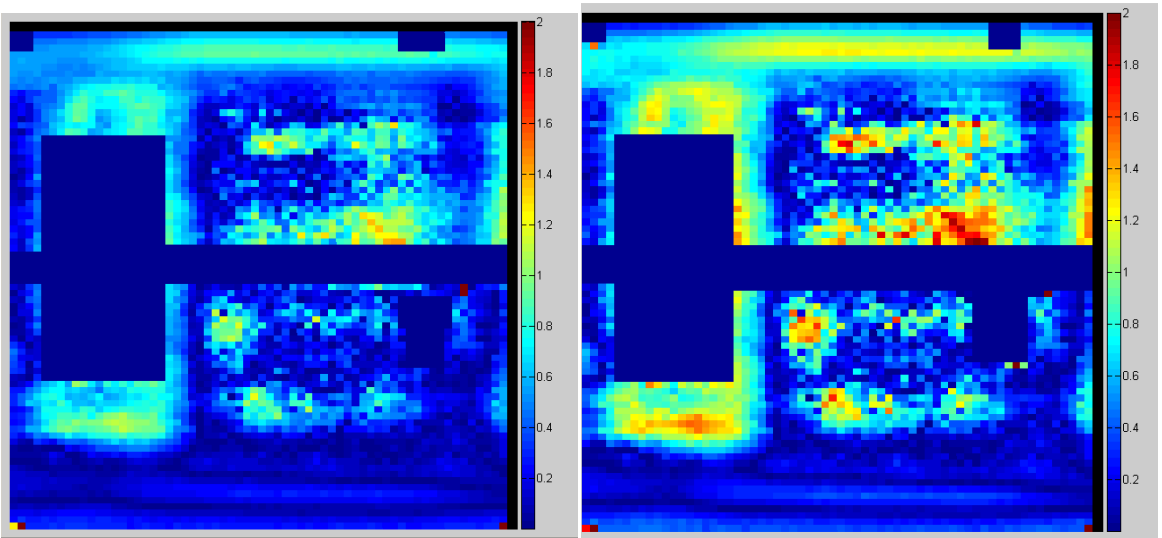
Figure D.140 Plan 4 (baseline) recalculated with the 600 series beam model and compared to the baseline machine delivery measurement 3 full axial region, 7%/4mm gamma index analysis with 90.14% pixels passing (left) and 5%/3mm with 72.51% pixels passing (right)

Figure D.141 Plan 4 (baseline) recalculated with the 600 series beam model and compared to the baseline machine delivery measurement 1 full sagittal region, 7%/4mm gamma index analysis with 97.72% pixels passing (left) and 5%/3mm with 84.77% pixels passing (right)

Figure D.142 Plan 4 (baseline) recalculated with the 600 series beam model and compared to the baseline machine delivery measurement 2 full sagittal region, 7%/4mm gamma index analysis with 97.31% pixels passing (left) and 5%/3mm with 86.71% pixels passing (right)
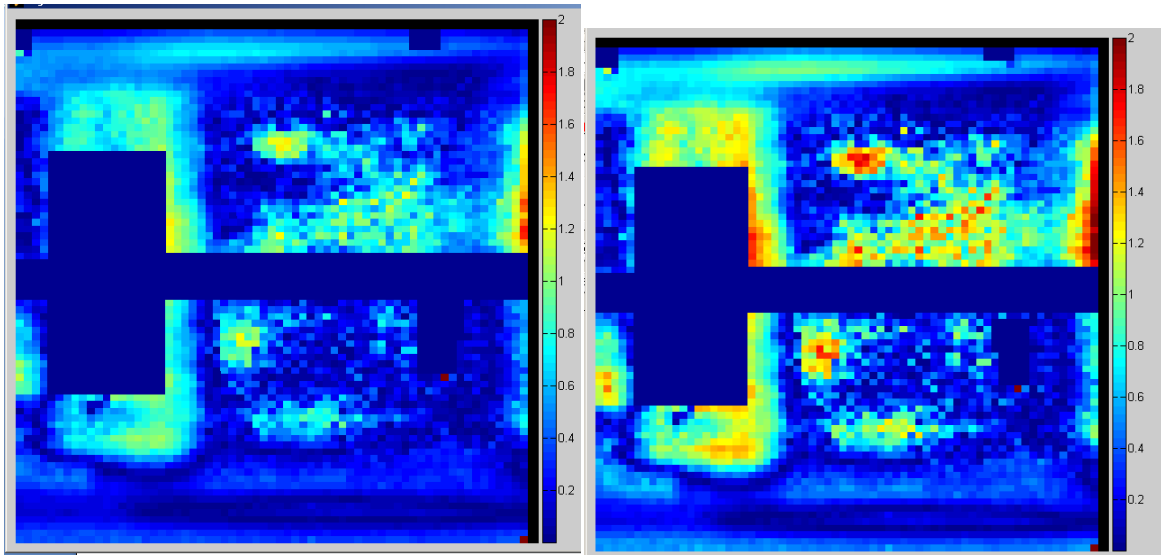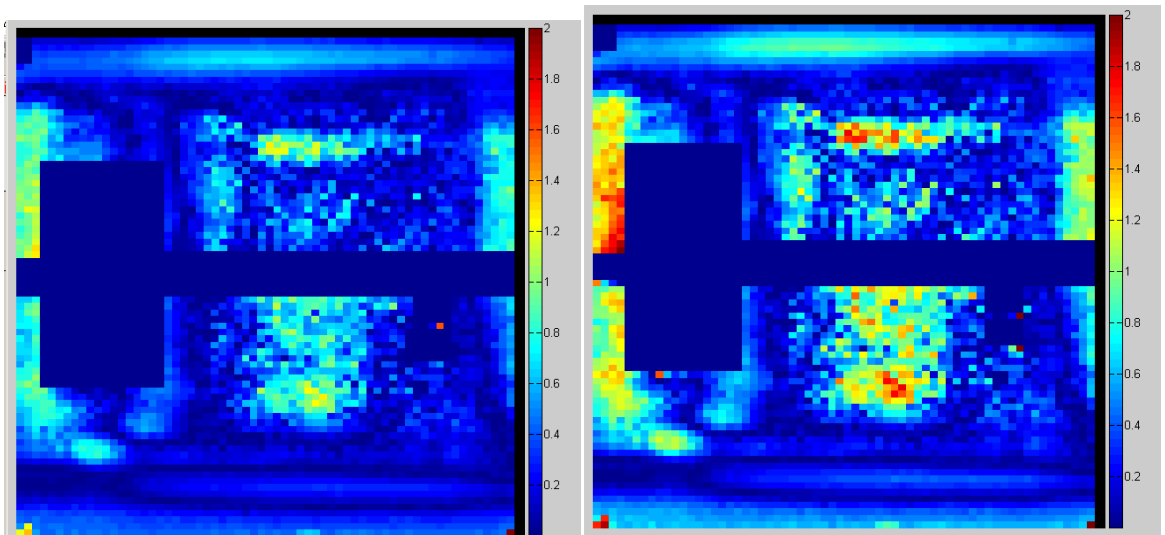

Figure D.143 Plan 4 (baseline) recalculated with the 600 series beam model and compared to the baseline machine delivery measurement 3 full sagittal region, 7%/4mm gamma index analysis with 98.57% pixels passing (left) and 5%/3mm with 90.75% pixels passing (right)

Bibliography

[1] S. Webb, Use of a quantitative index of beam modulation to characterize dose conformality: illustration by a comparison of full beamlet IMRT, few-segment IMRT (fsIMRT) and conformal unmodulated radiotherapy, Physics in Medicine and Biology 48 (2003) 2051-2062.

[2] A.L. McNiven, M.B. Sharpe, T.G. Purdie, A new metric for assessing IMRT modulation complexity and plan deliverability, Medical Physics 37 (2010) 505-515.

[3] N. Giorgia, F. Antonella, V. Eugenio, C. Alessandro, A. Filippo, C. Luca, What is an acceptably smoothed fluence? Dosimetric and delivery considerations for dynamic sliding window IMRT, Radiat Oncol 2 (2007) 42.

[4] D. Craft, P. Süss, T. Bortfeld, The Tradeoff Between Treatment Plan Quality and Required Number of Monitor Units in Intensity-modulated Radiotherapy, International Journal of Radiation Oncology*Biology*Physics 67 (2007) 1596-1605.

[5] J.S. Li, T. Lin, L. Chen, R.A. Price, Jr., C.M. Ma, Uncertainties in IMRT dosimetry, Med Phys 37 (2010) 2491-2500.

[6] R. Mohan, M. Arnfield, S. Tong, Q. Wu, J. Siebers, The impact of fluctuations in intensity patterns on the number of monitor units and the quality and accuracy of intensity modulated radiotherapy, Medical Physics 27 (2000) 1226-1237.

[7] G. Zhang, Z. Jiang, D. Shepard, M. Earl, C. Yu, Effect of beamlet step-size on IMRT plan quality, Med Phys 32 (2005) 3448-3454.

[8] T.S. Hong, W.A. Tomé, R.J. Chappell, P. Chinnaiyan, M.P. Mehta, P.M. Harari, The impact of daily setup variations on head-and-neck intensity-modulated radiation therapy, International Journal of Radiation Oncology*Biology*Physics 61 (2005) 779-788.

[9] J.V. Siebers, P.J. Keall, Q. Wu, J.F. Williamson, R.K. Schmidt-Ullrich, Effect of patient setup errors on simultaneously integrated boost head and neck IMRT treatment plans, International Journal of Radiation Oncology*Biology*Physics 63 (2005) 422-433.

[10] W. Luo, J. Li, R.A. Price, Jr., L. Chen, J. Yang, J. Fan, Z. Chen, S. McNeeley, X. Xu, C.M. Ma, Monte Carlo based IMRT dose verification using MLC log files and R/V outputs, Med Phys 33 (2006) 2557-2564.

[11] G. Mu, E. Ludlum, P. Xia, Impact of MLC leaf position errors on simple and complex IMRT plans for head and neck cancer, Phys Med Biol 53 (2008) 77-88.

[12] B.E. Nelms, J.A. Simon, A survey on planar IMRT QA analysis, J Appl Clin Med Phys 8 (2007) 2448.

[13] J.J. Kruse, On the insensitivity of single field planar dosimetry to IMRT inaccuracies, Med Phys 37 2516-2524.

[14] G.S. Ibbott, D.S. Followill, H.A. Molineu, J.R. Lowenstein, P.E. Alvarez, J.E. Roll, Challenges in credentialing institutions and participants in advanced technology multi-institutional clinical trials, Int J Radiat Oncol Biol Phys 71 (2008) S71-75.

[15] W. Bogdanich, Radiation Offers New Cures, and Ways to Do Harm, The New York Times, The New York Times Company, New York, 2010.

[16] W. Bogdanich, As Technology Surges, Radiation Safeguards Lag, The New York Times, The New York Times Company, New York, 2010.

[17] B.E. Nelms, H. Zhen, W.A. Tome, Per-beam, planar IMRT QA passing rates do not predict clinically relevant patient dose errors, Med Phys 38 1037-1044.

[18] P.R. Almond, P.J. Biggs, B.M. Coursey, W.F. Hanson, M.S. Huq, R. Nath, D.W.O. Rogers, AAPM's TG-51 protocol for clinical reference dosimetry of high-energy photon and electron beams, Medical Physics 26 (1999) 1847-1870.

[19] G.F. Knoll, Radiation detection and measurement, 3rd ed., Wiley, New York, 2000.

[20] T.H. Kirby, W.F. Hanson, D.A. Johnston, Uncertainty analysis of absorbed dose calculations from thermoluminescence dosimeters, Med Phys 19 (1992) 1427-1433.

[21] A. Niroomand-Rad, C.R. Blackwell, B.M. Coursey, K.P. Gall, J.M. Galvin, W.L. McLaughlin, A.S. Meigooni, R. Nath, J.E. Rodgers, C.G. Soares, Radiochromic film dosimetry: recommendations of AAPM Radiation Therapy Committee Task Group 55. American Association of Physicists in Medicine, Med Phys 25 (1998) 2093-2115.

[22] A. Molineu, D.S. Followill, P.A. Balter, W.F. Hanson, M.T. Gillin, M.S. Huq, A. Eisbruch, G.S. Ibbott, Design and implementation of an anthropomorphic quality assurance phantom for intensity-modulated radiation therapy for the Radiation Therapy Oncology Group, International Journal of Radiation Oncology*Biology*Physics 63 (2005) 577-583.

[23] B. Arjomandy, R. Tailor, A. Anand, N. Sahoo, M. Gillin, K. Prado, M. Vicic, Energy dependence and dose response of Gafchromic EBT2 film over a wide range of photon, electron, and proton beam energies, Med Phys 37 (2010) 1942-1947.

[24] A.M. Stell, J.G. Li, O.A. Zeidan, J.F. Dempsey, An extensive log-file analysis of step-and-shoot intensity modulated radiation therapy segment delivery errors, Med Phys 31 (2004) 1593-1602.

Vita

Jacqueline Renee Tonigan was born in Albuquerque, New Mexico on June 7th, 1987, the daughter of Diane Moody Tonigan and Richard Eric Tonigan, D.D.S. She attended Eldorado High School in Albuquerque and graduated in 2005. She then attended the University of New Mexico and received a Bachelor of Science degree in Nuclear Engineering in May 2009. She matriculated at the University of Texas Health Science Center at Houston Graduate School of Biomedical Sciences in September 2009.

Permanent Address:
1309 Kentucky St. NE
Albuquerque, NM 87110